Neuropathology induced by sterol glucosides in mice

by

Rena Christina Tabata

B.Sc., The University of British Columbia, 2005

A THESIS SUBMITTED IN PARTIAL FULFILLMENT OF THE
REQUIREMENTS FOR
THE DEGREE OF

MASTER OF SCIENCE

in

The Faculty of Graduate Studies

(Experimental Medicine)

THE UNIVERSITY OF BRITISH COLUMBIA

(Vancouver)

August 2008

Abstract

Sterol glucosides are a family of compounds characterized by a carbohydrate unit bound to a tetracyclic carbon chain. They are found in high concentrations in cycad seeds which have been linked to the etiology of amyotrophic lateral sclerosis-parkinsonism dementia complex (ALS-PDC). The neurotoxicities of the three main cycad sterol glucosides, campesterol β-D-glucoside, stigmasterol β-D-glucoside (SG), and β-sitosterol β-D-glucoside (BSSG) have been demonstrated previously *in vitro*. In the present study, we demonstrate that SG and BSSG exert neurotoxic effects *in vivo*. An outbred strain of mice was fed BSSG or SG (1000 μg daily) for a period of 15 wk and sacrificed immediately after or at 17 wk later. A battery of behavioural tests, including rotarod, wirehang, modified leg extension reflex test, treadmill, and open field were used to monitor behavioural disturbances. An array of histological measures was also conducted to assess the cellular impact of BSSG and SG. Behavioural test performance scores revealed that BSSG and SG impaired spinal reflexes and decreased overall movement. In addition to this, SG was found to impair motor coordination and strength. Also, ventral plane videography of performance on a treadmill and open field tests indicated that SG-exposed animals were more anxious and tended to drag and shuffle their limbs during forward movement. The cellular impact of dietary BSSG and SG exposures were also different. Animals exposed to each of the sterol glucosides showed an upregulation of activating transcription factor-3 and an increase in the incidence of phosphorylation of c-jun^{ser73} in response to stress. However, BSSG-exposure induced neurodegeneration that primarily targeted large motor neurons whereas SG impacted a more diverse motor neuron population, including large and small motor neurons. Exposure to each of the sterol glucoside caused intense proliferation of astrocytes and microglia as well as a depletion of dopamine levels in the *substantia nigra* and striatum. Lastly, SG-exposure induced the pathological aggregation of either tau or transactivating DNA binding protein-43 in some animals. The insights gained from this study will be useful for elucidating the pathogenesis of ALS-PDC and related disorders.

Table of contents

List of tables

List of figures

List of abbreviations

AD: Alzheimer's disease

ALS: amyotrophic lateral sclerosis

ALS-PDC: amyotrophic lateral sclerosis – parkinsonism dementia complex

ATF-3: activating transcription factor-3

BMAA: β-N-methylamino-L-alanine

BOAA: β-N-oxalylamino-L-alanine

BSSG: β-sitosterol β-D-glucoside

ChAT: choline acetyl transferase

CNS: central nervous system

GFAP: glial fibrillary acidic protein

HSP: heat shock protein

L-DOPA: L-deoxyphenyl alanine

MAM: methyl-azoxymethanol-β-D-glucoside

NFT: neurofibrillary tangle

PD: Parkinson's disease

SG: stigmasterol β-d-glucoside

Acknowledgements

I am grateful to my supervisory committee, Drs. Christopher Shaw, Doris Doudet, and Neil Cashman for their support and guidance throughout my graduate program in Experimental Medicine Graduate at the University of British Columbia, as well as for their support for my future academic endeavours.

I am also grateful to Drs. Reyniel Cruz-Aguado, Jason Wilson, and Denis Kay for practical guidance in all aspects of medical experimentation. Similarly, I am thankful to the members of the Shaw laboratory, past and present, for all of the inspiration, expertise, and laughter which made my graduate experience memorable and enjoyable.

With respect to the access to resources, I thank Drs. C. Schwab and P. McGeer for AD patient CNS tissue and Dr. K. McElwee and the members of his laboratory for unrestricted use of his laboratory equipment.

To my family, there are no words fitting for the gratitude I feel for you supporting me throughout my journey and the journeys to come.

I also thank J. K. Yeung and my friends for their unconditional love and encouragement they have provided. They have been a source of balance and contributed greatly to my personal development.

This work was supported by grants from the ALS Association, ALS Society of Canada, U.S. Department of Defense and the National Institutes of Health.

1.1 Overview of age-related neurological disorders

1.1.1 Background on age-related neurological diseases

This introduction is intended to provide a brief summary of the characteristics of the age-related human neurodegenerative diseases, Alzheimer's disease (AD), Parkinson's disease (PD), amyotrophic lateral sclerosis (ALS), and amyotrophic lateral sclerosis-parkinsonism dementia complex (ALS-PDC) that were pertinent to designing the experimental procedures and providing a basis for interpretation of the findings of the present study.

The neurodegenerative diseases, AD, PD, and ALS are typically diagnosed only once behavioural deficits can be detected clinically (Arasaki and Tamaki, 1998; Leenders et al., 1990; Whitehouse et al., 1982). In Alzheimer's disease, neurons are lost from various regions of the cerebral cortex and hippocampus and manifest as the loss of cognitive functions (Odle, 2003). Parkinson's disease involves the degeneration of select portions of the nigral-striatal system (Schapira and Olanow, 2003). Initially, terminal projections of dopamine-containing neurons are lost. Then eventually, the cell bodies of the dopaminergic neurons are lost from the substantia nigra (SN). This outcome results in disturbance of motor control and induces tremor, hypokinesia and rigidity (Dauer and Przedborski, 2003). Amyotrophic lateral sclerosis at end-stage is characterized by paralysis and death due to the progressive loss of spinal and cortical motor neurons controlling motor function, particularly the diaphragm (Rowland and Shneider, 2001).

In each of the aforementioned diseases, relatively specific neuronal populations degenerate and result in particular behavioural outcomes. It has been long-held that AD, PD, and ALS are distinct diseases, arising from distinct etiologies and resulting in mutually exclusive behavioural and neuropathological outcomes. This view has been based on the differential primary symptoms and pathological findings. However, more recent work has pointed to considerable cross-over between the neurodegenerative diseases (see Calne and Eisen, 1989; Muchowski and Wacker, 2005). For example, both PD and ALS patients

can exhibit a decline in cognitive function which is conventionally an AD attribute (Aarsland et al., 2003; Vaphiades et al., 2002). Also, AD patients can experience tremors, which is a feature primarily associated with PD (Yokoyama et al., 2002). Another overlap between AD and PD is that the gait disturbances experienced by some PD patients is a predictor for developing AD-like dementia (Verghese et al., 2002). ALS and PD have been shown to overlap significantly, and ALS cases with dementia and/or parkinsonism features are accordingly called ALS-plus (Zoccolella et al., 2002).

Assessments of post-mortem AD, PD, and ALS tissue have also uncovered many commonalities. In particular, the similarities in the molecular mechanisms associated with protein folding and aggregation have been gaining increasing attention (Muchowski and Wacker, 2005). Although the specific proteins that aggregate in particular neurodegenerative diseases are often unrelated in primary amino acid (aa) sequence, the characteristic lesions of AD, PD, and ALS typically contain fibrillar, amyloid-like structures with similar biochemical features (Dobson, 2003). However, instances of proteinacious inclusions possessing a common primary aa sequence have been observed across disease classifications. For example, neurofibrillary tangles (NFT) which are primarily associated with AD have been identified in some ALS (Kokubo et al., 2000) and PD (Arima et al., 1999) cases. On the same note, α-synuclein first identified in the amyloid plaques of AD patients has also been identified in PD Lewy bodies and Lewy neurites (Lucking and Brice, 2000).

1.1.2 A neurological disease model to decipher all other neurological diseases

As remarkable is the finding that the age-related diseases, AD, PD and ALS share commonalities to each other, the parallels are still limited. In contrast, the neurological disease, amyotrophic lateral sclerosis-parkinsonism dementia complex (ALS-PDC) is characterized by a wide range of behavioural and neuropathological attributes shared with each of the age-related diseases and many other neurological diseases. ALS-PDC can express as the classical form of ALS or as a form of parkinsonism with AD features, but some ALS-PDC

patients of Guam or Rota have been observed to present with a combination of these symptoms (Steele and Guzman, 1987). Based on these observations, some believe that understanding ALS-PDC can serve to better understand neurological diseases as a whole.

1.2 Amyotrophic lateral sclerosis-parkinsonism dementia complex

1.2.1 The history of ALS-PDC

Amyotrophic lateral sclerosis-parkinsonism dementia complex (ALS-PDC) is a progressive neurodegenerative disease with an unknown but suspected aetiology. Neuropathologically, ALS-PDC is similar to classical forms of ALS and atypical forms of Parkinson's disease and Alzheimer's disease (Kurland, 1988c; Steele and Guzman, 1987). The island of Guam in the 1950s was remarkable for its prevalence of these neurodegenerative diseases. The first formal report of a high incidence of ALS among the indigenous people of Guam was by a US Navy pathologist after the Second World War (Hirano et al., 1967). High numbers of parkinsonism cases were also reported around the same period (Hirano et al., 1961; Kurland, 1988c). The indigenous people of Guam and Rota, Chamorros, called ALS 'lytico' or 'paralytico', atypical AD and PD 'bodig', and the combinatorial manifestation 'lytico-bodig' (Reed et al., 1987). This disease complex accounted for nearly 25% of adult deaths among the Guamanians during the 1950's and 1980's (Kurland and Mulder, 1954; Plato et al., 2003; Waring et al., 2004) with an overall incidence 50 to 100 times higher than that of related disorders elsewhere (Kurland and Mulder, 1954). Today, the incidence of Guamanian ALS is about 3 per 100,000 people per year and PDC is about 32 per 100,000 people per year (Plato et al., 2003).

1.2.2 Clinical findings of ALS and ALS-PDC

The clinical features of classical ALS and Guamanian ALS (G-ALS) are nearly identical: progressive muscle weakness and atrophy, hyperreflexia and fasiculations (Mukai et al., 1982; Kurland and Mulder, 1987). With an insidious onset of disease, patients often lose the ability to initiate and control all

movement except of the eyes and succumb to the disease on average 3 to 5 years after diagnosis usually due to the failure of respiratory muscles (Hirano et al., 1966a; Mukai et al., 1982; Kurland and Mulder, 1987). Age of onset, however, differs between G-ALS and classical ALS with the former typically presenting 10 years earlier (Mukai et al., 1982). Although ALS and G-ALS share many features, they also have many differences. While cognitive function is generally spared in classical ALS and G-ALS, in ALS-PDC, the PDC component is characterized by parkinsonism features of cognitive decline similar to AD. Symptoms include tremor, rigidity, gait disturbances and bradykinesia. Speech difficulties (Coates and Bakheit, 1997) and olfactory dysfunction (Ahlskog et al., 1998) have also been reported. Fine motor movement impairment, facial masking with reptilian stare, and infrequent blinking are characteristic (Hirano et al., 1966a; Rodgers-Johnson et al., 1986). Almost all PDC patients suffer from some degree of dementia presenting as memory deficits, disorientation to place and time, difficulty with reasoning, and personality changes including increase in aggression (Lessell et al., 1962; Hirano et al., 1966a; Doty et al., 1991). Unlike classical PD, PDC patients do not respond to standard L-deoxyphenyl alanine (L-DOPA) treatment. ALS-PDC represents a spectrum of neurological disorders. Patients present with varying features of ALS and PDC. In a study of 104 Guamanian ALS cases, 5 patients eventually developed PDC (Hirano et al., 1966a). Additionally, they observed that 27 of the 72 PDC cases developed ALS (Hirano et al., 1966a).

1.2.3 Neuropathologic features of G-ALS, classical ALS, and ALS-PDC

The spinal cord neuropathology of Guamanian ALS and classical ALS is also very similar (Hirano et al., 1966a). Typical features include loss of spinal and cortical motor neurons (Hirano et al., 1966b; Rowland and Shneider, 2001). Guamanian ALS specifically has an abundance of neurofibrillary tangles (NFT) composed of the microtubule-associated protein tau throughout the central nervous system (Rodgers-Johnson et al., 1986). Tau regulates the assembly and stability of microtubules and its functionality is dependent upon the degree of

phosphorylation (Brich et al., 2003). Abnormally high levels of hyperphsphorylated tau are implicated in other neurological disorders such as AD (Alonso et al., 1996; Iqbal and Grundke-Iqbal, 1998), PD (Sperfeld et al., 1999; Rosso and van Swieten, 2002; Ishizawa et al., 2003) and PSP (Hof et al., 1991; Hof et al., 1994).

There are other neuropathological features of Guamanian ALS. In a study of ALS patients without PDC symptoms, 46% showed significant neuronal loss with increased NFTs in the hippocampus, which is normally associated with AD and other types of dementia (Rodgers-Johnson et al., 1986). Another more recent study showed reduced uptake of 6-fluorodopa in the striatum of Guamanian ALS patients; indicating a decreased number of dopaminergic cells in the substantia nigra, a hallmark pathology of PD (Snow et al., 1989). These findings could represent a concomitant PDC that has not yet progressed to a clinically detectable point (Snow et al., 1989). Other studies have observed significant neuronal disease in clinically undetectable states. For example, there needs to be greater than 80% depletion of dopaminergic neurons in the substantia nigra before a patient exhibits symptoms of PD (McGeer et al., 1988). In addition, it has been estimated that there is up to a 70% decrease in alpha motor neurons before ALS can be diagnosed clinically (Arasaki and Tamaki, 1998).

PDC shares neuropathological findings with PD and AD. Post-mortem analysis has revealed a loss of dopaminergic neurons in the substantia nigra and reduced 6-fluordopa uptake in the striatum of PD and PDC patients (Hirano et al., 1961; Lessell et al., 1962; Snow et al., 1989). One major difference, however, is that PDC patients have far fewer Lewy bodies, intracellular inclusions of synuclein protein which are classic of PD (Calne and Eisen, 1989; Forman et al., 2002; Winton et al., 2006). Similarities to AD include the marked cortical atrophy and NFTs in the hippocampus and entorhinal cortex (Hirano et al., 1961). The ultrastructure and immunohistochemical profile of the NFTs are identical to that in AD (Hirano et al., 1961; Forman et al., 2002; Winton et al., 2006). However, the

preference for NFTs to be in cortical layer 3 in Guamanian PDC differs from NFTs in cortical layer 5 of AD patients (Hirano et al., 1961).

As discussed earlier, there is often evidence of neuropathological changes in asymptomatic Guamanians who may represent preclinical ALS-PDC states. One study showed 95% of asymptomatic Guamanians over 60 years of age had extensive NFTs in various regions of the central nervous system.

The similarities and subtle differences in the neuropathology of Guamanian ALS-PDC and classical forms of ALS, PD, and AD could represent a complex interconnectivity. The study of Guamanian ALS-PDC, therefore, is promising in what it may tell us about neurodegenerative diseases as a whole.

1.3 Aetiology of ALS-PDC

1.3.1 Gene-environment hypotheses revisited

The aetiology of ALS-PDC remains uncertain. A multi-factorial inheritance seems to take into account both observed genetic and environmental factors. The genetic inheritance is inferred from the relatively homogeneous genetic background of the indigenous population of Guam, the Chamorros (Plato et al., 2003). While pure genetic inheritance has not been confirmed (Lilienfeld et al., 1994; Plato et al., 2003; Reed et al., 1975), the Chamorros of Saipan, an island 80 miles north of Guam, have a nearly identical genetic background as those of Guam yet have not experienced a high incidence of ALS-PDC (Yanagihara et al., 1984; Garruto et al., 1980). Furthermore, detailed screening over many years has failed to identify a specific causal gene(s) (Reed et al., 1975; Lilienfeld et al., 1994, Chen et al., 1995; Plato et al., 2003; Ince and Codd, 2005). Since completion of these screening studies, the focus shifted to finding potential environmental toxins. The levels of various minerals and heavy metals in soil and ground water, native food products, and industrial and military activity-associated materials and its correlation to ALS-PDC have been investigated (Chen et al., 1995; Durlach et al., 1997; Spencer et al., 2005). None of these studies were conclusive and have been discounted as causal factors to the disease. The first clue implicating cycad seeds with ALS-PDC came from

historical records detailing the toxic effects of the cycad seed (Kurland and Mulder, 1954; Plato et al., 2003). Furthermore, it was subsequently found that that the incidence of ALS-PDC was directly related to the level of cycad consumption by the Chamorros (Kurland, 1988a). Specifically, the increase in consumption of cycad seeds during food shortages of World War II (Kurland, 1988c; Plato et al., 2003; cited in Shaw and Wilson; 2003; Neumann et al., 2006) resulted in a spike in the incidence of ALS-PDC. When cycad consumption lessened post-war and when Guamanians adopted an 'Americanized' diet, a large decline in the incidence was observed (Zhang et al., 1990; Leenders et al., 1990). Allegedly, the Chamorros were originally introduced to the practice of eating cycad by Mexican natives who themselves were taught the practice by the Spanish. Supposedly, prior to learning the methods to "remove" the acutely toxic factors, Chamorros avoided the consumption of cycads, knowing the risks. The toxicity of unwashed cycad seeds are documented in ship records from Captain Cook's visit to Australia in the late 1700's. When several of Cook's sailors consumed unwashed cycad, they experienced violent vomiting, vertigo (1997) and even acute neurological symptoms (Hall, 1987). Reports detailing the acutely toxic effects of unwashed cycad in cattle and other animals have also been made (Hall, 1987).

The Chamorro practice of processing the cycad seeds for consumption began with the harvest of the seeds from the cycad palm, dehusking and cutting them to expose the endosperm, chopping the starchy portion into 'chips', then washing the chips for days up to a month prior to grinding the chips into a finely ground form resembling flour. As their ingestion of cycad seeds decreased with the increased popularity of a Western diet, the incidence of ALS-PDC was found to decrease (Zhang et al., 1990; Neumann et al., 2006). In addition, Kurland (1988) found that the Saipan natives who were genetically similar to Guamanians did not have a high incidence of ALS-PDC and curiously also did not consume cycad (Kurland, 1988c).

1.3.2 The cycad hypothesis

The cycad seeds ingested and implicated in the aetiology of ALS-PDC were consumed by Western Pacific populations after being thoroughly washed and ground into flour. It is probable that the Guamanians assumed that the intensive washing process rendered cycads safe to consume (Kurland, 1972; Kurland, 1988c; Spencer et al., 1991) particularly since their processing method removed the water soluble toxins, which were associated with the well known acute toxic effects and also because the link between insoluble toxins and development of ALS-PDC many years down the line would have been a difficult one to make (Schulz et al., 2005). Accordingly, the prevailing hypothesis is that the clinical aspects of ALS-PDC that develop over months and years after first exposure to cycad are caused by insoluble toxins that remain even after cycad seed washing (Kurland, 1988b).

1.3.3 A murine model of ALS-PDC

To compliment the dietary link between cycad seed consumption and ALS-PDC found in dietary studies, our laboratory developed a mouse model of ALS-PDC which linked cycad consumption to ALS-PDC. One quarter of the animals' daily intake by weight was calculated to be equivalent to the amount Guamanian natives may have consumed prior to WW2 (Wilson et al., 2002a). Daily feedings of washed cycad seed flour pellets to mice produced outcomes that were similar to human ALS-PDC (Wilson et al., 2002a; Wilson et al., 2003b; Wilson et al., 2004b; Wilson et al., 2004b). Control mice were fed an identical amount of standard mouse chow. Since both groups maintained similar weight throughout the duration of the study, systemic metabolism was assumed to be the same (Wilson et al., 2002a; Wilson et al., 2003c; Wilson et al., 2004b; Valentino et al., 2006). Cycad-flour fed mice were found to be impaired on the leg extension reflex and wire hang. Reduced gait length, a feature of PD was also observed (Wilson et al., 2002a). Tests for spatial, working and reference memory all showed impaired cognition (Wilson et al., 2002a; Schulz et al., 2003).

1.3.4 Candidate cycad toxins

Since the original epidemiological studies suggesting a correlation between consumption of cycad and development of ALS-PDC, researchers have sought to identify a toxic compound(s) responsible for causing the disease. Past studies have investigated various toxic amino acids, including methyl-azoxylmethanol-β-D-glucoside (MAM) derived from cycasin (Hoffmann and Morgan, 1984), as well as β-N-oxalylamino-L-alanine (BOAA) and β-N-methylamino-L-alanine (BMAA) (Spencer et al., 1987; Weiss et al., 1989). Rigorous studies conducted more recently have refuted earlier hypotheses that these compounds are causal to ALS-PDC (Wilson et al., 2002a; Wilson et al., 2003a; Cruz-Aguado et al., 2006). When monkeys were exposed to BOAA, they developed neurological lathyrism but none of the features overlapped with ALS-PDC (Spencer et al., 1986). In a study where mice were exposed to BMAA, no remarkable change was found in motor strength, coordination, spinal reflexes or cognition, or histopathologically (Perry et al., 1989). Cycasin and MAM have been shown to induce developmental abnormalities in rodents and an acute loss of motor system function in cattle, but again, the outcomes did not mimic ALS-PDC (Campbell et al., 1966; Hooper et al., 1974). These compounds failed to reproduce ALD-PDC features likely due to the high solubility in water. Prior to consuming the cycad seeds, the Chamorros soaked and washed the seeds repeatedly over the course of several days, nearly completely eliminating these compounds. Also, BMAA does not appear to cross the blood brain barrier (Montine et al, 2008).

The direction for the search of a causal cycad neurotoxin shifted after studies showed that it was unlikely that a water-soluble compound was causal to ALS-PDC (Duncan et al., 1990; Wilson et al., 2002a). Specifically, our research group began searching for a water-insoluble and lipophilic compound since the traditional washings eliminated water-insoluble compounds and a toxic compound that can exert effects on the CNS would need to be able to cross the blood brain barrier (reviewed in Shaw and Wilson, 2003). Three such candidate toxins, all β-D-glucosides, identified as campesterol β-D-glucoside, stigmasterol

β-D-glucoside (SG), and β-sitosterol β-D-glucoside (BSSG) (Figure 1) were isolated through a series of chemical extractions of washed cycad flour (Khabazian et al., 2002b). Cell death assays conducted after exposing cortical culture neurons to BSSG, campesterol glucoside and SG showed that BSSG is the least toxic and SG the most toxic (Khabazian et al., 2002). Furthermore, in rat cortical cultures, each of these sterol glucosides were found to induce depolarizing field potentials, induce the excitotoxic release of glutamate, activate protein kinases implicated in apoptotic and survival pathways, and induce apoptosis (Khabazian et al., 2002a). In a motor neuron-derived cell line, NSC-34, synthetic BSSG was found to induce a dose-dependent decrease in cell viability (Ly and Shaw, 2007). BSSG had similar effects on organotypic spinal, hippocampal and striatal cultures, inducing significant neuron loss compared to controls (K. Andreasson; C. Mathews; S. Jaffery; personal communication). These studies provided new support for the cycad hypothesis that washed cycad seed consumption may be causal for ALS-PDC. To date, the studies assessing the toxicity of these sterol glucosides have been limited to *in vitro* experimentation. With the stage set with earlier *in vitro* toxicity studies and the need for detailed *in vivo* work in mind, the theme of the present study was determined.

1.3.5 Sterol glucosides are ubiquitous in plants

The cycad phytosterol glucosides isolated from washed cycad seed flour falls under a broader classification termed sterol glucosides (Figure 1 for examples). Sterol glucosides characteristically have a carbohydrate unit bound to a tetracyclic carbon chain. A great variation exists in the carbohydrate unit, and can be anything from a glucose, galactose, or fructose amongst others. Well-known sterols that can be glycosylated with the basic structure include sitosterol, campesterol, stigmasterol, brassicasterol, and cholesterol.

Sterol glucosides are found in the glycolipids of plant cell membranes (Wojciechowski, 1983; Misiak et al., 1991) but their function remains poorly

understood. It is know however, that BSSG acts as a primer for *de novo* cellulose biosynthesis (Figure 1) (Peng et al., 2002).

The role and effect of phytosterols and phytosterol glucosides in mammals is contentious. Some have claimed that plant sterol glucosides can exert significant beneficial effects for patients with hypercholesterolemia and several products containing sterol glucosides have been produced (Bouic, 2002; Nestel et al., 2001). In contrast, other sterol glucosides have been shown to exert extremely toxic effects. One notable example is ouabain. Ouabain is a toxic compound that can be extracted from the seeds of certain native Aftrican plants and can block ion pumps in heart muscle cells and neurons (Erdmann et al., 2005). A related sterol glucoside cocktail, digitalin, which is a mixture of sterol glucosides that can be extracted from the seeds and leaves of foxglove (Wasserstrom and Aistrup, 2005), is also very toxic. The toxin scillirosidin, found in a semi-arid desert plant, contains a high concentration of sterol glucosides and causes paralysis upon ingestion (Azoyan et al., 1991). Solanine, found in unripe potato skin, which also has a high concentration of sterol glucosides, is known to cause neurological symptoms after ingestion (Bodart et al., 2000). A recent study examined the content of the three sterol glucosides found in cycad seeds in other plant species. Non-cycad species of plants and plant derivatives have a sterol glucoside content up to several orders of magnitude lower than in cycad seeds (Marler et al., 2005). Combined, these findings point to dosing as the crucial factor that determines whether or not sterol glucoside-containing plants and plant derivatives will induce neurological symptom(s) or disease. Most humans will ever only consume species with low sterol glucoside content and will likely never develop a sterol glucoside-related neurological condition.

1.3.6 Neural cell stress, survival and apoptosis

In the present study, I investigated the differential up-regulation of key stress-inducible genes and the expression of an apoptotic marker to assess the neural response to sterol glucoside exposure. The following is meant to serve as

a background summary surrounding key molecules chosen for molecular assays in the present study and is not intended to serve as an exhaustive review.

Following physical (Fawcett and Geller, 1998) or chemical insult, injured neurons initiate a cascade of molecular responses to promote survival and repair (Fawcett and Geller, 1998). When these molecular responses are inadequate or inappropriately expressed, neurons undergo cell death.

Heat shock proteins are considered one of the major lines of defense for neurons to overcome cellular stress and avert cell death. Heat shock protein (Hsp) synthesis is induced when an environmental stimulus perturbs an animal's physiological system to the extent that the cellular environment is disrupted and proteins become denatured. Under such perturbations, Hsps and other related molecular chaperones stabilize denaturing proteins, refold any reversibly denatured proteins back to their native conformation, and orchestrate the degradation of irreversibly denatured proteins (Lindquist, 1986; Lindquist and Craig, 1988; Parsell and Lindquist, 1994; Feige et al., 1996; Frydman, 2001; Hartl and Hayer-Hartl, 2002). Hsps are also required for protein trafficking and to facilitate the hand-over of misfolded proteins to the proteasome for degradation (Becker and Craig, 1994). Of particular interest to the present study is Hsp-70. Hsp-70 is a potent anti-apoptotic chaperone protein and the inadequate expression of Hsp-70 is known to trigger cell death. Furthermore, the role of Hsp-70 in delaying the degeneration of motor neurons has been investigated rigorously in recent years, and the differential expression levels of various Hsps have been revealed for AD, PD, and ALS and mouse models of these diseases (Chen and Brown, 2007).

It is thought that the expression of certain early transcription factors is central to determining the fate of a neuron because of their ability to regulate multiple gene expressions (Nakagomi et al., 2003). In the case of neuronal injury, activating transcription factor-3 (ATF-3) (also known as transcription factor LRG-21) and c-Jun, both members of the cAMP response element-binding protein CREB/ATF family of transcription factors are thought to be such essential early transcription factors (Nakagomi et al., 2003; Ohba et al., 2003). ATF-3 is

not expressed in healthy neurons but becomes highly expressed in response to neuronal injury (Masliah et al., 2000; Tsujino et al., 2000). The stress inducibility (Liang et al., 1996; Hai et al., 1999) and transcription repression properties (Chen et al., 1994) of ATF-3 are also well-documented. The differential action of ATF-3 is determined by its counterpart and its own configuration (Chen et al., 1994). ATF-3 as a homodimer functions as a repressor, whereas the heterodimer, for example when coupled with c-Jun, activates specific promoters in non-neuronal cells in the CNS (Hsu et al., 1992; Hai and Hartman, 2001). Like ATF-3, c-Jun is also a stress-inducible gene found in both neuronal and non-neuronal cells alike. Under stressful conditions, c-Jun is activated by c-Jun N-terminal kinase/stress-activated protein kinase (JNK/SAPK), which is a member of the MAP kinase superfamily (Xia et al., 1995; Herdegen et al., 1997). The survival of neurons is tightly coupled to c-Jun activation (Tsujino et al., 2000). For example, in c-Jun activated superior ganglion cells, activation of ATF-3 promotes expression of heat shock protein 27 (Hsp 27) (Benn et al., 2002) and leads to the survival of the cells. However, once phosphorylated, Jun operates as a cell death-promoting signal (Ham et al., 1995; Eilers et al., 1998; Tsujino et al., 2000).

Apoptosis research exploded soon after its first appearance in the biomedical literature in 1972 (Kerr et al., 1972). Apoptosis is a structurally distinctive mode of cell death observed to occur within living tissues (Kerr et al., 1972). The cardinal cellulo-morphological features of apoptosis include cell shrinkage, transient blebbing of the cell membrane, and eventual fragmentation of the cell into numerous, small, membrane-bound bodies (Kerr et al., 1972; Cohen, 1993). In apoptosis, organelle structure is relatively preserved, except for the nucleus, which undergoes a condensation of chromatin (Kerr et al., 1972). Cell surface molecules undergo more drastic changes so that apoptotic cells are recognized, phagocytosed and eliminated quickly (Kerr et al., 1972; Cohen, 1993). The highly conserved family of cysteine proteases, or caspases, play essential roles in mediating apoptotic cell death (Kerr et al., 1972; Alnemri et al., 1996). Caspases exert their effects at several stages of signaling during apoptosis, ranging from responding to extracellular factors at transmembrane

receptors to downstream proteolytic breakdown of cellular components (Alnemri et al., 1996). Among the group of 11 caspases identified to date, caspase-3 (also called CPP32, Yama and apopain) is studied most extensively due to its recognition as a central player in mediating apoptosis, for its role in enacting the final, irreversible commitment to death, and also for its the numerous clinical implications. For example, caspase-3 is the predominant enzyme involved in the cleavage of amyloid β 4A precursor protein, which is implicated in neuronal death in AD. In viable cells, caspases exist in the cytoplasm as an inactive pro-enzyme. In cells undergoing apoptosis, the inactive pro-enzyme is self-proteolysed and/or cleaved by other upstream proteases (e.g. caspase 8, 9 or 10) to generate active enzymes. As the processed form, caspase-3 is comprised of 17kDa and 12kDa heterodimer subunits derived from the 32 kDa pro-enzyme, which react to form the active caspase-3 enzyme. The activated form of caspase-3 in turn proteolytically cleaves and activates other caspases as well as relevant cytoplasmic targets.

The characterization of the role of stress-induced upregulation of the aforementioned chaperone proteins, transcription factors and apoptosis mediators will be crucial to constructing a detailed timeline of pathogenesis following sterol glucoside exposure and to compare to human AD, PD, and ALS.

1.3.7 Neuronal metabolism

Neural tissue is comprised of a heterogeneous population of neurons and glial cells whose activity level can be accurately assessed by measuring the level of oxidative energy metabolism, making cytochromes excellent endogenous markers (Wong-Riley, 1989). The cytochromes are a family of energy-deriving molecules essential for electron transport and oxidative phosphorylation (Wong-Riley, 1979; Wong-Riley, 1989). Cytochrome c oxidase (also known as cytochrome aa_3, ferrocytochrome c, oxygen oxidoreductase) occurs as an integral transmembrance protein of the inner mitochondrial membrane in all eukaryotes and in the cell membrane of prokaryotes (Wikstrom et al., 1981). In the electron transport chain, cytochrome c oxidase is the terminal enzyme that

catalyses the transfer of electrons from its reduced substrate ferrocytochrome c to molecular oxygen, effectively producing water (Wikstrom et al., 1981). This reaction is coupled to the generation of ATP.

Cytochrome c oxidase is said to account for greater than 90% of oxygen consumption by living organisms (Wikstrom et al., 1981). Accordingly, it is an essential component of all organs, including the brain and spinal cord. While the mature brain makes up approximately 2% of the total body weight, it consumes over 20% of the total oxygen intake at the resting state (cited in Wong-Riley, 1989). A steady supply of ATP is essential to maintaining ion pump function, axoplasmic transport processes, and the synthesis and secretion of neurotransmitters and so forth (reviewed in Wong-Riley, 1989). Increased neuronal metabolism can result under a variety of conditions due to a heightened demand for ATP. The differential demands placed on neuronal mitochondria are of particular interest in diseases and toxicology studies such as the present study to map the sequence of neuropathological changes, cellular responses and to provide potential targets for therapeutic intervention. The usage of cytochromes in histochemical methods has allowed neuroscientists to observe the regional functional diversity among the neurons. To date, the metabolic activity of cells following treatment with cycad and sterol glucoside have not been assessed.

1.4 Research theme and objectives

1.4.1 Research theme

Epidemiological and experimental studies have found a link between consumption of washed cycad seeds and development of ALS-PDC (Borenstein et al., 2007; Kurland, 1988b; Wilson et al., 2002a; Wilson et al., 2004b). A family of bioactive, insoluble compounds called sterol glucosides found in washed cycad seeds has been shown to exert toxic effects *in vitro* (Khabazian et al., 2002b). Accordingly, we hypothesized that one or more of the sterol glucosides is the neurotoxin instrumental in the pathogenesis of ALS-PDC yet crucial *in vivo* work had not yet been conducted.

1.4.2 Objectives

The objective of the present study was to map the behavioural and cellular outcomes of dietary exposure to two separate, pure cycad sterol glucosides: β-sitosterol β-D-glucoside (BSSG) and stigmasterol β-D-glucoside (SG) in an outbred strain of mice. A battery of behavioural tests was employed to determine whether motor strength, general coordination, emotionality, or gait was affected due to sterol glucoside exposure.

This study aims to contribute to the goal of identifying and revealing the effects of the putative causative molecule(s) in ALS-PDC and to shed light on the processes underlying this and other related neurodegenerative diseases. The information obtained from this study will contribute to defining a timeline of cellular and behavioural milestones of neurodegenerative disease in order to design timely pharmacologic interventions for ALS, PD, and AD.

1.4.3 Hypotheses

Hypotheses:

1) Dietary exposure to β-sitosterol β-D-glucoside (BSSG) will induce progressive motor and other deficits in mice (Chapter 3).
2) Dietary exposure to stigmasterol β-D-glucoside (SG) will induce progressive motor and other deficits in mice (Chapter 4).

A

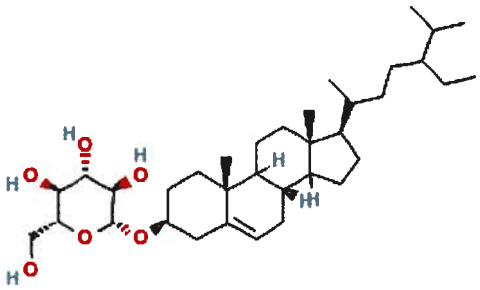

B

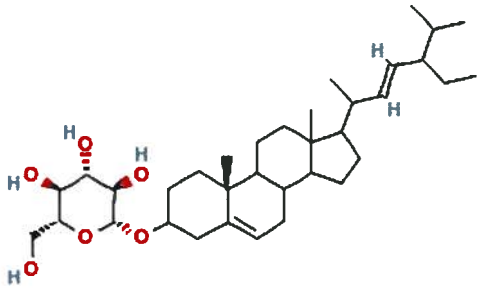

Figure 1. **Molecular structure of two of the water insoluble sterols found in washed cycad seed flour.**

Molecular structure of β-sitosterol β-D-glucoside (BSSG) (A) and stigmasterol β-D-glucoside (SG) (B). BSSG has a molecular weight of 576.8473 g/mol, molecular formula $C_{35}H_{60}O_6$ and the IUPAC name (2R,3R,4S,5S,6R)-2-[[(3S,8S,10R,13R,17R)-17-(5-ethyl-6-methylheptan-2-yl)-10,13-dimethyl-2,3,4,7,8,9,11,12,14,15,16,17-dodecahydro-1H-cyclopenta[a]phenanthren-3-yl]oxy]-6-(hydroxymethyl)oxane-3,4,5-triol). SG has a molecular weight of 574.83142 g/mol, molecular formula $C_{35}H_{58}O_6$ and is (2R,3R,4S,5S,6R)-2-[[(10R)-17-[(E)-5-ethyl-6-methylhept-3-en-2-yl]-10,13-dimethyl-2,3,4,7,8,9,11,12,14,15,16,17-dodecahydro-1H-cyclopenta[a]phenanthren-3-yl]oxy]-6-(hydroxymethyl)oxane-3,4,5-triol)) according to IUPAC guidelines. The outcomes following dietary exposure to BSSG and SG is highlighted in Chapter 3 and 4 respectively.

Chapter 2. Material and Methods

2.1 Materials

2.1.1 Chemical reagents

Chemicals and abbreviations	Company
Acetic acid	Sigma
Acetic acid, glacial	Fisher
BlokHen blocking reagent	Aveslab
Bovine serum albumin (BSA)	Sigma
2-Bromo-2-chloro-1,1,1 trifluoroethane	Sigma
Cresyl violet acetate	Sigma
Cytochrome c, type III	Sigma
4'6 diamidino-2-phenylindole (DAPI) mounting media	Vector
3,3'-diaminobenzidine tetrahydrochloride (DAB) kit	Vector
Entellen	Merck
Ethanol	Vancouver General Hospital
Ethyl violet (methyl green)	Sigma
Haematoxylin	Richard Allan
Isofluorane	Sigma
Isopentane	BDH
Isopropanol	Fisher
MOM immunodetection kit	Vector
Normal goat serum	Vector
Normal rabbit serum	Vector
Oil red O	Sigma
Paraformaldehyde	Sigma
Sodium azide	Fisher
Sodium chloride (NaCl)	Fisher
β-sitosterol β-D-glucoside	UBC Dept. Chemistry
Stigmasterol	Sigma

Stigmasterol β-D-glucoside	UBC Dept. Chemistry
Triton X-100	Fisher
Vectastain Elite ABC kit	Vector

2.1.2 Laboratory supplies

Laboratory supplies	**Company**
Optimum cutting temperature (OCT) gel	Tissue-tek
Platinum cured silicon tubing	Cole-Parmer
Superfrost Plus charged glass slides	Fisher
Slide coverslips	VWR
Cryomold	Tissue-tek

2.1.3 Primary and secondary antibodies

Antibody	**Company**	**Dilution**
Activated caspase-3	Chemicon	1:250
Activating transcription factor-3 (ATF-3) (H-90)	Santa Cruz	1:500
AlexaFluor 548-goat anti-rabbit IgG conjugate	Invitrogen	1:500
AlexaFluor 568-goat anti-rabbit IgG conjugate	Invitrogen	1:500
Choline acetyl transferase (ChAT)	Chemicon	1:100
Cytochrome oxidase	Sigma	1:25
Glial acidic fibrillary protein (GFAP)	GeneTex	1:250
Fluorescein isothiocyanate-goat anti-chicken IgY conjugate	Aveslab	1:1000
Fluorescein isothiocyanate-goat anti-rabbit IgG conjugate	Invitrogen	1:500
Heat shock protein-70 (Hsp-70)	Chemicon	1:200
Ionized calcium binding adaptor molecule-1 (IBA-1)	Wako	1:100
Phosphorylated-Tau (PHF-1, AT8 clone)	Pierce	1:500
Phosphorylated Jun^{Ser-73}	Santa Cruz	1:100
HyperphosphorylatedTAR DNA binding protein-43 (TDP-43)	ProteinTech	1:500
β-Tubulin III	Aveslab	1:1000
Tyrosine hydroxylase (TH)	Affinity	1:500

2.1.4 Behavioural testing equipment

Behavioural testing equipment	**Company**
Gait analysis runway	Mouse Specifics
Open field	Noldus
Rotarod	Shaw Laboratory
Wirehang	Shaw Laboratory

2.2 Methods

2.2.1 BSSG and SG synthesis and purity verification

Gram quantities of SG were synthesized on a contract basis by the laboratory of Dr. Stephen Withers (Department of Chemistry, University of British Columbia). Stigmasterol (95% purity) was purchased in bulk (Sigma-Aldrich Co., Oakville, ON, Canada) to use as the starting material for the synthesis of BSSG and SG. Stigmasterol was converted to stigmasterol tosylate which was treated with methanol and pyridine to yield stigmasterol methyl ether. Hydrogenation of stigmasterol methyl ether was accomplished in ethanol using 5% palladium on carbon as a catalyst. Finally, β-sitosterol was produced in a reaction with tosic acid in water and dioxane at 80°C. A multi-step process converted unglycosylated stigmasterol into BSSG and SG. Synthesized compounds were characterized using NMR (^{1}H and ^{13}C) and high-resolution mass spectrometry (HRMS). A purity of at least 95% was verified by HPLC.

2.2.2 Mice

All procedures were performed in strict compliance with the National Institutes of Health Guide for the Care and Use of Laboratory Animals and the Society for Neuroscience "Guidelines for the Use of Animals in Neuroscience Research" using protocols approved by the University of British Columbia Animal Care Council (Protocol number: A06-0181).

Five-month old male CD-1 mice (30.1-35.7 g, 7.5 cm – 8.8 cm) were purchased from Charles River (Wilmington, MA) (Appendix B). CD-1s were selected for the neurotoxicity experiments as our laboratory has demonstrated

the effects of cycad flour consumption in this same strain (Wilson et al., 2002a; Shaw and Wilson, 2003; Wilson et al., 2004a; Shaw et al., 2005). Adult mice were deliberately chosen to mimic the mean age of onset of ALS-PDC (Kurland, 1988; Kurland et al., 1994). Thirty-one mice for the BSSG study and 30 mice for the SG study were randomly divided into 2 groups (BSSG study: 15 control and 16 experimental animals; SG study: 14 control and 16 experimental animals). All animals were housed singly in a virus-free barrier facility in a room maintained at 22°C under a 12 h light/dark cycle. The mice were provided *ad libitum* access to food and water. The behavioural tests, including pre-testing were conducted in the same room.

2.2.3 BSSG and SG feeding

The synthetic BSSG or SG was mixed with finely ground Purina Chow mouse pellets (Mouse Diet™, Purina) to create the experimental pellets with a BSSG or SG content of 1000 µg per pellet. Dry materials were blended with a sterile silicon spatula. For every 5 g of standard feed, 2.5 mL of ddH_2O was added and the dough was kneaded and round up into pellets. A single sterol glucoside containing pellet was placed in the feeding tray each morning before the addition of regular mouse chow (*ad libitum*). All experimental pellets were entirely consumed by the mice each day. Control mice were fed standard mouse chow pellets of identical weight with no additives. SG feeding was conducted daily for 15 wk and mice were behaviourally monitored up until sacrifice at 35 wk (time point 1) or 52 wk (time point 2).

2.2.4 Behavioural testing

Motor behaviour is a reflection of the state of components that make up the motor system. In order to ascertain the cumulative effects of sterol glucosides on the entire mouse, I tested animals rigorously on a battery of behavioural tests. Here, I will provide summaries of the tests that were utilized to study the behaviours that result following dietary sterol glucoside exposure.

The mice were tested singly in each of the behavioural experiments between 10 a.m. and 5 p.m. under standard light conditions (Crawley, 2000) in the virus-free facility. The testing sequence of mice was randomized across groups at every session. The experimental group to which each animal belonged was unknown to the observer at the time of behavioural recording.

The rotarod was used to evaluate motor function, coordination and balance (Jones and Roberts, 1968; Sango et al., 1995; Gerlai et al., 1996a; Sango et al., 1996; Chapillon et al., 1998; Carter et al., 1999; Crawley, 1999;Gerlai and Roder, 1996). The time that a mouse could remain walking on a horizontal (Norflus et al., 1998), rotating axle (3.6 cm diameter; speed of rotation: 16 rpm) elevated above an area of padding without falling, clenching on, or jumping off the axle was measured (Crawley, 1999). Each mouse was placed in the center of the rod (Chen et al., 1995) and tested for a maximum of 160 s (Barneoud et al., 1997; Crawley, 1999) twice per week.

Neuromuscular strength was tested by the wire hang (or hanging wire) test (Wilson et al., 2003d; Wilson et al., 2004c; Wilson et al., 2005; Tabata et al., 2008). Both balance and grip strength are required for a mouse to keep its body suspended (Crawley, 2000). Mice were placed on a wire cage lid elevated 50 cm above a soft landing surface. The latency to fall off the wire (maximum 60 s) (Sango et al., 1996) was measured from the moment the wire apparatus was inverted (180°). Wirehang testing was also conducted biweekly.

The leg extension reflex test was used as a measure of motor neuron dysfunction (Barneoud and Curet, 1999). An altered form of this was used to discriminate more subtle behavioural changes. A 0-4 scale developed with consideration of possible animal responses was utilized (Wilson et al., 2002a): A score of 4 was assigned to an animal that exhibited complete extension of both legs. Such a response was considered a normal response. A score of 3 was assigned when an animal extended both legs with some tremors and/or punching of one leg. A score of 2 indicated that the animal extended one leg and retracted the other, or that the animal exhibited tremors in both legs. A score of 1 indicated that the animal retracted one leg and exhibited tremors in the other leg.

A score of 0 was assigned when both legs were retracted. The leg extension reflex was measured three times per week in each animal. This scaled test was designed to show the progressive loss of function as the normal reflex has been found to deteriorate progressively to tremor and then to total retraction in previous cycad and sterol glucoside studies (Wilson et al., 2002b; Tabata et al., 2008).

Spontaneous activity in an open field is considered one of the most standardized general measures of motor function (Crawley, 2000). The open field test can also reveal stress response in animals (i.e. defensive burying or thigmotaxis) (Karl et al., 2003). Open field testing of each animal was conducted every two weeks. A single mouse was placed in one of four round open field arena/tubs (approximately 1 m diameter) to permit the testing of four animals per 5 min trial. Five min has been shown to be sufficient for evaluation of gross abnormalities in locomotion and highly significant hyperactivity or behavioural sedation (Crawley, 2000). Large arenas were employed since they have better defined "regions" (i.e. center and perimeter) and permit mice to cover longer distances and demonstrate a wider variation in movement. This in turn, increases the likelihood of detection of fear-based behaviour (Crawley, 2000) and minimize habituation of the animal to the open field (Crawley, 2000). Testing arenas were cleaned with 70% ethanol before the testing of each animal and with quatricide at the end of each testing session. Movements were recorded using a video camera mounted on the ceiling. Video clips were reviewed and were manually scored or automatically analysed on an automated video tracking software (Ethovision® 3.1, Noldus Information Technologies Inc., Leesburg, VA, USA). Scoring was done on videotaped sessions, rather than in-person at the time of testing to avoid the introduction of confounding variables by the presence of an observer in close proximity to the mice (Crawley, 2000).

In order to examine spatial and temporal indices of front and hind limb stepping patterns during forward locomotion, mice were required to run on a colorless (PVC and polycarbonate), straight, level, walled motorized belt (Digigait™, treadmill motor: DC, ¼ HP; torque 45 lb-in, Mouse Specifics, Inc.,

Boston, MA, USA) set at 30 rpm with a no-flicker light source (90-250 VAC; 25 kHZ, Mouse Specifics, Inc., Boston, MA, USA) and camera mounted ventrally (relative to the animal) to facilitate continuous ventral plane videography (up to 150 frames per second) of activity. Gait indices were analyzed with the complementary digital imaging software (Digigait™, Mouse Specifics, Inc., Boston, MA, USA) as per manufacturer's instructions. Briefly, the software converts "paw prints" into a digital signal and generates a temporal record of paw placement and breaks down the digital file into three main parameters: stride duration, swing duration, and stance duration (please see Appendix C for a sample software conversion figure). The stance duration is the period during which the paw of a limb is in contact with the belt surface. The software further subdivides the stance duration into two components: braking duration (the increase in paw contact area over a discrete time interval) and propulsion duration (the decrease in paw contact area over a discrete time interval). The swing duration is the period of time that a paw is not in contact with the belt surface. In addition to these factors, over a dozen additional characteristics, including stance factor, step-sequence pattern, propulsion, and cadence are generated to provide a spreadsheet format report of twenty-five gait indices.

2.2.5 Animal sacrifice and organ harvesting

Mice were sacrificed for histological analysis at 35 wk (35.9-48.6 g) and 52 wk (41.2-51.4 g) of age for the SG study (Chapter 4) and at 52 wk (42.8-50.1 g) for the BSSG study (Chapter 3). Age-matched control mice from each time point were included for comparison. The mice were deeply anaesthetized in a chamber with 4% isoflurane and perfused intracardially with filtered PBS (pH 7.4) until the effluent was cleared of blood (2 min), followed by perfusion with cold (4°C) 4% paraformaldehyde (PFA) in 0.1 M phosphate buffer (pH 7.4) for 5 min (30 mL). The PBS and the PFA were delivered through separate sterile platinum-cured silicon tubing (Cole-Parmer Canada Inc., Montreal, Canada) and peristaltic pumps (MasterFlex peristaltic pump, Cole-Parmer Canada Inc., Montreal, Canada). The brains and spinal cords were dissected out and fixed

overnight at 4°C and equilibrated in increasing concentrations of sucrose in phosphate-buffered saline, pH 7.4 (10, 20, and 25%) over a 3-day period. Complete equilibration of the tissues was taken as the moment the tissues sank to the bottom of the scintillation tubes filled with 25% sucrose. After equilibration, the spinal cord and brain specimens were set in molds (Tissue-tek Cryomold, Sakura Finetek, USA, Torrance, CA) with an optimum cutting temperature (OCT) gel-sucrose mixture frozen by immersion in an isopentane (BDH Laboratory Supplies, UK) bath on dry ice and stored at -80°C until processing.

2.2.6 Tissue cryosectioning

Frozen, coronal sections (spinal cord: 20 µm, brain: 30 µm) were cut with a Hacker-Bright cryostat (Hacker Instruments and Industries Inc., Winnsboro, SC) and mounted on charged glass slides (Superfrost Plus; Fisher Scientific, Pittsburgh, PA) so that adjacent CNS sections on each slide represented regions 100 µm and 150 µm apart for spinal cord and brain, respectively ((Tabata, Wilson et al. 2008)). The slides were stored at -80°C until histological processing. To ensure CNS sections were matched between animals, anatomical landmarks were verified using a mouse brain atlas (Paxinos and Franklin 2001).

2.2.7 Histology and quantification of motor neurons

Spinal cord and brain sections from each animal were stained for Nissl body substance. At room temperature (RT), sections were rinsed in a graded ethanol series (95%: 15 min; 70%: 1 min; 50%: 1 min) to rehydrate and remove lipids and fixation chemicals from the tissue. The tissue were then rinsed for 2 min in two exchanges of distilled water, stained with twice-filtered cresyl violet stain (1.25 g cresyl violet acetate, 0.75 mL glacial acetic acid to 250 mL distilled water), rinsed in distilled water (1 min), and then dehydrated (50% ethanol: 1 min; 1% glacial acetic acid-70% ethanol: 2 min; 95% ethanol: 2 min; 95% ethanol: 3 dips; 100% ethanol: 1 min) and cleared in xylene. The slides were then cover-slipped in Entellen mountant (Merck, Darmstadt, Germany).

The tissue mounted slides were selected with a randomized start and sampled starting from the lumbar 2 region to the 6th. The superior-inferior boundaries of the lumbar and thoracic spinal cord were initially determined by a ventral and dorsal root count and verified by comparison to a stereotaxic mouse atlas (Sidman, Angevine et al. 1971). The boundaries for the ventral horn was determined by the margins of the gray matter for the lateral, medial and ventral boundaries as well as with the aid of an artificial line drawn laterally through the central canal. Both the left and right ventral horns from 12 sections from each animal were counted. Alpha-motor neurons and γ-motor neurons with and without apoptotic structural changes were counted using strict morphological and size criteria. Non-apoptotic α-neurons were considered as the following: Large, multipolar cells with a round, pale nucleus; visible nucleolus; globular Nissl body staining of the cytoplasm; and a diameter of 30 – 45 μm. In doing so, astrocytes, oligodendrocytes and microglia were excluded from the "α-motor neuron" counts (Martin, 1999; Sepkuty et al., 2002; Tabata et al., 2008). Pyknotic or karyopyknotic α-neurons undergoing apoptosis were considered as those with a diameter of 30 μm and greater with a condensed and darkly stained nucleus, with or without vacuolization outside of the cell. Chromatolytic α-neurons undergoing apoptosis were considered as those with a diameter of 30 μm and greater with no discernable nucleus, with or without shifting of the nucleus from its central position to the periphery, disintegration of the Nissl bodies (chromophil substance), with or without vacuolization outside of the cell. Healthy γ-motor neurons were considered as those cells between 18 μm and 30 μm in size (Szumanska and Gadamski, 1977). Apoptotic γ-motor neurons were considered as those between 18 μm and 30 μm in size with a condensed and darkly stained nucleus with or without vacuolization outside of the cell. Those motor neurons with the nucleus (in the count for "healthy" α- and γ- motor neurons), nucleolus, and cytosol intact were included in the counts. Counts performed on non-treated animal sections served as controls.

2.2.8 Immunofluorescence

Tissue-mounted slides were processed for fluorescence microscopy as follows: Sections were rinsed in coplin jars for 45 min at RT in three changes of PBS. Sections were then incubated at RT for 30 min in a blocking-permeabilization solution made of 5% normal goat serum (NGS), 5% normal rabbit serum (NRS) or 5% BlokHen II (Aves Labs, Inc., Tigard, OR), 0.05% Triton X-100 and PBS. Subsequently, the blocking solution was tipped off and the slides were rinsed in PBS for 2 min. Sections were then incubated overnight in a humidified chamber at 4°C with a PBS buffered solution that contained 1% NGS or 1% NRS, 1% bovine serum albumin (BSA) and one of the following primary antibodies: (a) rabbit anti-human/mouse ATF-3 (H-90) IgG (polyclonal, 1:500; Santa Cruz Biotechnology, Inc., Santa Cruz, CA), (b) anti-activated caspase-3 IgG (monoclonal, 1:250; Chemicon International, Temecula, CA), (c) goat anti-human/mouse choline acetyl transferase (ChAT) IgG (polyclonal, 1:100; Chemicon International, Temecula, CA), (d) rabbit anti-mouse glial fibrillary acidic protein IgG (polyclonal, 1:250; GeneTex Inc., San Antonio, TX), (e) rabbit anti-human/mouse ionized calcium binding adaptor molecule 1 (IBA-1) IgG (polyclonal, 1:500; Wako Pure Chemical Industries, Ltd, Richmond, VA), (f) mouse anti-human/mouse clone AT8 PHF-1 Tau (monoclonal, 1:200; Pierce Biotechnology Inc., Rockford, IL), (g) rabbit anti-human/mouse TAR DNA-binding protein 43 (TDP43) (1:100; ProteinTech Group Inc., Chicago, IL), (h) chicken anti-human/mouse β-tubulin 3 (TuJ1 antigen) (polyclonal, 1:100, Aves Labs, Inc., Tigard, OR), (i) rabbit anti-mouse tyrosine hydroxylase (polyclonal, 1:500, Chemicon International, Temecula, CA or polyclonal 1:1000, Affinity BioReagents, Golden, CO), (j) rabbit anti human/mouse anti-pJun^{ser73} IgG (polyclonal, 1:200; Chemicon International, Temecula, CA), (k) rabbit anti human/mouse anti-HSP-70 IgG (polyclonal, 1:200; Chemicon International, Temecula, CA), or (l) rabbit anti human/mouse anti-HSP-25 IgG (polyclonal, 1:100; Chemicon International, Temecula, CA). In each experiment, additional slides were incubated with the primary antibody and the secondary antibody omitted or with secondary antibody and primary antibody omitted to test for non-

specific staining. Where appropriate, positive control slides (Alzheimer's disease patient entorhinal cortex, kindly donated by Drs. Claudia Schwab and Patrick McGeer of the Kinsmen Laboratory (University of British Columbia, Vancouver, BC, Canada) were also processed as above for comparison. Following overnight incubation with the primary antibody, slides were rinsed for 45 min at RT in three changes of PBS. Immediately after, the slides were incubated in black chambers that excluded light for 1 hr at RT with the secondary antibody solutions containing 5% NGS or 5% NRS and fluorophore conjugated antibodies: AlexaFluor 568 goat anti-rabbit or rabbit anti-goat IgG (monoclonal, 1:250, absorption: 578 nm, emission 603 nm; Molecular Probes, Eugene, OR), AlexaFluor 546 goat anti-rabbit or rabbit anti-goat IgG (monoclonal; 1:250, absorption 556 nm, emission 573 nm; Molecular Probes, Eugene, OR) or fluorescein isothiocyanate (FITC) goat anti-rabbit IgG (polyclonal, 1:500, absorption: 494 nm, emission: 518 nm; Sigma, Saint Louis, MO). The secondary antibody solution was tipped off and slides were rinsed for 15 min in three changes of PBS. Tissue sections were cover-slipped with a 4'6 diamidino-2-phenylindole (DAPI) fluorescent mounting media (Vectashield, absorption: 360 nm, emission: 460 nm, Vector Laboratories, Burlington, ON, Canada) in order to label the nuclei and stored at 4°C in dark slide boxes to retard bleaching of the fluorescent labels.

2.2.9 Tau immunohistochemistry

Slide-mounted lumbar and thoracic spinal cord and brain sections were first rinsed for 45 min in 3 changes of PBS then quenched in 3% H_2O_2 in PBST (PBS + 0.5% Triton X-100) for 10 min. The slides were rinsed for 4 min in 2 changes of PBST. The MOM mouse Ig blocking reagent was prepared as per the manufacturer's instructions. Two drops of mouse Ig stock solution was added to 2.5 mL of PBS. The sections were incubated with this solution for 1 hr at RT. Following this step, sections were rinsed for 4 min in 2 changes of PBST and incubated (5 min) with the MOM diluent solution prepared by adding 600 µl of MOM protein concentrate to 7.5 mL of PBS. The diluent was tipped off the slides and replaced by a solution comprised of primary phospho-Tau antibody

diluted at 1:100 in the diluent solution prepared in the same manner as previous. The sections were incubated for 60 min at RT. Subsequently, sections were rinsed for 4 min in 2 changes of PBST and incubated for 10 min in the MOM biotinylated anti-mouse IgG reagent (10 µl of MOM biotinylated anti-mouse IgG diluted in 2.5 mL of the MOM diluents). The sections were then rinsed in PBST and incubated (1 hr at RT) with the secondary antibody prepared by combining one drop of secondary antibody (biotinylated goat-anti-rabbit IgG) from the Vectastain ABC Elite kit (Vector Laboratories, Burlingame, CA, USA) was combined with 3 drops of serum stock to 10 mL of PBST. At 30 min after start of slide incubation with the secondary antibody, an immunoperoxidase solution was prepared by adding 2 drops of reagent A and 2 drops of reagent B (Vectastain Elite ABC kit, Vector Laboratories, Burlingame, CA, USA) to 2.5 mL of PBST. After one hour incubation of the slides with the secondary antibody solution, the slides were rinsed for 4 min in two changes of PBST and incubated for 30 min in the working immunoperoxidase solution. Next, the sections were rinsed for 4 min in 2 changes of PBST. During the rinses, the DAB liquid substrate was prepared for the next step. As per manufacturer's instructions, 2 drops of buffer stock solution, 5 mL of ddH_2O, 4 drops of DAB stock solution, and 2 drops of hydrogen peroxide solution were combined. The slides were incubated for 3 min at RT with this DAB solution and monitored for color development. The sections were rinsed for 5 min in ddH_2O to stop the reaction and rid slides of DAB substrate. A methyl green nuclear counterstain was used to elucidate nuclei and motor neuron somata. The 0.5% methyl green counterstain was prepared in the following manner: First, the sodium acetate buffer was prepared with 1.36 g of sodium acetate trihydrate to 100 mL of distilled water adjusted to pH 4.2 using glacial acetic acid. For every 100 mL of buffer, 0.5 g of methyl green (ethyl violet, Sigma-Aldrich, Oakville, ON, Canada) was added to make a 0.5% methyl green solution. Slide-mounted sections were stained in the above methyl green solution for 5 min at RT. Sections were rinsed in distilled water, until the water became clear. Next, sections were dehydrated quickly with 95% ethanol (5 dips) and 2 changes of 100% ethanol (5 dips in each change), then cleared by 10 dips

of xylene. Finally, the slides were dried under a fume hood and cover-slipped with a resinous mounting media (Entellen, Merck, Darmstadt, Germany).

2.2.10 Tyrosine hydroxylase immunohistochemistry

Labelling of tyrosine hydroxylase-containing neurons in brain sections was identified by antibodies for tyrosine hydroxylase (Morrow et al., 2001) and indirect immunoperoxidase staining. Sections were incubated in blocking serum for 2 hr then with the primary antibody (rabbit anti-tyrosine hydroxylase, 1:500, Affinity Bioreagents, Golden, CO, USA) for 3 hr at RT. Sections were rinsed and incubated in biotinylated goat anti-rabbit IgG (1:100; Vector laboratories Inc., Burlingame, USA) for 30 min at RT, then visualized using the ABC method (Vectastain Elite ABC kit, Vector Laboratories Inc.).

2.2.11 Cytochrome c oxidase histochemistry

Tissue-mounted slides were processed for fluorescence immunohistochemistry in a manner adapted from Seligman et al. (1968) and Wong-Riley (1979). Sections were rinsed in coplin jars for 15 min at RT in three changes of PBS and subsequently incubated with a media comprised of 50 mg of 3,3'-diaminobenzidine tetrahydrochloride (DAB) (DAB substrate system, Vector Laboratories, Burlingame, CA, USA), 90 mL 0.1M phosphate buffer, 20 mg cytochrome c (type III, Sigma-Aldrich Co., Oakville, ON, Canada), and 4 g of sucrose in a dish submerged in a water bath maintained at 37°C in the dark for 2 h. The sections were monitored closely for the brown reaction product to appear within the tissue. Once a medium-brown color was achieved, slides were removed from the incubation media and rinsed for 15 min in three changes of PBS to stop the reaction. This was followed with a 2 min rinse in distilled water to remove residue from the slides. The slides were dried under a fume hood and cover-slipped with Entellen (Merck, Darmstadt, Germany).

2.2.12 Oil red O histochemistry

Tissue-mounted slides were processed to evaluate lipid distribution with light microscopy with a protocol adapted from Dr. Roy Ellis (IMVS Division of Pathology, The Queen Elizabeth Hospital, Woodville, South Australia). First, an oil red O stock solution was prepared 2 hr prior to execution of the histochemical procedures. The oil red O stock stain solution was made by mixing oil red O (0.5 g, Sigma-Aldrich, Oakville, ON, Canada) and isopropanol (100 mL, Fisher Scientific, Nepean, ON, Canada) over a 40°C water bath. Immediately prior to beginning the oil red O histochemical procedures, the oil red O working solution was made by combining 20 mL of distilled water for every 30 mL of oil red O stock stain solution. This working solution was filtered five times to remove any oil red O that did not dissolve in the solvent. Slide-mounted sections were rinsed in coplin jars for 15 min at RT in three changes of PBS. Sections were then rinsed at RT with 60% isopropanol for 5 min. The spinal cord sections were then stained with a freshly prepared working solution of oil red O for 20 min and then rinsed with 60% isopropanol. Nuclear counterstaining was achieved by staining the sections with haematoxylin (haematoxylin, 7211, Richard Allan Scientific, Kalamazoo, MI, USA) for 1 min. Finally, the sections were rinsed with distilled water, dried under a fume hood and cover-slipped with Entellen (Merck, Darmstadt, Germany).

2.2.13 Tissue visualization and image capture

Immunofluorescence protocol processed tissue sections were examined and captured using a Zeiss Axiovert 200M (Carl Zeiss Canada Limited, Toronto, ON). DAPI (blue fluorescence) visualization required a 359/461 nm absorption/emission filter. FITC required a 490,494/520 nm filter. Alexa Fluor 546™ (red fluorescence) utilized a 556,557/572,573 nm filter. During quantification at 40x magnification, two images were captured per lumbar and thoracic spinal cord section (i.e. left ventral horn and right ventral horn). Similarly, two images were captured per brain region and per dorsal or ventral root section. 40x images were 350 x 275 μm in dimension. Images were

captured using AxioVision 4.3 software. Data processed through immunofluorescence was analyzed using Zeiss Axiovert Zoom Axiovision 3.1 with AxioCam HRM. Non-fluorescent protocol processed tissue sections were examined and captured using the Motic B5 Professional Series 3.0 microscope (Motic Instruments Inc., Richmond, ON) and data were analyzed using Motic B5 Professional, Motic Images Advanced 3.0 (Motic Instruments Inc., Richmond, ON).

2.2.14 Quantification of immunoreactive cell somata or inclusions

The numbers of immunoreactive somata or inclusions were counted across the ventral horn of the spinal cord, across brain hemispheres, or per dorsal or ventral root with the 40x objective lens in a 600 µm / 600 µm area within region perimeters defined by a mouse brain atlas (2001). For each animal, eight cross-sections per spinal cord or brain region were studied. An average of both the right and left ventral horn for each of the eight cross sections was generated giving a final averaged number for each animal in each of the spinal cord areas.

For quantification of the level of mitochondrial activity (cytochrome c oxidase labelling) in the lumbar spinal cord or tyrosine hydroxylase immunoreactivity in the substantia nigra pars compacta and striatal sections, images captured using the Motic B5 Professional Series 3.0 microscope (Motic Instruments Inc., Richmond, ON) and analyzed using Motic B5 Professional, Motic Images Advanced 3.0 (Motic Instruments Inc., Richmond, ON) were scanned into a TIFF format file and analysed using the NIH Image J 1.37 software to measure density levels of antibody labelling. Eight to 12 sections from each mouse per region of interest were included.

2.3 Statistical analyses

Quantitative data obtained from each hemisphere of each spinal cord or brain section was averaged to generate a hemispherical average, then data averages for each animal was averaged prior to statistical analyses. Differences between the control and SG-fed mice were statistically evaluated using the

Student's t-test with a $p<0.05$ being required for significance. All data are expressed as mean ± standard deviation (SD). Statistical significance was established using either an unpaired two-tailed *t*-test, one-way or two-way ANOVA followed by a Tukey's post-hoc or Fisher's LSD (GraphPad Prism v3.0, GraphPad Software Inc., San Diego, CA; Statistica for Windows v. 6.1 statistical software package, Statsoft, Tulsa, OK). Statistical analyses conducted in each of the studies have been reviewed by several statistics advisors in the Department of Statistics, University of British Columbia.

Chapter 3. The effects of dietary β-sitosterol β-D-glucoside treatment

Work in this chapter was partially published as: Tabata, R.C., Wilson, J.M.B., Ly, P., Zwiegers, P., Kwok, D., Van Kampen, J.M., Cashman, N. and Shaw, C.A. 2008. *Chronic exposure to dietary sterol glucosides is neurotoxic to motor neurons and induces an ALS-PDC phenotype,* Journal of Neuromolecular Medicine 10(1):24-39.

Hypothesis:

Dietary exposure to β-sitosterol β-D-glucoside (BSSG) will induce progressive motor deficits and neuropathological changes in adult mice.

Specific aims:

1. To determine if dietary BSSG can induce ALS-PDC-like behavioural and pathological outcomes similar to those observed with washed cycad flour exposure.
2. To determine some of the key mechanisms underlying cellular changes that occurs as a result of dietary BSSG.

3.1 Results

In order to investigate whether BSSG is neurotoxic to an out-bred strain of mice, I fed 1000 µg of synthetic BSSG per day to CD-1 mice for 15 wk (Figure 2). The mice were monitored behaviourally prior to feeding commencement (in order to obtain baseline values) as well as during and after BSSG-feeding to detect for any dietary BSSG-induced behavioural changes (Figure 2). Seventeen weeks after the last BSSG pellet was provided, mice were sacrificed for behavioural analysis (Figure 2). Brain and spinal cord tissue were subjected to a variety of histological measures to detect for changes in motor neuron numbers, response(s) to stress, signs of apoptotic mechanisms at play, changes in the number of cholinergic motor neuron numbers, tyrosine hydroxylase levels in

dopaminergic neurons, signs of lipid accumulation, as well as changes in the level of mitochondrial activity.

3.1.1 Body weight of mice

At baseline and throughout the experiment, there were no significant differences in the weekly average body weight between treatment groups (Figure 3).

3.1.2 Dietary BSSG exposure induces behavioural changes

Motor deficits began to appear 13 wk post-BSSG-feeding. BSSG-fed mice showed a progressive decrease on the leg extension test that became statistically significant after week 30 compared to controls (Student's t-test: $p<0.05$, Figure 4). As in previous studies using cycad, the decline in leg extension was not a simple monotonic decline, but rather showed periods of increasing deficit followed by short-term recovery toward control values (Wilson et al., 2002a). The hind limb extension deficits were accompanied by a noticeable tremor and/or a punching motion that progressively intensified over time. When the mice were tested for open field exploratory behavior, both control and BSSG-fed groups were found to show a tendency for a decrease in open field activity over the course of the study. Statistically significant inter-group differences were first observed at 28 wk (or 48 wk in age). The decrease in movement exhibited by BSSG-fed mice was marked, with a -40% (Student's t-test, $p<0.05$) decrease in overall movement as measured by grid-crossings compared to controls (Figure 5). However, assessment of performance on the rotarod and wire hang test did not indicate motor coordination or strength deficits (Tabata et al., 2008).

3.1.3 Dietary BSSG induces motor neuron loss

Nissl body staining of BSSG-fed mice spinal cord tissue showed a significant decrease in the number of large α-motor neurons in the ventral horn of both the lumbar (-35%; Student's t-test: $p<0.05$) and thoracic (-19%; Student's t-

test, $p<0.05$) spinal cord compared to controls (Figure 6). Further, many surviving motor neurons of BSSG-fed mice at both levels showed abnormal morphological features, the most notable being shrunken somata with intense labelling and/or indiscrete nuclei (indicative of pyknosis) (dashed arrows). The motor neurons undergoing pyknosis appeared to be undergoing "classical" or "central" pyknosis where Nissl bodies are first lost centrally then eventually lost peripherally (Levine et al., 2004). Other remaining cells were large with disrupted membranes (solid arrows) indicative of chromatolysis. The appearances and the numbers of motor neurons were the same on both sides of the cord (i.e. bilateral symmetry in neurodegeneration).

Anti-ChAT immunoreactive cells were counted as cholinergic neurons. As was the case with the Nissl body stain-facilitated motor neuron quantification, the quantification of cholinergic neurons was conducted in the ventral horn of the lumbar spinal cord (Figure 7). Large anti-ChAT immunoreactive cells with a distinct nucleus were included in the count. Anti-ChAT labelling of motor neurons was significantly decreased in BSSG-fed mice compared to controls (-40%, Student's t-test). Anti-ChAT immunoreactive cells of BSSG-fed mice showed abnormal morphological features compared to controls (Figure 7). As with cresyl violet staining, motor neurons appeared to be undergoing central pyknosis (Figure 7). Motor neuron counts visualized with cresyl violet histology and cholinergic cell counts elucidated with anti-ChAT immunofluorescence histology correlated remarkably well (-35% and -40%, respectively), suggesting that the majority of the cells that were lost were motor neurons.

3.1.4 Glial response to dietary BSSG

The number of reactive astrocytes was determined by counting anti-GFAP immunoreactive cells with stellate (star-shaped) cell bodies in the ventral horns of lumbar spinal cord (L2-L5) sections (Figure 11). BSSG-fed mice showed significantly increased GFAP labelled cells (+82%) compared to the controls (Student's t-test, $p<0.05$). A quantification of microglia labelling in the ventral horn of the lumbar spinal cord in control and BSSG-fed mice revealed that

BSSG-fed mice had significantly more microglia (+307%) compared to the controls (Student's t-test, $p<0.0001$) (Figure 12).

3.1.5 Signalling pathways involved in the response to BSSG toxicity

The Nissl body stain and ChAT immunofluorescence demonstrated a striking depletion of motor neurons in the lumbar and thoracic spinal cord (Figure 5 and 6) but provided no indication regarding the mechanism of degeneration. Accordingly, in order to assess BSSG-fed animal neurons' responses to BSSG toxicity, I used antibodies that recognize Hsp-70, phosphorylated-Jun^{ser73}, ATF-3, as well as the active form of caspase-3.

Quantification of Hsp-70 immunoreactive cells indicated that BSSG-fed animals had 644% more cells positively labelled in the ventral horn of the lumbar spinal cord (Student's t-test: $p<0.001$). The ventral horn of the thoracic spinal cord did not show a statistically significant inter-group difference (Student's t-test: not significant: $p=0.8263$) (Figure 8). Based on morphology and size, it appeared that the majority of cells that expressed Hsp-70 were large motor neurons 30 µm or greater.

A quantitative assessment of cells expressing p-Jun^{ser73} revealed that BSSG-fed animals had more cells expressing p-Jun^{ser73} compared to age-matched controls, but these values did not reach statistical significance. However, an assessment of the morphology and size of the cells immunoreactive to anti-p-Jun^{ser73} also indicated that the cells that labelled are primarily large α-motor neurons (Figure 10). Large α-motor neurons were found to be immunoreactive to ATF-3 as well. Compared to the immunoreactivity level to anti-p-Jun^{ser73} however, a greater number of motor neurons were positively labelled with anti-ATF-3 (Figure 9 and 10).

An antibody to the active form of caspase-3 was used to differentiate apoptotic cells. Examination of the ventral horns of the lumbar spinal cord showed that a significantly greater number of cells were immunoreactive to anti-caspase-3 (Student's t-test: +199%, $p<0.05$) in BSSG-fed animals compared to controls. Scrutiny of the size (30 – 45 µm) and morphology of the cells confirmed

that these anti-caspase-3 immunoreactive cells were large α-motor neurons (Figure 13).

3.1.6 Mitochondrial activity levels in BSSG-fed animals are unchanged

Cytochrome c oxidase, a sensitive marker for neuronal metabolic activity (Wong-Riley, 1979; Wong-Riley, 1989), was used to assess metabolic activity in the lumbar spinal cord sections of BSSG-fed animals. An inter-group assessment of the optical density of cytochrome c oxidase levels showed that at 52 wk, there was not a statistically significant difference (Student's t-test, $p>0.05$) (Figure 14).

3.1.7 The effects of dietary BSSG on the nigral-striatal pathway

Anti-tyrosine hydroxylase (TH) labelling of neurons in the striatum and substantia nigra pars compacta (SNpc) showed that BSSG-fed mice had significantly decreased anti-TH labelling in the striatum (-13%) and in the SNpc (-12%) compared to controls (Student's t-test, $p<0.05$, Figure 15).

3.1.8 Lipids accumulate in the ventral roots of BSSG-fed animals

Lipid deposition/accumulation levels were assessed in BSSG-fed animals and their age matched controls with the oil red O lipid stain. The lumbar spinal cord and the dorsal and ventral roots were examined for signs of abnormal lipid accumulation. An inter-group statistical assessment revealed that the degree of lipid accumulation was not statistically significant in the motor neurons of the lumbar spinal cord (Student's t-test: $p=0.0674$) or throughout the dorsal roots (Student's t-test: $p=0.3778$) (Figure 16). However, the ventral roots of BSSG-fed animals showed a significantly greater number of lipid deposits (Student's t-test: $p<0.05$, +13%) (Figure 16). While BSSG-fed animals had a greater number of lipid deposits, the distribution, morphology, and staining intensity of the lipid deposits were similar across groups and CNS regions (Figure 16).

3.2 Discussion

3.2.1 The loss of cholinergic neurons and tyrosine hydroxylase containing neurons correlate with behavioural findings

The results of the present study show for the first time that BSSG can be neurotoxic *in vivo*, in an out-bred strain of mice, and induce behavioural and histological pathologies that mimic, in many respects, early features of ALS-PDC. At a dose of 1000 µg per day for 15 wk, out-bred CD-1 mice exhibited leg extension deficits beginning at week 30 and a decrease in overall movement beginning at week 28. These findings correlate well with the reduction of tyrosine hydroxylase in "dopaminergic" neurons and fibres or decrease in dopamine precursor production in the nigro-striatal regions (Figure 15), as well as with the profound loss of motor neurons from the lumbar spinal cord (Figure 6). Further, these pathological changes involving the motor and the nigro-striatal systems mimic findings obtained in cycad-flour feeding studies involving the same strain of mice (Wilson et al., 2002c) as well as studies involving other rodents (Valentino et al., 2006).

3.2.2 Multiple weeks of BSSG-feeding overwhelm survival/repair mechanisms and induce apoptosis of neural cells

This study investigated the response of motor neurons and non-motor neuronal populations to stress induced by BSSG *in vivo*, in an out-bred strain of mice, also for the first time. I assessed the stress response by quantifying the degree of up-regulation of the molecular chaperone, Hsp-70, and the pro-apoptotic, stress-inducible factors, activating transcription factor-3 (ATF-3) and p-Jun (Tsujino et al., 2000; Lu et al., 2005). Hsps, particularly Hsp-70, play essential roles associated with protein quality maintenance, including protein folding, targeting, transport, and degradation (Becker and Craig, 1994; Kline and Morimoto, 1997). Based on these functions, Hsps are thought to provide a line of defence against protein misfolding in neurodegenerative diseases. ATF-3 is a member of a family of leucine zipper transcription factors that bind to promoters responsive to cAMP and phorbol ester at the cAMP (CRE) and phorbol ester

response elements (Chu et al., 1994). Both ATF-3 and Jun have been shown to be expressed by sensory and motor neurons under stress both *in vitro* and *in vivo* (Nakagomi et al., 2003), just prior to the cell death commitment point (Eilers et al., 1998). The results of this BSSG-feeding study are consistent with the current literature. When the spinal cord sections were analyzed for Hsp-70, ATF-3, and p-Jun^{ser73} expression at 52 wk (17 wk post BSSG-feeding), anti-Hsp-70 was slightly elevated and anti-ATF-3 immunoreactivity was markedly higher in BSSG-fed animals compared to age-matched controls. Further, p-Jun^{ser73} expression also appeared to be greater in BSSG-fed animals, despite a lack of statistical significance. ATF-3 is a crucial determinant of cell mortality. When the heightened expression is accompanied by ample activation of c-Jun, neurons are rescued and repaired (Benn et al., 2002). Further, when c-Jun, which is regulated by JNK, is phosphorylated, cells are induced to die (Ham et al., 1995). Thus, in the present study, by 17 wk post-BSSG-feeding, it appears that many cells were just approaching the critical survival/repair threshold- many cells showed a significant up-regulation of ATF-3 but without fatal phosphorylation of c-Jun accompanied by an inadequate Hsp-70 up-regulation. This interpretation is supported by the apoptosis assay conducted in the present study. While I observed numerous, large motor neurons undergoing apoptosis (Figure 11A), inspection of motor neurons separately with a cresyl violet stain, haematoxylin stain (done with oil red O), and an antibody to ChAT indicated that 15 wk of BSSG feeding did not abolish the neuronal population (Figure 6, 7, 16) and permitted the animals to perform at a relatively high level on behavioural tests (Figure 4 and 5).

Mitochondrial activity level assessment in the CNS of BSSG-fed animals, revealed no inter-group differences. I chose to examine the level of cytochrome c oxidase labelling since it plays a critical role in energy metabolism in neurons (Wong-Riley, 1979). The cytochrome c oxidase activity levels change within neurons according to cellular activity levels. When neurons, for example, are actively growing or undergoing repair, mitochondrial activity increases (Wong-Riley et al., 1978; Wong-Riley et al., 1978). In this current study, we examined

the quantity of cytochrome c oxidase in the CNS to evaluate whether the mitochondrial activity level changes following BSSG feeding. An inter-group difference in cytochrome c oxidase levels was not observed, possibly indicating that such changes might reflect early transient event.

3.2.3 The neuronal response to BSSG includes glial cell activation

The increased anti-GFAP labelling of reactive astrocytes (Figure 11) confirms results previously reported with cycad flour feeding (Wilson et al., 2002c; Wilson et al., 2003; Wilson et al., 2005). Activated astrocytes were observed throughout the ventral horn of lumbar spinal cord sections near both morphologically normal and abnormal motor neurons. In human and mouse models of ALS, abundant gliosis is readily discernible in affected CNS regions (Kawamata et al., 1992; Hall et al., 1998; Sasaki and Iwata, 1999; Anderson and Swanson, 2000; Barbeito et al., 2004; Rao and Weiss, 2004). Evidence of a more general neuroinflammatory process was observed in the present study. A significant number of hyperramified microglia was found in the lumbar spinal cord of BSSG-exposed animals. This finding is supported by our ongoing studies using cycad flour that clearly demonstrate proliferation and hyper-ramification of microglia as one of the earliest pathological events to occur in the spinal cord (Lee et al., 2007). It thus seems clear that both forms of glial activation can occur following exposure to cycad neurotoxins. Whether such events occur in parallel, in tandem, or transiently are not yet known. Indeed, there is considerable controversy in the experimental literature about the relative roles of astrocytes and microglia in neurodegeneration (Sargsyan et al., 2005). While a statement about whether the activation of astrocytes and microglia is beneficial to an animal in response to a neurotoxic insult cannot be made here, the finding that these cellular entities are players in the sequence of events that eventually amounts to the loss of motor neurons is important as the application of this information can help develop a standard to base prognosis of neurological disease. Specifically, by correlating the numbers of astrocytes and microglia activated at an early time point to the degree of general neuronal loss,

cholinergic motor neuron loss, and behavioural disturbances that occur later in the disease, outcomes of other toxin exposure may become predictable. To illustrate this point, for example, a biopsy of the spinal cord of an animal with suspected toxin exposure can be assessed for the level of astrocyte and microglia proliferation. From there, a report on the prognosis can be made.

Cumulatively, all of the observed changes in the lumbar spinal cord and the basal ganglia are consistent with many aspects of our cycad model of ALS-PDC, as well as with the disease itself (Table 1). Work in progress is designed to examine other CNS regions involved in ALS-PDC in order to evaluate the extent of BSSG-induced neuropathology (i.e. olfactory bulb).

3.3 Conclusion

Overall, the data from the *in vivo* experiments show that BSSG is neurotoxic to motor neurons with some additional effects on non-motor neuron populations but do not severely impair the whole animals' performance on behavioral tests as severe as cycad-feeding does (Wilson et al., 2002c; Wilson et al., 2003; Wilson et al., 2004c; Wilson et al., 2005). This outcome may suggest that BSSG alone is not sufficient to fully replicate the widespread behavioural deficits and pathology seen in cycad-fed mice or in ALS-PDC. In regard to this point, Khabazian et al. (2002) showed that cycad contains several primary sterol glucoside variants that are neurotoxic *in vitro*, with the level of toxicity up to one hundred times greater than that of BSSG (Khabazian et al., 2002d). Thus, in washed cycad flour, the different sterol glucoside molecules may synergistically operate to generate the overall ALS-PDC phenotype. Another possibility is that the each of the cycad sterol glucosides may have differential neurotoxic actions on the various neuronal populations. This differential may depend on either access to the CNS and/or the still unknown type(s) of binding site for these molecules.

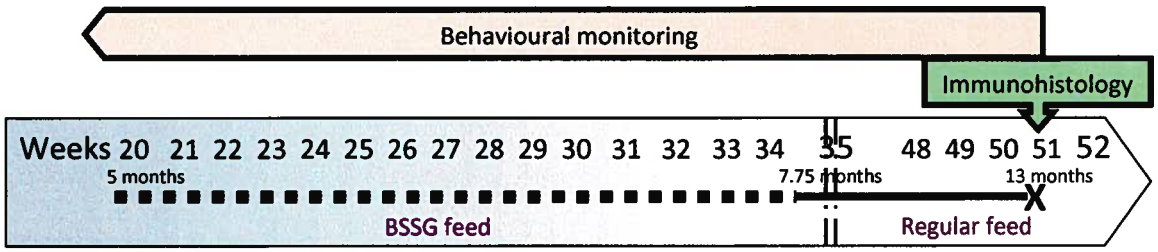

Figure 2. **Schematic depicting the timing of β-sitosterol β-D-glucoside-containing pellet feeding, animal sacrifice, and histological and behavioural analyses.**

Male, outbred CD-1 mice, 20 wk of age were fed BSSG-containing mouse chow pellets daily for 15 wk (dashed horizontal line). At 15 wk, BSSG animals were switched back to a diet of standard mouse chow pellets (solid horizontal line), survived an additional 17 wk and were sacrificed (X symbol). Animals were monitored behaviourally for the duration of the study and a histological analysis was conducted on tissue of animals 52 wk old.

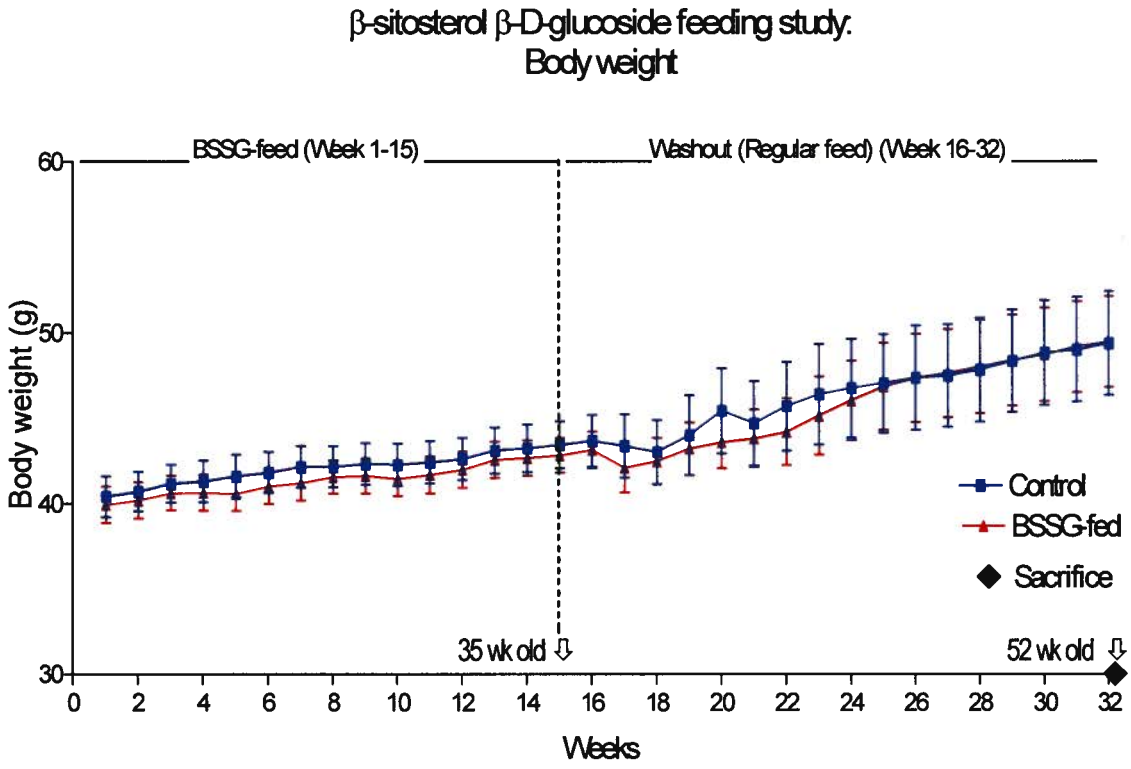

Figure 3. **Body weights of BSSG-fed animals and their age-matched controls.**

A comparison of weight values between control and BSSG-exposed animals indicated that body weights were not significantly different between the groups and increased steadily over-time.

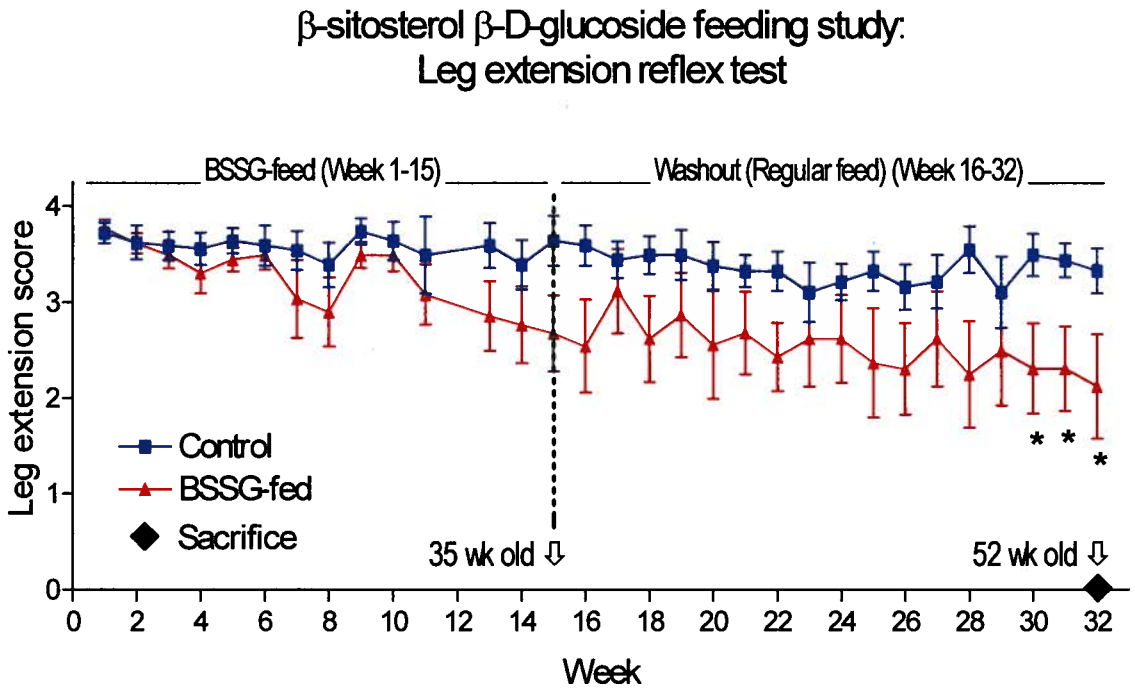

Figure 4. **BSSG-fed animals' hind limb reflex declines progressively.**

The leg extension (LE) reflex test was used to monitor motor defects. BSSG-fed mice showed a progressively declining score on the LE test that became significant after week 30 compared to controls. A-B: Student's t-test, *p<0.05.

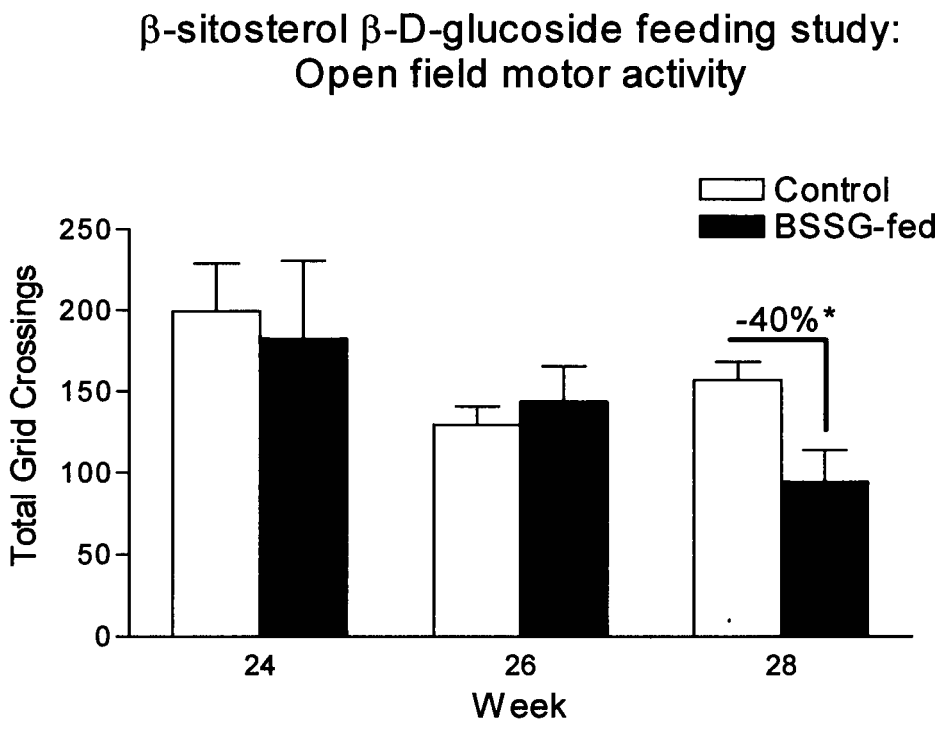

Figure 5. **BSSG-fed animals move progressively less over time.**

BSSG-fed mice showed significantly decreased movement as measured by grid crossings at week 28 compared to age-matched controls. A statistically significant intergroup difference was not detected prior to week 28 (data from earlier weeks omitted for clarity).

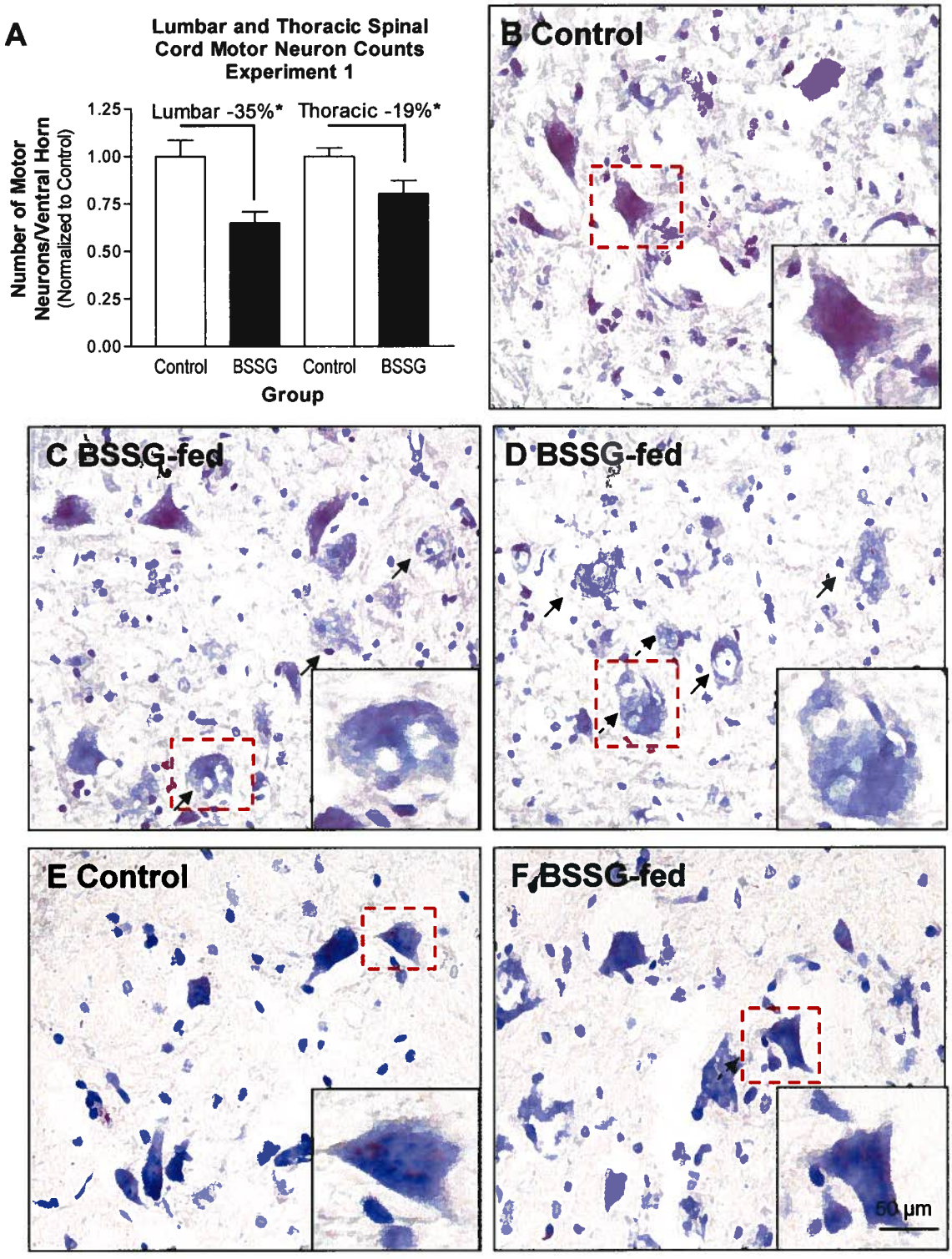
A
Lumbar and Thoracic Spinal Cord Motor Neuron Counts Experiment 1
Number of Motor Neurons/Ventral Horn (Normalized to Control)
1.25
1.00
0.75
0.50
0.25
0.00
Lumbar -35%*
Thoracic -19%*
Control
BSSG
Control
BSSG
Group
B Control
C BSSG-fed
D BSSG-fed
E Control
F BSSG-fed
50 µm

Figure 6. **Motor neuron counts following BSSG feeding.**

CD-1 mice were fed 1000 µg of BSSG per day for 15 wk. Seventeen weeks later, mice were sacrificed and the spinal cords were collected for histology. (A) Lumbar and thoracic spinal cord motor neuron counts revealed a decrease in motor neurons of -35% and -19%, respectively, compared to age-matched controls (t-test, *$p<0.05$). Motor neuron morphology was differentiated with cresyl violet staining of Nissl substance. A representative micrograph of a control animal (B) shows numerous healthy α- and γ-motor neurons. Motor neurons and glia are distributed evenly throughout the neuropil. In contrast, BSSG-exposed animals showed pyknosis (dashed lines), chromatolysis (solid lines) and an overall decrease in the number (-35%) of motor neurons (C and D). Cresyl violet staining in the thoracic spinal cord of a control (E) and BSSG-fed animal (F) revealed that control animals showed healthy distribution and morphology of motor neurons and glia, while BSSG-fed animals had a slight decrease (-19%) in the number of motor neurons as well as pyknotic and chromatolytic motor neurons. Images were captured using a light microscope under a 40x objective lens. Scale bars =50 µm.

A

β-sitosterol β-D-glucoside feeding study:
Anti-choline acetyl transferase
immunoreactive cells in the lumbar spinal cord

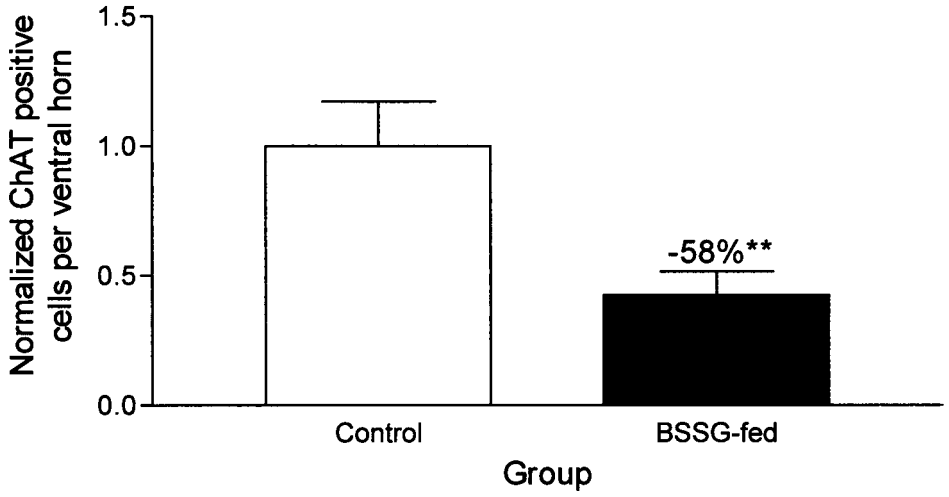

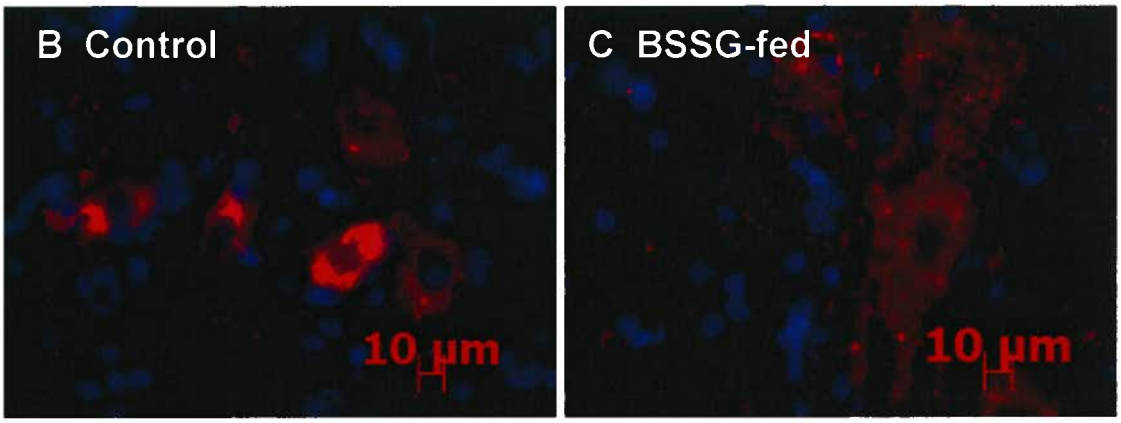

Figure 7. **Cholinergic motor neurons are reduced in the spinal cord of BSSG-fed mice.**

An antibody to choline acetyl transferase (ChAT) was used to detect cholinergic neurons in the lumbar spinal cord of BSSG-exposed mice and age-matched controls. BSSG feeding for a 15 wk period was found to induce a significant (-58%, t-test; **$p<0.01$) decrease in the number of cholinergic cells in the ventral horn of the lumbar spinal cord (A). (B-C) Representative micrographs of anti-ChAT (red) labelled cells in control and BSSG-fed mice sections are depicted in panel B and C respectively. A qualitative comparison revealed normal cell morphology in control animals but a disruption in cellular integrity amongst BSSG-fed animals' motor neurons (C). The blue label is DAPI (nuclei). Images were captured using a fluorescence microscope under a 40x objective lens. Scale bars=10 μm.

A

β–sitosterol β-D-glucoside feeding study: Number of cells expressing Hsp-70 in the ventral horn of the lumbar spinal cord

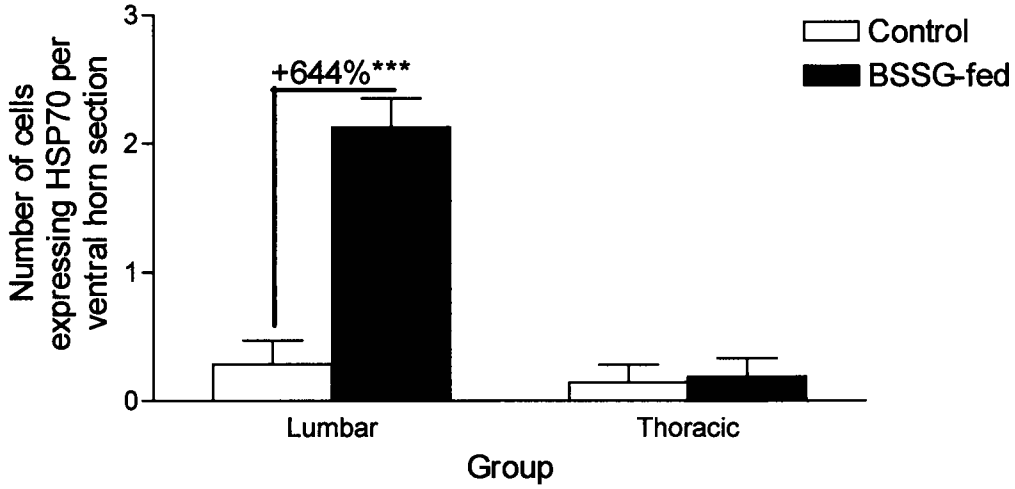

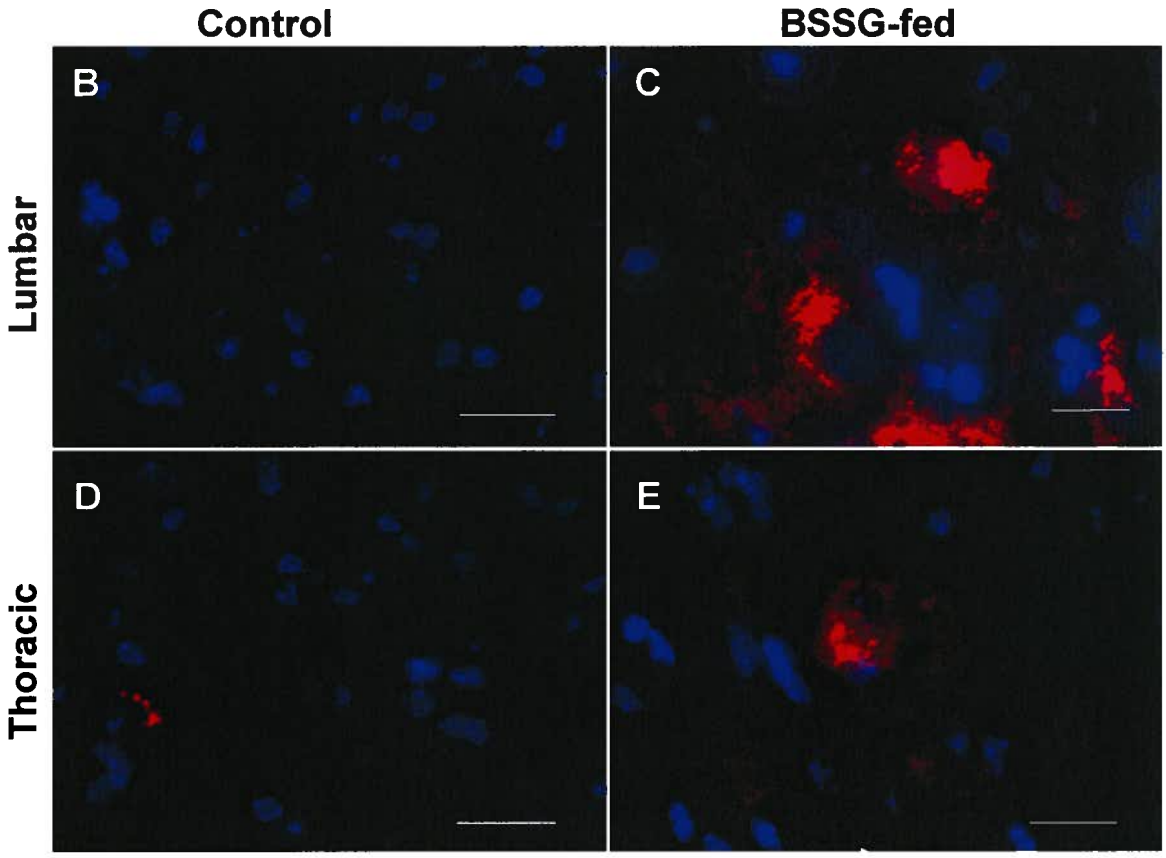
Control
BSSG-fed
Lumbar
Thoracic
B
C
D
E

Figure 8. **Heat shock protein-70 labelling in the lumbar and thoracic spinal cord of BSSG-fed mice.**

(A) Quantification of anti-heat shock protein-70 (Hsp-70) immunoreactive cells in the ventral horn of the lumbar and thoracic spinal cord. BSSG-fed mice had 644% more Hsp-70 immunoreactive cells in the ventral horn of the lumbar spinal cord at 52 wk of age (Student's t-test: ***$p<0.001$). An inter-group difference was not found in the ventral horn of the thoracic spinal cord (Student's t-test: not significant, $p=0.8263$). Panels B and D reflect the typical lack of anti-HSP-70 immunoreactivity observed amongst control animal lumbar and thoracic spinal cord regions respectively. Panels C and E show representative BSSG-fed animal sections with numerous cells positively labelled with anti-Hsp-70. Large motor neurons (C and E, arrows) were immunoreactive for anti-Hsp-70. The red label is anti-Hsp-70 while blue is showing DAPI nuclear labelling. Images were captured using a fluorescence microscope under a 40x objective lens. Scale bars = 20 μm.

A

β-sitosterol β-D-glucoside feeding study: Number of activating transcription factor-3 immunoreactive cells in the ventral horn of the lumbar spinal cord

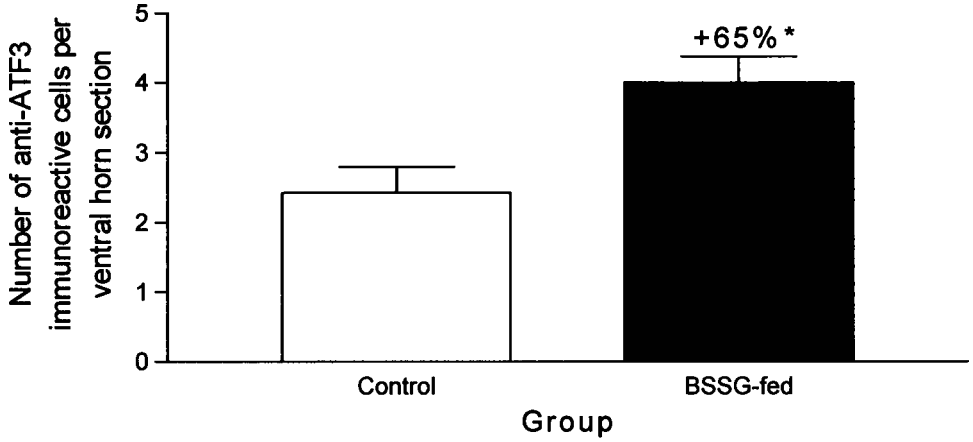

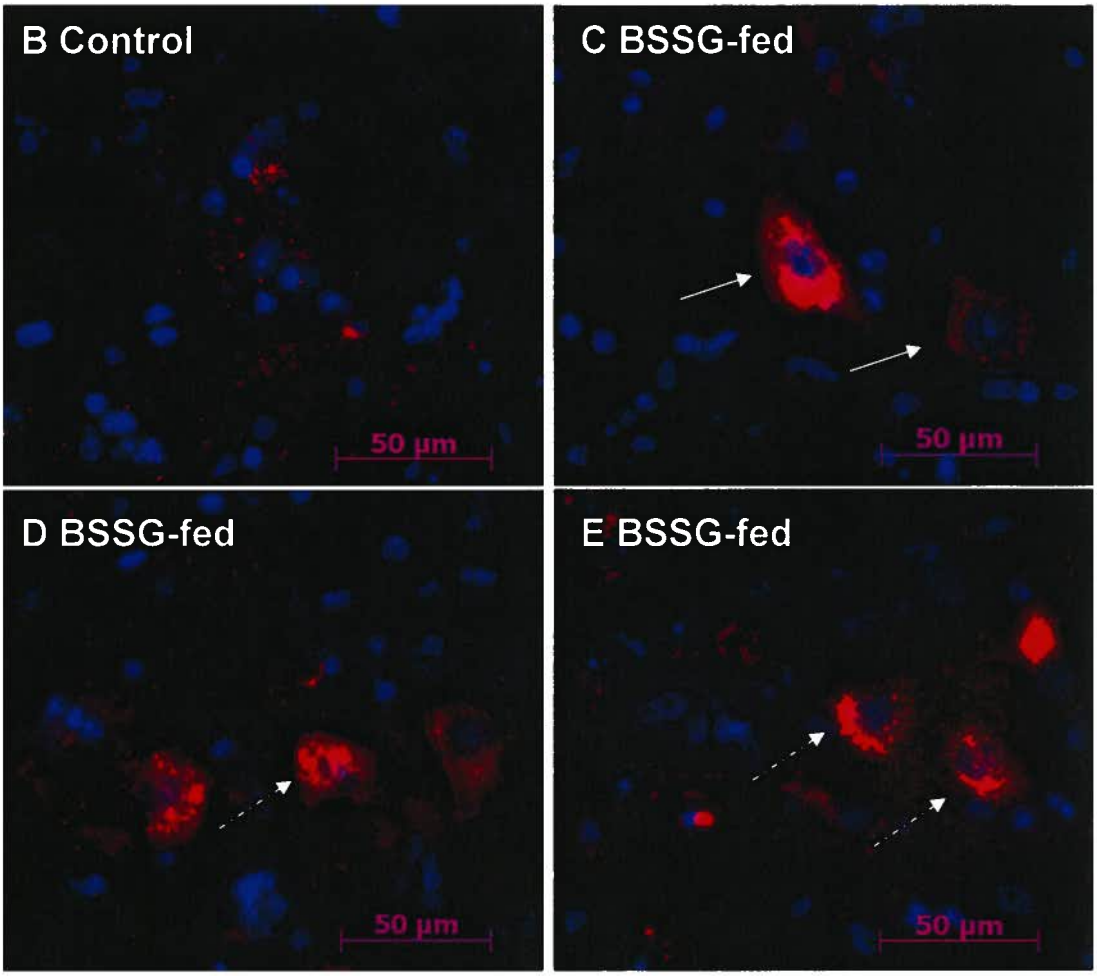

Figure 9. **Activating transcription factor-3 is activated in the lumbar spinal cord of BSSG-fed mice.**

(A) Quantification of anti-activating transcription factor-3 (ATF-3) immunoreactive cells in the ventral horn of the lumbar spinal cord (t-test, *$p<0.01$). Panel B reflects the typical lack of anti-ATF-3 immunoreactivity observed amongst control animal lumbar cord while panels C-E show representative BSSG-fed animal sections with numerous cells positively labelled with anti-ATF-3. Both large motor neurons (C, arrows) as well as smaller ones (D-E, dashed arrows) were immunoreactive for anti-ATF-3, suggesting that the general motor neuron population is under stress due to dietary BSSG exposure. The red label is anti-ATF-3 while blue is showing DAPI nuclear labelling. Images were captured using a fluorescence microscope under a 40x objective lens. Scale bars=50 µm.

A β-sitosterol β-D-glucoside feeding study: Number of anti-phosphorylated-jun^{ser73} immunoreactive cells in the ventral horn of the lumbar spinal cord

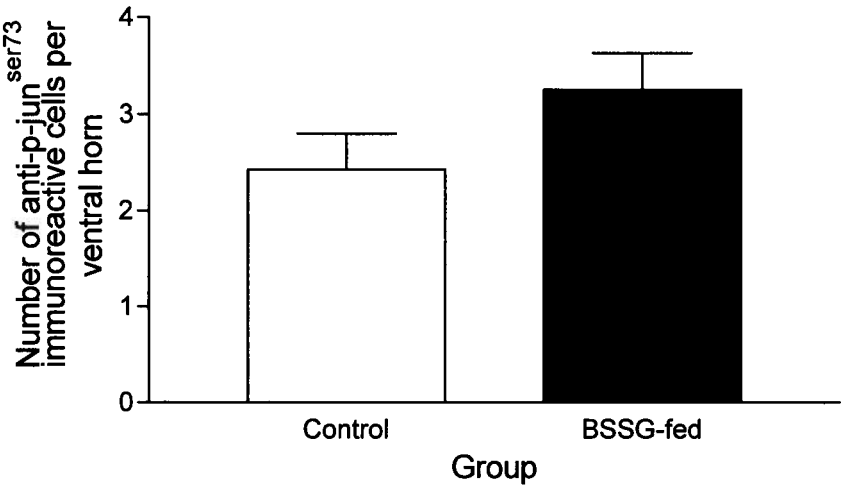

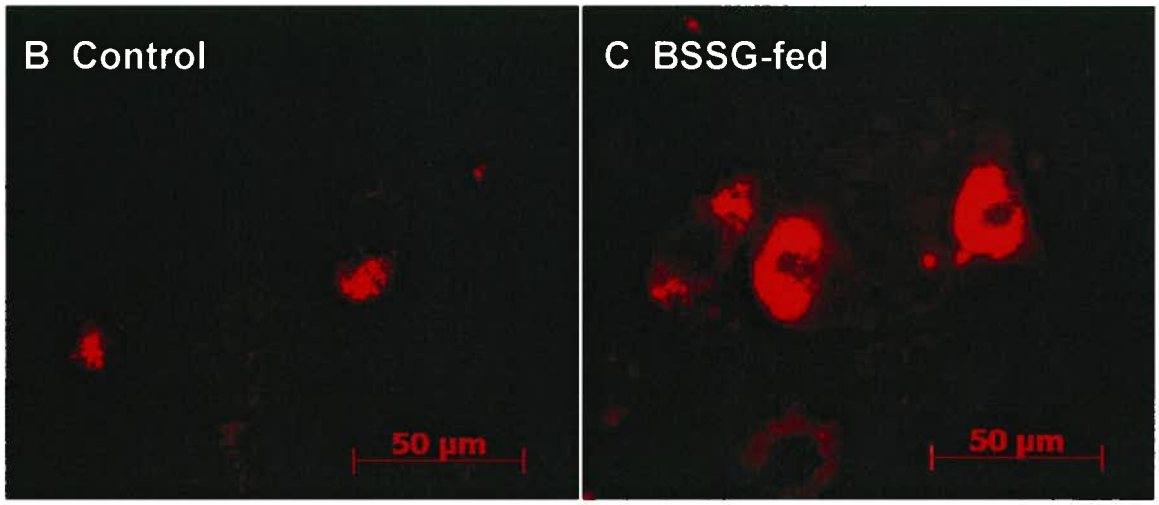

Figure 10. **BSSG-feeding induces the phosphorylation of c-Jun at serine 73.**

(A) Quantification of anti-phosphorylated jun at serine 73 (p-Jun ^{ser73}) immunoreactive cells in the ventral horn of the lumbar spinal cord at 52 wk. Statistical analysis revealed that the findings were not significant (Student's t-test: not significant, p=0.1440). Panel A is a representative photomicrograph depicting the lack of immunoreactivity to anti-p-Jun^{ser73} in the ventral horn of the lumbar spinal cord of a control mouse. Panel B is that of a BSSG-fed animal, showing anti-p-Jun ^{ser73} immunoreactive cells. Images were captured using a fluorescence microscope under a 40x objective lens. Scale bars=50μm.

A

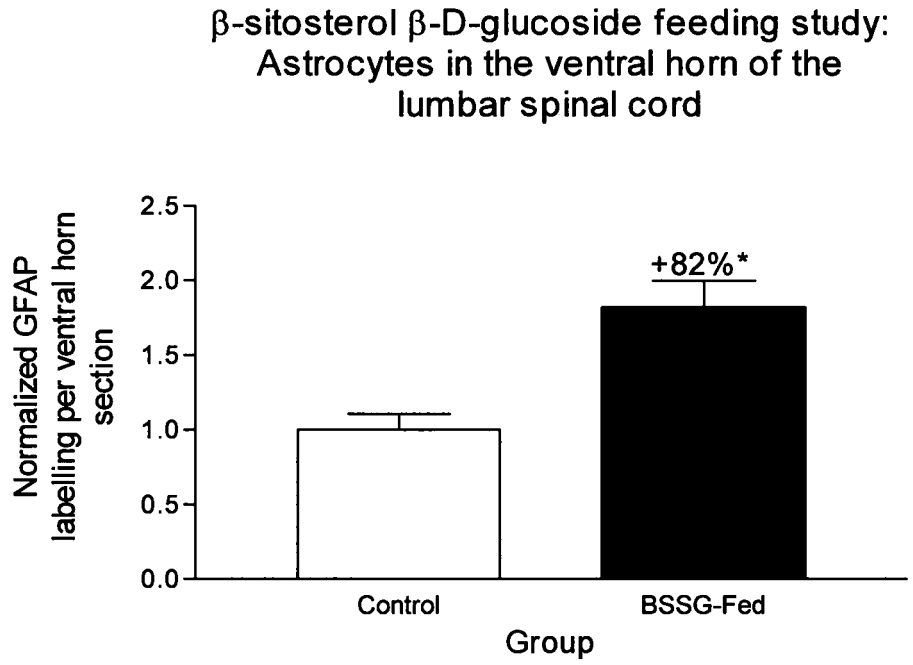
β-sitosterol β-D-glucoside feeding study:
Astrocytes in the ventral horn of the
lumbar spinal cord
Normalized GFAP
labelling per ventral horn
section
2.5
2.0
1.5
1.0
0.5
0.0
+82%*
Control
BSSG-Fed
Group

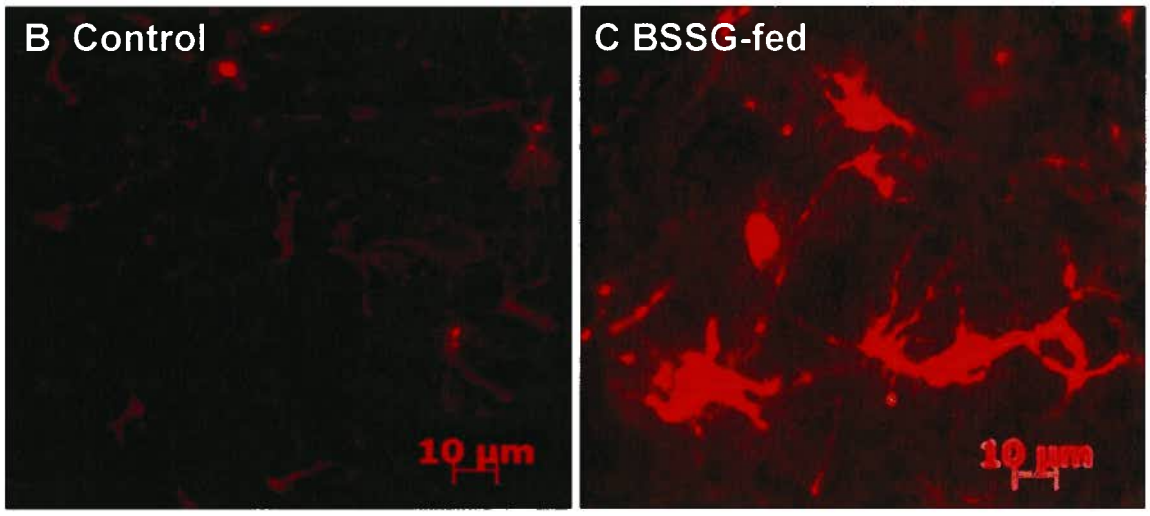
B Control
10 µm
C BSSG-fed
10 µm

Figure 11. **Proliferation of activated astrocytes occurs in the lumbar spinal cord of BSSG-fed mice.**

(A) Quantification of GFAP labelling in the ventral horn of the lumbar spinal cord in control and BSSG-fed mice. BSSG-fed mice showed significantly increased GFAP labelled cells (+82%) compared to the controls (Student's t-test, *$p<0.05$). Representative photomicrographs highlighting the lack of GFAP labelled cells in the ventral horn of the lumbar spinal cord of control mice (B) and hyper-ramified and proliferated astrocytes (red) in BSSG-fed mice (C). Images were captured using a fluorescence microscope under a 40x objective lens. Scale bars=10 μm.

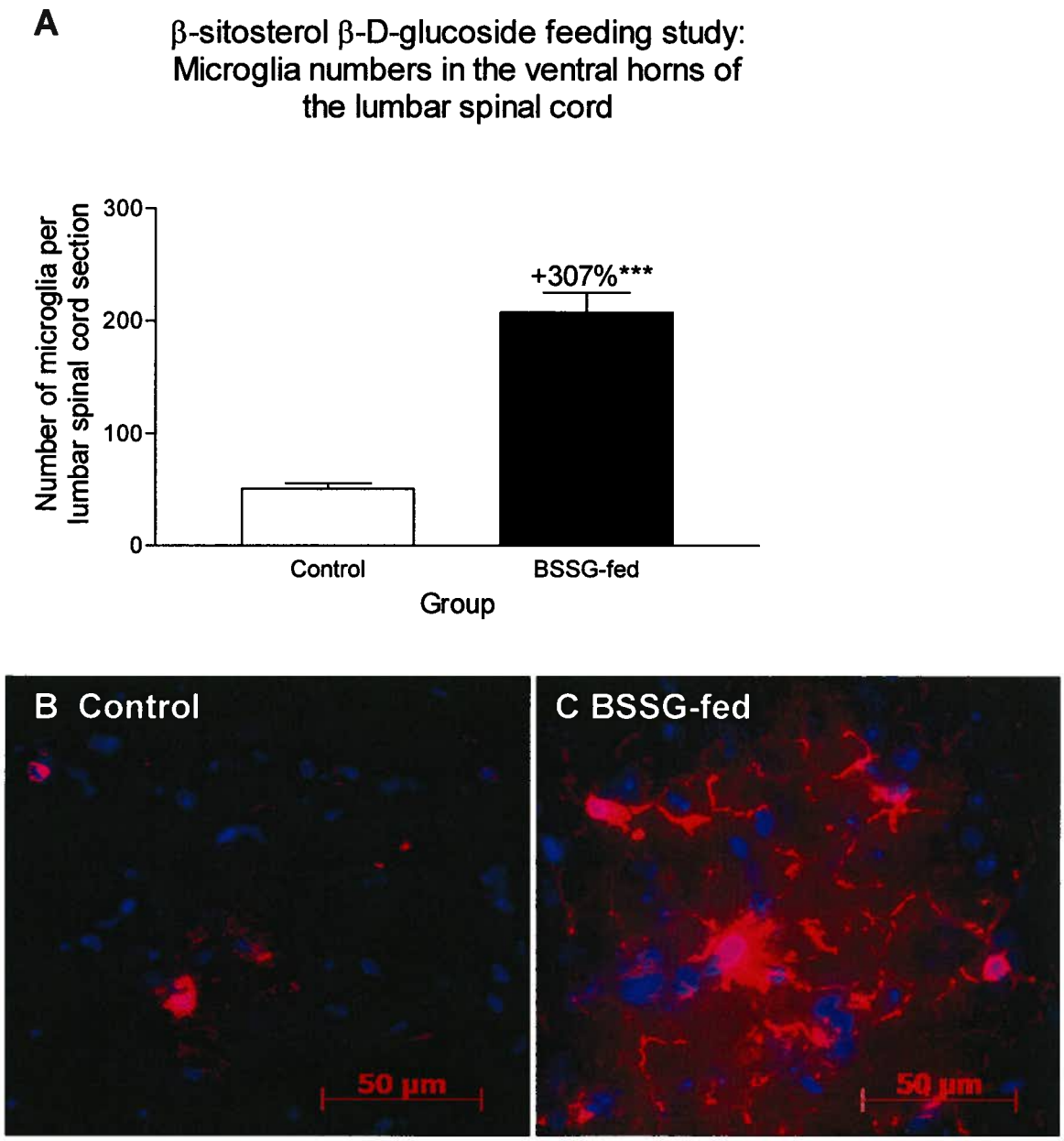

Figure 12. **Activated microglia in the lumbar spinal cord of BSSG-fed mice.**

(A) Quantification of microglia labelling in the ventral horn of the lumbar spinal cord in control and BSSG-fed mice. BSSG-fed mice showed significantly increased IBA-1 labelled cells (+307%) compared to the controls (Student's t-test, ***$p<0.0001$). Panel B is a representative photomicrograph highlighting the lack of activated microglia in the ventral horn of the lumbar spinal cord of control mice and while panel C depicts activated microglia (red) in BSSG-fed mice. The blue label is DAPI (nuclei). Images were captured using a fluorescence microscope under a 40x objective lens. Scale bars=50 µm.

A

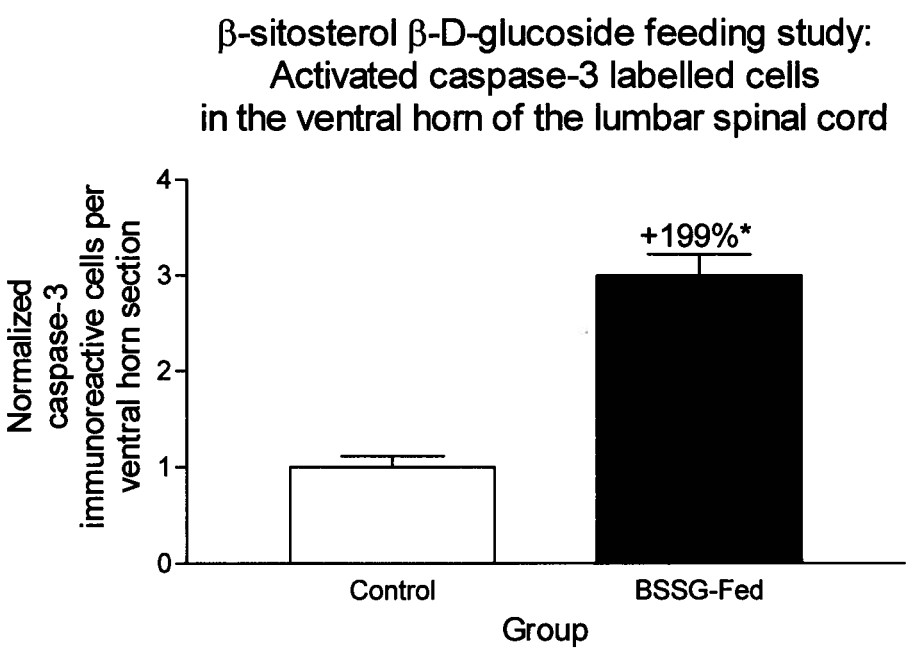
β-sitosterol β-D-glucoside feeding study:
Activated caspase-3 labelled cells
in the ventral horn of the lumbar spinal cord
Normalized caspase-3 immunoreactive cells per ventral horn section
0
1
2
3
4
+199%*
Control
BSSG-Fed
Group

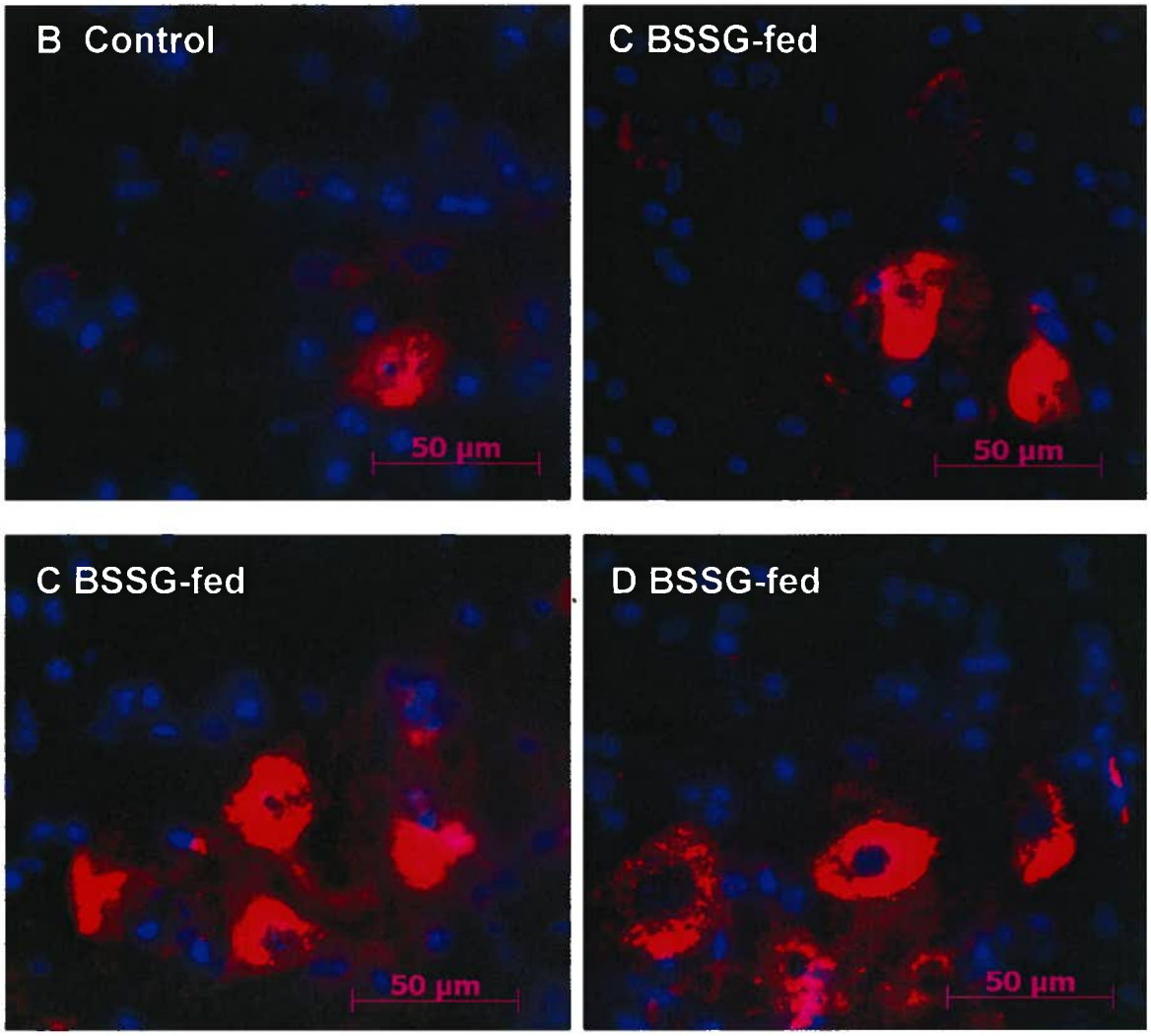

Figure 13. **Apoptosis in the lumbar spinal cord neurons following BSSG-feeding.**

Apoptotic activity was studied with an antibody to anti-active-caspase-3. (A) Active caspase-3 labelling was significantly increased (+199%) in the ventral horn of BSSG-fed animals (Student's t-test, *$p<0.05$). Active caspase-3 labelling in the ventral horn of the lumbar spinal cord of an age-matched control (B) and BSSG-fed mouse (C-D) at 52 wk. Images were captured using a fluorescence microscope under a 40x objective lens. Scale bars=50 µm.

A β-sitosterol β-D-glucoside feeding study: Cytochrome oxidase activity in the lumbar spinal cord

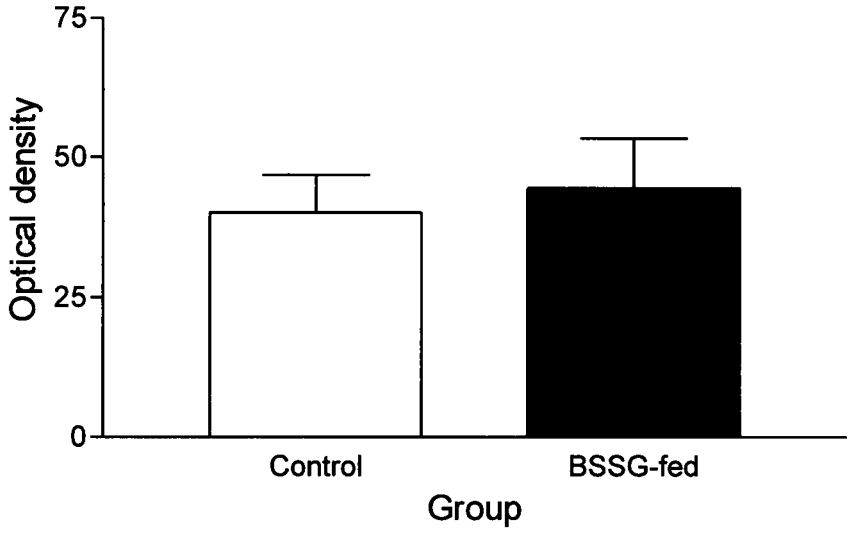

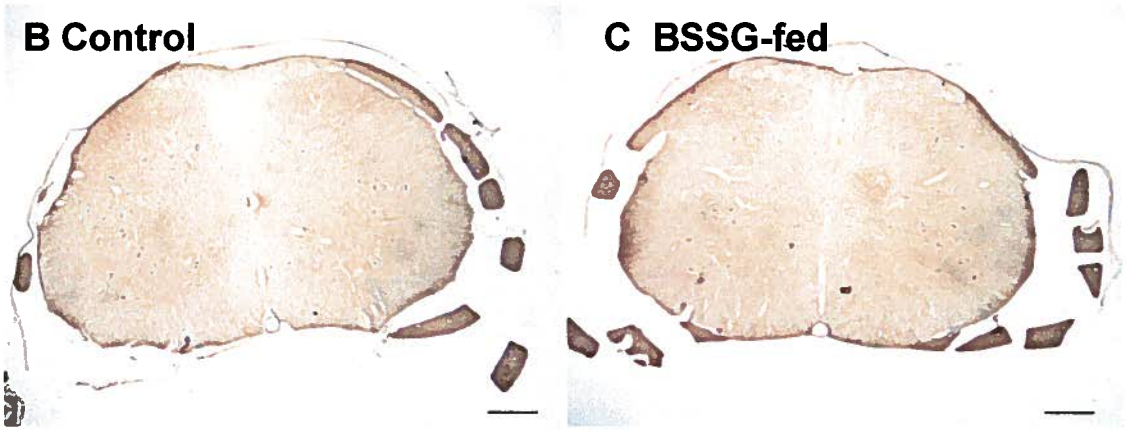

Figure 14. **Cytochrome c oxidase activity level is unchanged following BSSG-feeding.**

Cytochrome c oxidase activity was analyzed in the lumbar spinal cord of BSSG-fed animals and their age-matched controls. No significant difference was observed between the groups when their optical density profiles were compared (A), and gross examination of tissue also did not indicate such a difference (B-C). Images were captured using a light microscope under a 5x objective lens. Scale bars=1 mm.

A

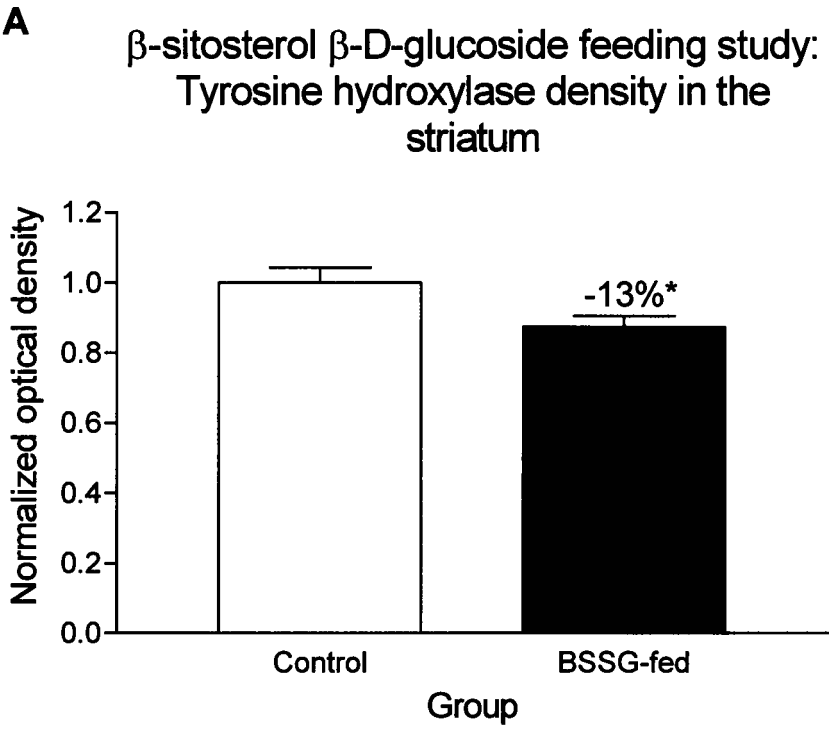
β-sitosterol β-D-glucoside feeding study:
Tyrosine hydroxylase density in the striatum
Normalized optical density
1.2
1.0
0.8
0.6
0.4
0.2
0.0
-13%*
Control
BSSG-fed
Group

B

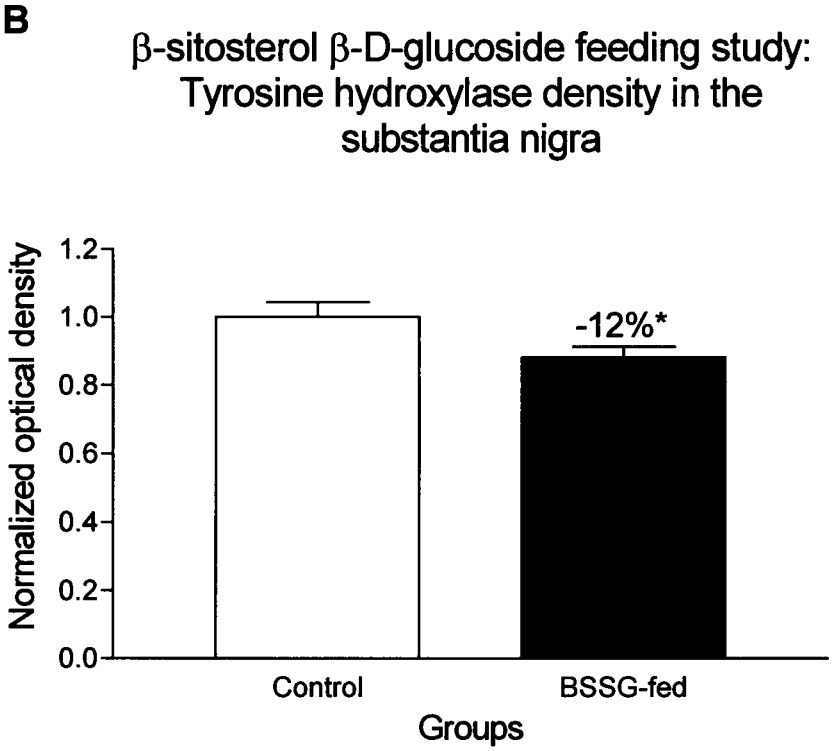
β-sitosterol β-D-glucoside feeding study:
Tyrosine hydroxylase density in the substantia nigra
Normalized optical density
1.2
1.0
0.8
0.6
0.4
0.2
0.0
-12%*
Control
BSSG-fed
Groups

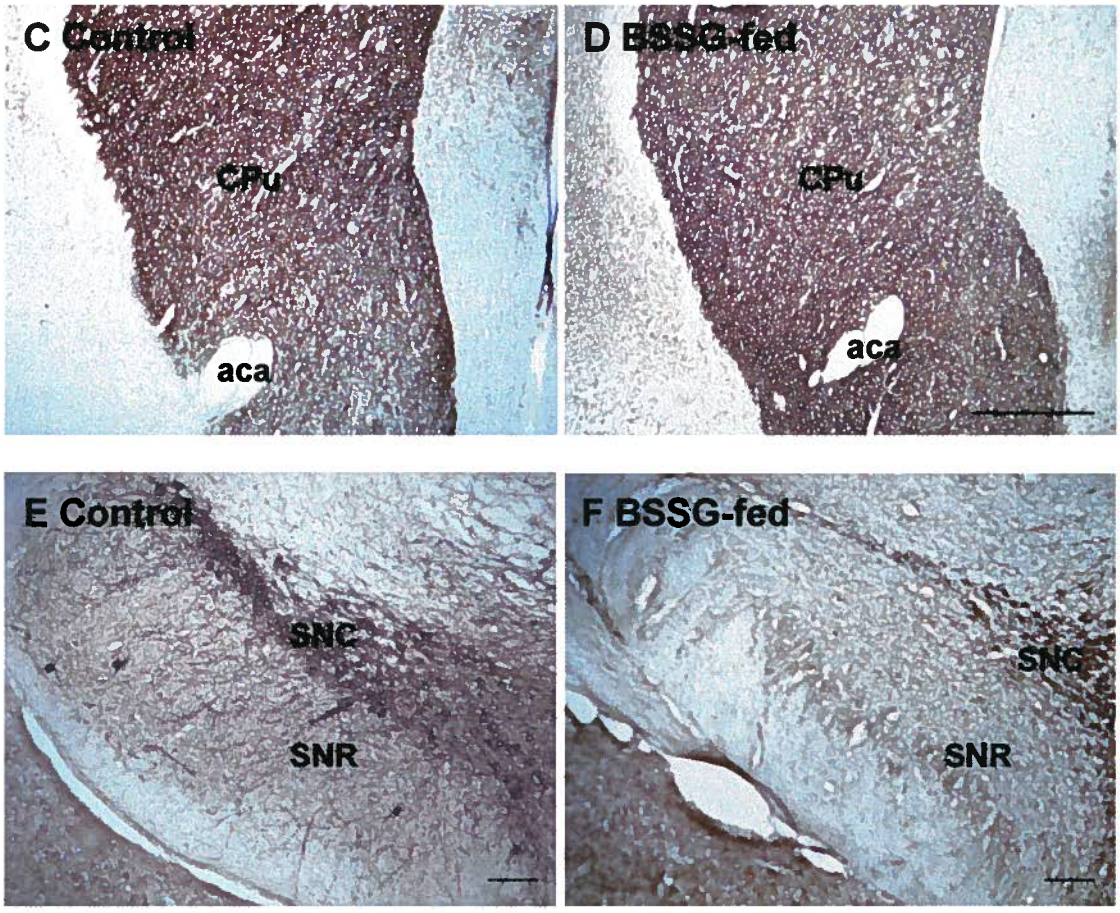

Figure 15. **Tyrosine hydroxylase labelling in the nigro-striatal region of BSSG-fed mice.**

Tyrosine hydroxylase containing-cell density measurement was achieved by immunohistology and subsequent optical density analysis of tyrosine hydroxylase (TH) immunoreactive cells and projections. Quantification of optical density of striatum (A) and substantia nigra pars compacta (SNpc) (B) are shown. BSSG-fed mice showed significantly decreased tyrosine hydroxylase labelling compared to the controls in both the striatum (panel A; Student's t-test: -13%, $p<0.05$) and SNpc (panel B; Student's t-test: -12%, $*p<0.05$). Panels C and D depict representative striatal sections of 52 wk old control and BSSG-fed animals respectively. A few anatomical landmarks have been indicated for orientation. The anterior commissure (aca) and striatum (CPu) are indicated in panels C and D. Panels E and F depict representative SNpc sections from a control and BSSG-fed mouse respectively. In the images, the reticular portion (SNR) and the compact portion (SNC) of the SN are shown. Images were captured using a light microscope under a 10x objective lens. Scale bars= 3 mm (C and D) and 200 µm (E and F).

A

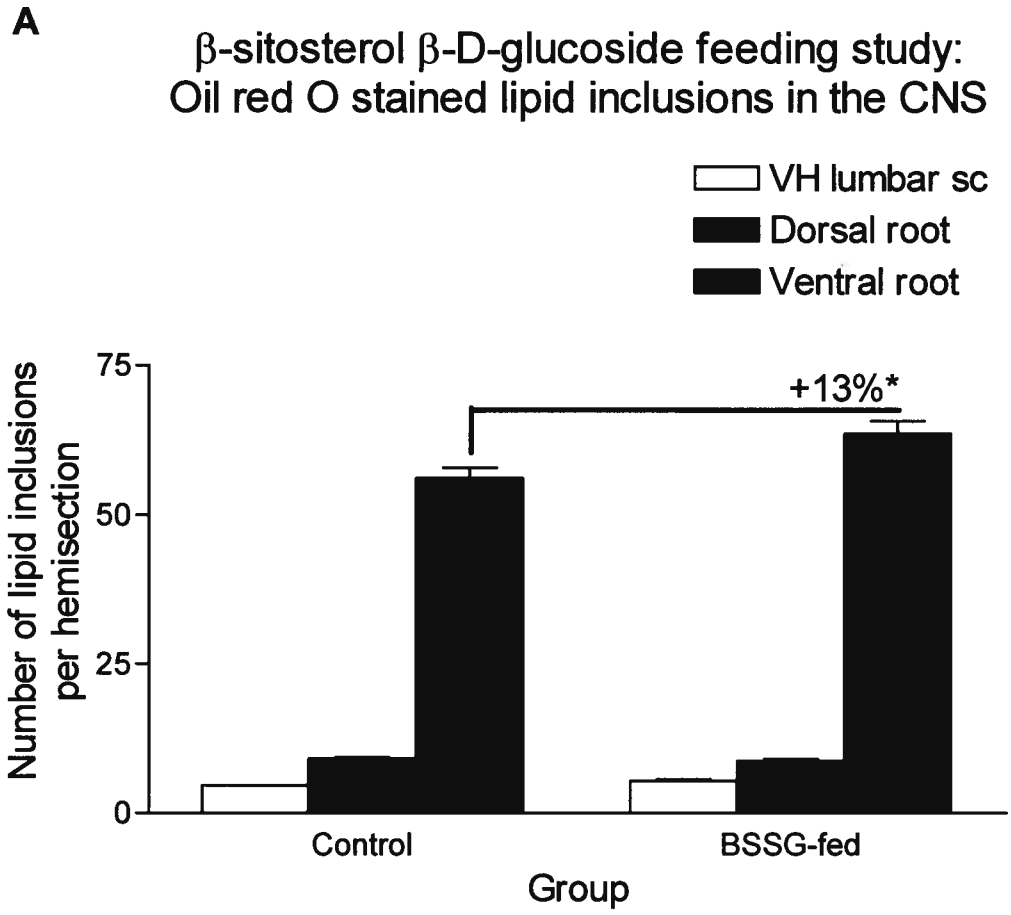
β-sitosterol β-D-glucoside feeding study:
Oil red O stained lipid inclusions in the CNS
VH lumbar sc
Dorsal root
Ventral root
Number of lipid inclusions per hemisection
75
50
25
0
+13%*
Control
BSSG-fed
Group

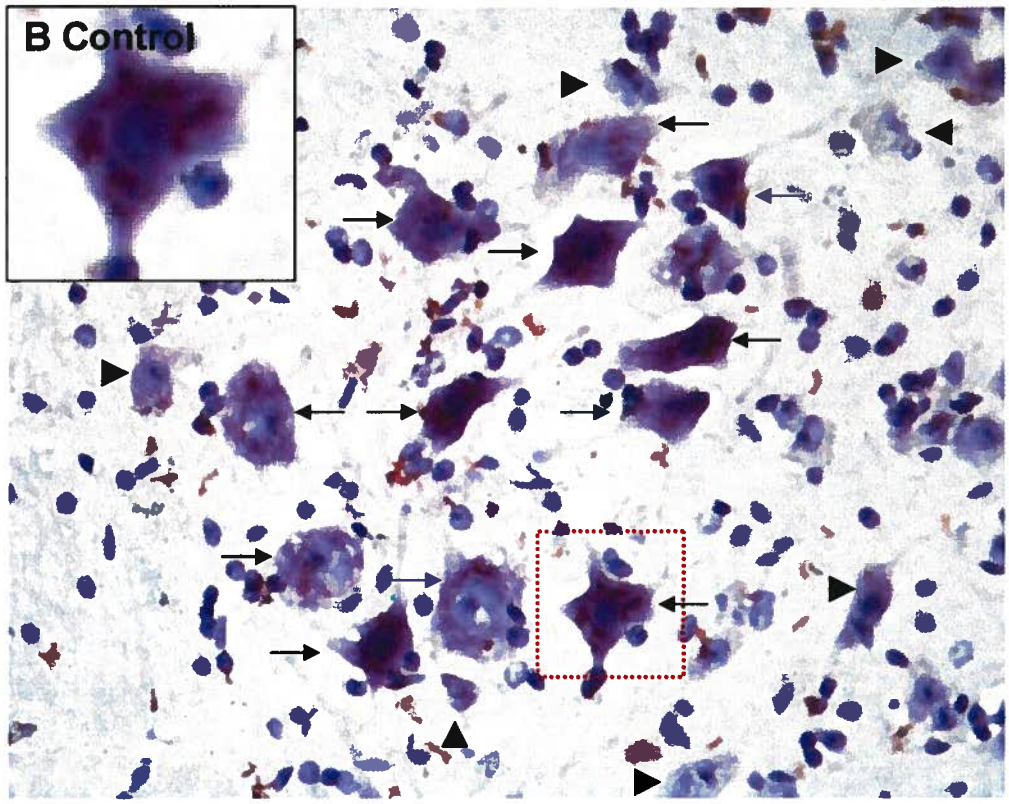
B Control

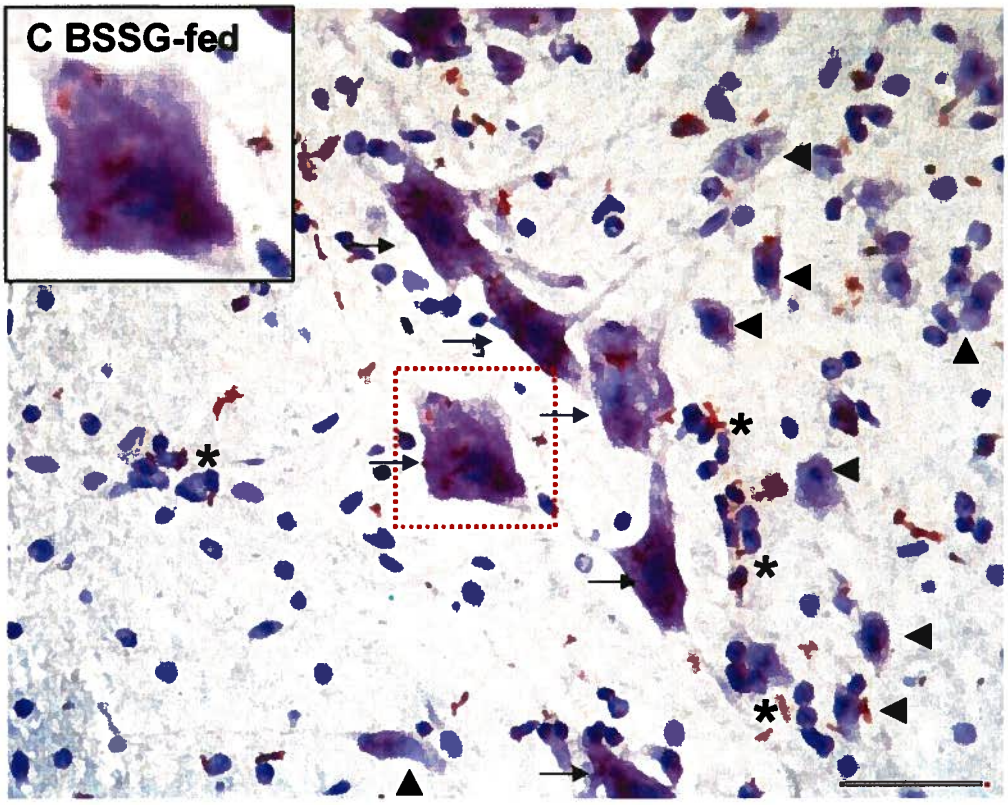
C BSSG-fed

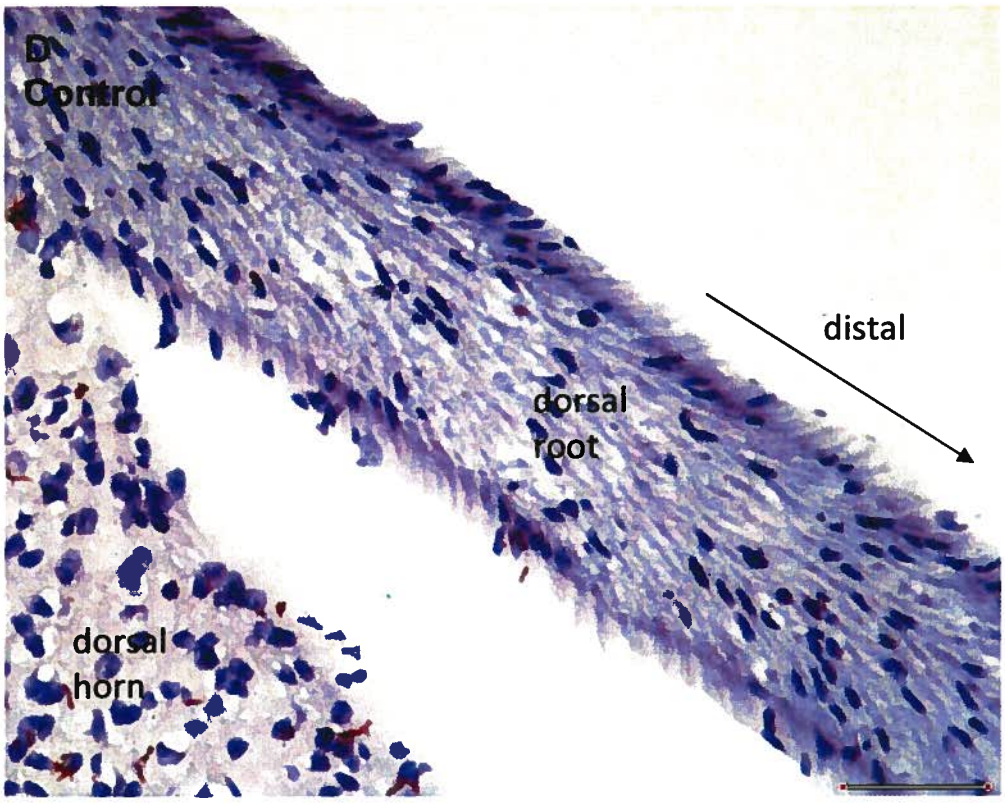
D
Control
distal
dorsal
root
dorsal
horn

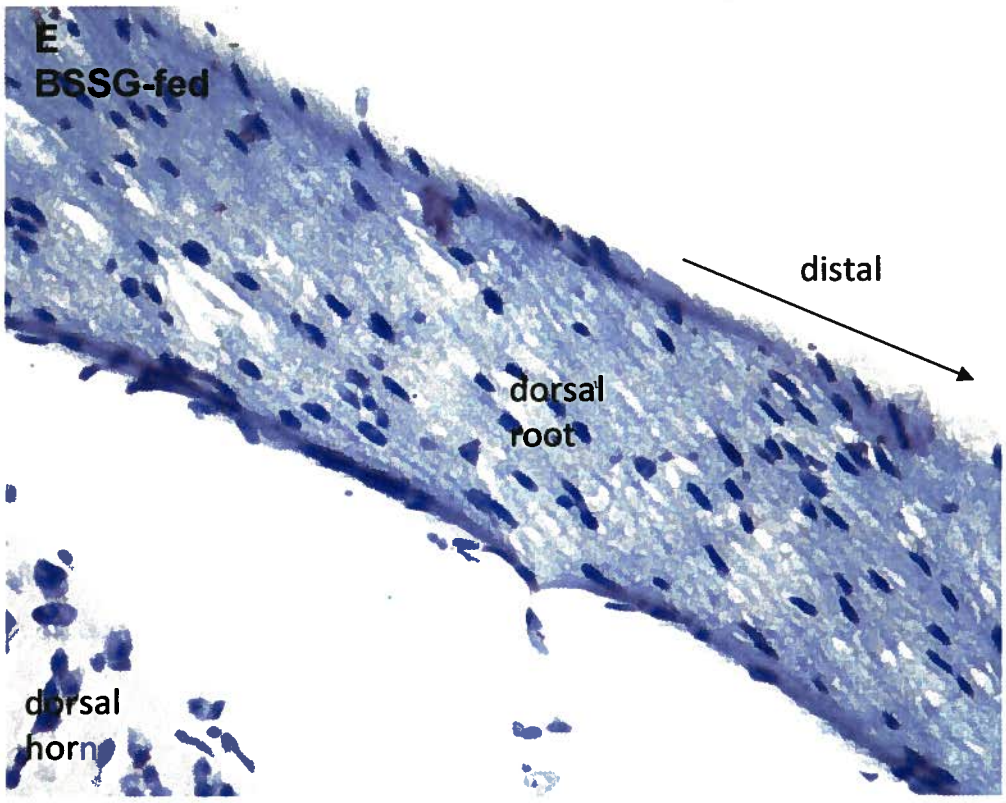
E
BSSG-fed
distal
dorsal
root
dorsal
horn

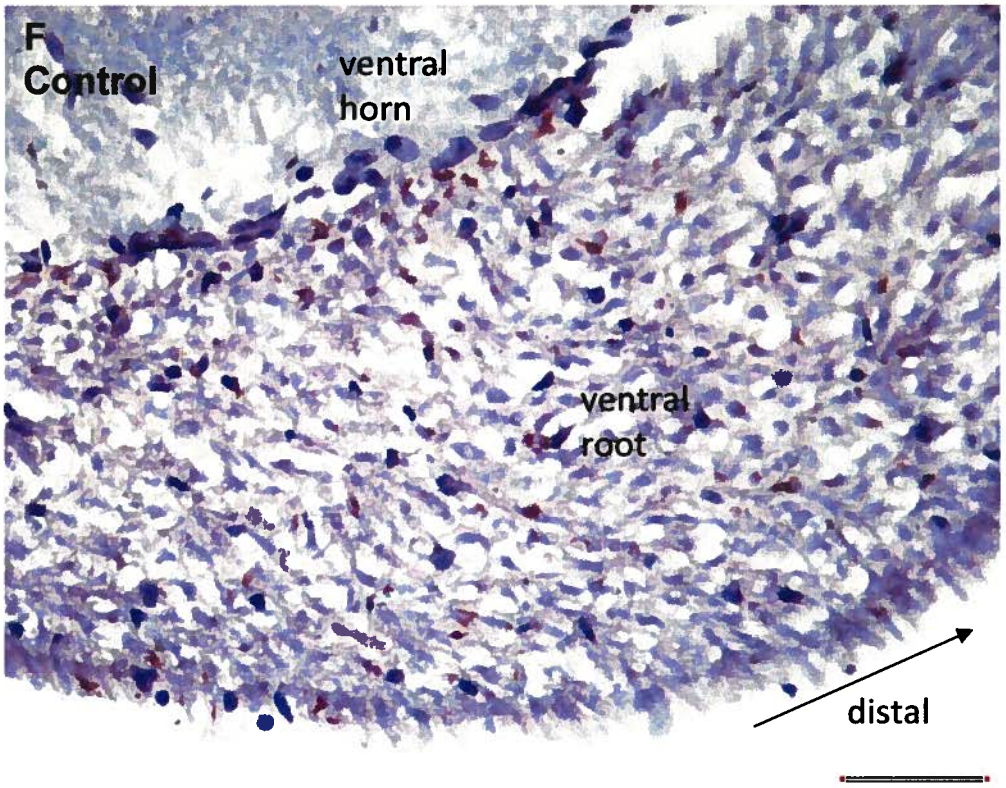
F
Control
ventral
horn
ventral
root
distal

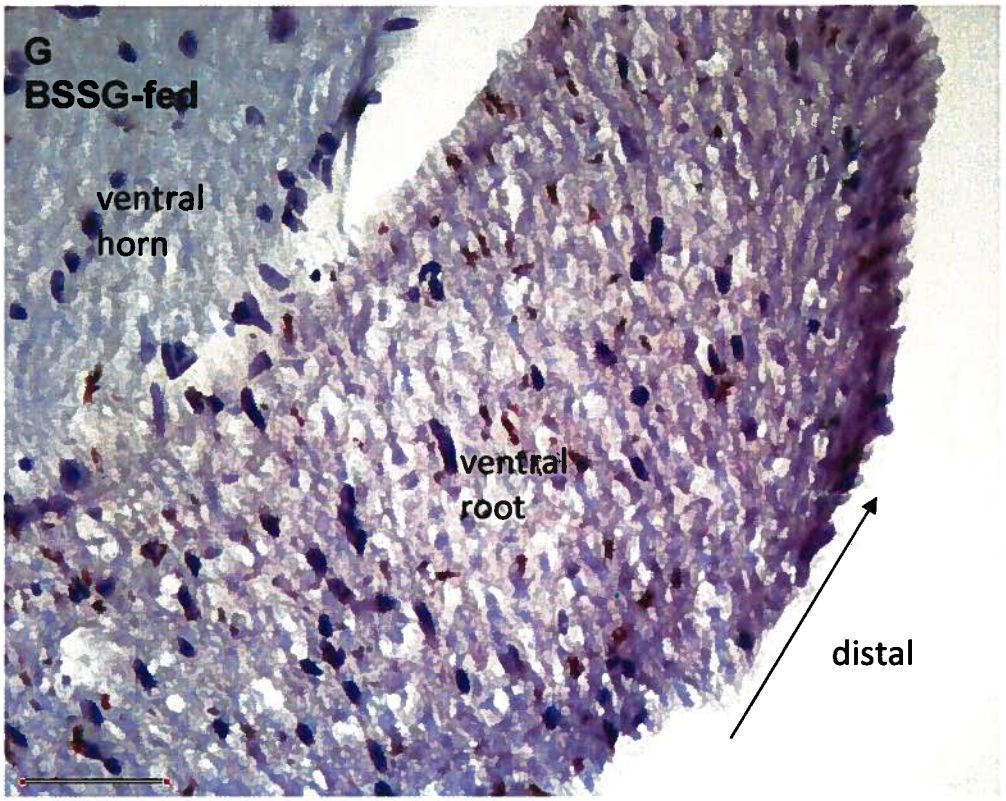
G
BSSG-fed
ventral
horn
ventral
root
distal

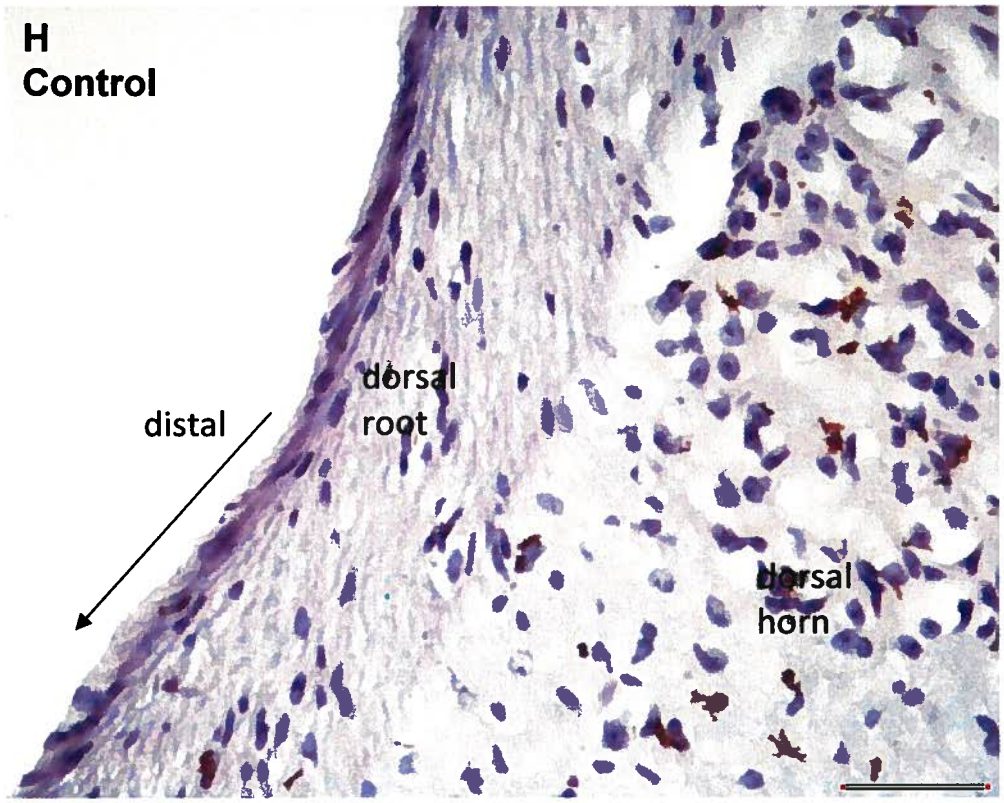
H
Control
distal
dorsal
root
dorsal
horn

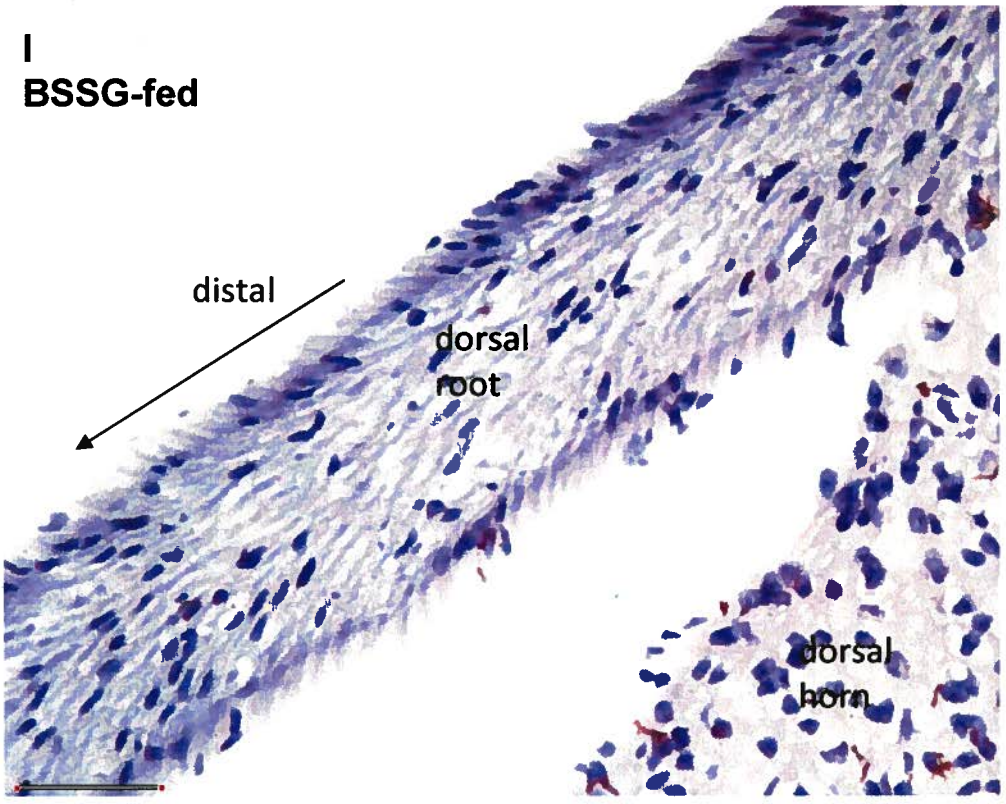
I
BSSG-fed
distal
dorsal
root
dorsal
horn

Figure 14. **Oil red O staining of lipids in the lumbar and thoracic spinal cord.**

Lipid deposits were revealed by staining with oil red O (red coloured stain). Counterstaining of nuclei was achieved with haematoxylin (blue/purple coloured stain). Lipid deposits were counted in the motor neurons (ventral horn of the lumbar spinal cord) and in the dorsal and ventral roots of control and BSSG-fed mice. Panel A shows a quantification of lipid deposits in control and BSSG-fed at 52 wk. BSSG-fed animals appeared to possess more lipid deposits, but the data did not reach statistical significance (Student's t-test: $p=0.0674$). Similarly, a statistical difference in the number of lipid deposits was not found in the dorsal roots (Student's t-test: $p=0.3778$). However, an inter-group difference in the number of deposits was found in the ventral root sections. BSSG-fed animals had a +13% increase compared to age-matched controls (Student's t-test: $*p<0.05$). Panels B and C show representative lumbar spinal cord ventral horn sections of a control and a BSSG-fed animal, respectively, at 52 wk (40x objective, scale bar=50 µm). Panel D shows gliosis in a BSSG-fed animal (100x objective, scale bar=20 µm). The dorsal and ventral roots of control and BSSG-treated animals are also shown. Micrographs were captured using a light microscope under a 40x or a 100x objective lens. Scale bars = 50 or 100 µm.

Mouse Strain	CD1 (out bred)
Sex	Male
Mouse age at start of feeding	20 wk
Numbers (n)	Control=15; BSSG-fed=16
BSSG Feeding Duration	15 wk
Post-feeding survival duration	17 wk
Mouse age at sacrifice	52 wk
Behavioural Tests	Open field motor activity* Leg extension*
Motor Neurons per lumbar cord section	-35%*
Motor Neurons per thoracic cord section	-19%*
Cholinergic cell number Choline acetyl transferase (ChAT)	-58%* (lumbar VH)
Stress induction Heat shock protein-70 Activating transcription factor-3 Phosphorylated jun^{ser73}	HSP-70: +644%*** (lumbar VH) ATF-3: +65%* (lumbar VH) Phospho-Jun^{ser73}: +34% (ns, p=0.1440)
Apoptotic activity Active caspase-3	+199%* (lumbar VH)
Astrocyte proliferation Glial fibrillary acidic protein (GFAP)	+82%* (lumbar VH)
Microglia proliferation Ionized calcium-binding adaptor molecule-1 (IBA-1)	+307%*** (lumbar VH)
Cytochrome c oxidase activity	+1% (ns) (lumbar VH)
Dopaminergic cell density Tyrosine hydroxylase (TH)	-13%* (striatum), -12%* (substantia nigra)
Lipid deposit accumulation Oil red O	+16% (lumbar VH) (ns, p=0.0674) -4% (dorsal spinal root) (ns, p=0.3778) +13%* (ventral spinal root)

*p<0.05; **p<0.01; ***p<0.001; not significant = ns; lumbar = lumbar spinal cord; ventral horn = VH

.

Table 1. **Summary of neurological outcomes following BSSG feeding.**

A summary of quantitative values for each of the experiments conducted are shown.

Chapter 4. The effects of dietary stigmasterol β-D-glucoside treatment

Hypothesis:

Dietary exposure to stigmasterol β-D-glucoside (SG) will induce progressive motor deficits and neuropathological changes in mice.

Specific aims:

1. To determine if dietary SG can induce ALS-PDC-like behavioural and pathological outcomes similar to those observed with washed cycad flour exposure.
2. To determine some of the key mechanisms underlying cellular changes that occurs as a result of dietary SG.

4.1 Results

In order to investigate whether SG is neurotoxic to an out bred strain of mice, I fed 1000 μg of synthetic SG per day to CD-1 mice for 15 wk. The mice were monitored behaviourally before, during, and after SG-feeding. Half of the mice were sacrificed immediately after receiving the last SG dose (35 wk of age) while the remaining mice survived an additional 17 wk (52 wk of age). Brain and spinal cord tissue, extracted from mice 35 and 52 wk of age, were subjected to a battery of histological and immunohistological measures to determine motor neuron numbers, detect signs of stress or apoptosis, determine the number of cholinergic neurons, tyrosine hydroxylase levels, and cytochrome c oxidase activity levels.

4.1.1 Body weight of subjects

At baseline and throughout the experiment, there were no significant differences in the weekly average body weight between the SG-fed group and the control group (Figure 18).

4.1.2 Dietary SG induces behavioural changes

Motor coordination and function (Gerlai et al., 1996b; Roder et al., 1996; Crawley, 1999;Gerlai and Roder, 1996) were assessed with the rotarod test. Performance data of the SG-fed animals indicated a shorter latency to fall, although data did not reach statistical significance (Figure 19). Some SG-fed animals were observed to clench onto the rotating axle or either one of the side barriers and/or fell off the rotarod soon after being placed onto the horizontal rod. Neuromuscular strength as tested by the wire hang test (Wilson et al., 2003d; Wilson et al., 2004c; Wilson et al., 2005; Tabata et al., 2008) indicated that SG-fed mice showed progressive impairment on this task beginning at 35 wk. By 14 wk post-feeding (or 49 wk of age), the difference in performance became statistically significant (Student's t-test: $p<0.05$) (Figure 20).

As observed in the BSSG study, SG-fed mice exhibited a progressive deficit on the leg extension test that became noticeable 15 wk into SG feeding and statistically significant after 19 wk (Figure 21). However, unlike what was observed with BSSG (Chapter 3 and Tabata et al., 2008) and cycad (Wilson et al., 2002a; Wilson et al., 2004b), where the diminished leg extension reflexes occurred non-monotonically with intermittent short-term recovery periods, SG-fed mice showed a steady decline in spinal reflexes (Figure 21).

As in the BSSG study, mice were tested for open field exploratory behaviour. However, at the start of the SG study, an automated open field videography and analysis system became available for use. With analysis and quantification automated, many more emotionality and movement variables became available for analysis. Most notably, SG-fed mice showed a trend in greater overall movement velocity (Figure 22A), angular velocity (Figure 22B), percent of time spent moving (Figure 22C) and total distance travelled (Figure 22D) in a 5 min interval. Further, SG-fed mice were observed to maintain a greater distance from the arena perimeter (Figure 22E) indicating decreased anxiety levels or disinhibition (Flint et al., 1995). In addition to these findings, 2 of 16 SG-fed animals exhibited rotational locomotion during every open field testing session until the time of sacrifice. The detection of these behavioural differences

among the two treatment groups is significant, since both automated and non-automated open field testing are normally only able to detect "highly significant" behavioural sedation and hyperactivity (Crawley, 2000). Inter-group differences were not found to be significant (Student's t-test, $p>0.05$) at 35 or 52 wk, except at a single time point (Figure 22E).

Two-way ANOVAs were conducted for each open-field variable. Each open-field variable was set as the dependent variable while the time (in weeks) and treatment groups were held as the independent variables. When the total distance to the arena border was analyzed, the time was found to have an effect ($F_{12, 168}=3.96$ ($p=0.000022$)) while the treatment group did not ($F_{1,168}=1.22$ ($p=0.271097$)). Similarly, when the mean distance to the arena border was analyzed, time was found to have an effect ($F_{12,168}=3.81$ ($p=0.000039$)). The treatment group did not have an effect on the mean distance to the arena border ($F_{1,168}=1.19$ ($p=0.275969$)). The total distance moved was unaffected by time ($F_{12,168}=0.86$ ($p=0.586949$)) and treatment group ($F_{1,268}=0.29$ ($p=0.589943$)). As expected, the mean distance moved was also unaffected by time ($F_{12,168}=0.98$ ($p=0.465622$)) and group ($F_{1,268}=1.34$ ($p=0.465622$)). The velocity of movement of the mice were unaffected by time ($F_{12,168}=0.86$ ($p=0.591534$)) and group ($F_{1,168}=0.29$ ($p=0.591394$)). Similarly, the angle velocity was unaffected by time ($F_{12,168}=0.26$ ($p=0.994221$)) and group ($F_{1,168}=0.70$ ($p=0.405016$). The heading speed of the mice were unaffected by time ($F_{12,168}=1.06$ ($p=0.39$)) and group ($F_{1,168}=3.35$ ($p=0.068866$)). The total turn angle of the mice was also unaffected by time ($F_{12,168}=1.47$ ($p=0.141231$)) and group ($F_{1,168}=0.48$ ($p=0.827422$)). When the mean turn angle was analyzed however, time was found to have an effect ($F_{12,168}=2.82$ ($p=0.001509$)) and the group still did not ($F_{1,168}=1.00$ ($p=0.319730$)). The meander of the mice were unaffected by time ($F_{12,168}=1.59$ ($p=0.097979$)) and group classification ($F_{1,168}=1.88$ ($p=0.171762$)). The total time spent moving was affected by time ($F_{12,168}=3.37$ ($p=0.000199$)) but not treatment group ($F_{1,168}=0.66$ ($p=0.418296$)). Related to this, the percent of time spent in arena moving was affected by time ($F_{12,168}=3.37$ ($p=0.000198$)) but not group ($F_{1,168}=0.66$ ($p=0.418213$)). When the frequency of rearing was analyzed, time

was found to have an effect ($F_{12,168}$=2.50 (p=0.004889)) but group did not ($F_{1,168}$=0.036022 (p=0.849699)).

The acquirement and analysis of gait indices was also automated by ventral plane videography (Appendix C). Ventral plane videography is the computerized version of the traditional footprint pattern analysis of mice, where ataxia and gait abnormalities are quantified from the footprint patterns of mice (Crawley and Paylor, 1997; Barlow et al., 1996; Carter et al., 1999). The computer-generated parameters including stride duration, swing duration, and stance duration were revealing of the effects of SG on the motor system. SG-fed animals showed a delay in motor responses. Specifically, the SG-fed animals took longer to initiate movement and alternate the direction of movement in both their forelimbs (Figure 23A) and hind limbs (Figure 23B, F, and E, respectively). Stance duration, the period during which the paw of a limb is in contact with the belt surface was also increased in both the forelimbs and hind limbs in SG-fed animals (Figure 23C and D, respectively). Taken together with the observation that SG-fed animals take shorter strides (Figure 23D), SG induces an overall shuffling and dragging of the limbs. Complementary to these findings, SG-fed animals were observed to take a greater number of steps (Figure 23I) to keep up with the motorized belt set at 30 rpm. Figure 23 provides graphical data on the left forelimb and hind limb. Similar findings were observed in the right forelimb and hind limb and are provided in the Appendix A.

Two-way ANOVAs were conducted on the various gait indices. The swing duration of each of the forelimbs and hind limbs were found to be affected by group but not time. Specifically, the left forelimb was unaffected by time ($F_{1,188}$=1.21 (p=0.273282)) and affected by group ($F_{16,188}$=12.83314 (p=0.000000)). Similarly, the right forelimb was found to be unaffected by time ($F_{1,188}$=0.02 (p=0.889980)) and affected by group ($F_{16,188}$=1.76 (p=0.039432)). The left hind limb was unaffected by time ($F_{1,188}$=1.47 (p=0.226706)) and affected by group ($F_{16,188}$=28.7 (p=0.000000)). The right hind limb was also unaffected by time ($F_{1,188}$=1.79 (p=0.182256)) and affected by group ($F_{16,188}$=37.19 (p=0.000000)) to a similar degree. Limb braking speeds were influenced by time

and group in various manners. Specifically, the left forelimb time was affected significantly by time ($F_{1,188}$=6.62 (p=0.010840)) and group ($F_{16,188}$=7.69 (p=0.000000)). Contrastingly, the right forelimb was unaffected by time ($F_{1,188}$=0.77 (p=0.380772)), affected by group ($F_{16,188}$=4.57 (p=0.000000)), and found to be affected by the interaction of time and group ($F_{16,188}$=1.99 (p=0.015631)). The left hindlimb braking speed was unaffected by time ($F_{1,188}$=0.08 (p=0.784047)), affected by group ($F_{16,188}$=61.03 (p=0.000000)), and affected by the interaction of the time and group variables ($F_{16,188}$=5.34 (p=0.000000)). Similarly, the right hind limb braking speed was unaffected by time ($F_{1,188}$=2.82 (p=0.095015)), affected by group ($F_{16,188}$=62.73 (p=0.000000)), and affected by the interaction of time and group ($F_{16,188}$=1.85 (p=0.027910)). The effects of time and group on the propulsion of each of the limbs were also analyzed. The left forelimb propulsion was found to be unaffected by time ($F_{1,188}$=1.67 (p=0.197696)), affected significantly by group ($F_{16,188}$=21.30 (p=0.000000)), and affected by the interaction of time and group ($F_{16,188}$=1.11 (p=0.347959)). The hind limbs were affected by the grouping variable on its own and/or by the interaction of time and the grouping variable. Specifically, the left hind limb was unaffected by time ($F_{1,188}$=2.16 (p=0.143040)), affected significantly by group ($F_{16,188}$=4.36 (p=0.000000)), and affected by the interaction of time and group ($F_{16,188}$=2.99 (p=0.000185)). The right hind limb was unaffected by time ($F_{1,188}$=1.31 (p=0.254243)) and affected by grouping ($F_{16,188}$=4.69 (p=0.000000)). Two-way ANOVA of limb stance width revealed the effects of treatment. The left forelimb stance was found to be unaffected by time ($F_{1,188}$=0.00 (p=0.997923)), affected by group ($F_{16,188}$=15.79 (p=0.000000)), and affected by the interaction of time and group ($F_{16,188}$=2.25 (p=0.005172)). The right forelimb stance was also unaffected by time ($F_{1,88}$=0.10 (p=0.755093)), affected by group ($F_{16,188}$=13.21 (p=0.000000)), and affected by the interaction of time and group ($F_{16,188}$=2.26 (p=0.004979)). Left hind limb stance was also unaffected by time ($F_{1,188}$=0.67 (p=0.414560)), affected by group ($F_{16,188}$=16.84 (p=0.000000)), and affected by the interaction of time and group ($F_{16,188}$=3.62 (p=0.000009)). Right hind limb stance was unaffected by time ($F_{1,188}$=0.99

(p=0.321233)) and the interaction of time and group ($F_{1,16}$=0.87 (p=0.607527)) but affected by group ($F_{16,188}$=10.94 (p=0.000000)). The stride times for each of the limbs were found to be affected by time and group. The left forelimb was affected by time, group, and by the interaction of time with group ($F_{1,188}$=7.99, p=0.005206; $F_{16,188}$=396.29, p=0.000000; and $F_{16,188}$=2.71, p=0.000661, respectively). The right forelimb was also affected by each of time, group, and the interaction of the two variables ($F_{1,188}$=7.19, p=0.007989; $F_{16,188}$=389.00, p=0.000000; and $F_{16,188}$=2.82, p=0.000413). The left hind limb was also affected by time, group, and the interaction of both ($F_{1,188}$=6.22, p=0.013461; $F_{16,188}$, p=0.000000; $F_{16,188}$=3.89, p=0.000003). The right hind limb in contrast was not affected by time ($F_{1,188}$=0.75, (p=0.388191)) or the interaction of time and group ($F_{16,188}$=0.74, (p=0.748971)), and affected by grouping only ($F_{16,188}$=314.86 (p=0.000000)). The left forelimb stride length was affected by time ($F_{1,188}$=10.16 (p=0.001680)), group ($F_{16,188}$=10.11 (p=0.000000)), but not by the interaction of the two variables ($F_{16,188}$=1.42 (p=0.134868)). The right forelimb stride length was affected by time and group on their own, as well as by the interaction of the two ($F_{1,188}$=12.40, p=0.000540; $F_{16,188}$=9.90, p=0.000000; and $F_{16,188}$=1.80, p=0.033803, respectively). The left hind limb stride length was affected by time, group, and the combination of the two ($F_{1,188}$=16.07, p=0.000088; $F_{16,188}$=19.09, p=0.000000; $F_{16,188}$=2.19, p=0.006786). The right hind limb was affected by group ($F_{16,188}$=11.56 (p=0.000000)), but not time ($F_{1,188}$=3.29 (p=0.071259)) or the interaction of time and group ($F_{16,188}$=0.83648 (p=0.643045)). The effect of time and group on stride frequency of each limb was also analyzed. Time, group, and the interaction of time and group were found to have an effect on the left forelimb stride frequency ($F_{1,188}$=0.28151, p=0.596336; $F_{16,188}$=46.657, p=0.000000; $F_{16,188}$=2.61, p=0.001045). Similarly, the right forelimb stride frequency was affected by time ($F_{1,188}$=6.27 (p=0.013106)), group ($F_{16,188}$=1.28 (p=0.214264)) and the interaction of group and time ($_{F16,188}$=1.77 (p=0.037337)). Similarly, the left hind limb was affected by time ($F_{1,188}$=15.00 (p=0.000148)), grouping ($F_{16,188}$=65.56 (p=0.000000), and time and group together ($F_{16,188}$=2.20 (p=0.006409)). The right hind limb was unaffected by time ($F_{1,188}$=1.20

(p=0.274023)) and the interaction of time and group ($F_{16,188}$=1.13 (p=0.328461)), and affected by grouping ($F_{16,188}$=7.048140 (p=0.000000)). The effect of time and group on the paw angle of each limb was assessed. The left forelimb was not affect by time ($F_{1,188}$=0.17183 (p=0.678966)) and affected by group ($F_{16,188}$=35.16283 (p=0.000000)). The interaction of time and group did not affect the left forelimb paw angle ($F_{16,188}$=0.81 (p=0.671408)). Similarly, the group was found to affect the right forelimb paw angle ($F_{16,188}$=4.90 (p=0.000000)), but not the time ($F_{1,188}$=0.25 (p=0.620891)) or time and group together ($F_{16,188}$=0.526401 (p=0.931053)). The left hind limb paw angle was affected by time ($F_{1,188}$=7.40 (p=0.007152)) and group ($F_{16,188}$=59.38 (p=0.000000), but not both together ($F_{16,188}$=0.91 (p=0.558381)). The right hind limb paw angle was unaffected by time ($F_{1,188}$=0.03 (p=0.858635)) and the interaction of time and group ($F_{16,188}$=0.66 (p=0.834761)), and affected by group on its own ($F_{16,188}$=3.885996 (p=0.000003)). Two-way ANOVAs were conducted on the number of steps taken by each limb. The time did not have an affect on the number of steps made by the left forelimb ($F_{1,188}$=0.10 (p=0.748667)) but the group did ($F_{16,188}$=64.10 (p=0.000000)). The interaction of time and group did not have an effect on the number of steps ($F_{16,188}$=0.77 (p=0.722964)). The number of steps made by the right forelimb was similarly unaffected by time ($F_{1,188}$=0.40 (p=0.527202)) and the interaction of time and group ($F_{16,188}$=1.38 (p=0.157539)) and was affected by group ($F_{16,188}$=56.76 (p=0.000000)). The number of steps made with the left hind limb was unaffected by time ($F_{1,188}$=0.04 (p=0.846690)) and the interaction of time and group ($F_{16,188}$=0.51 (p=0.940227)), and affected by group ($F_{16,188}$=0.50962 (p=0.940227)). The number of steps made by the right hind limb was unaffected by time ($F_{1,188}$=0.04 (p=0.837670)) and the combination of time and group ($F_{16,188}$=0.76787 (p=0.720362)), and was affected by group ($F_{16,188}$=79.21 (p=0.000000)). The paw area of each limb was found to be affected by time, group, and the combination of the two in different ways. Time and group was found to significantly effect the paw area of the left forelimb ($F_{1,188}$=4.04, p=0.045844; $F_{16,188}$=27.67, p=0.000000, respectively). The interaction of time and group did not affect the left forelimb paw area ($F_{16,188}$=0.95

(p=0.516827)). The right forelimb was not affected by time ($F_{1,188}$=0.01, (p=0.925829)) or the interaction of time and group ($F_{16,188}$=1.65 (p=0.060891)). The group, however, was found to significantly affect the right forelimb paw area ($F_{16,188}$=160.40 (p=0.000000)). The left hind limb paw area was affected by time ($F_{1,188}$=6.33 (p=0.012674)) and group ($F_{16,188}$=83.75 (p=0.000000)) but not by the interaction of the two ($F_{16,188}$=1.30 (p=0.203511)). In contrast, the right hind limb paw area was affected by group ($F_{16,188}$=200.17 (p=0.000000)) but not affected by time ($F_{1,188}$=1.52 (p=0.219176)) or the interaction of time and group ($F_{16,188}$=1.36 (p=0.163107)).

4.1.3 Dietary SG induces neuropathology

The purpose of this study was to reveal the cellular events that occur following SG-feeding. In the previous study, the up-regulation of ATF-3, phosphorylation of jun, accumulation of lipids, the programmed cell death pathway and activation of astrocytes and microglia were implicated in the degeneration of lumbar and thoracic spinal cord ventral horn motor neurons (Chapter 3 and Tabata et al., 2008). In the present study, immunohistochemical methods were again employed to study the number of glial cells activated, the number of motor neurons, the number of apoptotic motor neurons, the cytochrome c oxidase activity level, tyrosine-hydroxylase-containing cell density and the level of phosphorylation or up-regulation of stress/survival pathway-implicated transcription factors and chaperone proteins, and signs of lipid accumulation (Holderith et al., 2003; Lauckner et al., 2003; Lotocki et al., 2003; Vanni-Mercier et al., 2003; Yoshida et al., 1994). I incubated lumbar spinal cord sections of SG-fed animals and age-matched control animals with an antibody against the active form of caspase-3, GFAP, IBA-1, Hsp-70, ATF-3, and p-Jun^{ser73}, signalling molecules involved in stress and survival pathways; and phosphorylated tau (PHF-1 AT8 Tau) and TAR DNA-binding protein 43 (TDP-43). Thirty-five wk old (time point 1) and 52 wk old (time point 2) mice CNS tissue were analyzed to determine if the cells/transcription factors/chaperone proteins/lipid deposits were implicated in the response to SG toxicity. The most

pronounced pathological changes were observed within the lumbar spinal cord. No immunoreactivity was observed in control sections in which the primary antibody was omitted from the procedure.

Cresyl violet staining (for Nissl body substance) was used to ascertain the number of α- and γ-motor neurons. The counts were conducted on spinal cord sections of animals survived to 35 and 52 wks (Figure 24A). A detailed quantification of motor neurons was accomplished by sub-grouping motor neurons according to size, morphology, and Nissl substance distribution (for the detailed sub-grouping and counting methodology, please see Chapter 2). An inter-group comparison revealed that at both 35 and 52 wk, the control group had more healthy α- and γ- motor neurons in the ventral horn of the lumbar spinal cord (35 wk: Student's t-test: ns, $p>0.05$; 52 wk Student's t-test: -55%, $p<0.05$). An inter-group statistical assessment of the total number of α-motor neurons also showed significant differences at both time points (Student's t-test at 35 wk: -29%, $p<0.05$; 52 wk: -47%, $p<0.05$; Figure 24A). Furthermore, the SG-fed group was found to undergo a significant decline in the total number of α-motor neurons between 35 and 52 wk (Student's t-test: -36%, $p<0.05$) indicating that the neurotoxic impact of SG continues even after cessation of SG-feeding. As with BSSG-feeding (Figure 5), SG-feeding induced classical pyknosis (defined in Chapter 2). This interpretation comes from the observation that motor neurons with Nissl substance missing only centrally or both centrally and peripherally were found scattered throughout lumbar spinal cord sections of SG-fed mice at 35 wk (Figure 24B-E) and at 52 wk (Figure 24J-M).

An antibody that recognizes choline acetyl transferase in cholinergic neurons was again used to assess whether or not cholinergic neurons are affected following SG-feeding. Quantification of ChAT immunolabelling in the ventral horn of the lumbar spinal cord revealed a significant difference between the control and SG-fed groups at both pre-symptomatic and symptomatic time points. SG-treated animals exhibited a significantly lower number of cholinergic neurons with 18% (Student's t-test: $p<0.05$) and 32% (Student's t-test: $p<0.05$) fewer cholinergic neurons at 35 and 52 wk, respectively compared to controls

(Figure 25A). Furthermore, an intra-group assessment revealed a progressive decline in the number of cholinergic neurons (Student's t-test: -31%, $p<0.05$).

Neurons in the lumbar spinal cord of SG-fed animals were stressed following SG feeding. Quantitative analysis of Hsp-70 immunoreactive cells showed statistically significant inter-group differences in the number of Hsp-70 immunoreactive cells at 35 and 52 wk. Specifically, at 35 wk, SG-fed animals were found to have 1036% (Student's t-test: $p<0.001$) more cells expressing Hsp-70 (Figure 26A). At 52 wk, this number was found to decline yet remained significant with 425% (Student's t-test: $p<0.05$) more cells expressing Hsp-70 compared to the controls (Figure 26A). Quantitative analysis of ATF-3 immunoreactivity revealed that a significantly greater number of cells in the lumbar spinal cord of SG-fed were immunoreactive to anti-ATF-3 compared to age-matched controls at 35 (Student's t-test: +242%, $p<0.001$) and 52 wk (Student's t-test:: +101%, $p<0.01$) (Figure 27) as well as to the anti-phosphorylated-Jun ^{ser73} (p-Jun^{ser73}) (Student's t-test at 35 wk: +199%, $p<0.05$; 52 wk: not significant, $p>0.05$) (Figure 28). Control animal lumbar spinal cord sections were typically devoid of cells immunoreactive to both anti-ATF-3 and p-Jun^{ser73} (Figure 27, 28).

The level of glial cell involvement in dietary SG-exposure induced effects was determined with antibodies for GFAP and IBA-1. Quantification of anti-GFAP labelling in the ventral horn of the lumbar spinal cord of control and SG-fed mice at 35 wk and 52 wk revealed that SG-fed mice had a significantly greater number of reactive astrocytic compared to the controls at both the pre-symptomatic (Student's t-test: +337%, $p<0.001$) and symptomatic time-points (Student's t-test:: +119%, $p<0.05$) (Figure 29). Similarly, quantification of microglia in the ventral horn of the lumbar spinal cord of control and SG-fed mice at 35 wk and 52 wk revealed that SG-fed mice had significantly more reactive microglia compared to the controls (Student's t-test: +33%, $p<0.01$ and +59%, $p<0.05$, respectively) (Figure 30).

Lumbar spinal cord sections were incubated with a polyclonal antibody for the active form of caspase-3. Apoptosis of motor neurons was found to occur as

with BSSG-feeding (Figure 31). SG-fed mice had a significantly greater number of apoptotic cells compared to controls at both 35 and 52 wk (Student's t-test at 35 wk: +78%, $p<0.001$, 52 wk: not significant, $p>0.05$) (Figure 31A). Furthermore, a greater number of apoptotic cells were observed at 35 wk compared to 52 wk, suggesting that by the later time point, many motor neurons had undergone apoptosis, leaving a smaller number of residual motor neurons. In addition, at 52 wk, cells immunoreactive to caspase-3 appeared to be slightly smaller in size than those that labelled at 35 wk, suggesting that the type and size of motor neurons that undergo apoptosis during the later stages of SG-feeding are different from those that do so at the pre-symptomatic time-point. Alternatively, it is possible that sometime during the early stage of SG-feeding the larger α-motor neurons underwent significant contraction and became smaller in stature.

An antibody recognizing tyrosine hydroxylase in dopaminergic neurons was used to assess whether SG-feeding affected tyrosine hydroxylase levels in dopaminergic neural populations of the brain. SG-feeding was found to significantly decrease tyrosine hydroxylase labelling (optical density) in treated animals compared to controls (Student's t-test: $p<0.001$) in the substantia nigra pars compacta (SNpc) at 35 wk (Student's t-test: -34%, $p<0.001$) and at 52 wk (Student's t-test: -39%, $p<0.05$) (Figure 33A). Furthermore, TH optical density was found to decrease among SG-fed animals over the 17 wk post-SG-feeding period (Student's t-test: -22%, $p<0.05$) suggesting that a progressive depletion of tyrosine hydroxylase levels in dopaminergic neurons occurred as a result of SG-feeding.

Lipid accumulation was visualized by staining with oil red O. Lipid deposits were detected in the motor neurons and neuropil of both control and SG-fed animal lumbar spinal cord sections, but the average number (Student's t-test: +28%, $p<0.05$) and size of lipid deposits per cell were greater in the treatment group (Figure 34).

Neuronal metabolic activity was analysed with a histological analysis for cytochrome c oxidase levels. As was observed in the BSSG study, no

statistically significant differences were observed between groups at 35 or 52 wk (Figure 32A). However, in contrast, a decline in cytochrome c oxidase activity was observed to occur over time in each of the groups. The control group was found to undergo a 47% decrease (Student's t-test, $p<0.001$) in cytochrome c oxidase activity, while the SG-fed group saw a decline to a lesser degree of 36% (Student's t-test: $p<0.01$) (Figure 32A).

4.1.4 Dietary SG induces the formation of two distinct types of pathological proteins

Antibodies recognizing phosphorylated tau and phosphorylated TDP-43 were used to assess whether SG-fed animal CNS tissue harboured pathological tau or TDP-43 inclusions. Dietary SG was found to induce an abnormal accumulation of elongated and globular phosphorylated tau inclusions in the ventral horn of the lumbar spinal cord at 52 wk (in 2 of 8 animals) but not at the earlier time point (Figure 36). Double-immunofluorescence revealed that a subset of these phosphorylated tau-containing cells co-labelled with anti-caspase-3, indicating that the inclusion was actively undergoing apoptosis (Figure 35).

In healthy cells, TDP-43 is found in the nucleus, but redistributes and accumulates in the cytosol in neurological conditions, including sporadic ALS. Immunohistology further revealed that the inclusions that appeared oblong were also often twisted irregularly or entangled in a cluster of glia (Figure 37). Pathological redistribution of hyperphosphorylated TDP-43 into the cytosol was also observed in two animals belonging to the SG-fed group. The animals harbouring the pathologic TDP-43 inclusions were different from those that possessed the tau inclusions. No abnormal translocation of TDP-43 was observed in control animals (Figure 37), SG-fed animals at 35 wk, and in the remaining six SG-fed animals at 52 wk. Pathological tau or TDP-43 cytoplasmic inclusions were not detected in the frontal neocortex, dentate granule cells and in the hippocampal pyramidal neurons.

4.2 Discussion

4.2.1 SG induces the progressive loss of cells from the CNS and in turn, leads to behavioural impairment

The results of the present study show for the first time that SG can be neurotoxic *in vivo* and induce progressive behavioural and histological pathology distinct from dietary BSSG exposure that mimic in many respects, early features of ALS-PDC. At a dose of 1000 µg per day for 15 wk, outbred CD-1 mice exhibited progressive impairment of muscular strength (Figure 20) and spinal reflexes (Figure 21), and a slight disturbance of motor coordination (Figure 19). SG was also found to induce increases in overall movement velocity (Figure 22A), angular velocity (Figure 22B), percent of time spent moving (Figure 22C), total distance travelled (Figure 22D) and anxiety. Further, on certain tasks, animals were found to take shorter strides, shuffle and drag their limbs during tasks that required fast forward movement (Figure 23). SG-fed animals exhibited other parkinsonian attributes as well. Two of 16 SG-fed animals exhibited rotational locomotion at each of the open field testing sessions. Rotational locomotion is often observed as a consequence of a unilateral lesion in the nigrostriatal system (Ungerstedt and Arbuthnott, 1970; Mura et al., 1998). The motor neuron counts conducted at both time points indicated that over the course of the 15 wk of SG feeding, neurons in the lumbar spinal cord were lost *en masse*. Yet the behavioural findings over the same period did not indicate such a drastic degeneration of motor neurons. However, as mentioned in the introduction, many other studies have observed significant neuronal disease in clinically undetectable states. In PD, greater than 80% degeneration of dopaminergic neurons from the SN must occur before a patient becomes symptomatic (McGeer et al., 1988). In the case of ALS, a minimum of a 70% decrease in alpha motor neurons is required before a patient becomes symptomatic (Arasaki and Tamaki, 1998). Nonetheless, the range of behavioural findings is consistent with detailed assays of the types of cells lost from the CNS. SG-exposed animals showed a marked loss of large α-motor neurons, and to a lesser degree, γ-motor neurons, and dopaminergic neurons. Even more

importantly, the progressive decline in performance on the behavioural tests and accumulating neuropathology resemble ALS-PDC, where it is thought that exposure to some factor(s) triggers a cascade of neurodegeneration that take many years to achieve clinical presentation (Kurland, 1988).

4.2.2 Modulation of survival and pro-apoptotic signals in response to SG-exposure

This study also investigated the response of motor neurons and non-motor neuronal populations to stress. SG-feeding was found to induce significant elevation of Hsp-70, ATF-3 and $pJun^{ser73}$ at 35 and 52 wk. In contrast, BSSG-feeding induced a statistically significant increase of Hsp-70 and ATF-3 only at 52 wk. As discussed previously (Chapter 1), Hsp-70 is up-regulated when cells become stressed and ATF-3 is a crucial determinant of cell mortality that depends on the ample activation of c-Jun for neuronal rescue and survival (Benn et al., 2002), which in turn is regulated by JNK, and when phosphorylated induces cells to undergo apoptosis (Ham et al., 1995). Thus, in the present study, by 17 wk post-SG-feeding, unlike in the case of BSSG where cells appeared to just be approaching the critical survival/repair-apoptosis threshold with concurrent up-regulation of a rescue chaperone, SG-feeding induced cells to cross this line accompanied by a significant up-regulation of ATF-3, fatal phosphorylation of c-Jun, and futile up-regulation of Hsp-70.

The results from the BSSG and SG *in vivo* studies indicate a differential expression in suppressors and instigators of neurodegeneration. Accordingly, these chaperones and transcription factors could serve as potential therapeutic targets for neurodegenerative disorders (Sherman and Goldberg, 2001; Muchowski and Wacker, 2005). This notion has been explored in a few disease models. In animal Alzheimer models, over-expression of Hsp-70 can rescue neurons from Aβ42 mediated toxicity. Another survival chaperone, Hsp-27 has been demonstrated to decrease the level of hyperphosphorylated Tau and decrease the incidence of Tau-mediated apoptosis (Shimura et al., 2004). Other studies have demonstrated the induction of the opposite phenomenon with gene

delivery. Knockdown of Hsp-70 and Hsp-90 by RNAi increases the accumulation of pathogenic Tau (Dou et al., 2003). In a *Drosophila* model of Parkinson's disease, expression of human Hsp-70 suppresses α-synuclein-mediated dopaminergic neuron toxicity (Auluck et al., 2002). Similarly, *in vitro*, Hsp-70 (Klucken et al., 2004) and Hsp-27 (Zourlidou et al., 2004) over-expression protects cells from α-synuclein-mediated toxicity. In ALS models, similar findings have been made. Intranuclear microinjection of the expression vectors for mutant SOD1 and Hsp-70 into primary cultured motor neurons reduces the toxicity of SOD1 and promotes motor neuron survival (Bruening et al., 1999). When both Hsp-27 and Hsp-70 were over-expressed, further reduction of the toxicity of SOD1 and protection of motor neurons was conferred (Patel et al., 2005). When the heat shock response, in particular the expression of Hsp-70 in the spinal cord, was induced in transgenic mice with arimoclomol, the behavioural phenotype, motor neuron numbers and survival period was improved (Kieran et al., 2004).

Again, as in the BSSG study, when metabolic activity was assessed in the CNS of SG-fed animals, a change in neuronal activity in response to SG was not detected. Here, again, I interpret the lack of difference in mitochondrial activity to storage temperature/time degradation of cytochrome c oxidase.

4.2.3 Dietary SG induced proteinopathy

Proteinopathy (or proteopathy) is the abnormal accumulation of proteins that occur in certain disease states (Walker and LeVine, 2002a). Proteinopathies occur in over 30 diseases and affect all types of tissue, including the CNS in neurological diseases such as Alzheimer's dementia, Parkinson's dementia and amyotrophic lateral sclerosis (Walker and LeVine, 2002b). Proteinopathies are aptly named since they involve a conformational change of some protein causing it to misfold, polymerize, aggregate, and/or to become resistance to clearance (Dobson and Karplus, 1999). Since all proteins share a common polypeptide backbone all proteins have the potential to misfold (Dobson and Karplus, 1999) yet only certain proteins have been implicated in proteinopathies. It has been

suggested that the instability or structural characteristics of certain proteins increases their likelihood to misconform (Carrell and Lomas, 1997a; Dobson, 1999). In nearly all cases, misconformation of proteins has resulted in an increase in beta-sheet structure (Carrell and Lomas, 1997a; Dobson and Karplus, 1999; Selkoe, 2003). Other structural modifications have been found to increase the tendency of certain proteins to self-assemble. Post-translational modifications, for example hyperphosphorylation, and changes in the primary amino acid sequence of the protein have been shown to expedite disease processes (Carrell and Lomas, 1997b; Dobson and Karplus, 1999; Walker and LeVine, 2002a).

TDP-43 is a nuclear DNA binding protein expressed ubiquitously in a wide range of tissues. It is thought to be involved in transcription repression as well as in the activation of exon skipping (Buratti and Baralle, 2001; Mercado et al., 2005). Currently, the physiological function of the protein is undefined but it has become well-established in the last several years that in normal conditions, TDP-43 is localized to the nucleus of neurons and sometimes in glial cells (Neumann et al., 2006, Kwong et al., 2007). TDP-43 has been identified as the pathologic protein common to most forms of frontotemporal lobar degeneration with ubiquinated inclusions (FTLD-U) and sporadic amyotrophic lateral sclerosis (Mackenzie et al., 2008). In these pathological conditions, TDP-43 is hyperphosphorylated and is found to co-localize with ubiquitin. Further, in such cells, nuclear TDP-43 staining is lost, raising the possibility that in such cells there is some degree of loss or disruption of nuclear function or cellular mechanisms (Arai et al., 2006; Neumann et al., 2006). Aberrant tau expression and aggregates in the form of neurofibrillary tangles (NFT) are key aspects of AD and ALS-PDC. NFTs are also prevalent in Chamorros asymptomatic for ALS-PDC (Kurland et al., 1994). Further, studies have also suggested that the TAU gene may increase susceptibility to ALS-PDC in concert with an exogenous, environmental factor (Poorkaj et al., 2001).

The proteino-pathology observed in the SG-fed mice was heterogeneous in that 25% of mice exhibited accumulation of pathological phosphorylated tau, a

different 25% of the cohort exhibited accumulation of pathological phosphorylated TDP-43, and the remaining showed no signs of either aggregates (Figure 37). The finding that the glucuronide of stigmasterol can induce pathological aggregation of two distinct types of proteins is quite remarkable as no other compound has been shown to induce such effects *in vivo*. In humans, neurological disorders that exhibit tau or TDP-43 pathological accumulations are considered separate diseases. However, the results seem to indicate that an SG-feeding induced tau and TDP-43 proteinopathies are part of a clinicopathological spectrum of disease. These results are consistent with the fact that a range of neurological diseases can manifest in a genetically diverse human population living in similar environments. These findings may be attributable to the fact that an out-bred strain of mice was chosen for the studies. Had an inbred strain of mice been chosen, I may not have observed either one or both forms of pathological protein aggregates.

4.3 Conclusions

The results of the present study further contribute to support the hypothesis that sterol glucosides form a primary basis for the observed behavioural and pathological outcomes observed in mice (Wilson et al., 2002a; Wilson et al., 2001; Wilson et al., 2004a) and in ALS-PDC, in both cases following consumption of washed cycad flour. The neurological outcomes in this study occurred over the course of many weeks and resemble the presumed long-term development of ALS-PDC in human patients. I note, however, that the behavioural deficits observed amongst both the SG- (and BSSG-) fed animals are not nearly as overt as observed in ALS-PDC patients and that the majority of the pathology was detected via quantitative screening suggesting that the two sacrifice time-points used in the present study are equivalent to the "early" stage of human ALS-PDC. It would be interesting to see whether surviving the BSSG and SG-fed animals for an additional period will result in the symptoms to progress further and resemble "full-blown" or "end-stage" ALS-PDC.

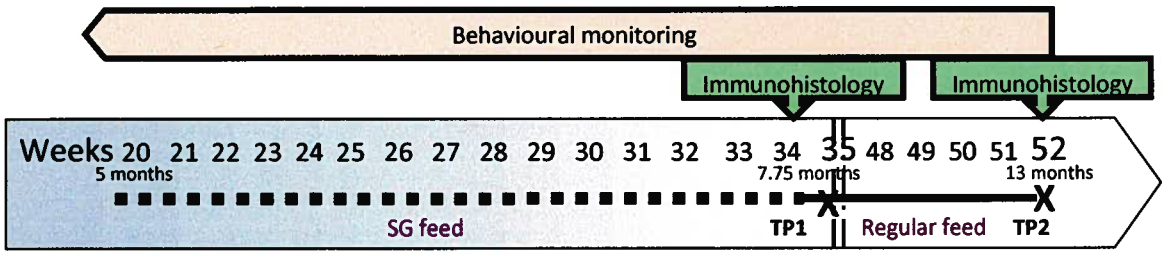

Figure 17. **Schematic depicting the timing of stigmasterol β-D-glucoside dietary exposure, animal sacrifice, histology and behavioural testing.**

Male, outbred CD-1 mice, 20 wk of age were fed SG-containing mouse chow pellets daily for 15 wk (dashed horizontal line). At 15 wk, half of the animals were sacrificed (X symbol), and the remaining SG-animals were switched back to a diet of standard mouse chow pellets (solid horizontal line), survived an additional 17 wk and sacrificed (X symbol). Animals were monitored behaviourally (orange) for the duration of the study and histological analysis (green) was conducted on tissue of animals 35 and 52 wk old.

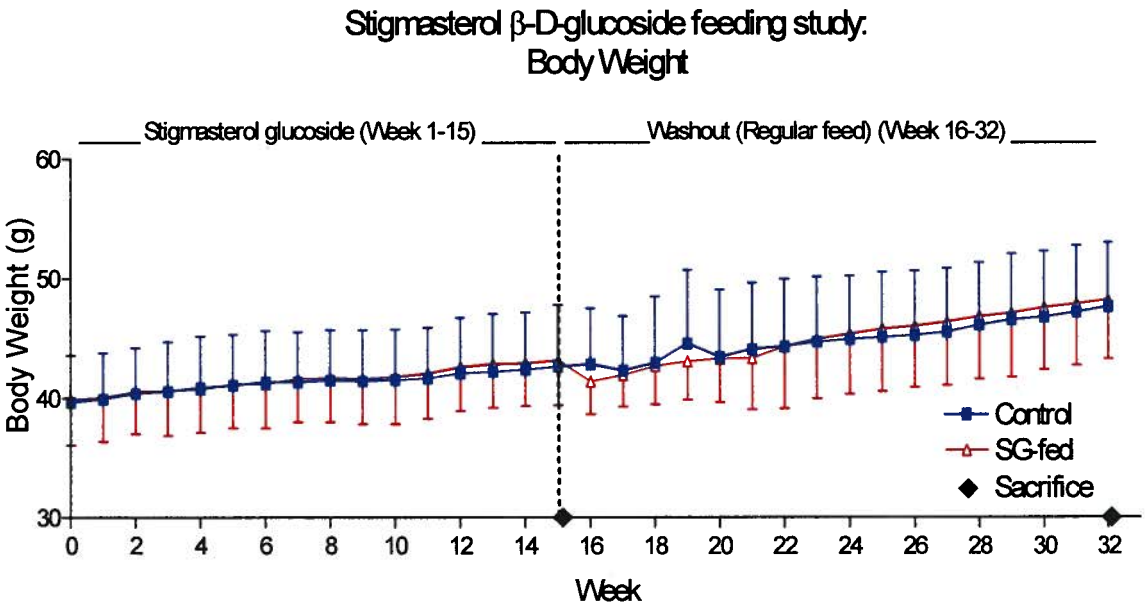

Figure 18. **Body weights of SG-fed animals and their age-matched controls.**

A comparison of weight values between control and SG-fed animals revealed that body weights are not significantly different between groups and increase steadily over-time.

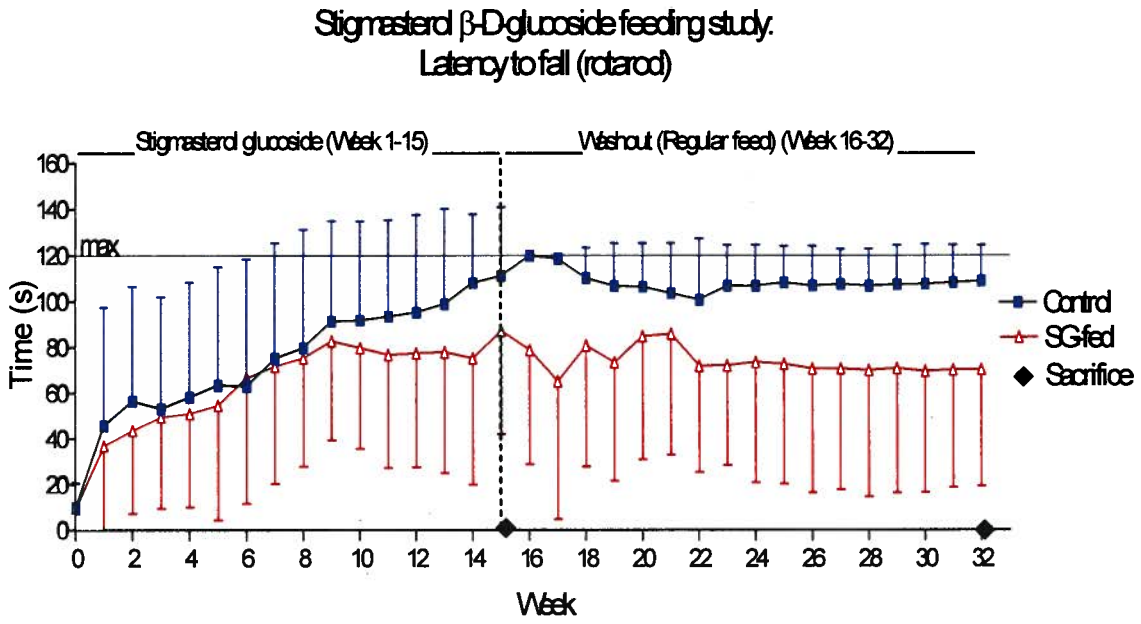

Figure 19. **SG-feeding reduces rotarod performance.**

The rotarod test was used for the duration of the study to monitor animals' motor coordination. SG-exposed animals demonstrated a trend in diminished performance on the rotarod but numbers did not reach statistical significance.

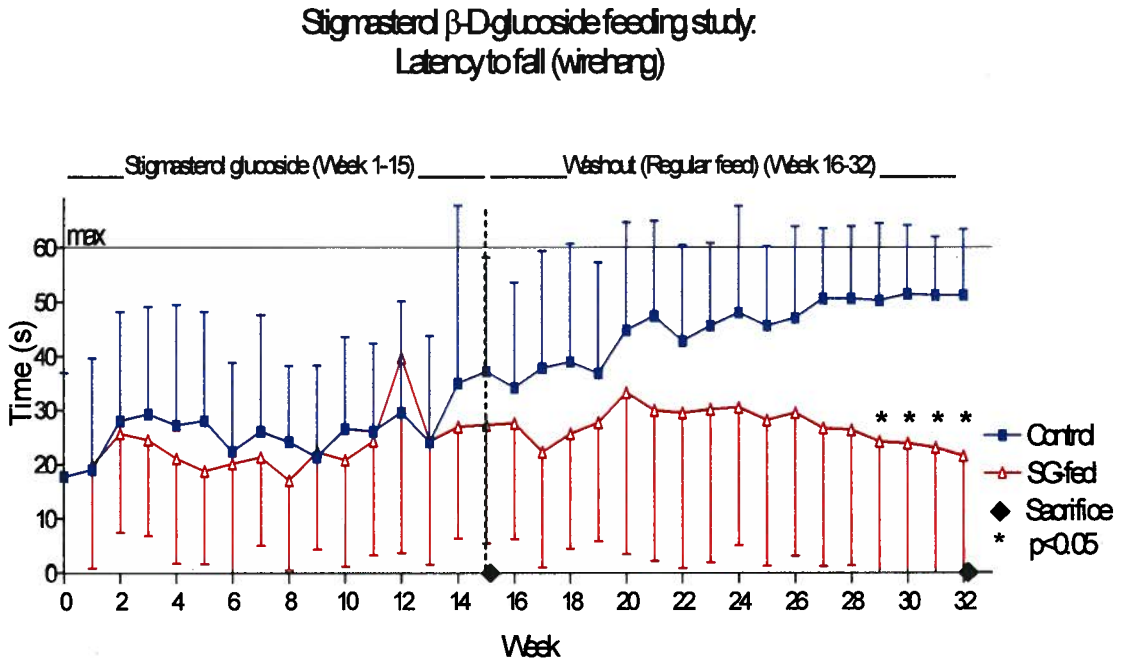

Figure 20. **SG-feeding reduces performance in a forelimb strength analysis test.**

The wirehang test was used to monitor muscle strength in SG-fed animals and their age-matched controls for the duration of the study. A decline in performance was evident prior to the first animal sacrifice (35 wk) and by fourteen wk post-feeding, the difference in performance was statistically significant (t-test: *$p<0.05$) and remained so until the time the remaining mice were sacrificed.

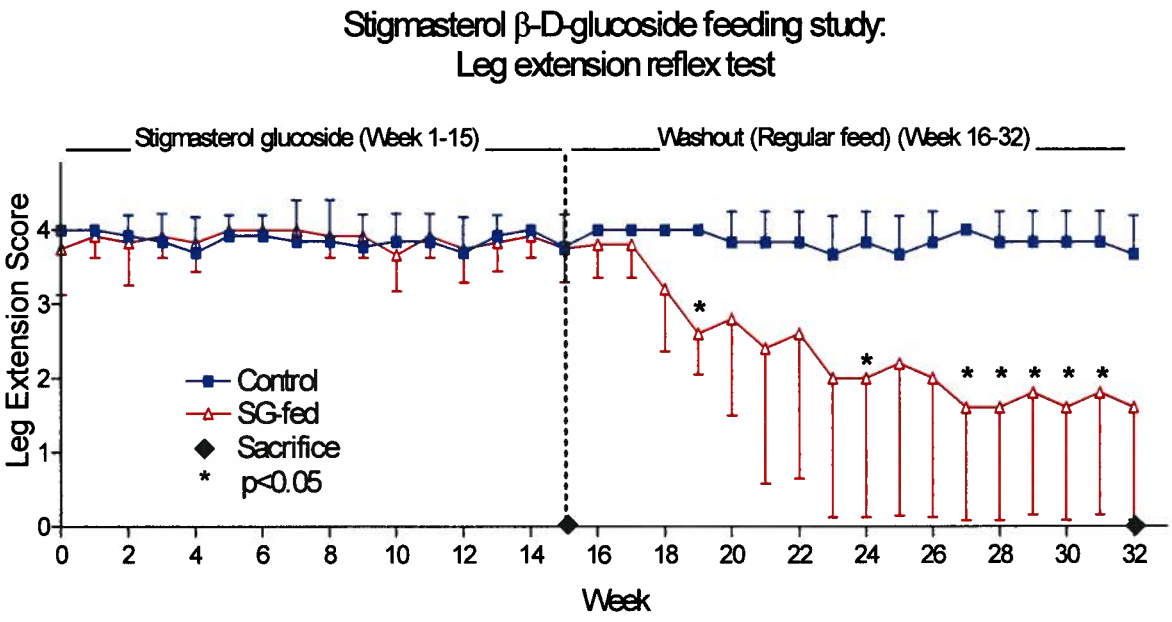

Figure 21. **SG-feeding induces a decline in performance on the leg extension reflex test.**

The leg extension reflex test was used to monitor hind limb reflex in SG-exposed animals and their age-matched controls for the duration of the study. A steady decline in performance was evident amongst SG-fed animals soon after the first animal sacrifice (35 wk). Time points at which the performance was found to be significant is marked with an asterisk (t-test: *$p<0.05$). In contrast, control animals showed no disturbance in hind limb reflex for the duration of the study.

A

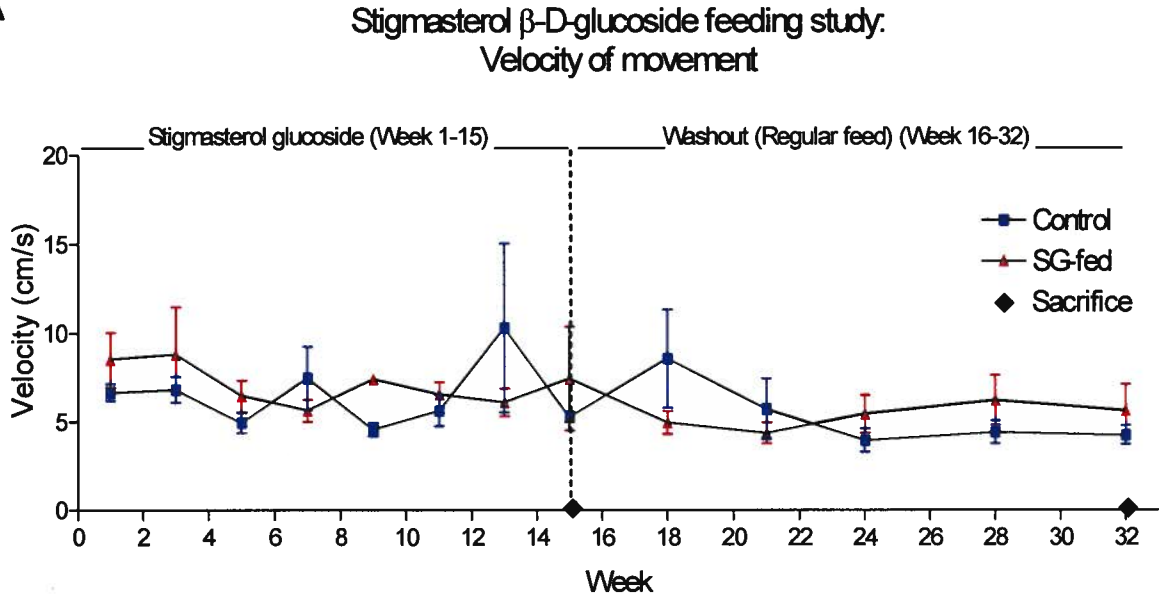
Stigmasterol β-D-glucoside feeding study:
Velocity of movement
Stigmasterol glucoside (Week 1-15)
Washout (Regular feed) (Week 16-32)
Control
SG-fed
Sacrifice
Velocity (cm/s)
Week

B

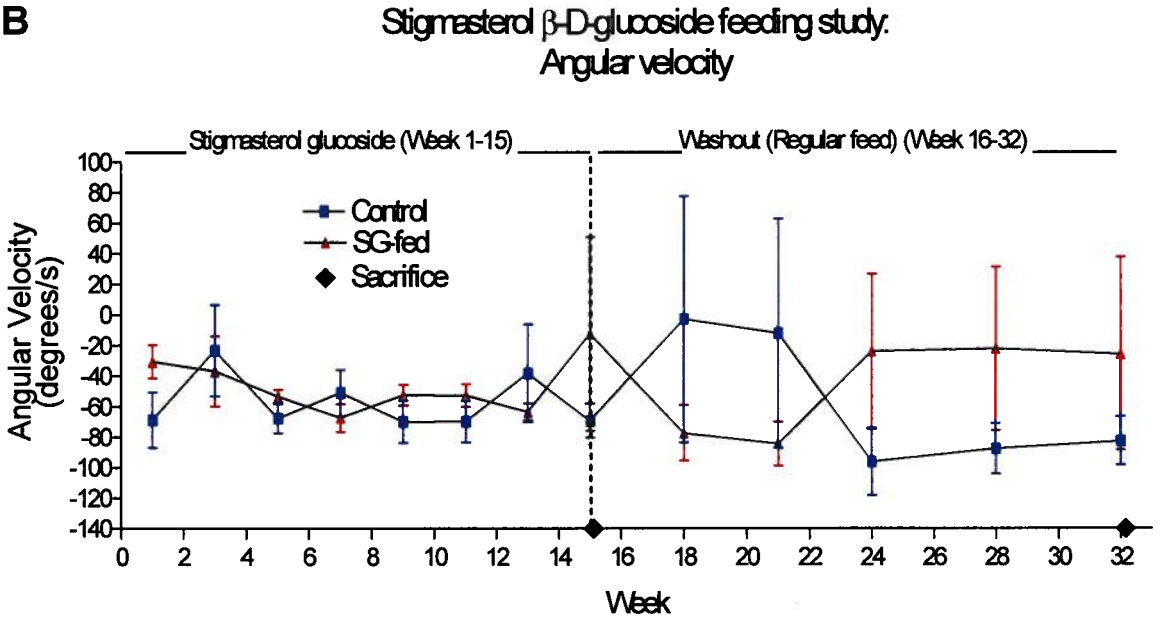
Stigmasterol β-D-glucoside feeding study:
Angular velocity
Stigmasterol glucoside (Week 1-15)
Washout (Regular feed) (Week 16-32)
Control
SG-fed
Sacrifice
Angular Velocity (degrees/s)
Week

C

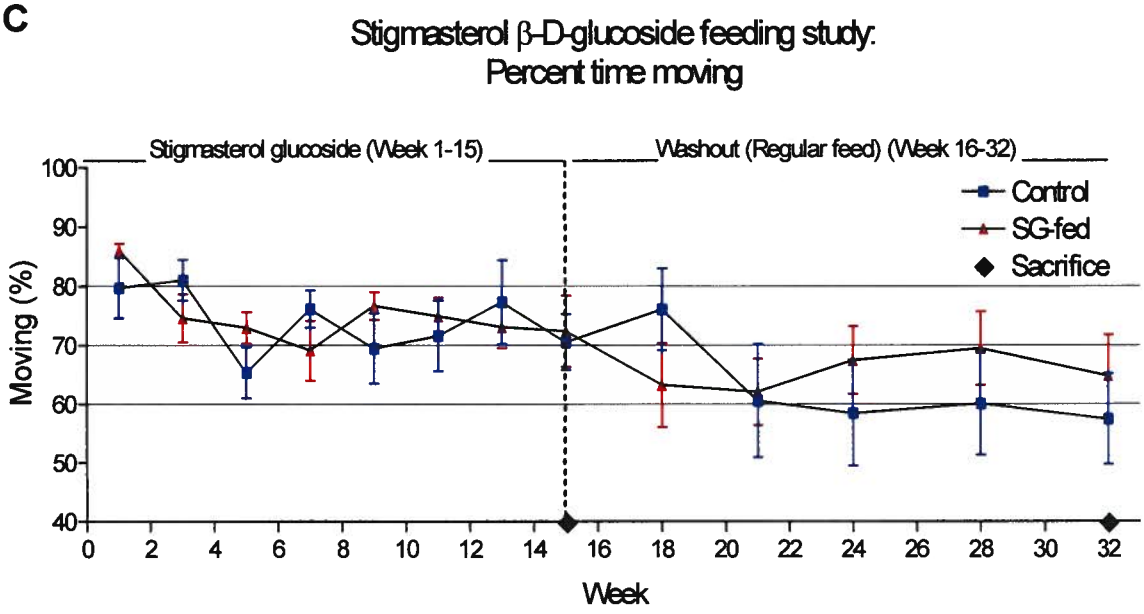
Stigmasterol β-D-glucoside feeding study:
Percent time moving
Stigmasterol glucoside (Week 1-15)
Washout (Regular feed) (Week 16-32)
Control
SG-fed
Sacrifice
Moving (%)
100
90
80
70
60
50
40
0
2
4
6
8
10
12
14
16
18
20
22
24
26
28
30
32
Week

D

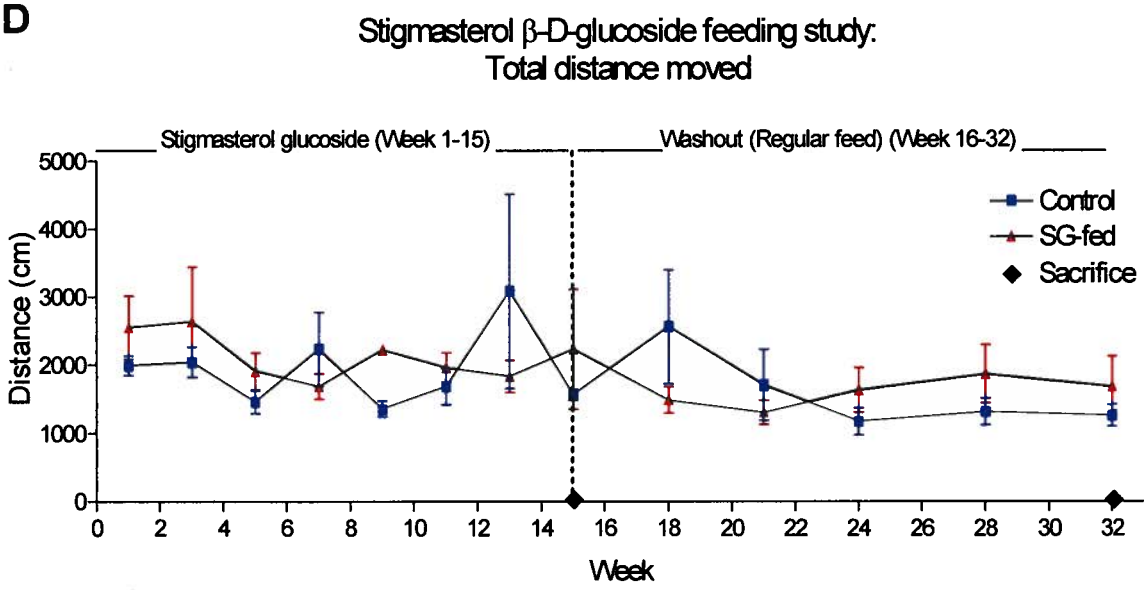
Stigmasterol β-D-glucoside feeding study:
Total distance moved
Stigmasterol glucoside (Week 1-15)
Washout (Regular feed) (Week 16-32)
Control
SG-fed
Sacrifice
Distance (cm)
5000
4000
3000
2000
1000
0
0
2
4
6
8
10
12
14
16
18
20
22
24
26
28
30
32
Week

E

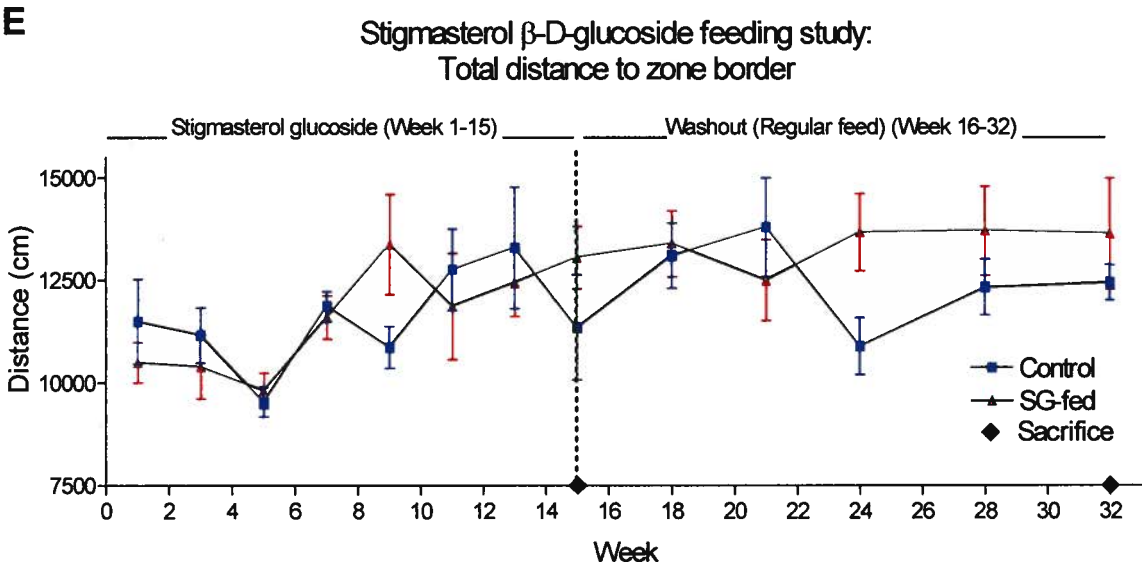
Stigmasterol β-D-glucoside feeding study:
Total distance to zone border
Stigmasterol glucoside (Week 1-15)
Washout (Regular feed) (Week 16-32)
Distance (cm)
15000
12500
10000
7500
0 2 4 6 8 10 12 14 16 18 20 22 24 26 28 30 32
Week
Control
SG-fed
Sacrifice

F

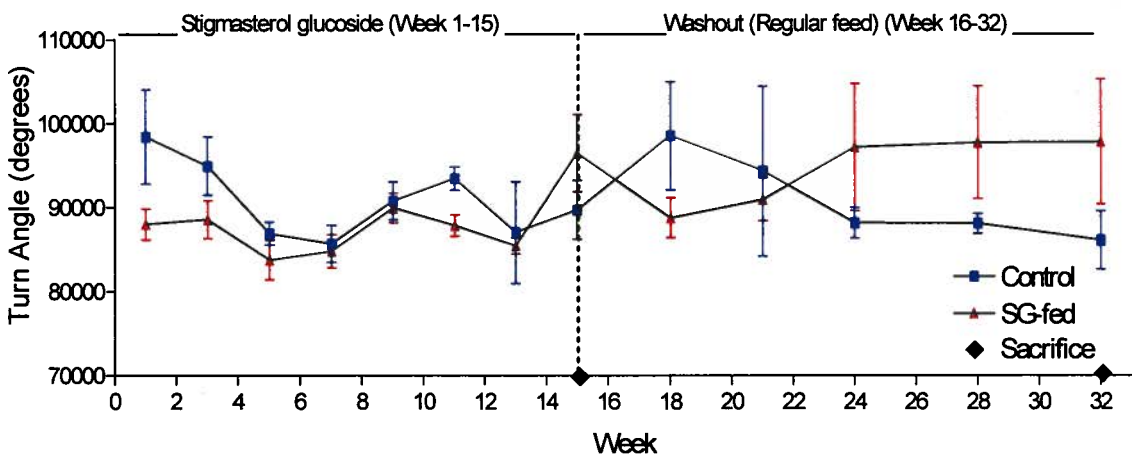
Stigmasterol β-D-glucoside feeding study:
Total turn angle
Stigmasterol glucoside (Week 1-15)
Washout (Regular feed) (Week 16-32)
Turn Angle (degrees)
110000
100000
90000
80000
70000
0 2 4 6 8 10 12 14 16 18 20 22 24 26 28 30 32
Week
Control
SG-fed
Sacrifice

Figure 22. **Open field test performances reveal a propensity amongst SG-fed animals to be more hyperactive, anxious, and rotate more frequently at tighter angles.**

SG-fed mice showed a trend in greater general movement velocity (A), angular velocity (B), percent of time spent moving (C), and total distance travelled (D) compared to age-matched controls, as measured by an automated open field camera and analysis program. SG-fed animals also showed a propensity to stay away from the periphery of the arena, which is indicative of anxiety (E) and spinning behaviour at tight angles (F). The Student's t-test did not reveal a statistically significant intergroup difference in any of the open field testing variables.

A

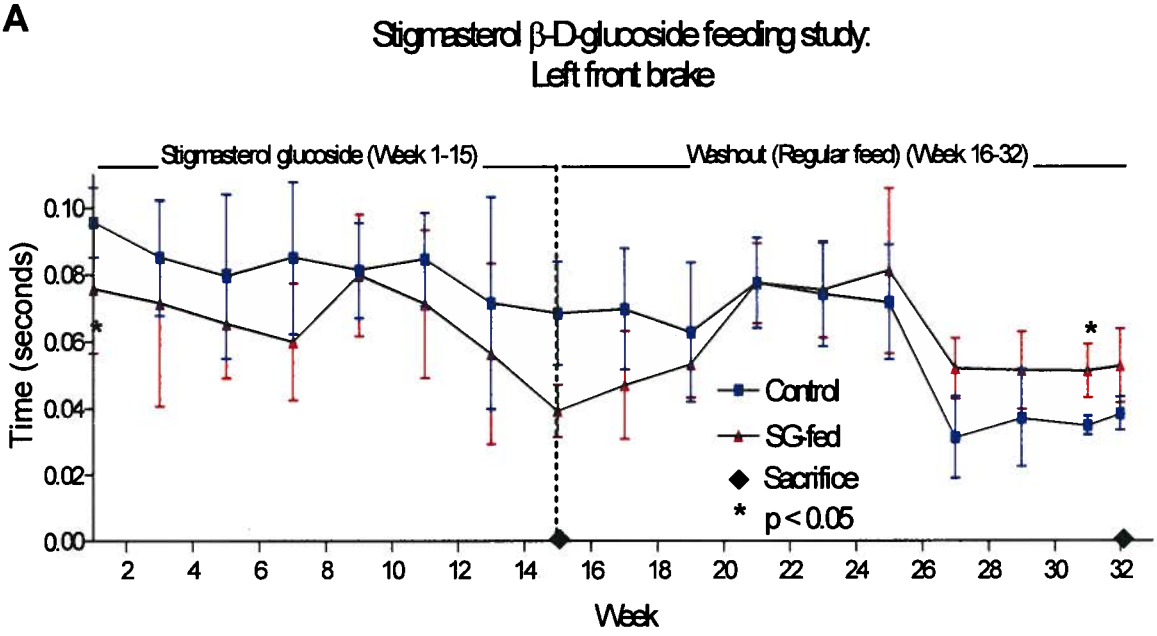
Stigmasterol β-D-glucoside feeding study:
Left front brake
Stigmasterol glucoside (Week 1-15)
Washout (Regular feed) (Week 16-32)
Time (seconds)
0.10
0.08
0.06
0.04
0.02
0.00
2 4 6 8 10 12 14 16 18 20 22 24 26 28 30 32
Week
Control
SG-fed
Sacrifice
* p < 0.05

B

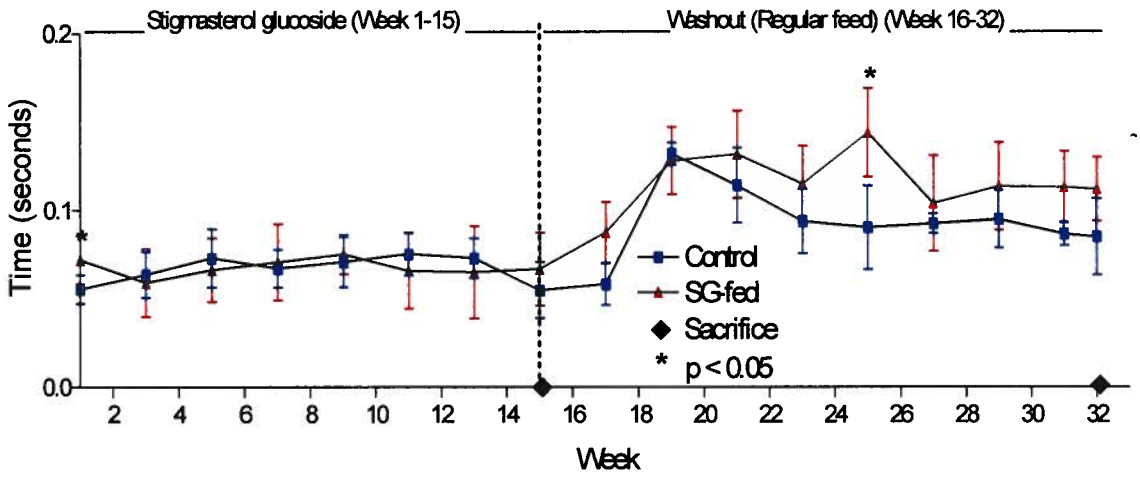
Stigmasterol β-D-glucoside feeding study:
Left front propel
Stigmasterol glucoside (Week 1-15)
Washout (Regular feed) (Week 16-32)
Time (seconds)
0.2
0.1
0.0
2 4 6 8 10 12 14 16 18 20 22 24 26 28 30 32
Week
Control
SG-fed
Sacrifice
* p < 0.05

C

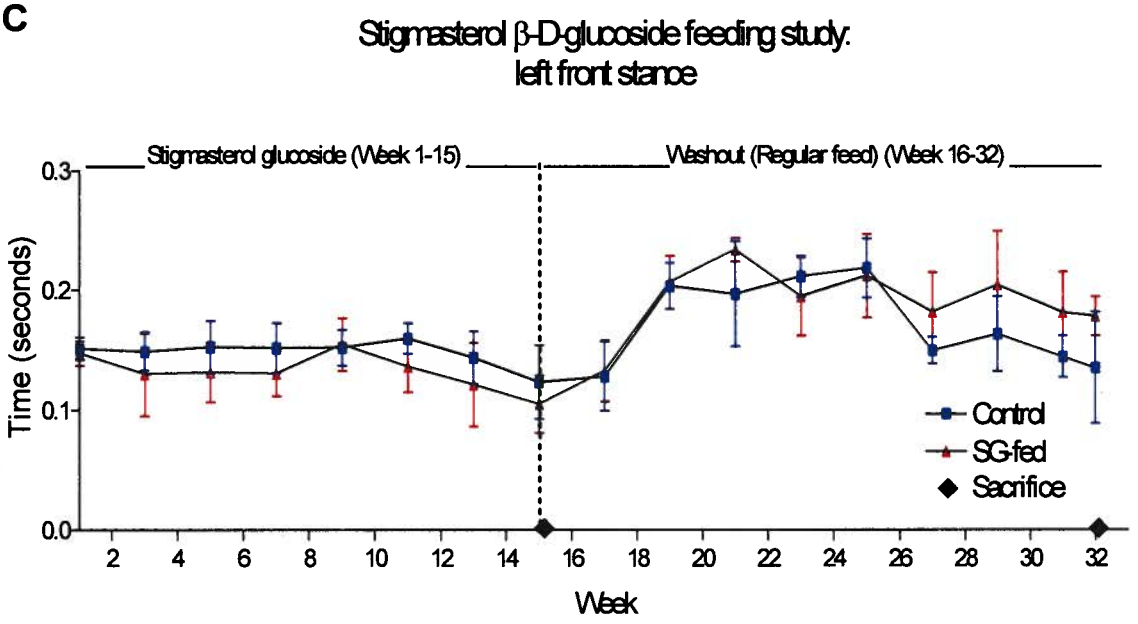
Stigmasterol β-D-glucoside feeding study:
left front stance
Stigmasterol glucoside (Week 1-15)
Washout (Regular feed) (Week 16-32)
Time (seconds)
0.3
0.2
0.1
0.0
2
4
6
8
10
12
14
16
18
20
22
24
26
28
30
32
Week
Control
SG-fed
Sacrifice

D

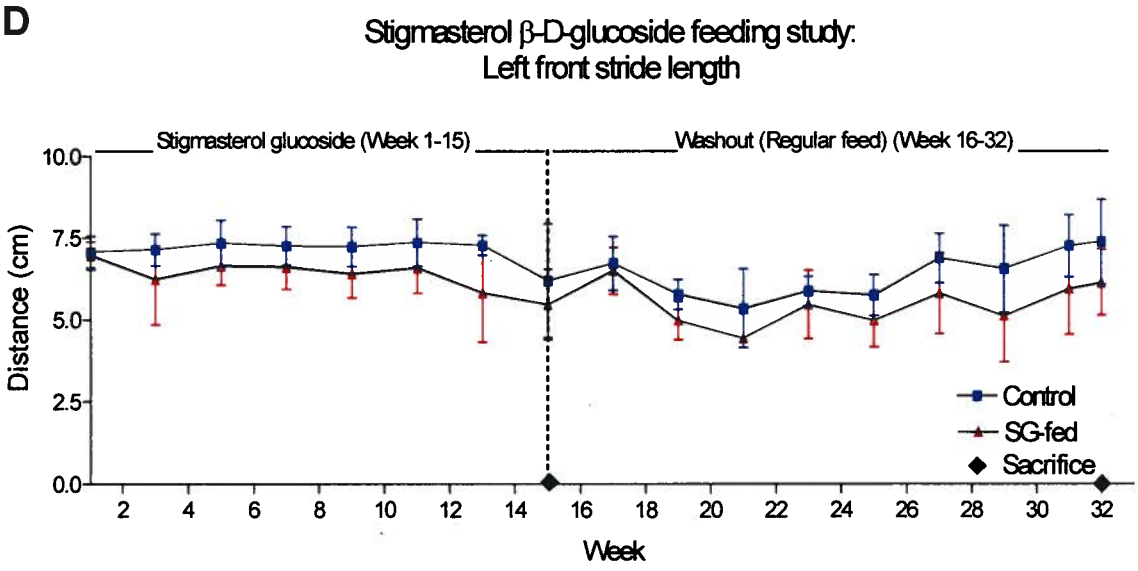
Stigmasterol β-D-glucoside feeding study:
Left front stride length
Stigmasterol glucoside (Week 1-15)
Washout (Regular feed) (Week 16-32)
Distance (cm)
10.0
7.5
5.0
2.5
0.0
2
4
6
8
10
12
14
16
18
20
22
24
26
28
30
32
Week
Control
SG-fed
Sacrifice

E

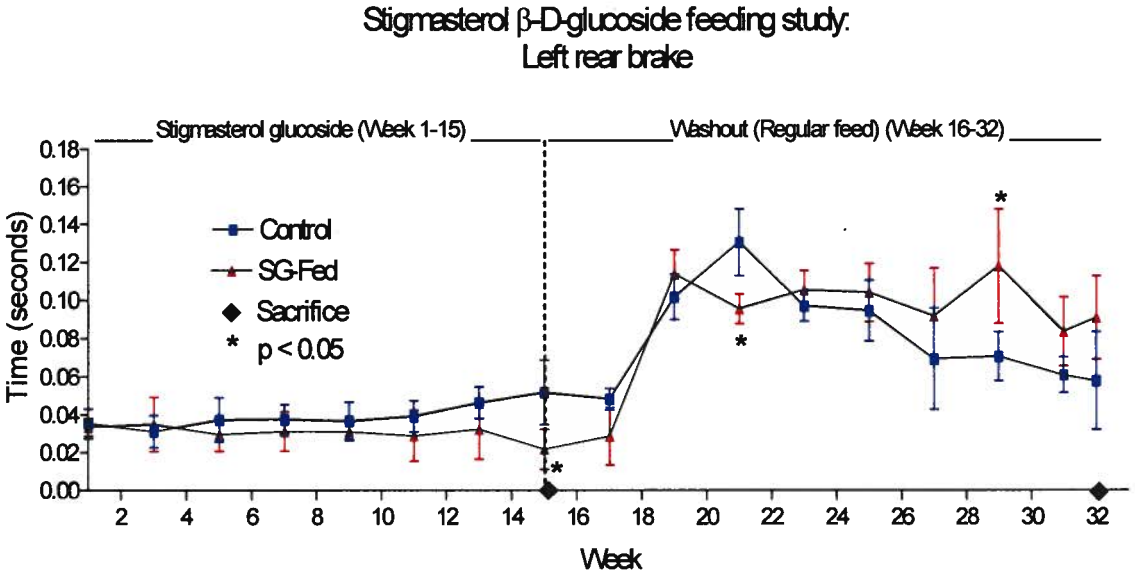
Stigmasterol β-D-glucoside feeding study:
Left rear brake
Stigmasterol glucoside (Week 1-15)
Washout (Regular feed) (Week 16-32)
Time (seconds)
Week
Control
SG-Fed
Sacrifice
* p < 0.05

F

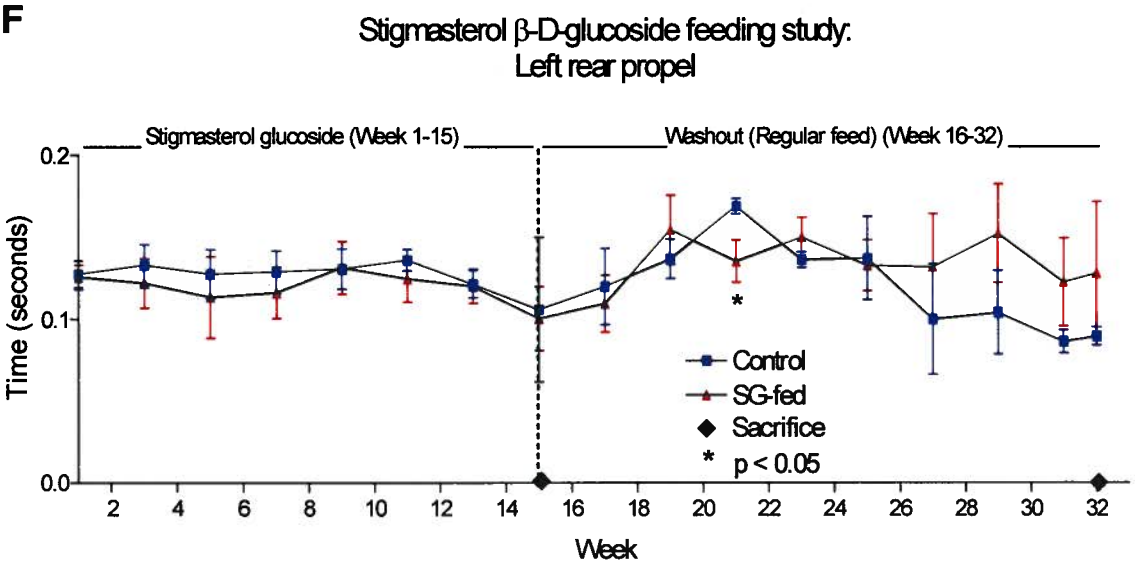
Stigmasterol β-D-glucoside feeding study:
Left rear propel
Stigmasterol glucoside (Week 1-15)
Washout (Regular feed) (Week 16-32)
Time (seconds)
Week
Control
SG-fed
Sacrifice
* p < 0.05

G

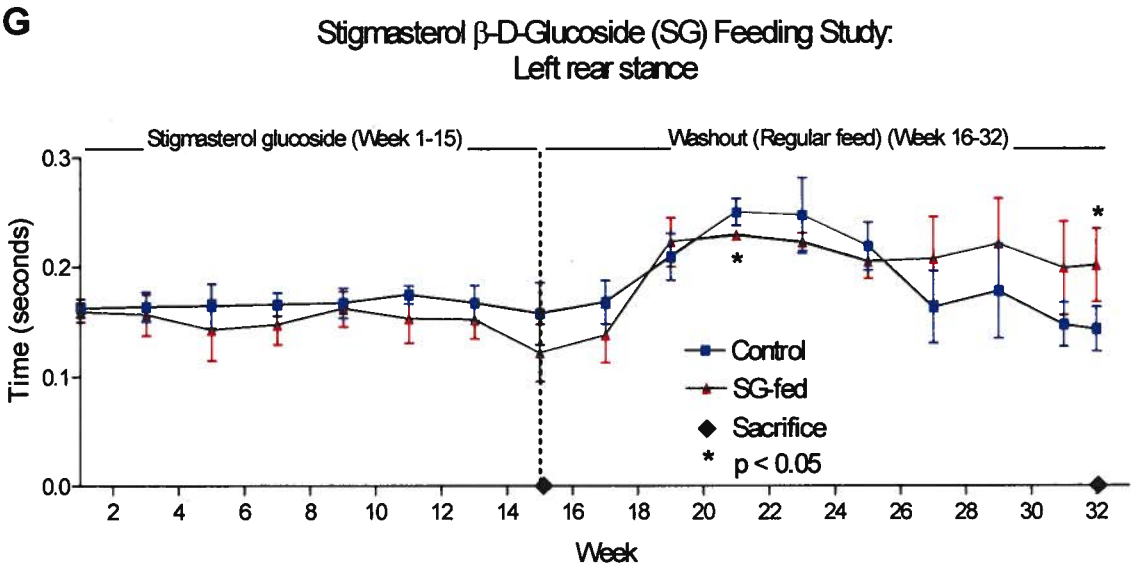
Stigmasterol β-D-Glucoside (SG) Feeding Study:
Left rear stance
Stigmasterol glucoside (Week 1-15)
Washout (Regular feed) (Week 16-32)
Time (seconds)
0.0
0.1
0.2
0.3
2
4
6
8
10
12
14
16
18
20
22
24
26
28
30
32
Week
Control
SG-fed
Sacrifice
* p < 0.05
*
*

H

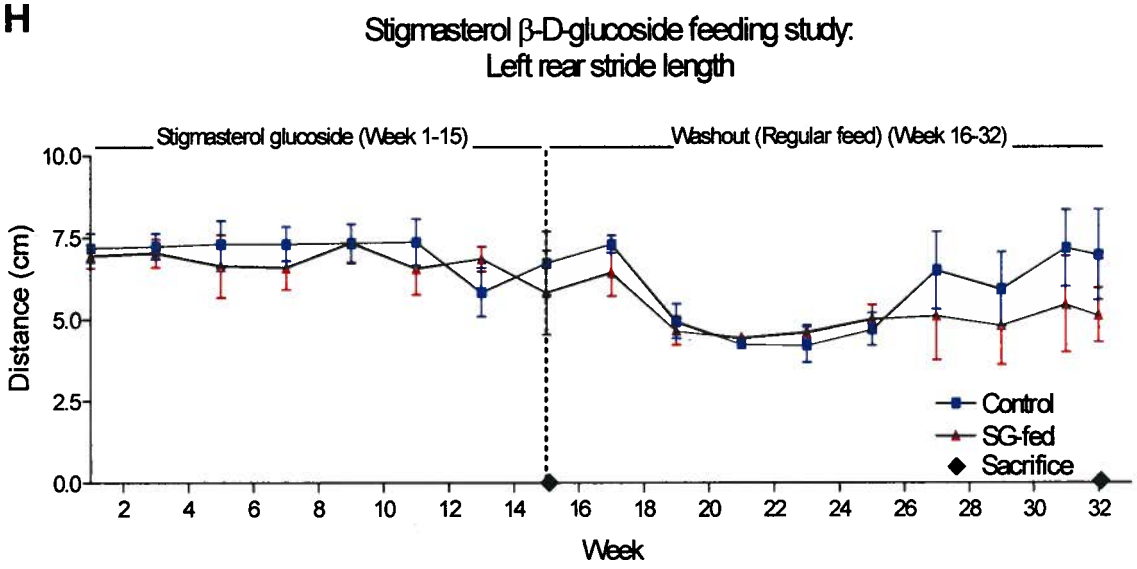
Stigmasterol β-D-glucoside feeding study:
Left rear stride length
Stigmasterol glucoside (Week 1-15)
Washout (Regular feed) (Week 16-32)
Distance (cm)
0.0
2.5
5.0
7.5
10.0
2
4
6
8
10
12
14
16
18
20
22
24
26
28
30
32
Week
Control
SG-fed
Sacrifice

I

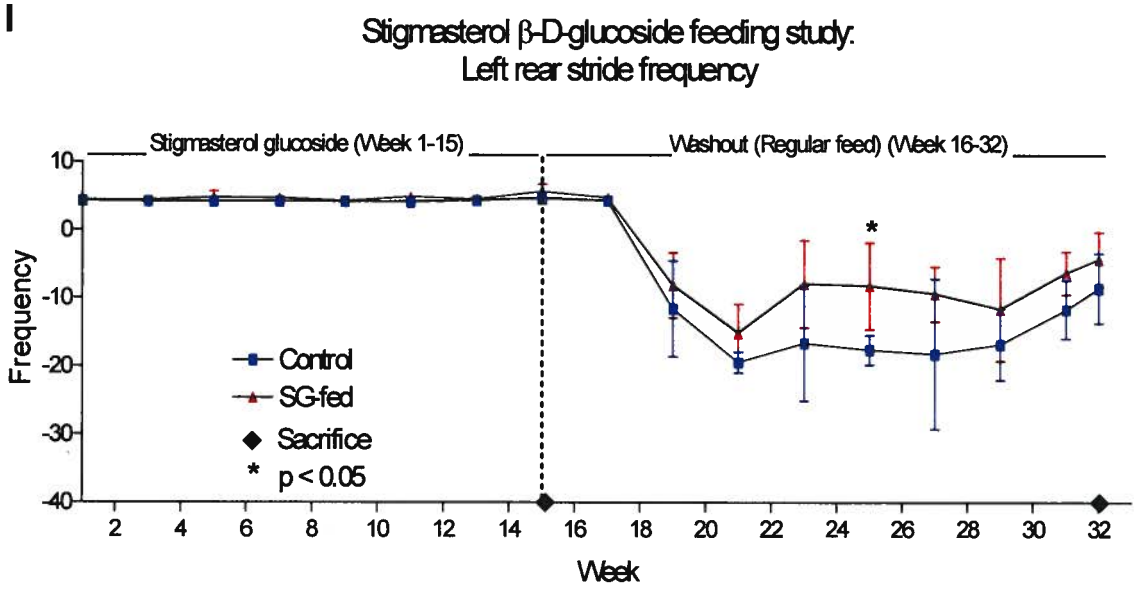

Figure 23. **Gait indices of SG-fed mice and their age-matched controls.**

Gait indices were obtained with computer-assisted vertical plane videography system and analysis software. SG-fed animals showed a decline in motor response and control which manifested as an increase in time required for an animal to brake with forelimbs (A) or hind limbs (E) or initiate propulsion (or forward movement) with either forelimb (B) or hind limbs (F). SG-fed animals exhibited longer stance durations in both the forelimbs and hind limbs (C, G respectively) but took shorter strides (D, H). As a result of the shorter stride lengths, SG-fed animals required a greater number of steps (I) to keep up with the standard belt speed of 30 rpm. For clarity, graphical data pertaining to the fore limb and hind limb are shown here. For a complete listing, please see the Appendix.

A

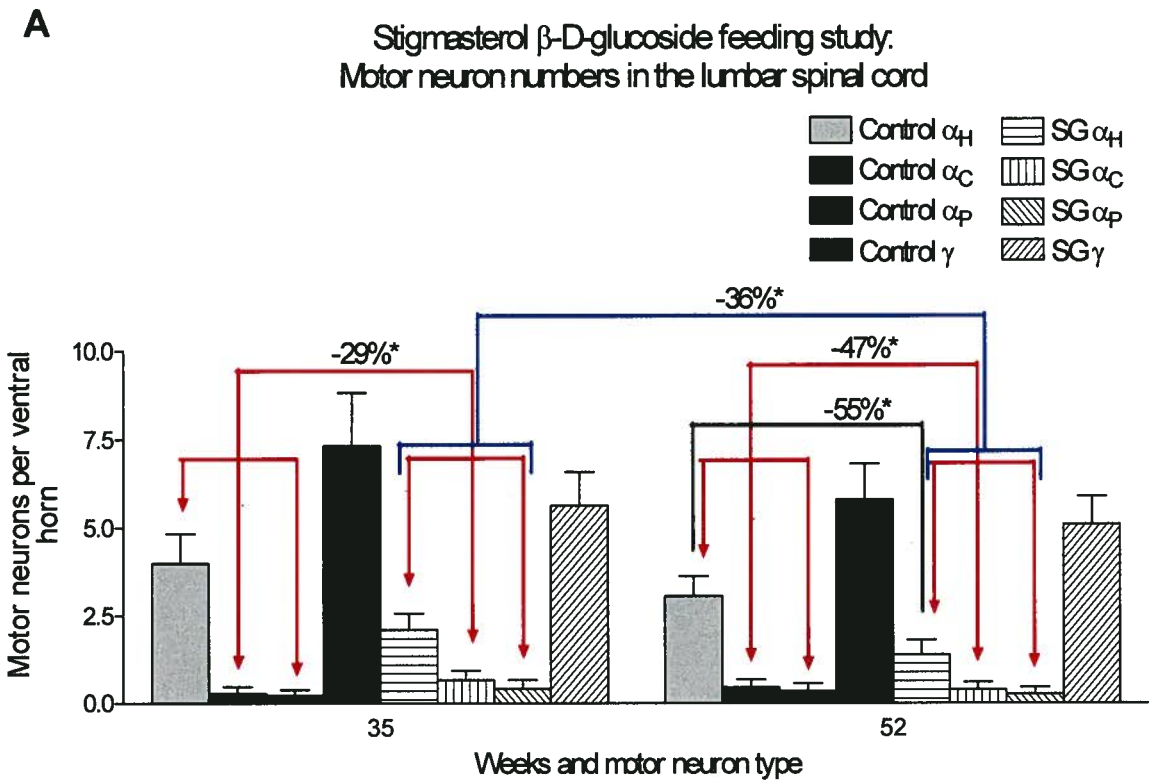
Stigmasterol β-D-glucoside feeding study:
Motor neuron numbers in the lumbar spinal cord
Control α_H
Control α_C
Control α_P
Control γ
SG α_H
SG α_C
SG α_P
SG γ
-36%*
-29%*
-47%*
-55%*
Motor neurons per ventral horn
10.0
7.5
5.0
2.5
0.0
35
52
Weeks and motor neuron type

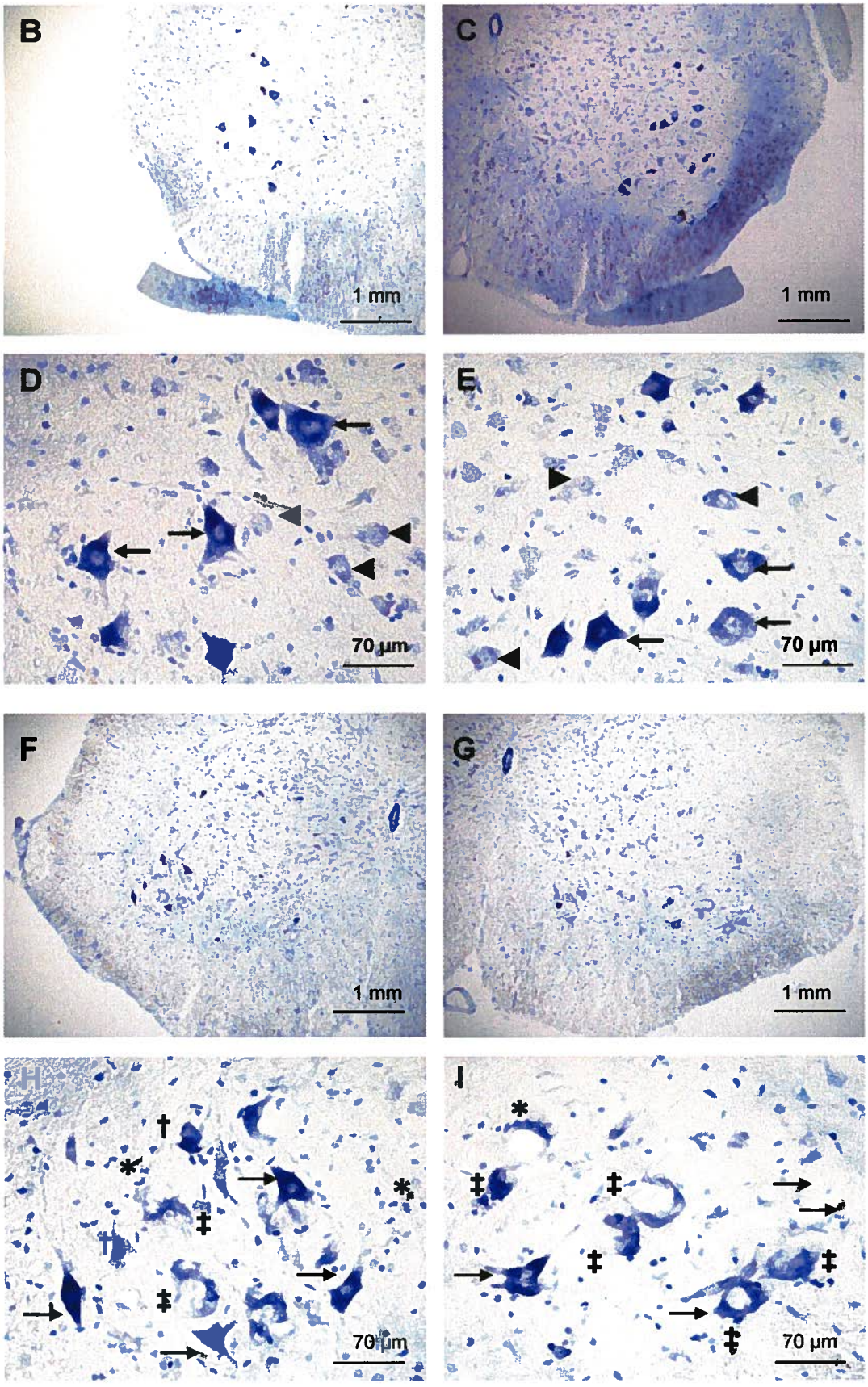
B
1 mm
C
1 mm
D
70 µm
E
70 µm
F
1 mm
G
1 mm
H
70 µm
I
70 µm

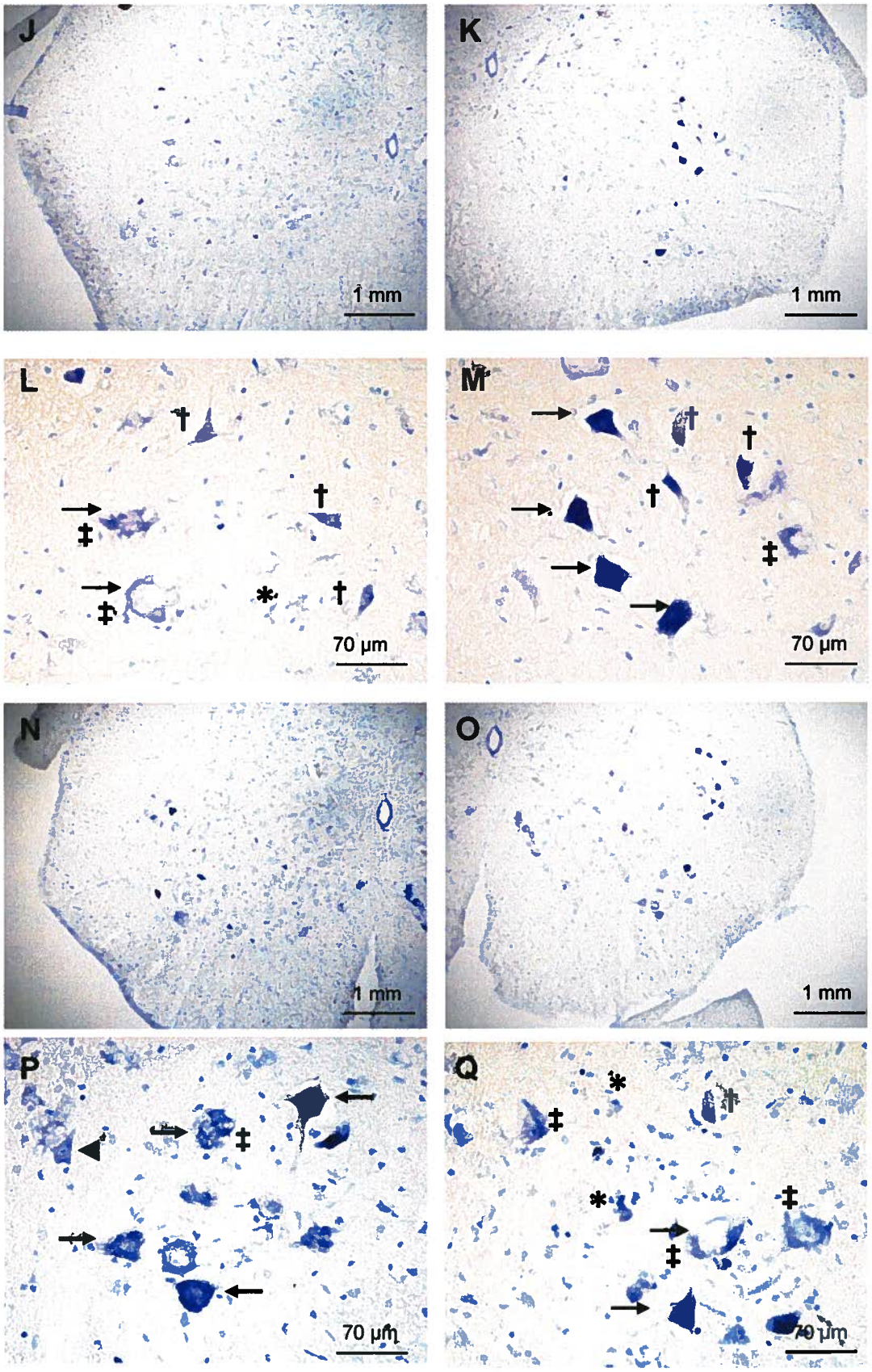
J
1 mm
K
1 mm
L
70 µm
M
70 µm
N
1 mm
O
1 mm
P
70 µm
Q
70 µm

Figure 24. **Motor neuron counts following SG-feeding.**

Motor neurons were differentiated with cresyl violet for Nissl bodies. Lumbar spinal cord α- and γ-motor neuron counts were conducted at 35 and 52 wk (A). Motor neurons were sub-grouped into those with a normal, healthy appearance (subscript "H"), those that were chromatolytic (subscript "C") and those that were pyknotic (subscript "p") (please see Chapter 2 for detailed classification criteria). At both 35 and 52 wk, the control group was observed to have numerous healthy α- and γ- motor neurons in the ventral horn of the lumbar spinal cord. With the detailed motor neuron counts, statistical significance was detected between the number of "healthy" α- motor neurons between the control and SG-fed group at 52 wk (t-test: -55%, $p<0.05$) only (A). When a statistical analysis was conducted between the total number of α-motor neurons between groups, a significant difference was detected at each of the time points (t-test at 35 wk: -29%, $*p<0.05$; t-test at 52 wk: -47%, $*p<0.05$; red lines indicate subcategories that were grouped to obtain a α-motor neuron "total"). Further, the SG-fed group was found to undergo a significant decline in the total number of α-motor neurons between 35 and 52 wk (t-test: -36%, $*p<0.05$; blue lines indicate the summation of subgroups in the graph). Representative micrographs of a control group animal lumbar spinal cord (ventral horn) exhibiting normal α- and γ-motor neuron quantity, distribution and morphology at 35 wk (B-E) and at 52 wk (J-M) are shown. Equivalent sections of an SG-fed mouse at 35 wk (F-I) and at 52 wk (N-Q) are also shown. Arrows point to α-motor neurons (35-50 μm in length) and arrow heads point to γ-motor neurons (<35 μm in length). SG-fed animals had more motor neurons in various states of degeneration compared to age-matched controls. Glial cell clustering and neuronophagic foci (asterisk: *), chromatolysis (dagger: †) and pyknosis (double dagger: ‡) were visible in SG-exposed animal tissues at both 35 and 52 wk. By 52 wk, the decrease in the number of α- and γ-motor neurons was more pronounced and gliosis at the ventral border of the ventral horns of the lumbar spinal cord. Empty beds encircled by high density clusters of glial cells that were once presumably occupied by α-motor neurons were found scattered throughout the ventral horn at the latter time point. Images were captured using a light microscope under a 20x (panels B, C, F, G, J, K, N, O) or a 40x (D, E, H, I, L, M, P, Q) objective lens. Scale bar=1mm (panels B, C, F, G, J, K, N, O) or 50 μm (D, E, H, I, L, M, P, Q).

A

Stigmasterol β-D-glucoside feeding study:
Choline acetyl transferase positive cells in
the ventral horn of the lumbar spinal cord

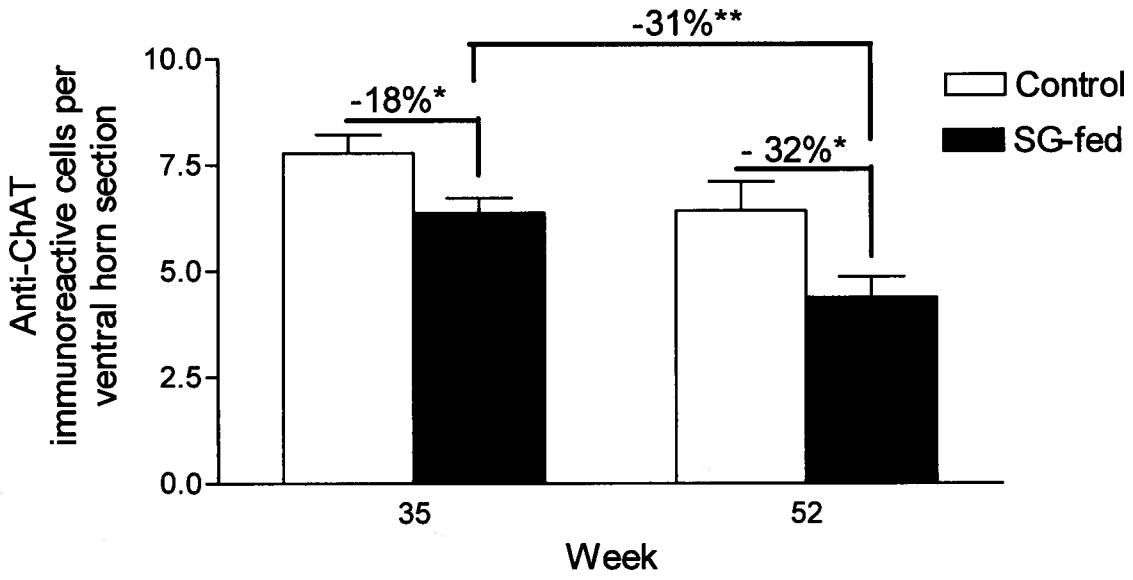

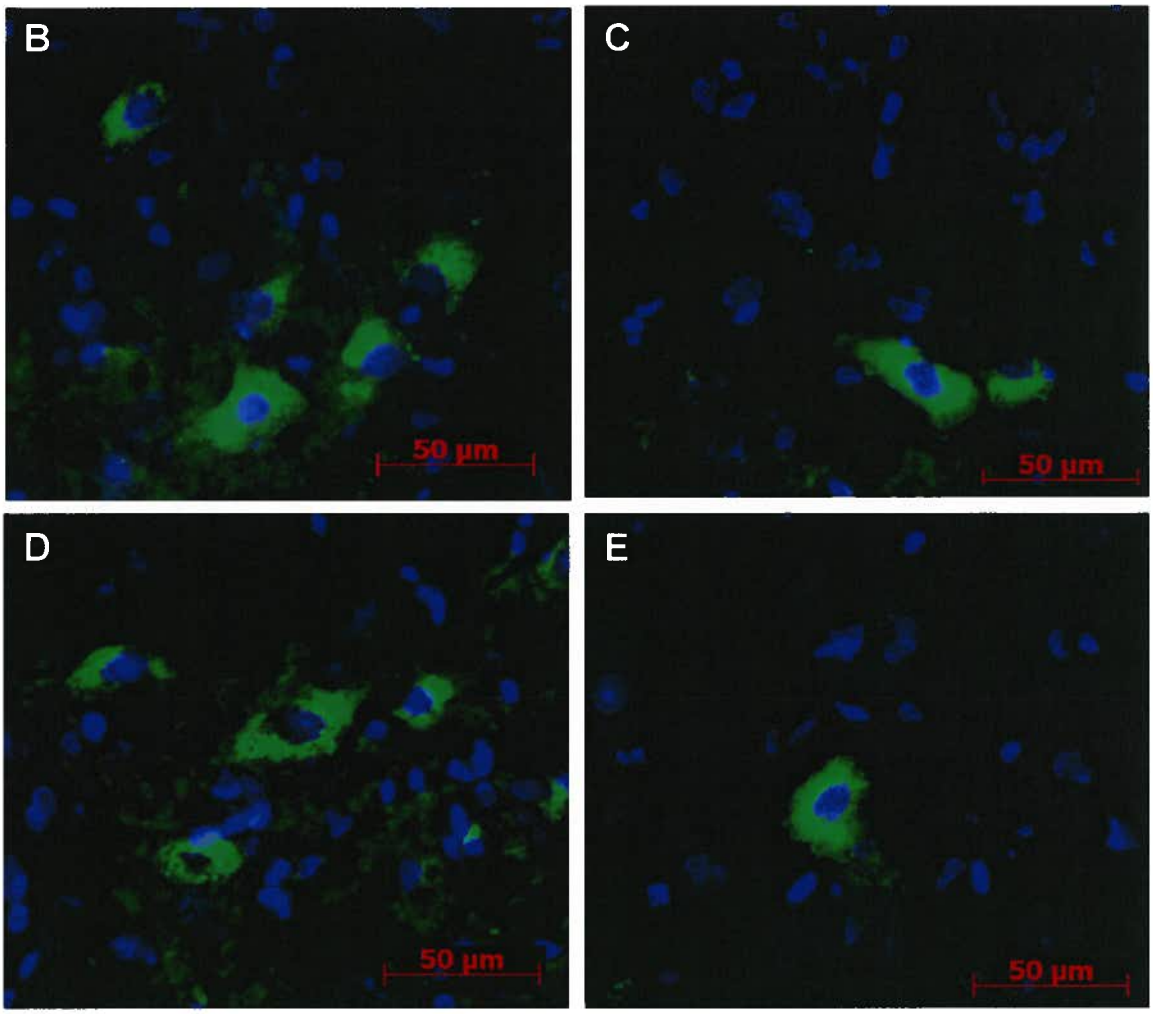

Figure 25. **Cholinergic motor neurons in the spinal cord of SG-fed mice.**

Anti-choline acetyl transferase (ChAT) immunoreactive cells were counted as cholinergic cells. Quantification anti-ChAT labelling in the ventral horn of the lumbar spinal cord revealed a significant difference between the control and SG-fed groups at 35 and 52 wk. SG-fed animals had 18% (t-test: *$p<0.05$) and 32% (t-test: *$p<0.05$) fewer cholinergic neurons at 35 and 52 wk, respectively (A). Further, the SG-fed animals experienced a significant decrease in the number of cholinergic neurons between 35 and 52 wk (t-test: -31%, *$p<0.05$). Representative micrographs of anti-ChAT labelled cells (red) with neuronal labelling (DAPI, blue) in control (B) and SG-fed (C) mice at 35 wk show normal, polygonal, even labelling of cholinergic cells. Micrographs of control (D) and SG-fed mice (E) at 52 wk also show normal morphology of cells. Images were captured using a fluorescence microscope under a 40x objective lens. Scale bar=50 µm.

A

Stigmasterol β-D-glucoside feeding study:
Number of cells expressing Hsp-70 in the ventral horn of the lumbar spinal cord

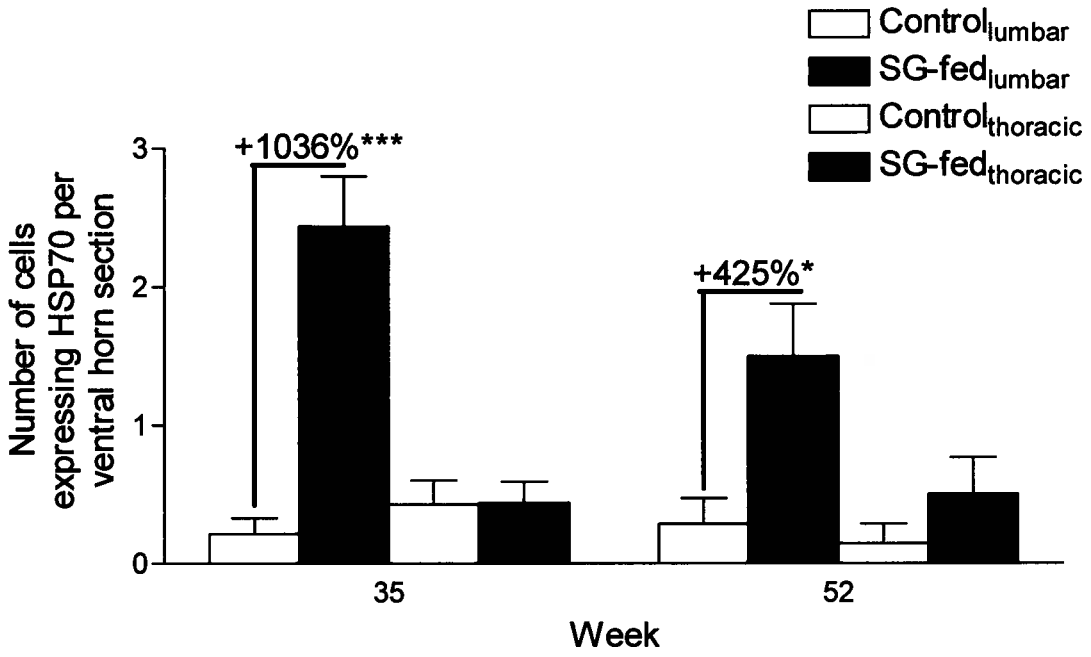

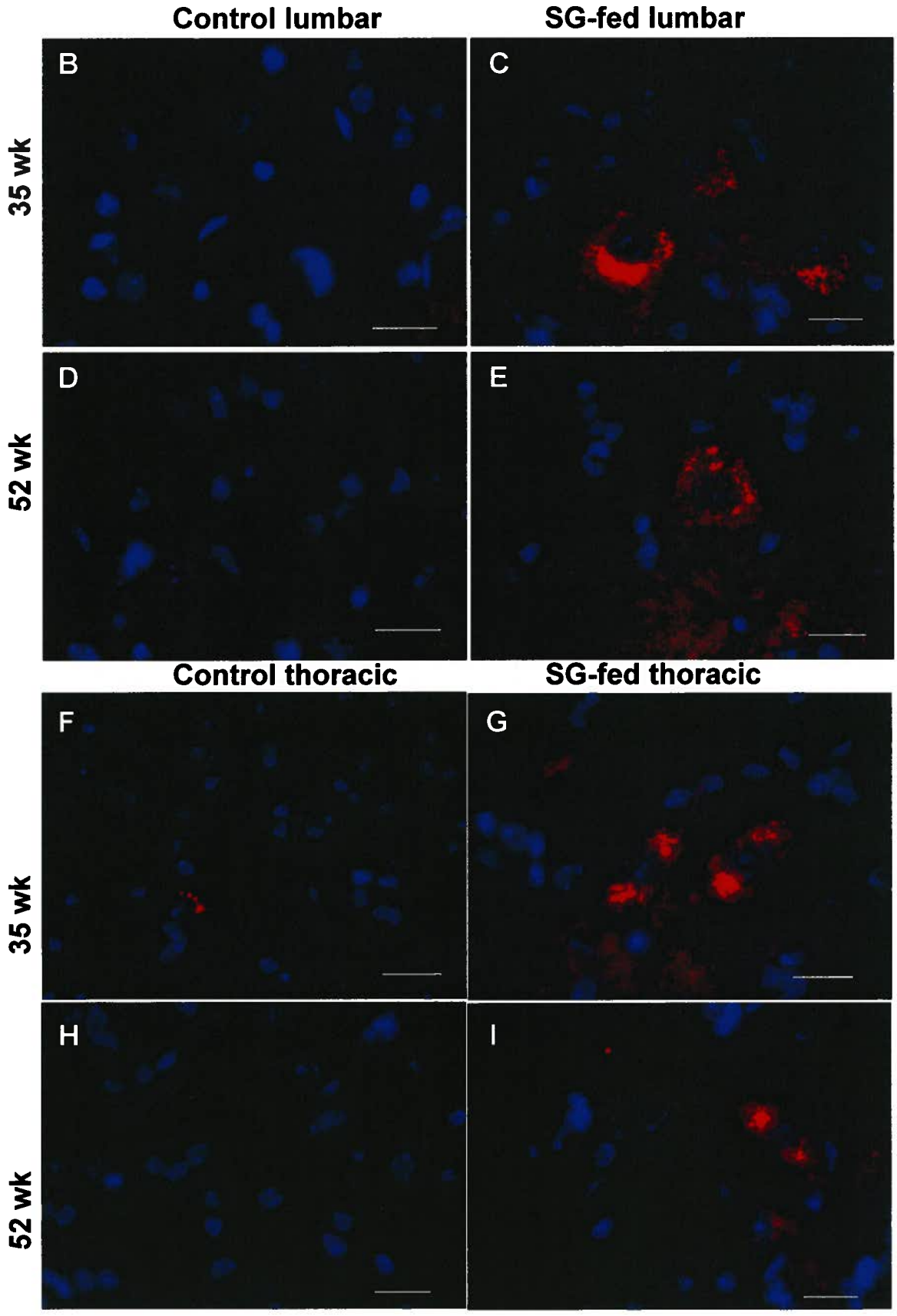
Control lumbar
SG-fed lumbar
B
C
35 wk
D
E
52 wk
Control thoracic
SG-fed thoracic
F
G
35 wk
H
I
52 wk

Figure 26. **Heat shock protein-70 labelling in the lumbar and thoracic spinal cord of SG-fed mice at 35 and 52 wk.**

(A) Quantification of anti-heat shock protein-70 (Hsp-70) immunoreactive cells in the ventral horn of the lumbar and thoracic spinal cord at 35 and 52 wk. SG-fed animals had a significantly greater number of anti-Hsp-70 immunoreactive cells in the ventral horn of the lumbar spinal cord at both 35 and 52 wk (Student's t-test: +1036%, $p<0.001$; +425%, $p<0.05$, respectively). In contrast, inter-group analysis of the total number of anti-Hsp-70 immunoreactive cells in the ventral horn of the thoracic spinal cord sections did not reveal a statistically significant difference (35 wk Student's t-test: not significant, $p=0.9697$; 52 wk Student's t-test: not significant, $p=0.2793$). An intra-group (time-dependent) assessment of the total number of anti-Hsp-70 immunoreactive cells did not reveal a statistically significant change over time for neither the lumbar nor thoracic spinal cord regions for either treatment group (Control animal group lumbar spinal cord- Student's t-test: not significant, $p=0.7334$; control animal group thoracic spinal cord- Student's t-test: not significant, $p=0.1223$; SG-fed group lumbar spinal cord- Student's t-test: not significant, $p=0.2967$; SG-fed group thoracic spinal cord- Student's t-test: not significant, $p=0.8319$). Panels B and D reflect the typical lack of anti-HSP-70 immunoreactivity observed in control animal lumbar spinal cord regions. Similarly, panels F and H are representative thoracic spinal cord sections of control mice at 35 and 52 wk, respectively. Panels C and E show SG-fed animal lumbar spinal cord sections with numerous large cells immunoreactive to anti-Hsp-70. Panels G and I depict representative SG-fed animal thoracic spinal cord sections with a lack of anti-Hsp-70 immunoreactivity. The red label is anti-Hsp-70 while blue is showing DAPI nuclear labelling. Images were captured using a fluorescence microscope under a 40x objective lens. Scale bars = 20 μm.

A

Stigmasterol β-D-glucoside feeding study: Number of cells expressing activating transcription factor-3 in the ventral horn of the lumbar spinal cord

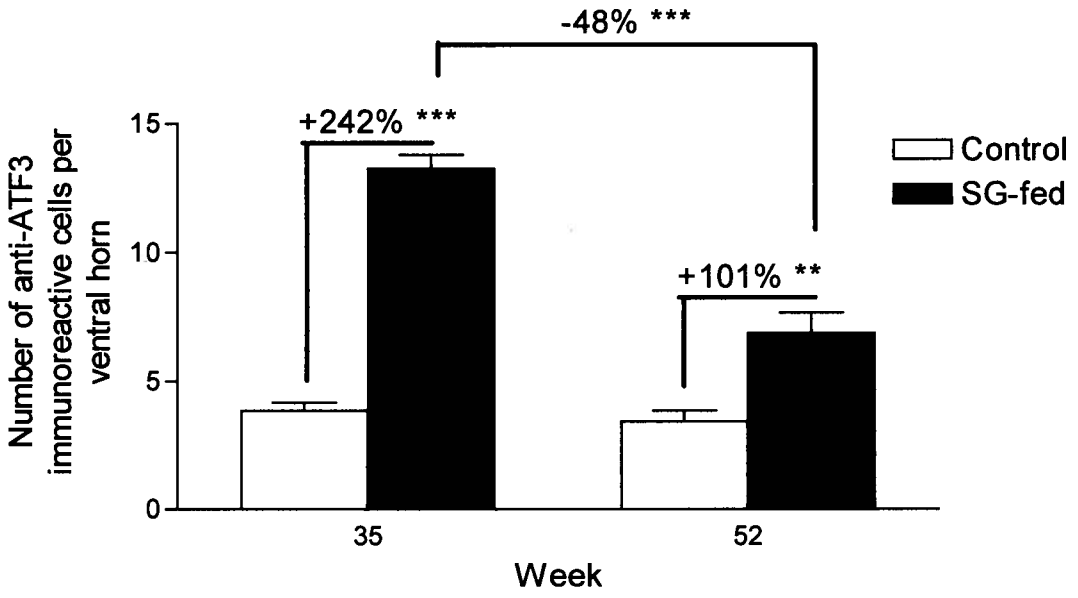

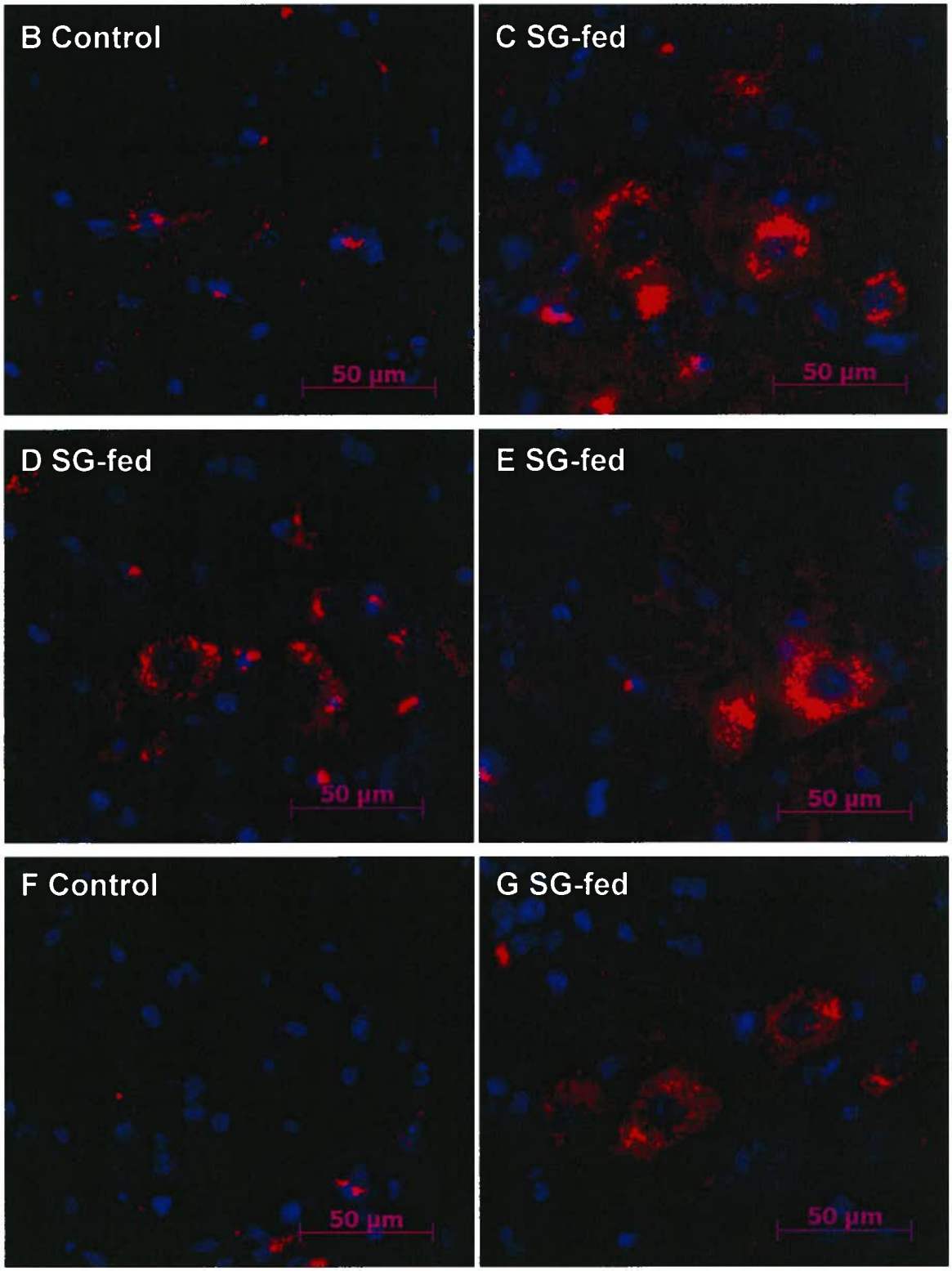
B Control
50 µm
C SG-fed
50 µm
D SG-fed
50 µm
E SG-fed
50 µm
F Control
50 µm
G SG-fed
50 µm

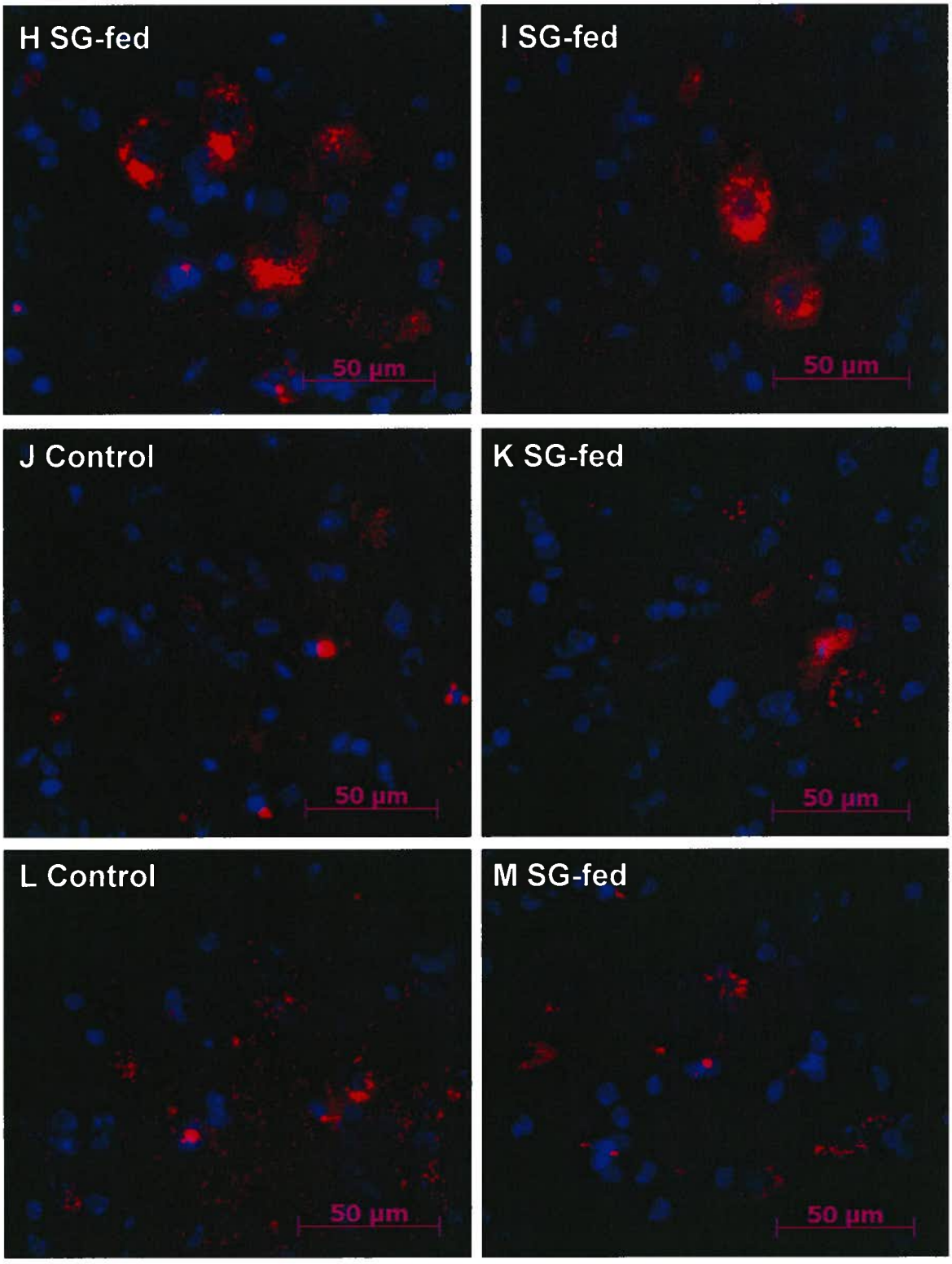
H SG-fed
50 µm
I SG-fed
50 µm
J Control
50 µm
K SG-fed
50 µm
L Control
50 µm
M SG-fed
50 µm

Figure 27. **Activating transcription factor-3 labelling in the lumbar and thoracic spinal cord of SG-fed mice.**

(A) Quantitative analysis of anti-activating transcription factor-3 (ATF-3) immunoreactivity in the lumbar and thoracic spinal cord. A significantly greater number of cells in the lumbar spinal cord of SG-fed were immunoreactive to anti-ATF-3 compared to age-matched controls at 35 (t-test: +242%, ***$p<0.001$) and 52 wk (t-test: +101%, **$p<0.01$). Further, the SG-fed animal sections were found to undergo a significant decrease in anti-ATF-3 immunoreactive cells over time (t-test: -48%, ***$p<0.001$). (B) Representative photomicrograph depicting the lack of immunoreactivity to ATF-3 in the lumbar spinal cord of control animals at 35 wk. In contrast, SG-fed animals showed intense cellular immunoreactivity to anti-ATF-3 in the lumbar spinal cord (C-E). Several sections are shown to illustrate the range in size of cells labelled with anti-ATF-3. Control animals at 52 wk also showed little immunoreactivity to anti-ATF-3 (F), while SG-fed animals showed numerous cells labelled with anti-ATF-3 (G-I). Control and SG-fed animals' thoracic spinal cord sections at 35 wk (J=Control 35 wk, K=SG-fed) and at 52 wk (L=Control, M=SG-fed) showed minimal immunoreactivity to anti-ATF-3. Images were captured using a fluorescence microscope under a 40x objective lens. Scale bars=50μm.

A

Stigmasterol β-D-glucoside feeding study:
Number of anti-phosphorylated-jun^{ser73} immunoreactive cells in the ventral horn of the lumbar spinal cord

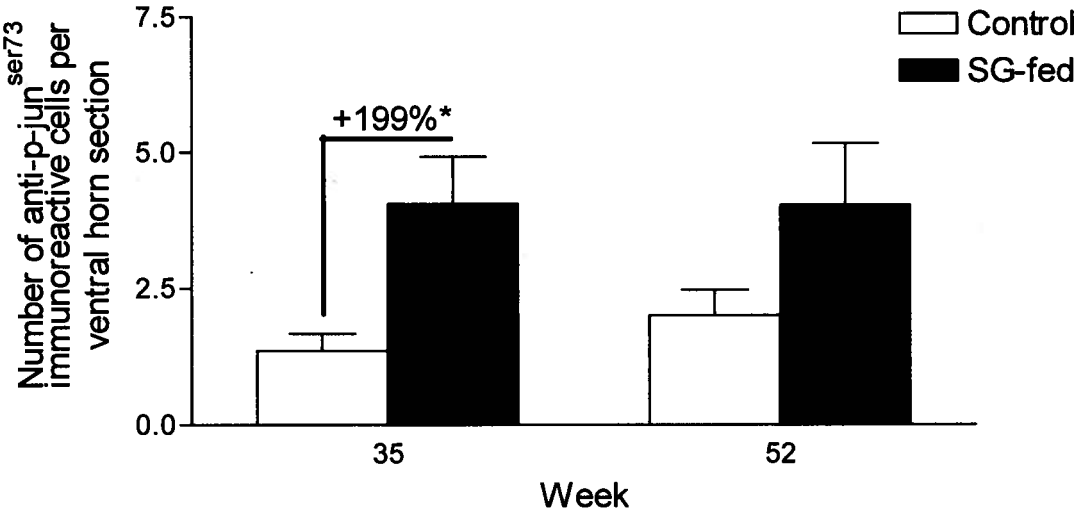

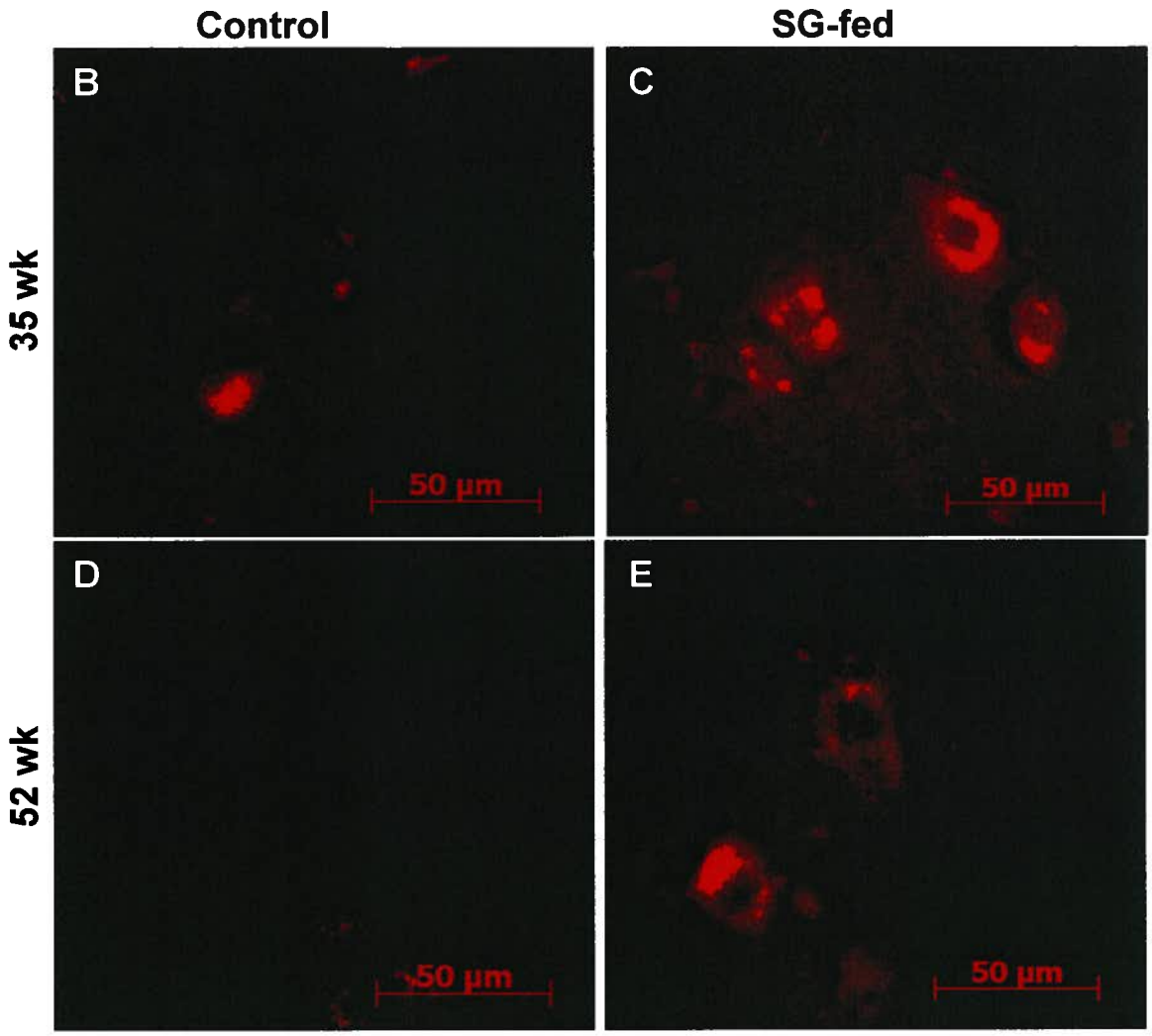
Control
SG-fed
35 wk
52 wk
B
C
D
E
50 µm
50 µm
50 µm
50 µm

Figure 28. **SG-feeding induces the phosphorylation of c-Jun at serine 73 in response to neuronal stress.**

(A) Quantitative analysis of anti-p-Jun^{ser73} immunoreactivity in the lumbar spinal cord. A significantly greater number of cells in the lumbar spinal cord of SG-fed were immunoreactive to anti-p-Jun^{ser73} compared to age-matched controls at 35 (t-test: +199%, *$p<0.05$). Also, at 52 wk, SG-fed animals appeared to have more numerous cells immunoreactive to anti-p-Jun^{ser73} but these values did not reach statistical significance. Representative photomicrograph depicting the lack of immunoreactivity to anti-p-Jun^{ser73} in the lumbar spinal cord of control animals at 35 and 52 wk (B and D). In contrast, SG-fed mice showed intense cellular immunoreactivity to anti-p-Jun^{ser73} in the lumbar spinal cord (C and E). Images were captured using a fluorescence microscope under a 40x objective lens. Scale bars=50μm.

A

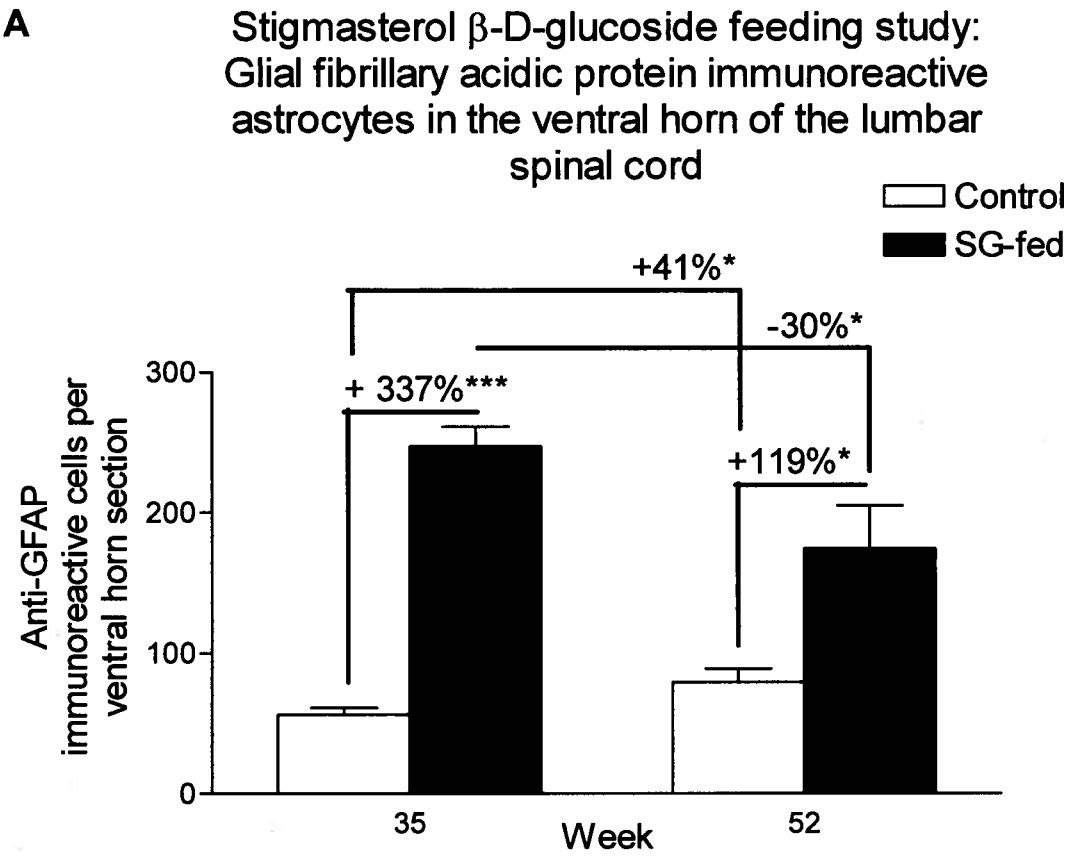
Stigmasterol β-D-glucoside feeding study:
Glial fibrillary acidic protein immunoreactive astrocytes in the ventral horn of the lumbar spinal cord
Control
SG-fed
+41%*
-30%*
+ 337%***
+119%*
Anti-GFAP immunoreactive cells per ventral horn section
300
200
100
0
35
Week
52

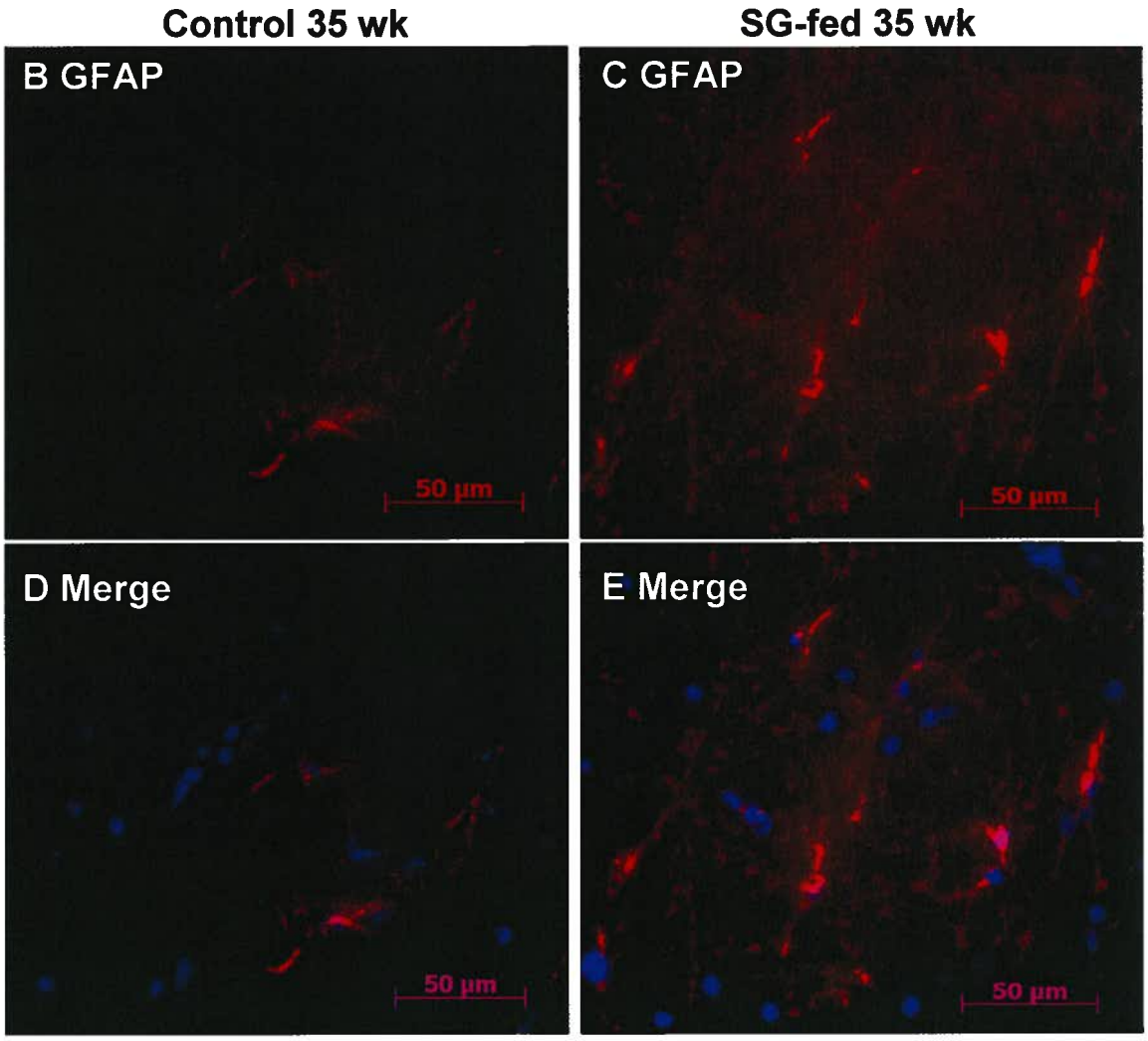
Control 35 wk
SG-fed 35 wk
B GFAP
C GFAP
D Merge
E Merge
50 µm
50 µm
50 µm
50 µm

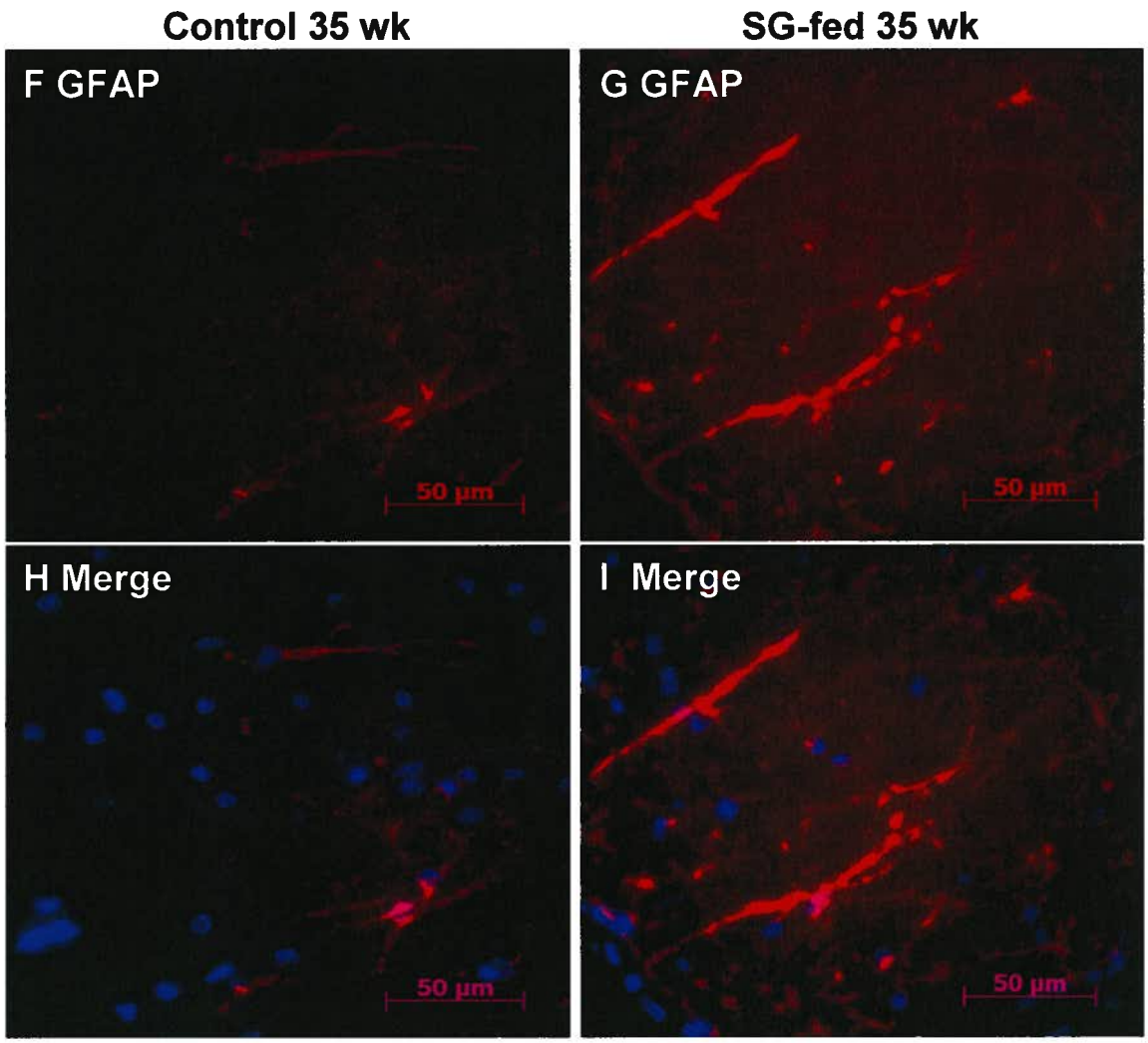
Control 35 wk
SG-fed 35 wk
F GFAP
G GFAP
H Merge
I Merge
50 µm
50 µm
50 µm
50 µm

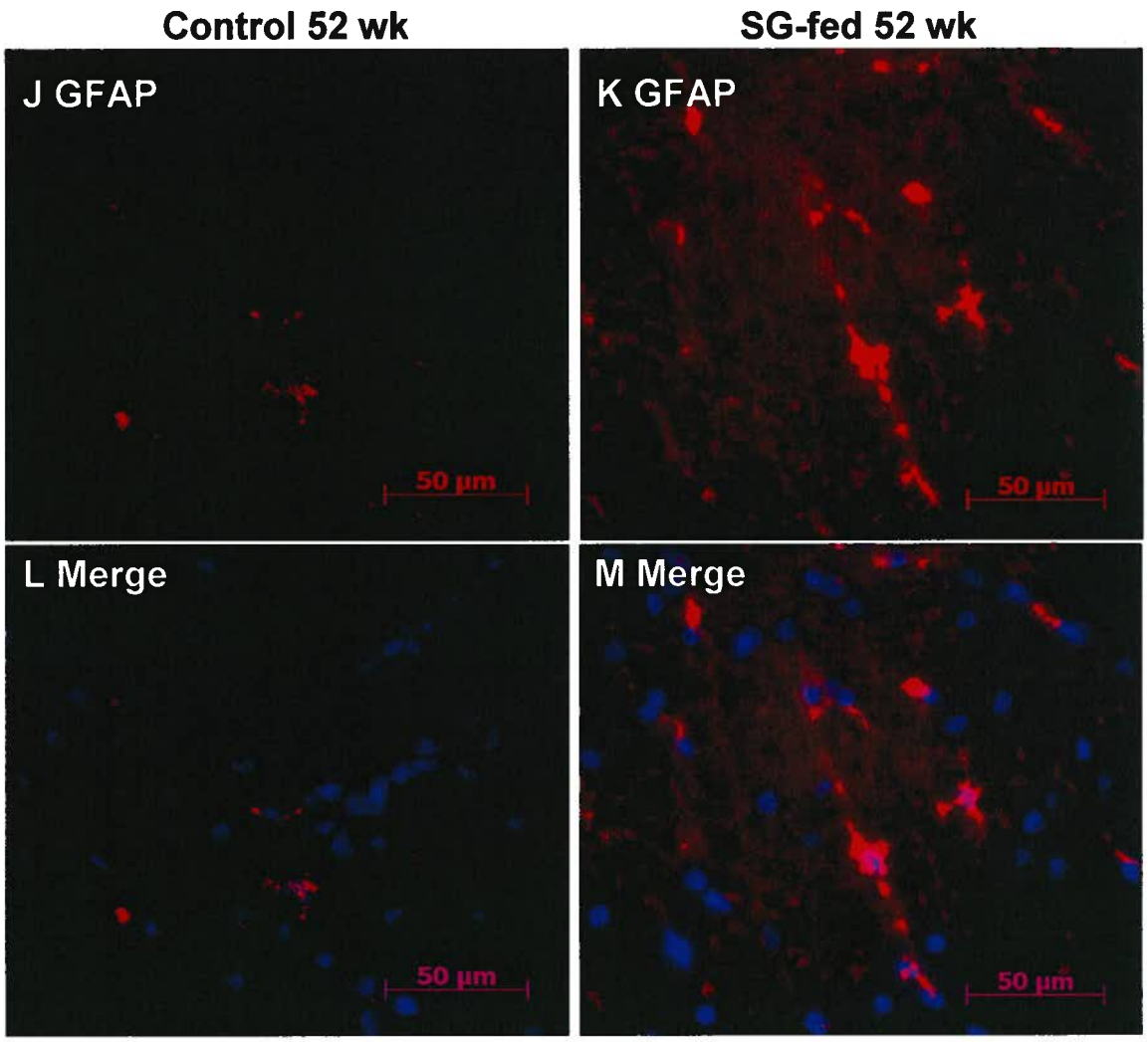
Control 52 wk
SG-fed 52 wk
J GFAP
K GFAP
L Merge
M Merge
50 µm
50 µm
50 µm
50 µm

Figure 29. **Activated astrocytes in the lumbar spinal cord of SG-fed mice.**

Anti-glial fibrillary acidic protein (GFAP) immunoreactive, stellate (both compact and elongated) cells were counted as astrocytes. Quantification of anti-GFAP labelling in the ventral horn of the lumbar spinal cord of control and SG-fed mice at 35 wk and 52 wk (A). SG-fed mice had a significantly greater number of astrocytic cells compared to the controls at both the pre-symptomatic (t-test: +337%, ***$p<0.001$) and symptomatic time-points (t-test: +119%, *$p<0.05$). Further, while the control animals experienced a significant increase in the number of astrocytes over time (t-test: +41%, *$p<0.05$), SG-fed animals were found to undergo a significant reduction in GFAP positive astrocytes (t-test: -30%, *$p<0.05$) over the same 17 wk period. Representative photomicrographs of control animals at 35 wk depict the lack of anti-GFAP labelled cells in the ventral horn (B and D) and distal lateroventral horn (F and H) of the lumbar spinal cord. Representative ventral horn sections of control mice at 52 wk (J and L) are also shown. The green label is anti-GFAP while the blue labels nuclei (DAPI). Scale bars=50 μm. Panels C and E, and K and M depict representative SG-fed animal lumbar spinal cord ventral horn sections containing numerous, stellate astrocytes intensely immunoreactive to anti-GFAP at 35 at 52 wk respectively. Panels G and I are representative micrographs of SG-fed animals' distal lateroventral horn of the lumbar spinal cord experiencing significant infiltration of hyper-ramified astrocytes. Images were captured using a fluorescence microscope under a 40x objective lens. Scale bar = 50 μm.

A

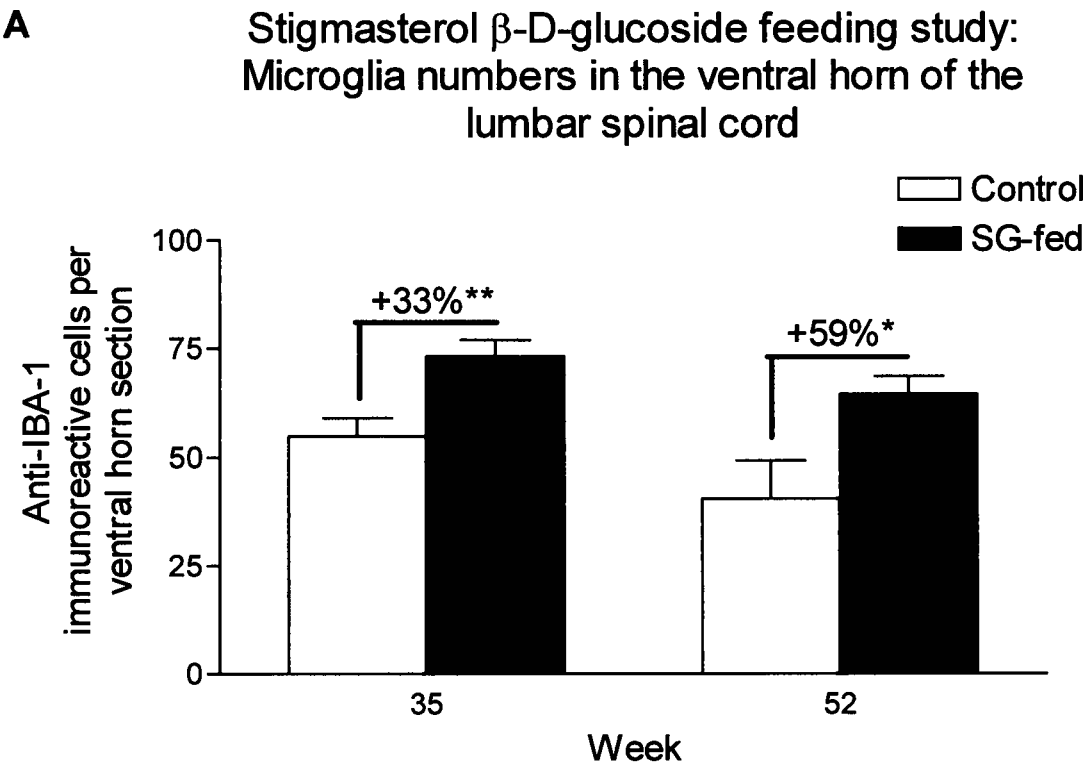
Stigmasterol β-D-glucoside feeding study:
Microglia numbers in the ventral horn of the lumbar spinal cord
Control
SG-fed
Anti-IBA-1 immunoreactive cells per ventral horn section
100
75
50
25
0
+33%**
+59%*
35
52
Week

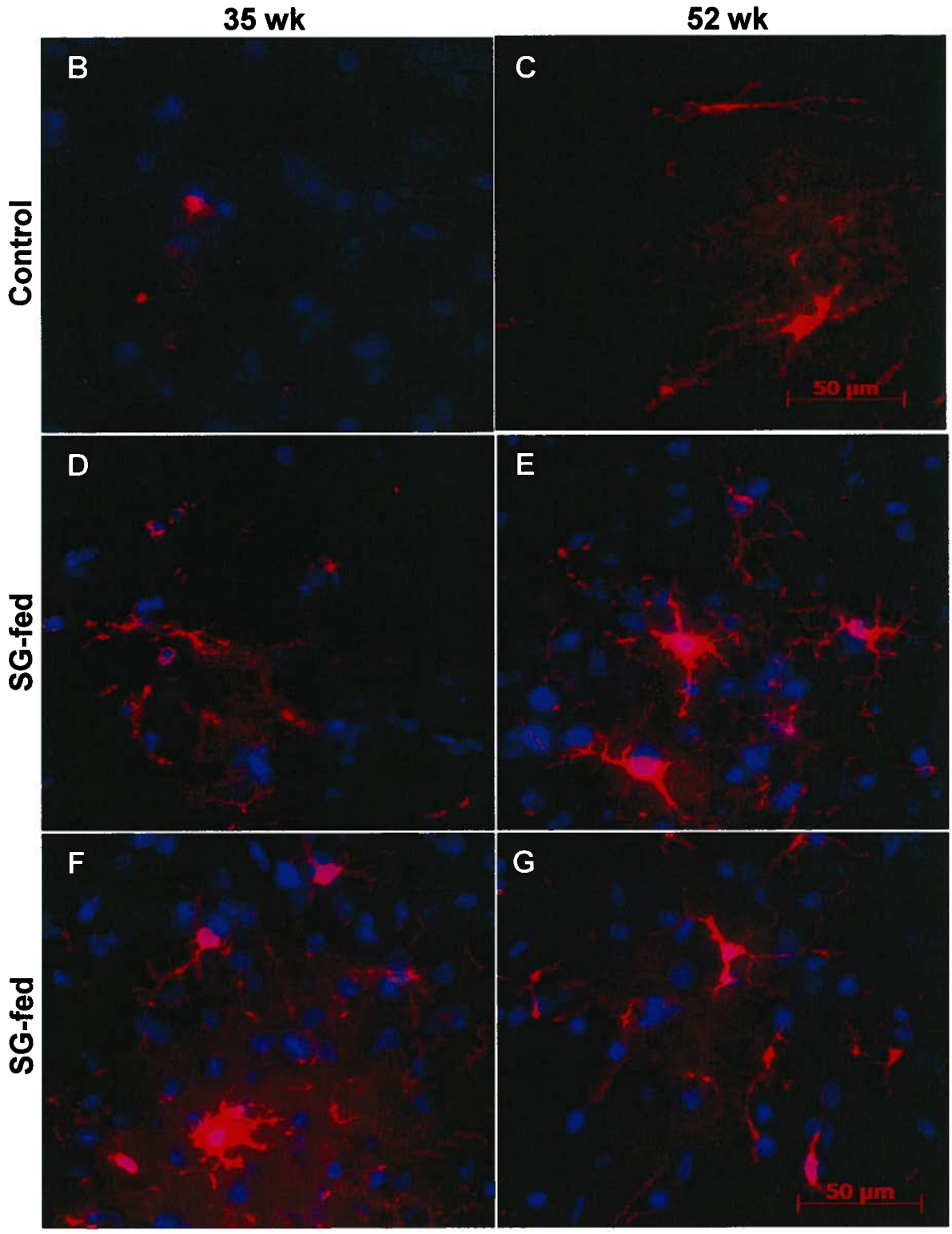
35 wk
52 wk
Control
SG-fed
SG-fed
B
C
D
E
F
G
50 µm
50 µm

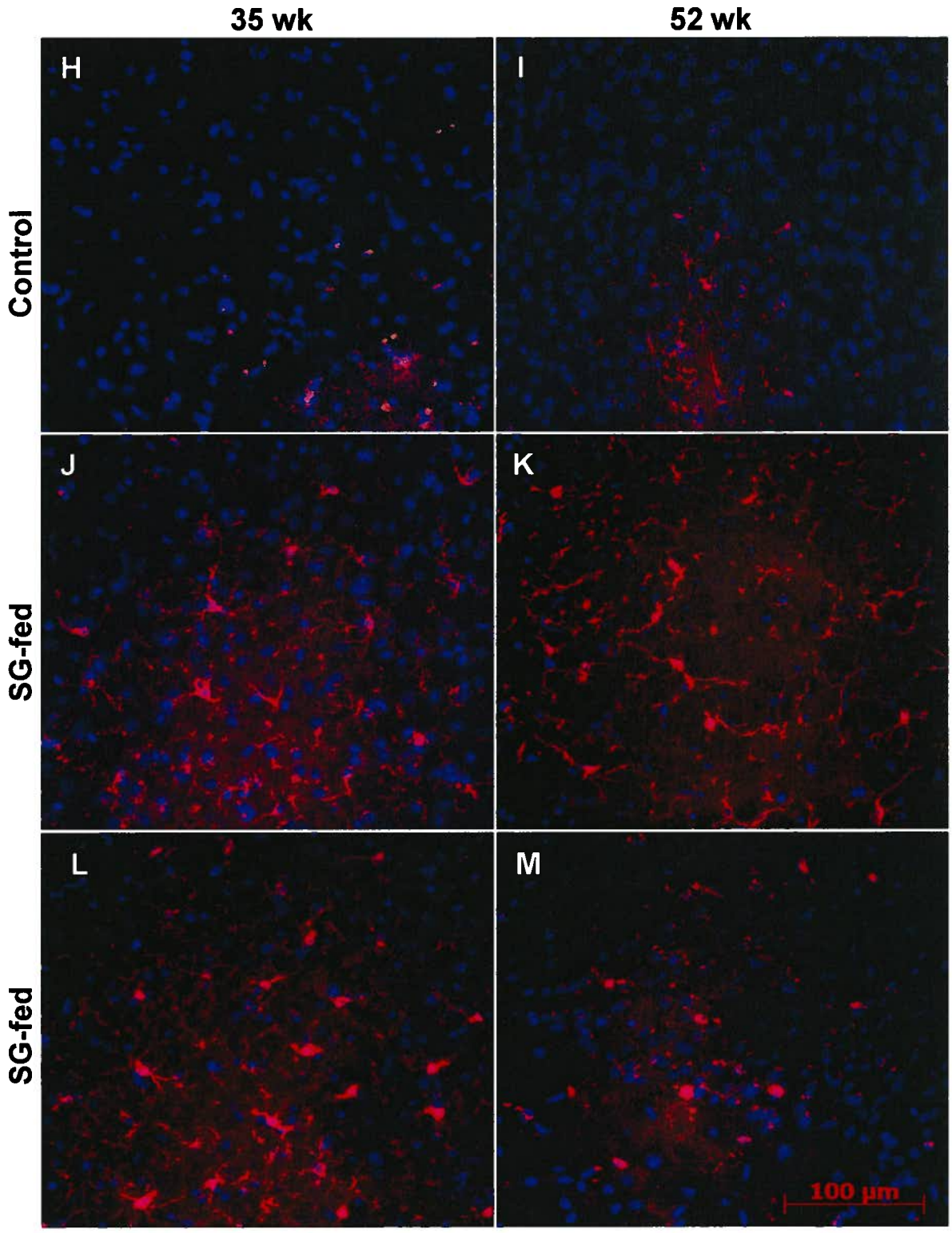
35 wk
52 wk
H
I
J
K
L
M
Control
SG-fed
SG-fed
100 µm

Figure 30. **Microglial proliferation in the lumbar spinal cord of SG-fed mice.**

Cells immunoreactive to ionized calcium binding receptor-1 (IBA-1) were counted as microglia. (A) Quantification of microglia in the ventral horn of the lumbar spinal cord of control and SG-fed mice at 35 wk and 52 wk. SG-fed mice had significantly more microglia compared to the controls at both the pre-symptomatic (t-test: +33%, $^{**}p<0.01$) and symptomatic (t-test: +59%, $^{*}p<0.05$) time-points (Student's t-test, $^{*}p<0.05$). Representative photomicrographs of control animals at 35 (40x objective: B; 10x objective: H) and 52 wk (40x objective: C; 10x objective: I) show weak immunolabelling of microglia in the lumbar spinal cord. In contrast, SG-fed animals showed numerous, large, microglia at both 35 (40x objective: D, F; 10x objective: J, L) and 52 wk (40x objective: E, G; 10x objective: K, M). Immunofluorescent images were captured using a fluorescence microscope under a 40x (B-G) or 10x (H-M) objective lens to provide both a detail of microglial morphology with a higher power and a depiction of expansive ventral horn microglia activation with a lower power. In SG-fed animals, both the soma and projections were found to be larger (C, E, G, I, K, M). Scale bars = 50 µm (B-G) and 100 µm (H-M).

A

Stigmasterol β-D-glucoside feeding study:
Anti-caspase-3 immunoreactive cells in
the venral horn of the lumbar spinal cord

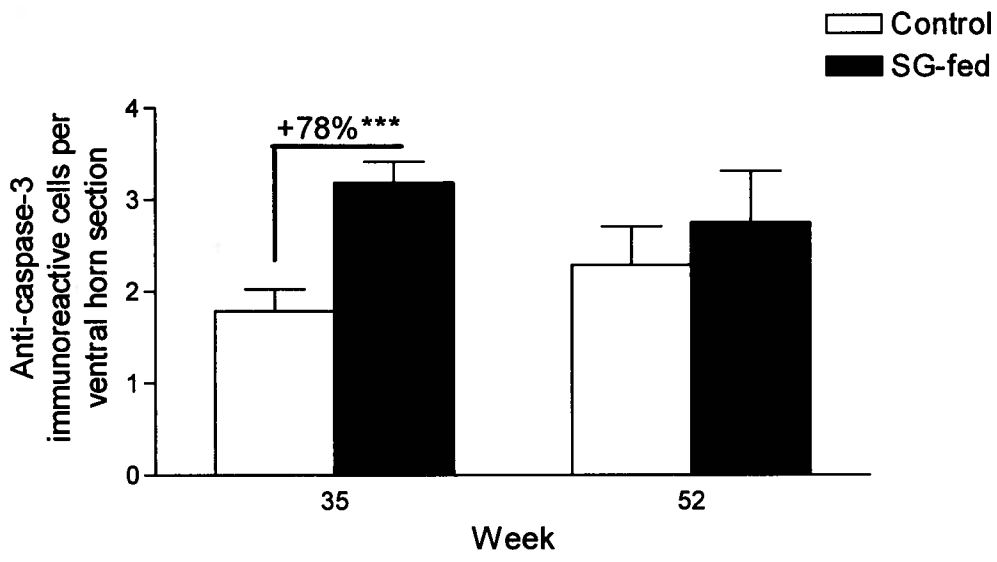

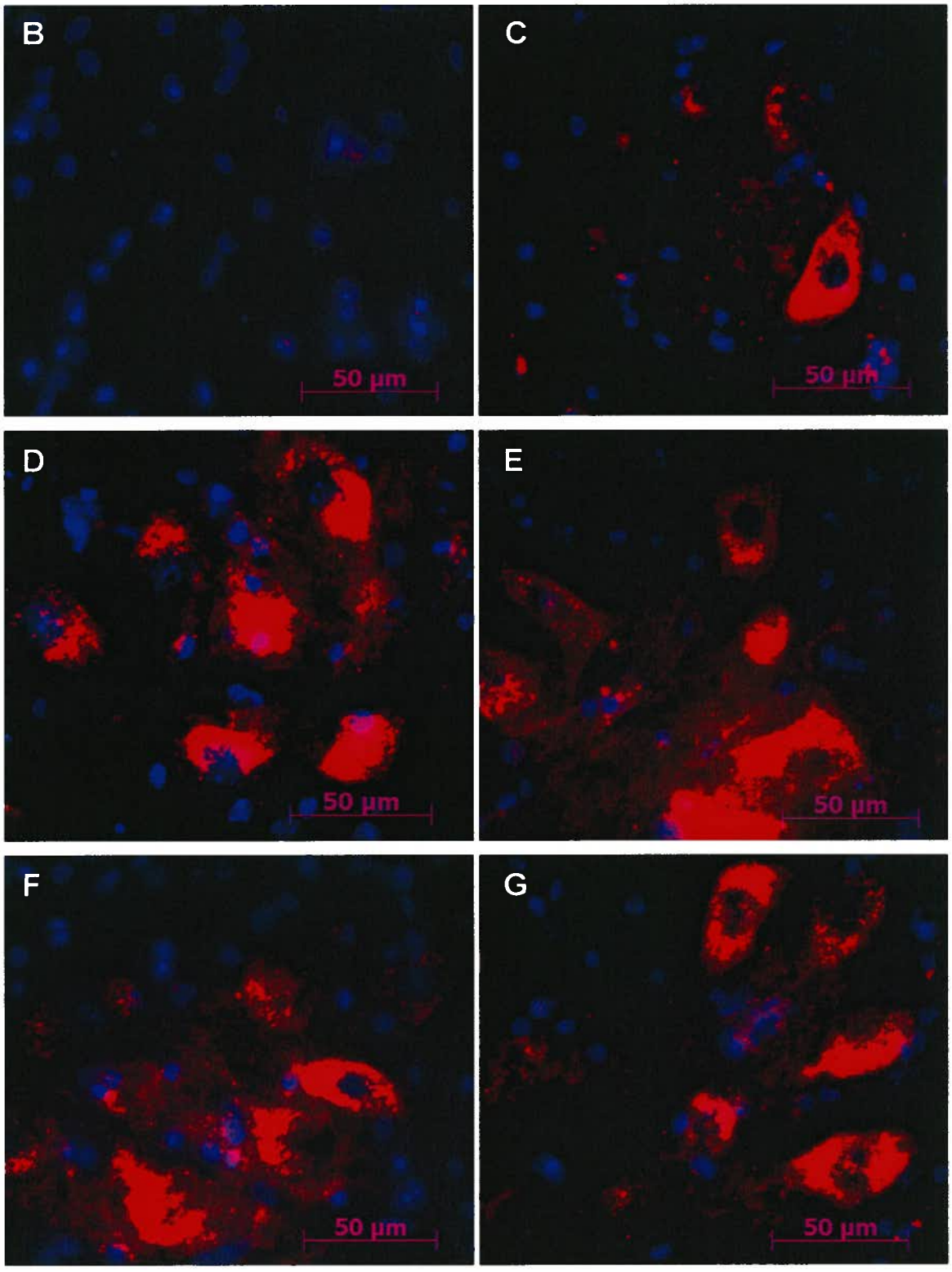
B
50 µm
C
50 µm
D
50 µm
E
50 µm
F
50 µm
G
50 µm

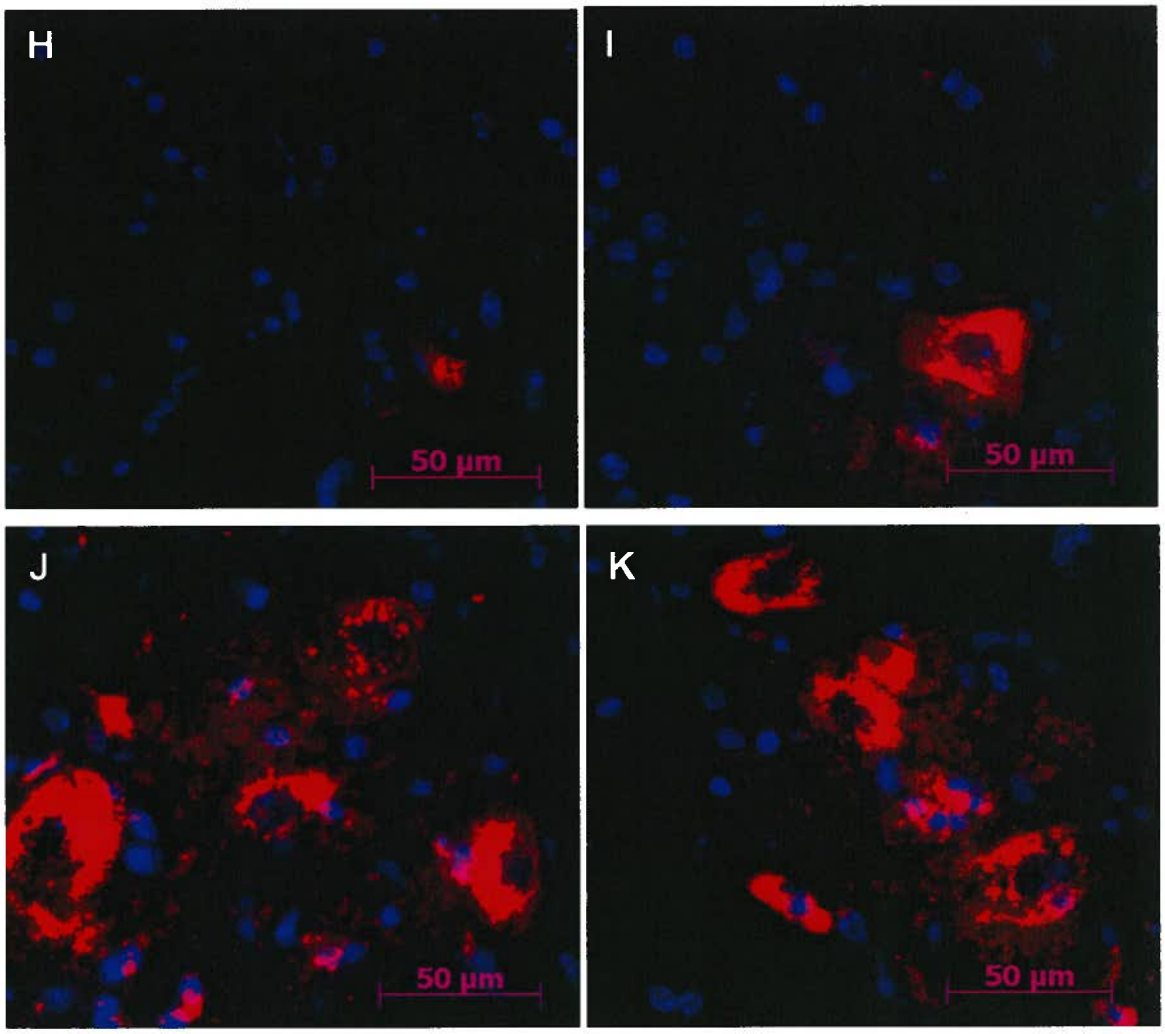
H
50 µm
I
50 µm
J
50 µm
K
50 µm

Figure 31. **Caspase-3 labelling in the spinal cord of SG-fed mice.**

Quantification of anti-caspase-3 immunoreactive cells in the ventral horn of the lumbar spinal cord at 35 and 52 wk revealed that SG-feeding induced cells to undergo apoptosis at pre-symptomatic and symptomatic time points. At 35 wk, a significant greater number of apoptotic neurons were observed in SG-fed animals (t-test, +78%, ***$p<0.001$) (A). A greater number of apoptotic cells were also observed in SG-fed animals at 52 wk, but numbers did not reach significance (A). (B-C) Active caspase-3 labelling in the ventral horn of the lumbar spinal cord of control mice and SG-fed mice (D-G) at the pre-symptomatic time point (35 wk). Representative photomicrographs of control mice (H-I) and SG-fed animals at the symptomatic time point (52 wk) are also depicted (J-K). At both time-points, SG-fed animals exhibited significantly more anti-active-caspase-3 positively labelled cells. At 52 wk, cells immunoreactive to caspase-3 appeared to be slightly smaller in size than the cells that labelled at 35 wk, suggesting that the type and size of motor neurons that undergo apoptosis during the later stages of SG-feeding are different from those that do so at the pre-symptomatic time-point. Alternatively, it is possible that sometime during the early stage of SG-feeding, the larger α-motor neurons underwent significant shrinkage and became γ-motor neuron-like in size. Several examples of control and SG-fed mice at 35 wk and 52 wk are provided to illustrate the distribution of cells and range of size and morphology of cells that were actively undergoing apoptosis. Images were captured using a fluorescence microscope under a 40x objective lens. The red label is anti-caspase-3, while the blue indicate nuclei (DAPI). Scale bar = 50 μm.

A

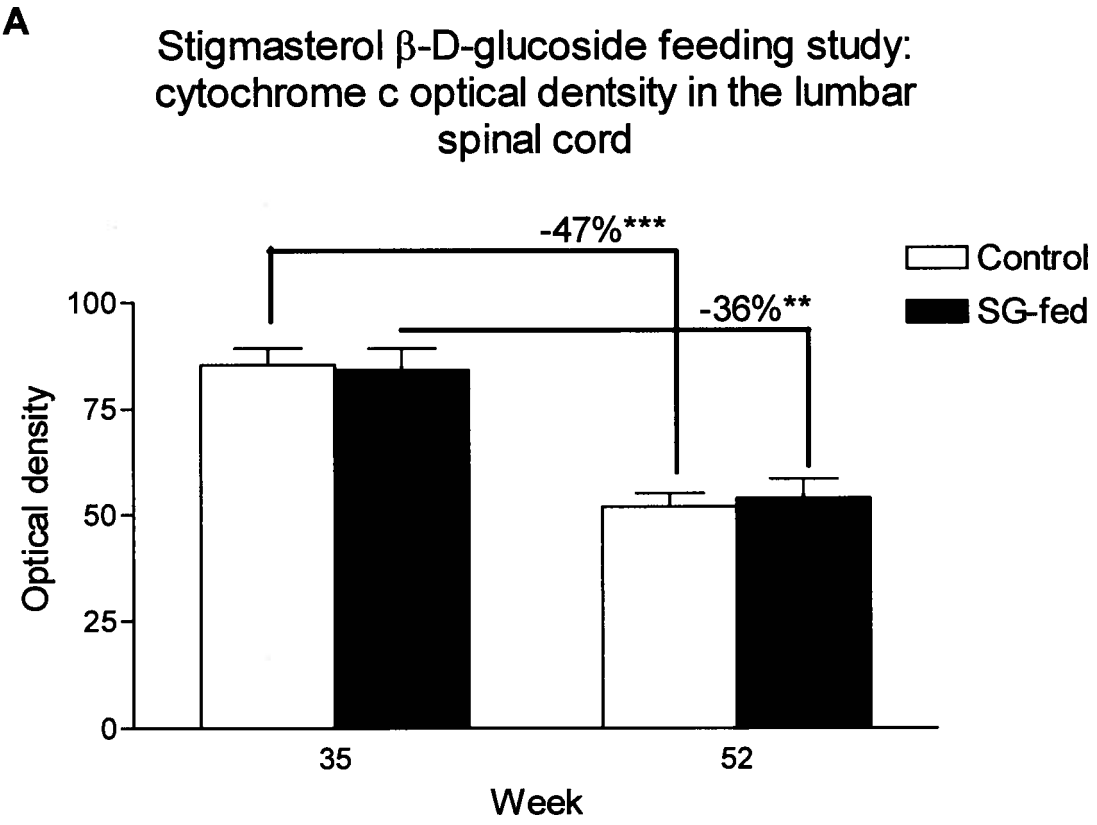
Stigmasterol β-D-glucoside feeding study: cytochrome c optical dentsity in the lumbar spinal cord
-47%***
-36%**
Control
SG-fed
Optical density
100
75
50
25
0
35
52
Week

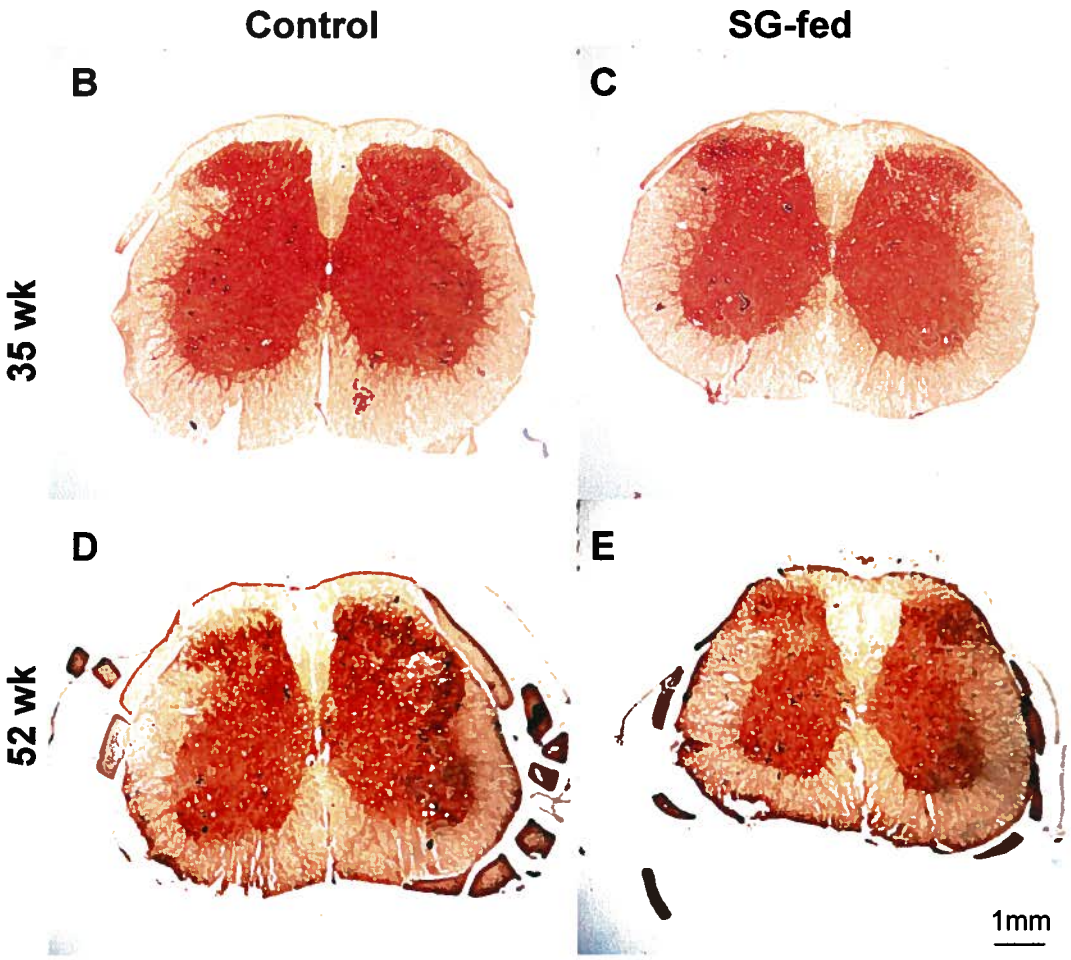

Figure 32. **Cytochrome c oxidase activity is unaffected in SG-fed animals.**

Cytochrome c oxidase activity was analyzed in SG-fed animals and age-matched controls. No significant differences were observed between groups at 35 or 52 wk (A). A decline in cytochrome c oxidase activity was observed to occur over time in each of the groups (A). Micrographs were captured using a light microscope under a 40x objective lens. Scale bars=1mm

A

Stigmasterol β-D-glucoside feeding study:
Tyrosine hydroxylase optical density in the
substantia nigra pars compacta

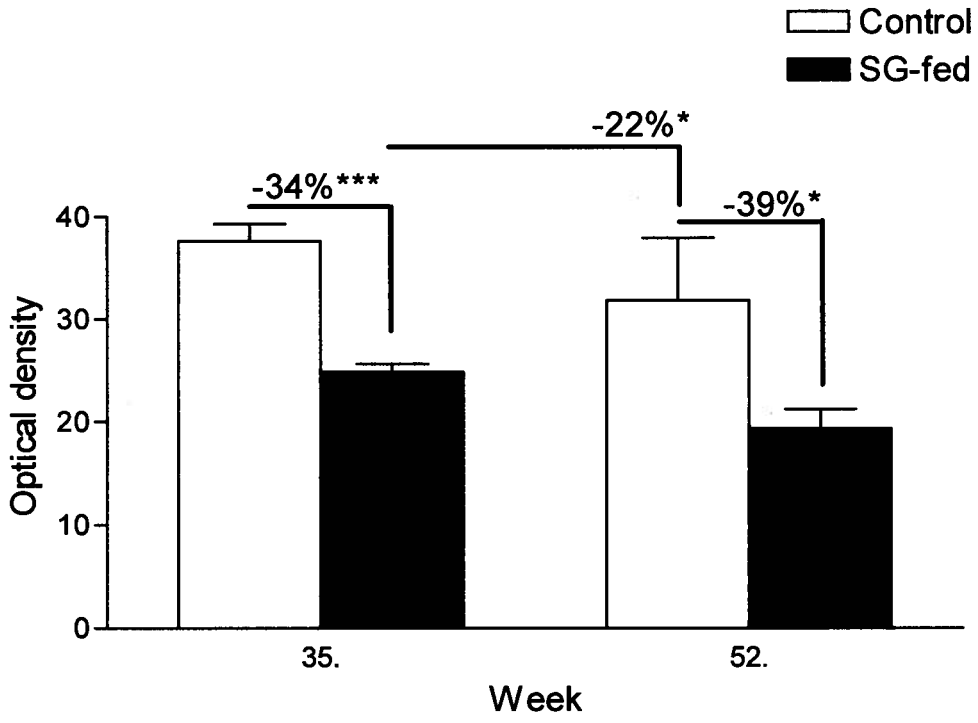

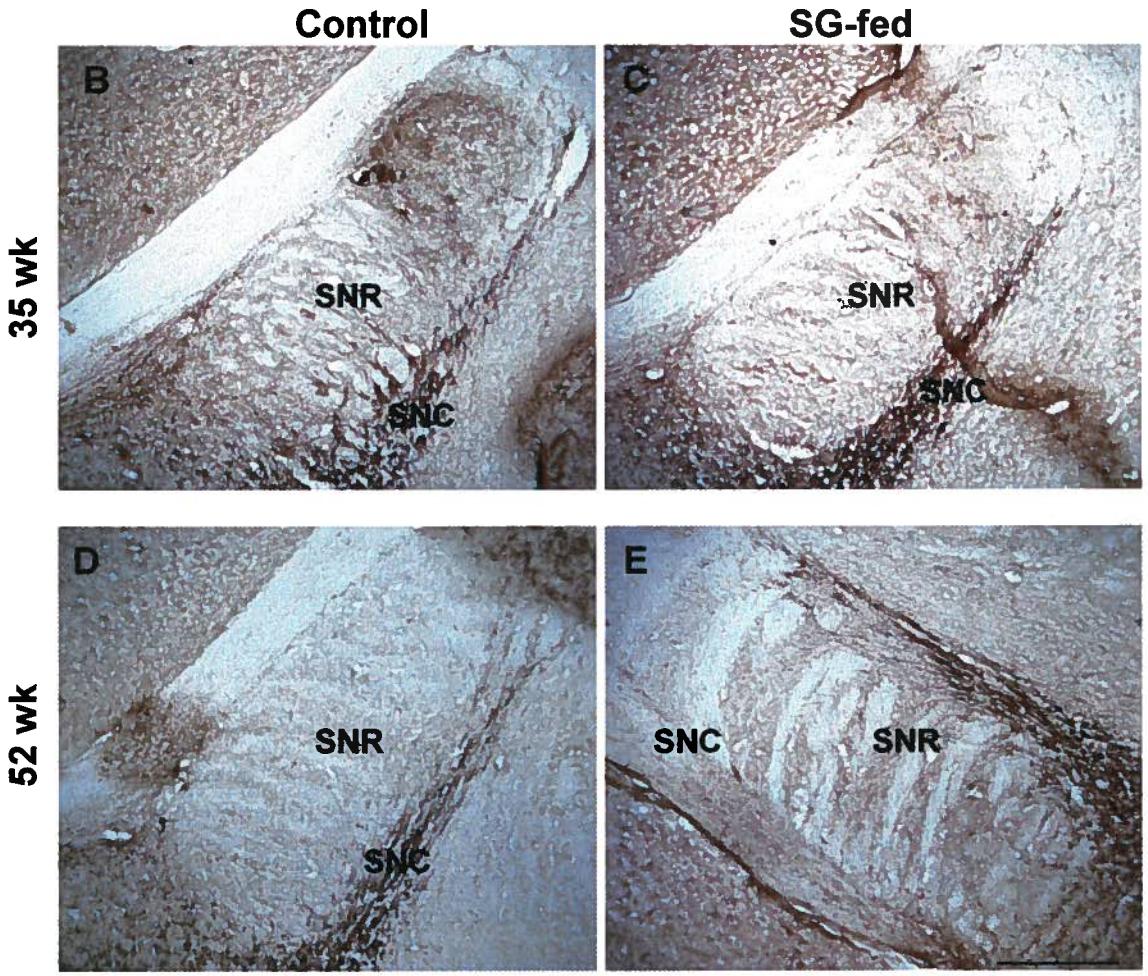
Control
SG-fed
35 wk
52 wk
B
C
D
E
SNR
SNC
SNR
SNC
SNR
SNC
SNC
SNR

F

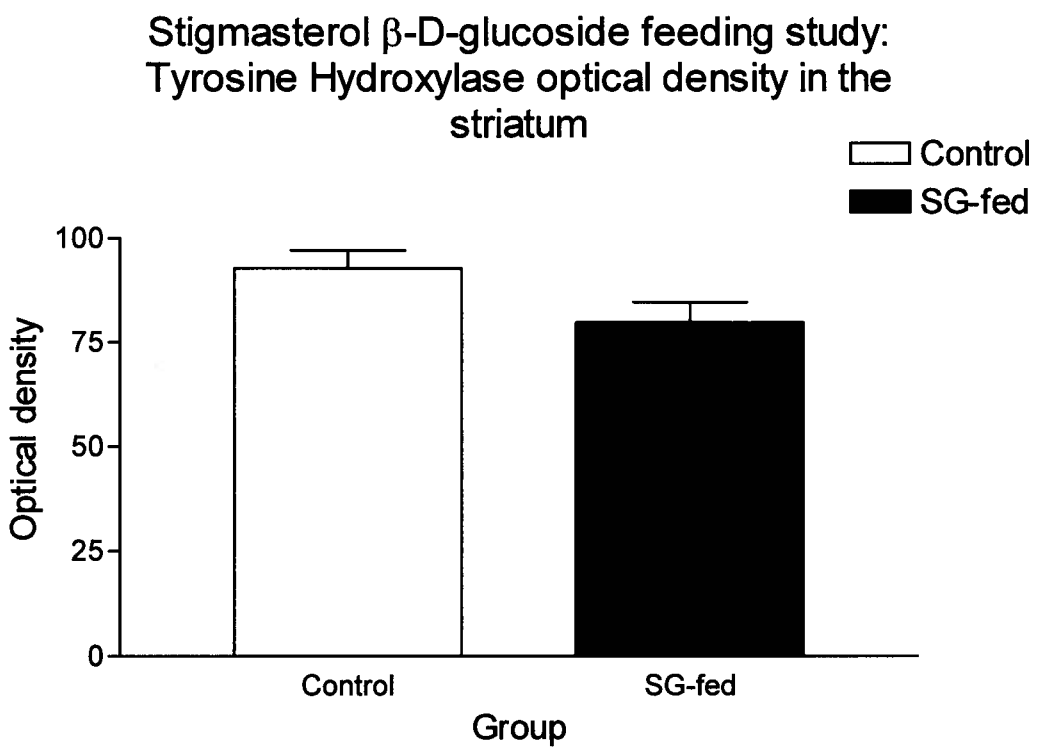
Stigmasterol β-D-glucoside feeding study:
Tyrosine Hydroxylase optical density in the striatum
Control
SG-fed
Optical density
100
75
50
25
0
Control
SG-fed
Group

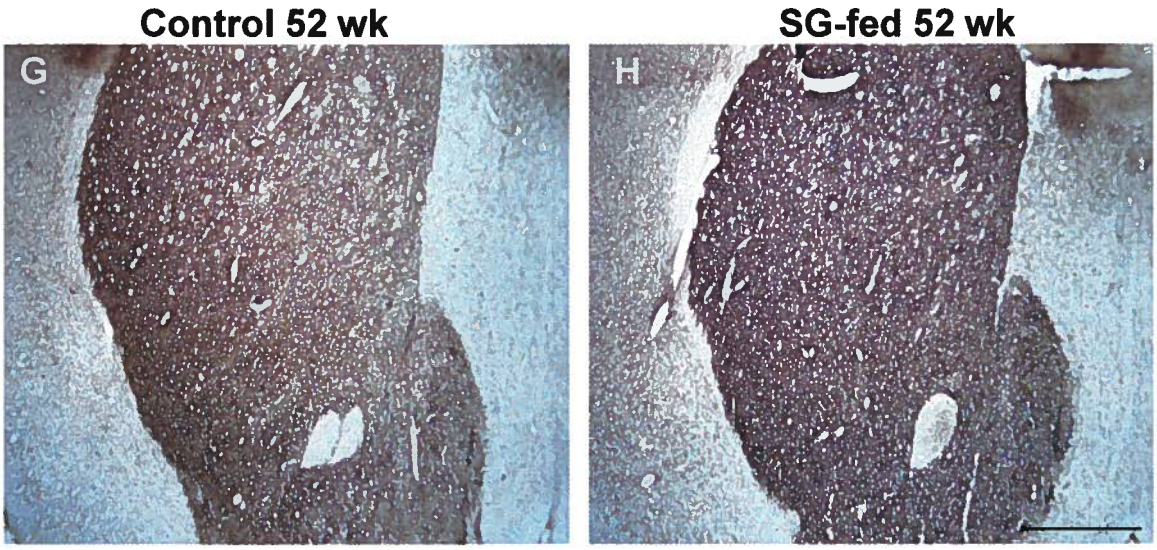

Figure 33. **Tyrosine hydroxylase labelling is lost in the striatum of SG-fed mice.**

SG-fed mice showed significantly decreased tyrosine hydroxylase labelling (optical density) compared to controls in the substantia nigra pars compacta (SNpc) at 35 wk (t-test: -34%, ***$p<0.001$) and at 52 wk (t-test: -39%, *$p<0.05$). TH optical density was found to decrease among SG-fed animals over time (t-test: -22%, *$p<0.05$) in the SNpc (A). A decrease in optical density was not found among the SG-fed animals' striata at either time-point (t-test: not significant $p=0.0846$) (F). Panel B and C depict representative SNpc sections of control and SG-fed animals at 35 wk. Similarly, panels D and E depict representative sections at 52 wk of control and SG-fed animals. Panels G and H depict representative striatal sections of 52 wk old control and SG-fed animals respectively. Micrographs were captured using a light microscope under a 40x objective lens. Scale bars=1.25 mm (B through E) and 3 mm (F and G).

A

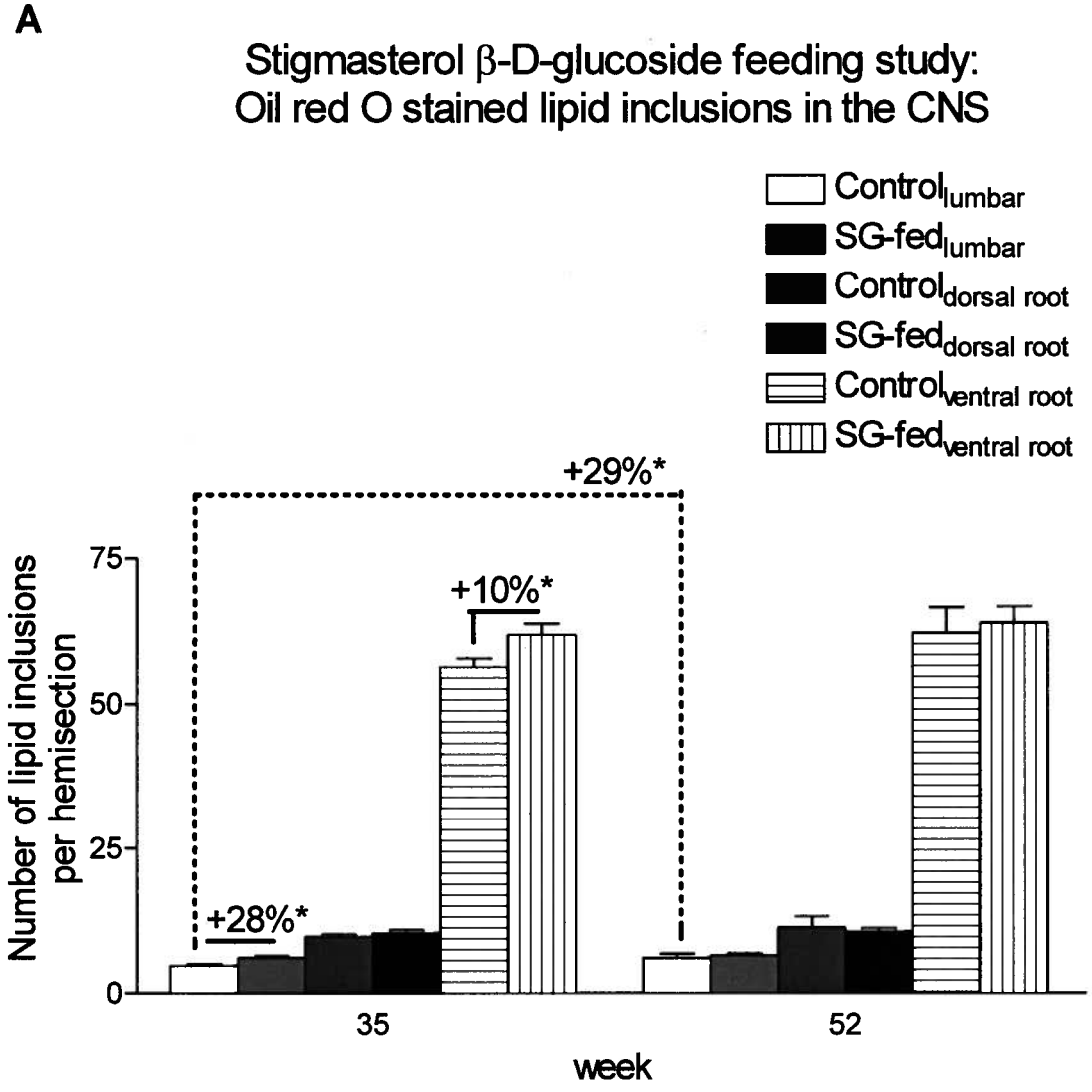
Stigmasterol β-D-glucoside feeding study:
Oil red O stained lipid inclusions in the CNS
Control lumbar
SG-fed lumbar
Control dorsal root
SG-fed dorsal root
Control ventral root
SG-fed ventral root
+29%*
+10%*
+28%*
Number of lipid inclusions per hemisection
75
50
25
0
35
52
week

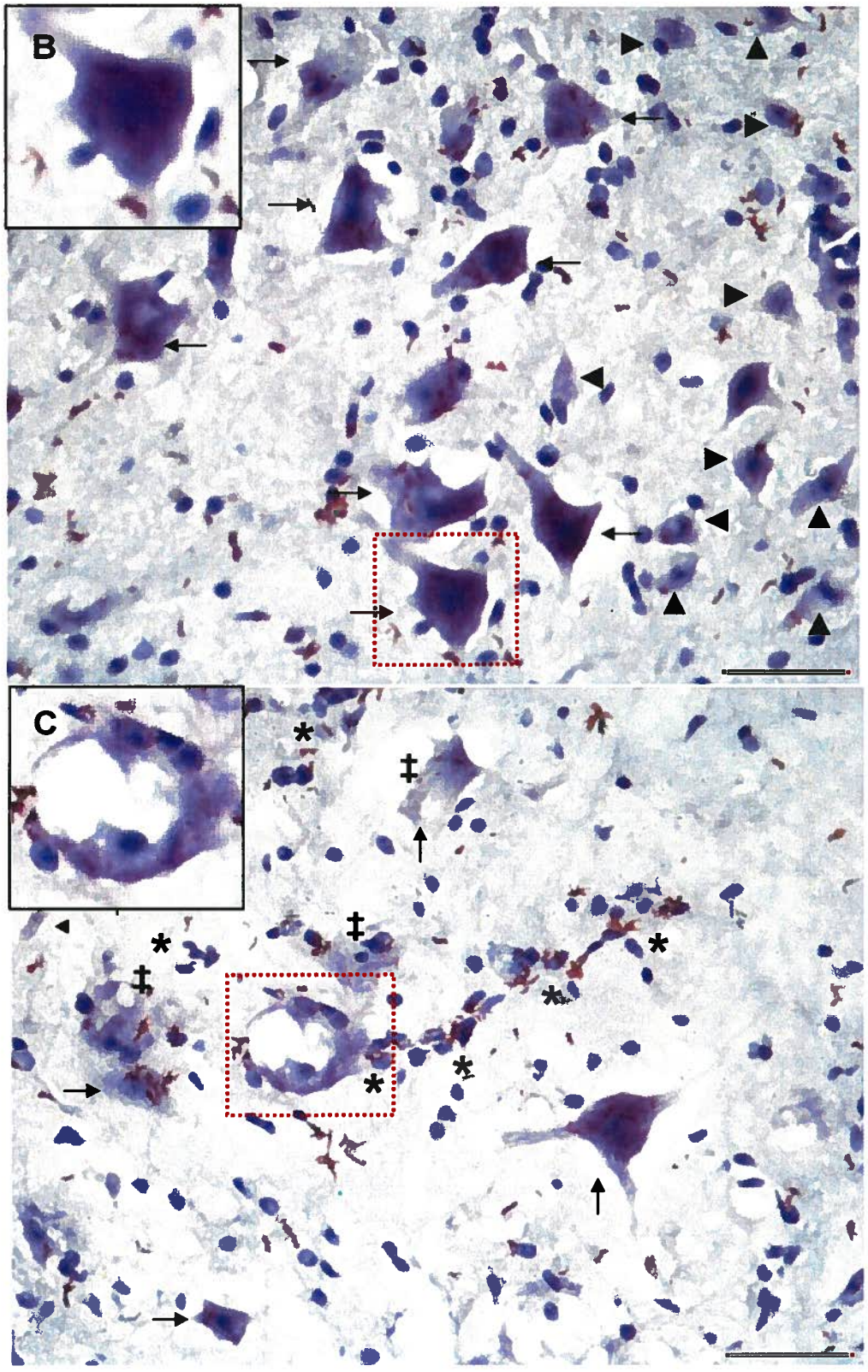
B
C

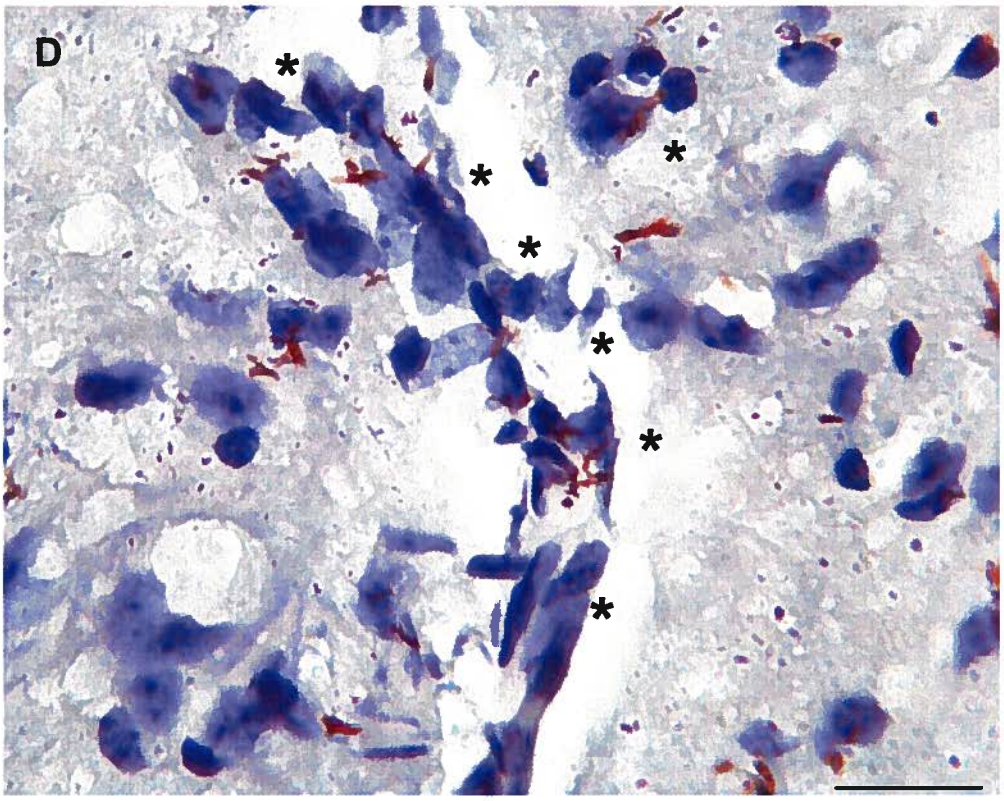
D

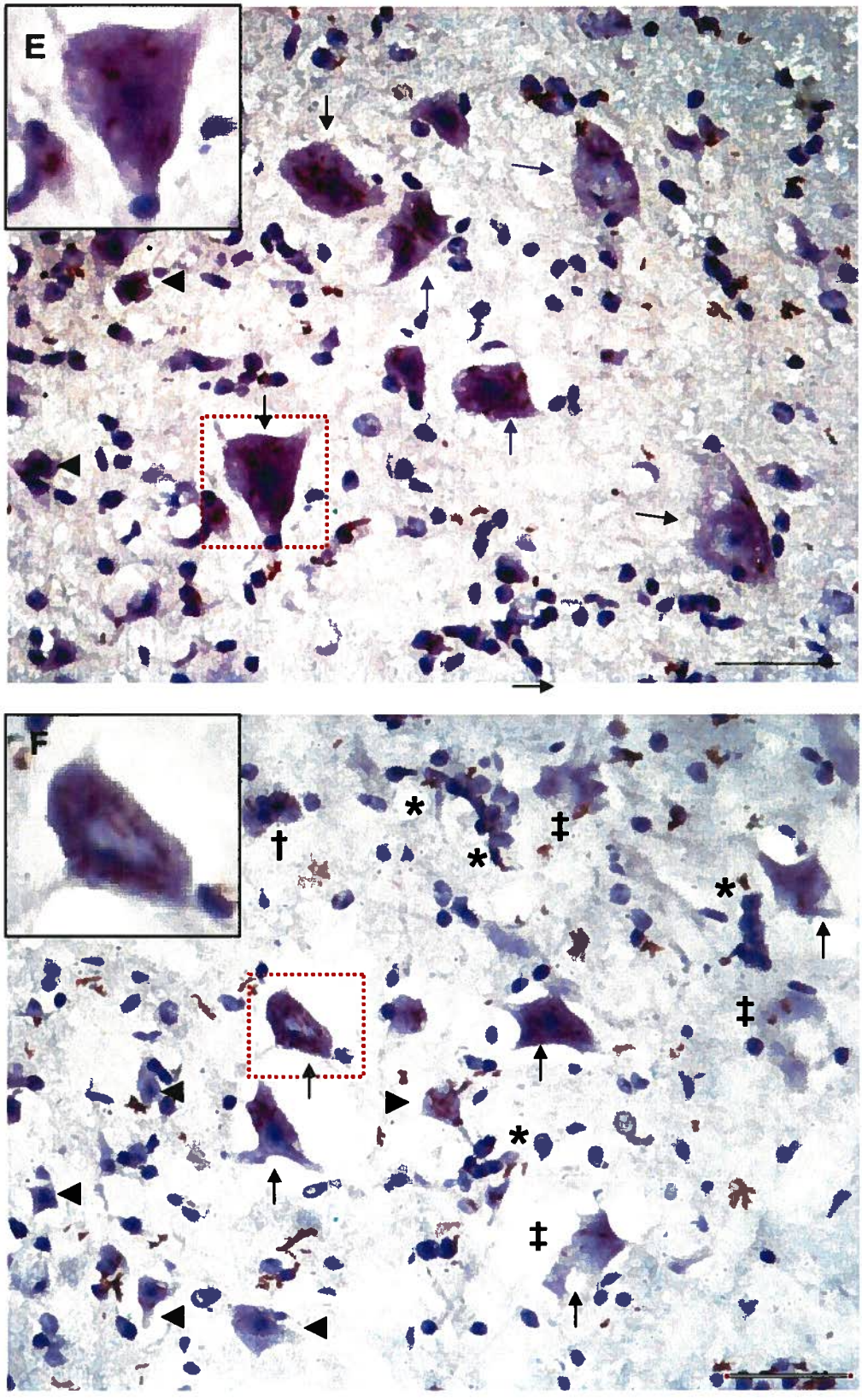
E
F

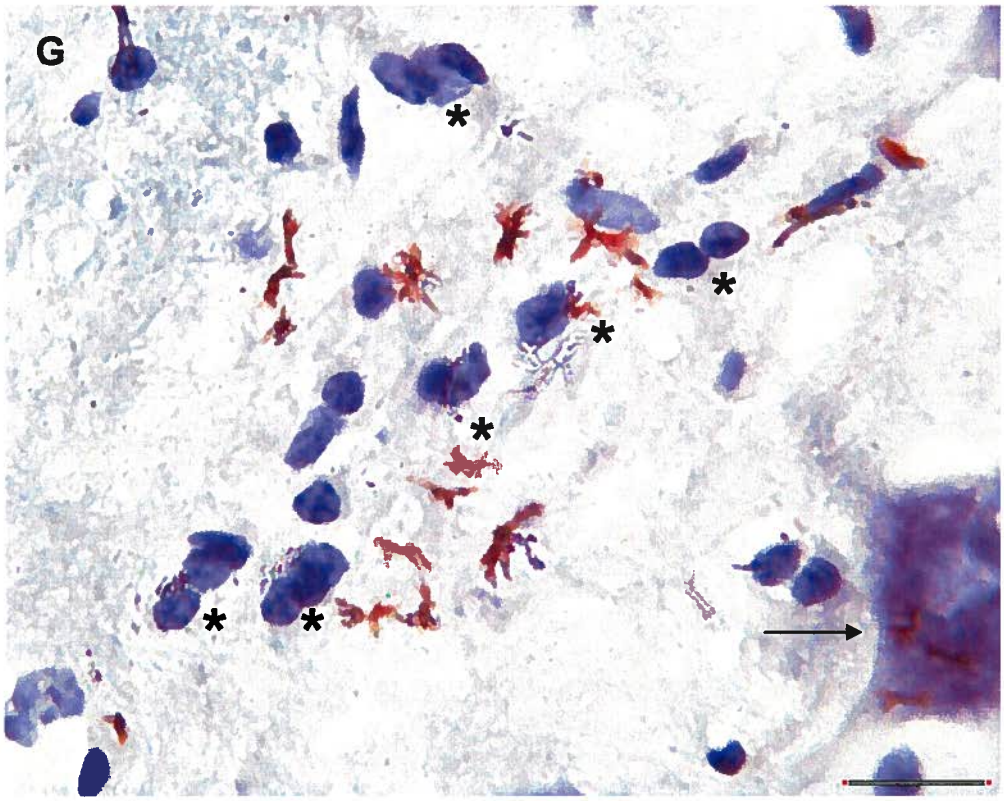
G

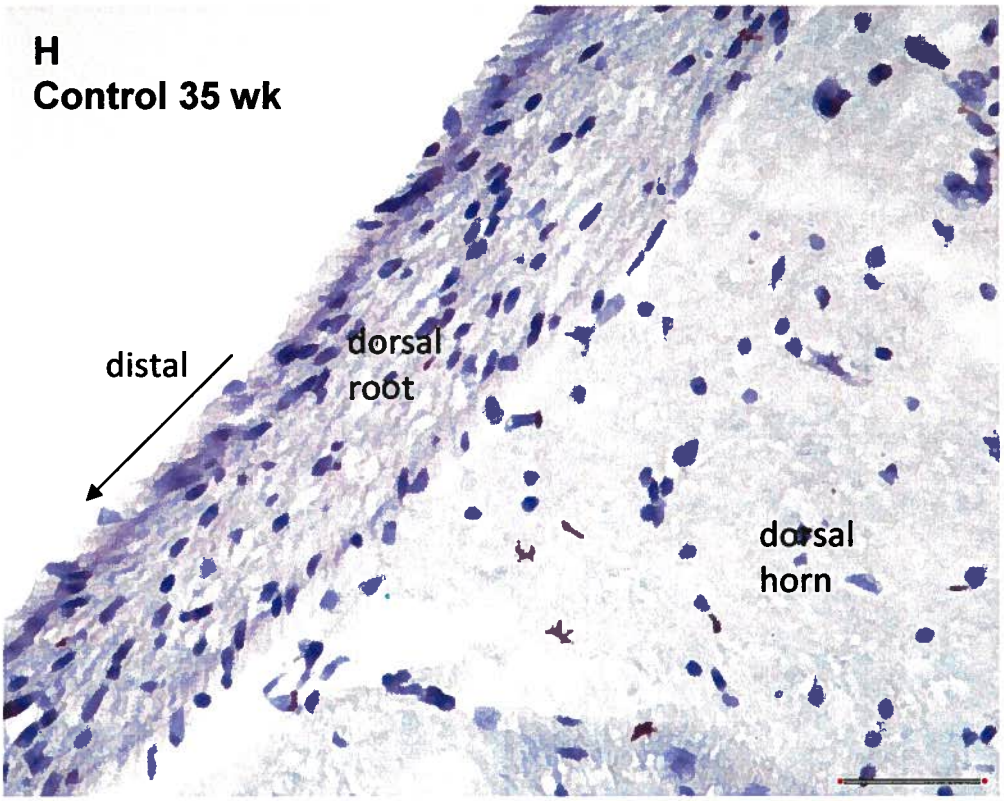
H
Control 35 wk
distal
dorsal
root
dorsal
horn

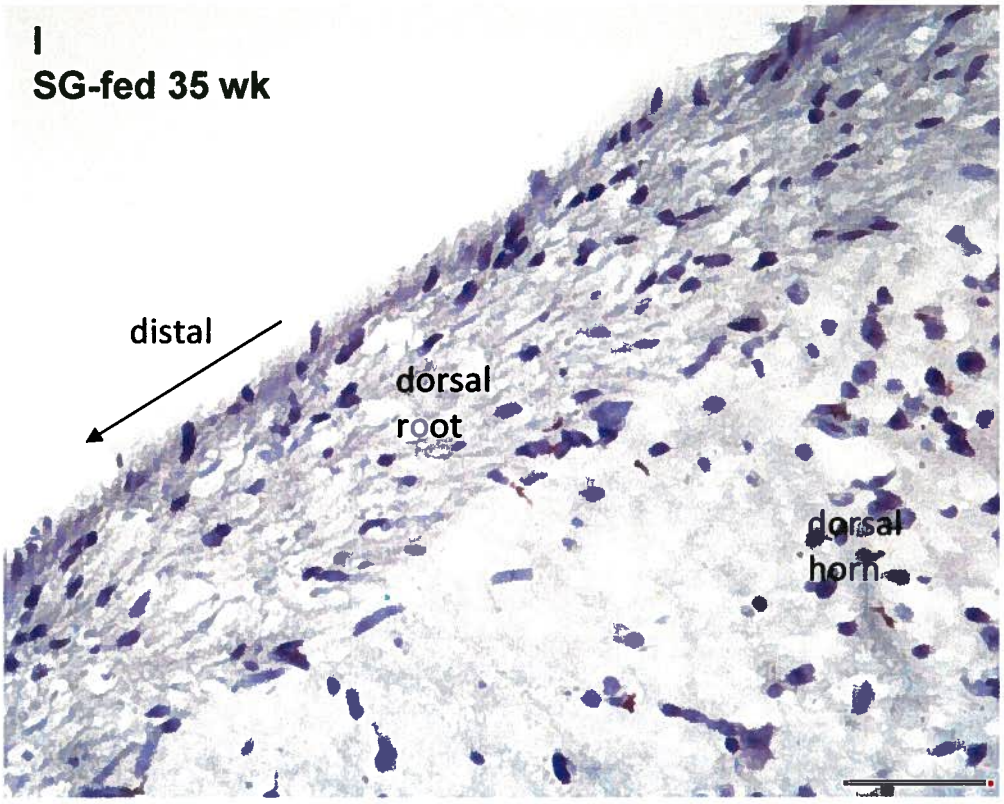
I
SG-fed 35 wk
distal
dorsal
root
dorsal
horn

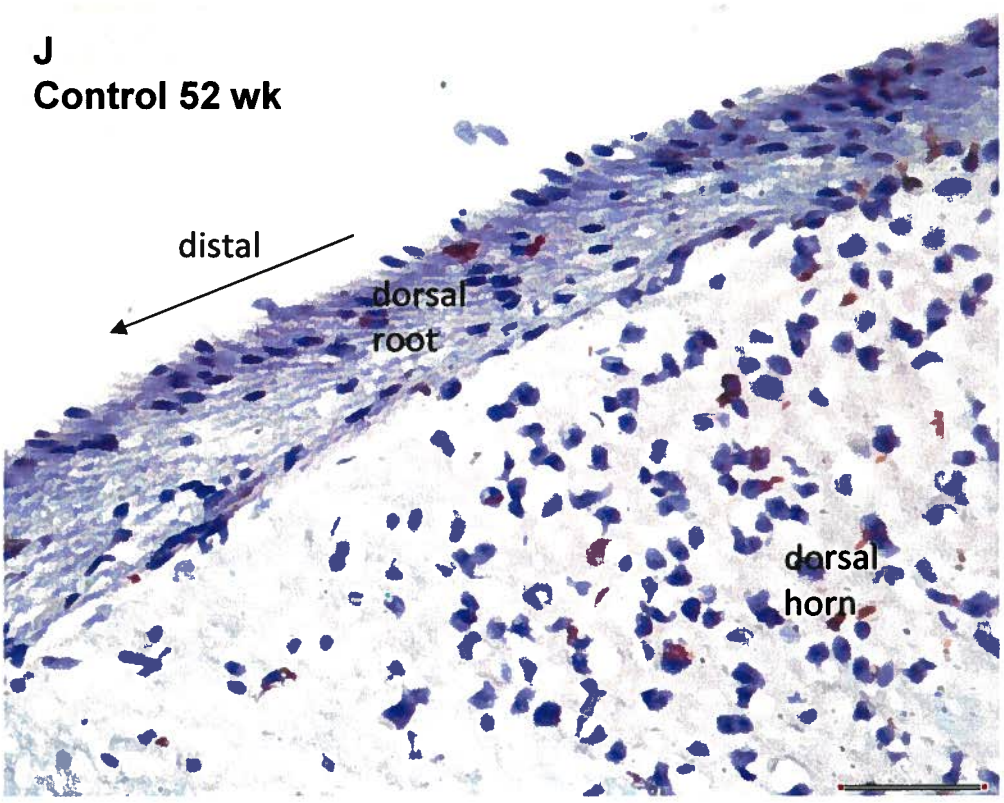
J
Control 52 wk
distal
dorsal
root
dorsal
horn

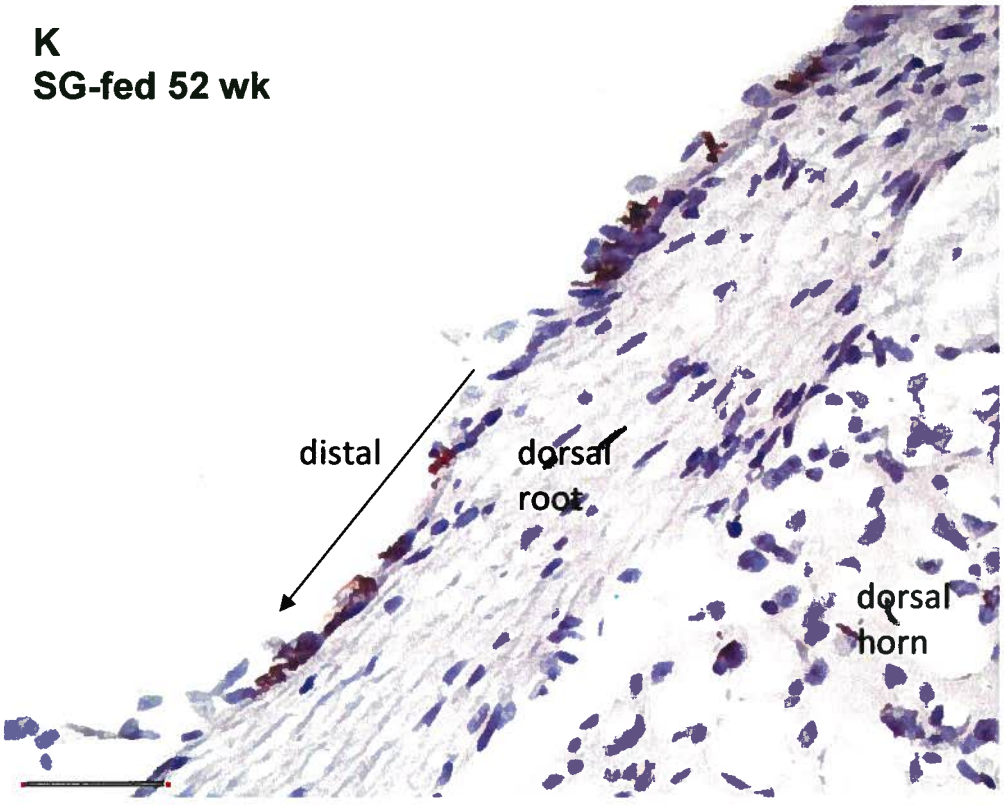
K
SG-fed 52 wk
distal
dorsal
root
dorsal
horn

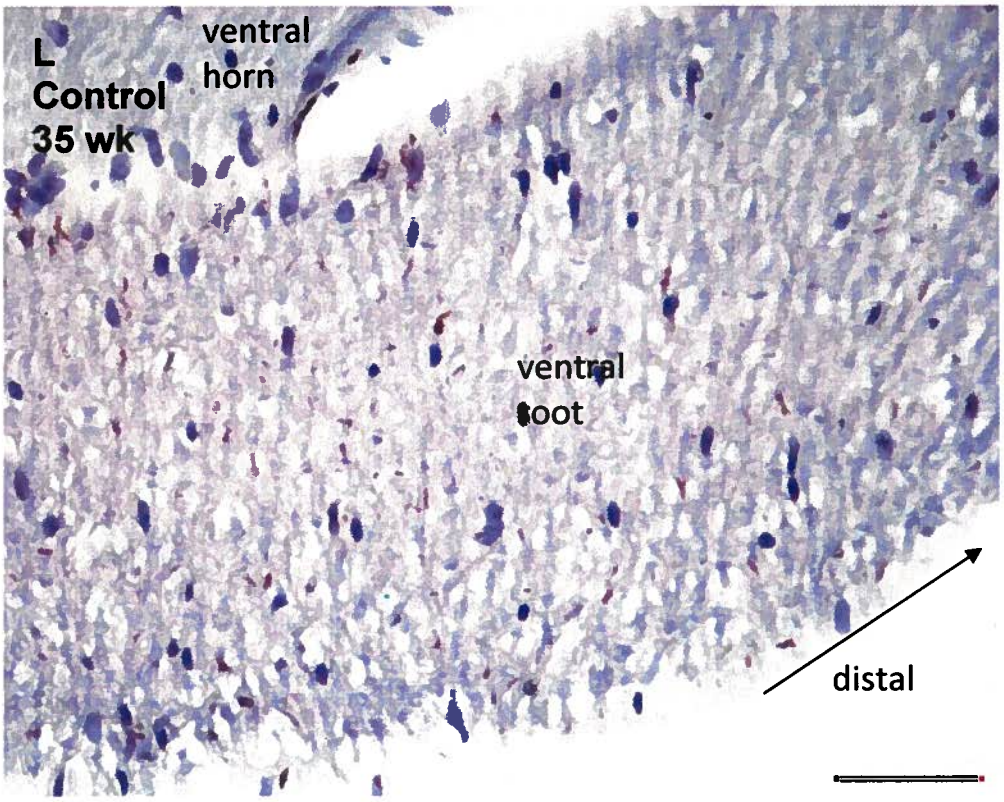
L
Control
35 wk
ventral
horn
ventral
root
distal

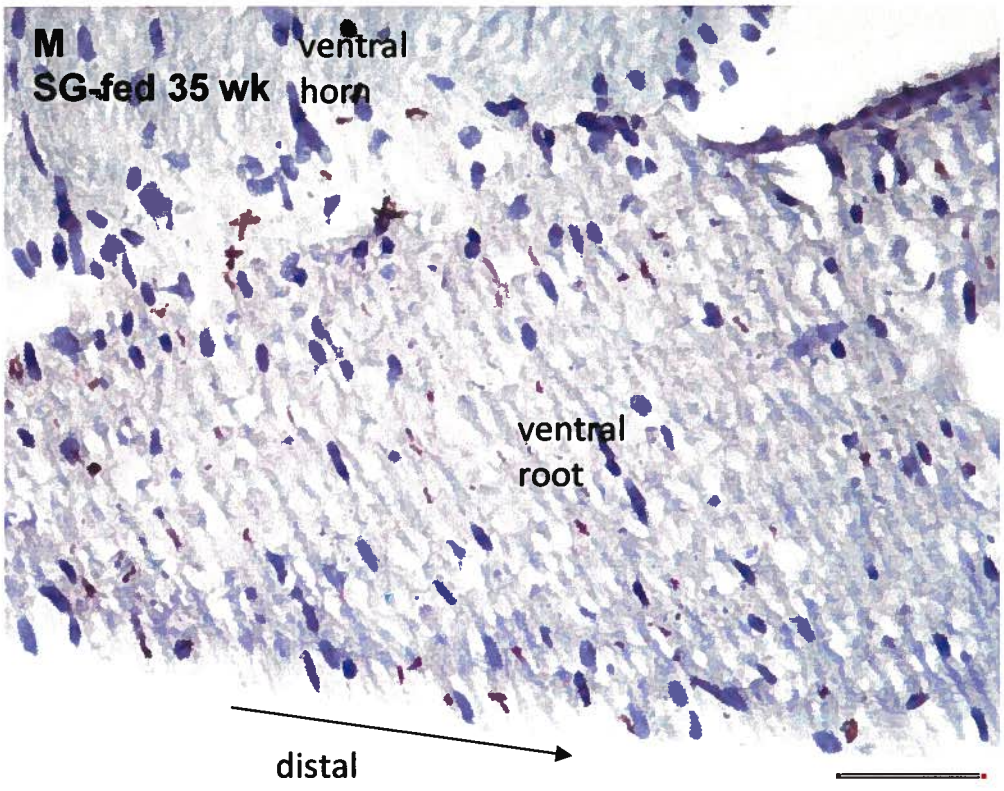
M
SG-fed 35 wk
ventral
horn
ventral
root
distal

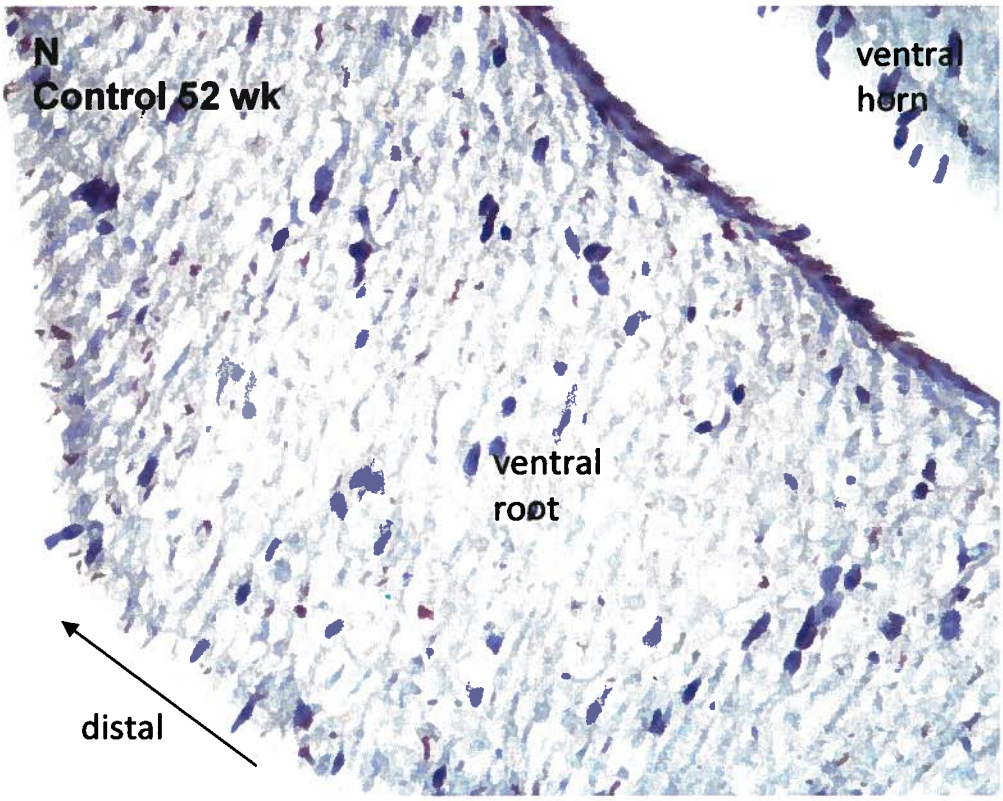
N
Control 52 wk
ventral
horn
ventral
root
distal

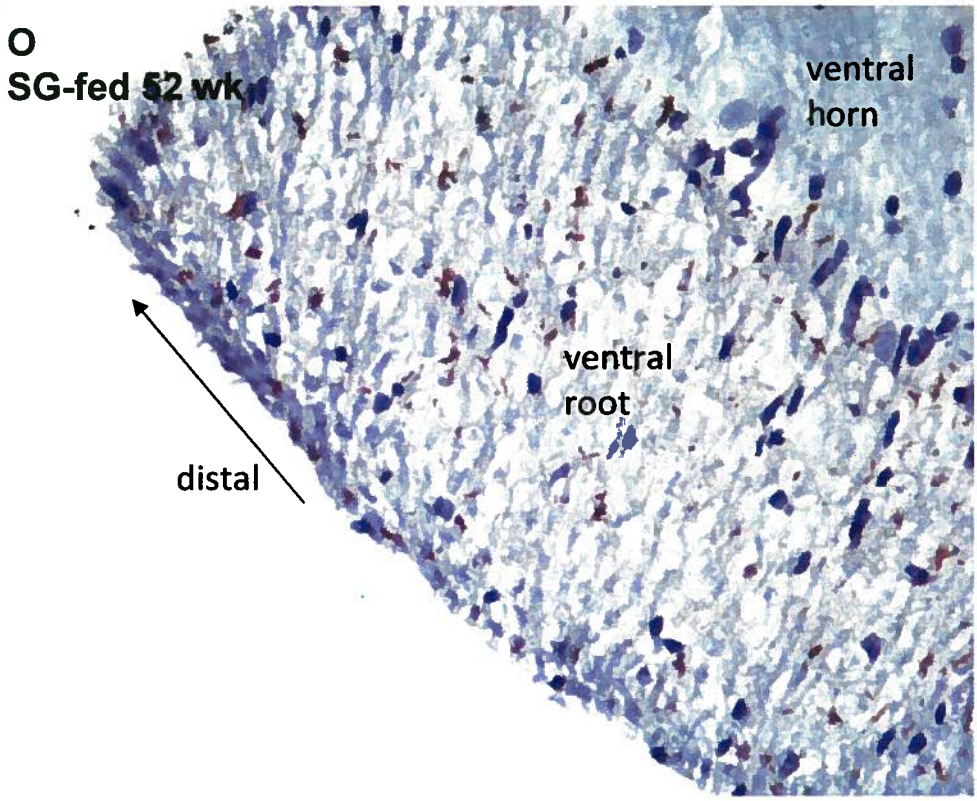
O
SG-fed 52 wk
ventral
horn
ventral
root
distal

Figure 34. **Oil red O staining of lipids in the lumbar spinal cord and dorsal and ventral spinal roots.**

Lipid deposits in various CNS regions were revealed by oil red O (red coloured stain). Nuclei were stained with haematoxylin (blue/purple coloured stain). Lipid deposits were observed in the motor neurons of control and SG-fed mice, but the number and size of the deposits were greater in lumbar spinal cord and ventral roots of SG-fed animals. Panel A shows a quantification of lipid deposits in control and SG-fed animals at 35 and 52 wk. An inter-group assessment of the ventral horn of the lumbar cord revealed that at 35 wk, SG-fed animals had significantly more lipid deposits in the ventral horn of the lumbar spinal cord (Student's t-test, +28%, *$p<0.05$). SG-fed animals also had significantly more lipids in the ventral spinal roots compared to control animals at 35 wk (Student's t-test: +10%, *$p<0.05$). A similar comparison of the dorsal roots did not show a statistically significant difference (Student's t-test: not significant, $p=0.3778$). At 52 wk, statistically significant inter-group differences were not found in the three CNS regions that were assessed (lumbar spinal cord: Student's t-test, $p=0.6406$; dorsal root: Student's t-test, $p=0.6958$; ventral root: Student's t-test, $p=0.7422$). Time-dependent effect assessment of lipid accumulation in SG-fed animals and age-matched controls was also performed. Control animals showed a statistically significant increase in the total number of lipid deposits over time (Student's t-test: +29%, $p<0.05$). SG-fed animals did not experience an accumulation of deposits over time (Student's t-test, $p=0.4864$). Both SG-fed animals and controls did not show time-dependent effects in the dorsal (Student's t-tests- control: $p=0.4864$; SG-fed: $p=0.5478$) or ventral roots (Control: $p=0.1301$; SG-fed: $p=0.5478$). Panels B and C show representative lumbar spinal cord ventral horn sections of a control and SG-fed animal respectively at 35 wk (40x objective, scale bars=50 µm). Panel D shows gliosis seen commonly in SG-fed animals (100x objective, scale bar=20 µm). Panel E and F are lumbar spinal cord ventral horn micrographs of control and SG-fed animals respectively at 52 wk (40x objective, scale bars=50 µm). Gliosis was again observed in the SG-fed animals at 52 wk (100x objective, scale bars=20 µm). The dorsal roots of control and SG-fed animals at each of the time points are also shown. At 35 wk, the number of lipid deposits in the dorsal and ventral roots was not statistically significant. However, at 52 wk, SG-fed animals were observed to have significantly more lipid deposits in both the dorsal (J, K) and ventral roots (N, O). Micrographs were captured using a light microscope under a 40x or a 100x objective lens. Scale bars = 50 µm (B, C, E, F, H, I, J, K, L, M, N, O) or 100 µm (D, G).

A

Stigmasterol β-D-glucoside feeding study: phosphorylated tau aggregates in the lumbar spinal cord at 52 wk

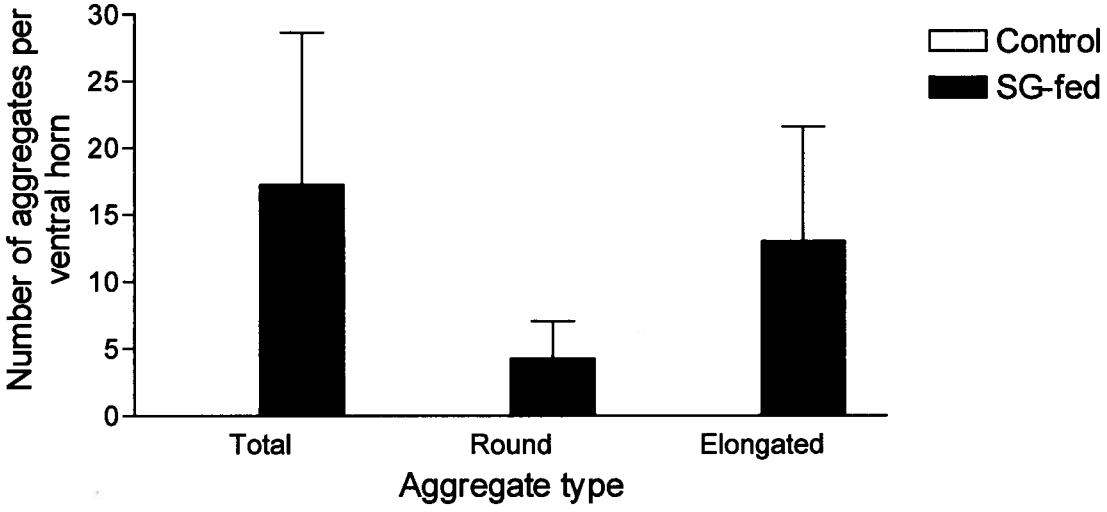

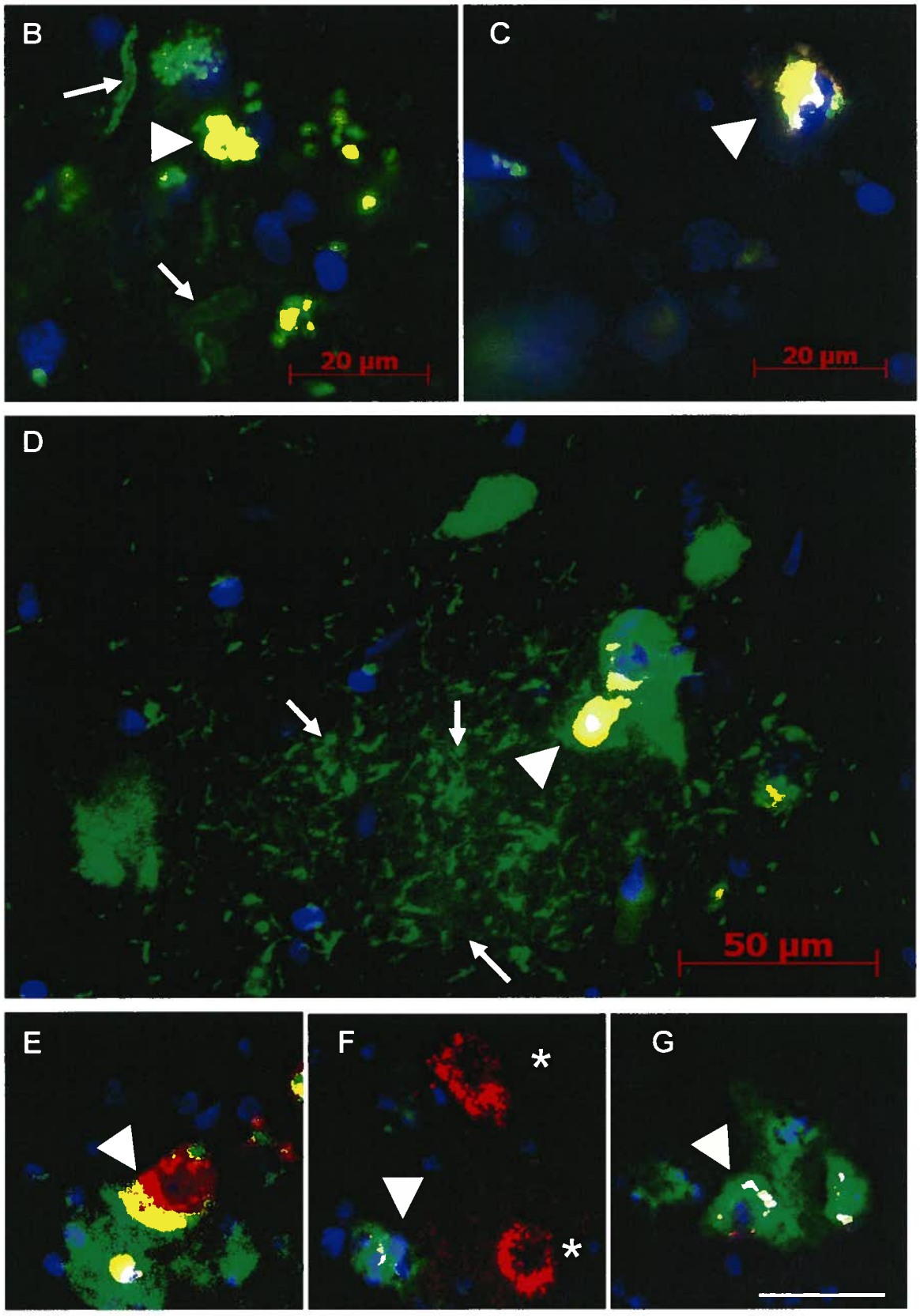
B
20 µm
C
20 µm
D
50 µm
E
F
*
*
G

Figure 35. **Select SG-fed mice accumulated phosphorylated tau in the ventral horn of the lumbar spinal cord and a subset of these phosphorylated tau-containing cells underwent apoptosis.**

Dietary SG-feeding induced accumulation of phosphorylated tau. A subset of these phosphorylated tau-containing cells was found to be actively undergoing apoptosis. Labelling of active caspase-3 (Casp-3) and pair-helical filament (PHF) tau phosphorylated at Ser-202 (AT8 clone) in the ventral horn of the lumbar spinal cord showed co-labelling. The majority of the phosphorylated-tau-containing cells were actively undergoing apoptosis in animals at 52 wk. (A) The number of elongated and round aggregates was quantified separately (A). Images were captured using a fluorescence microscope under a 40x objective lens. Panels B and C show positive control Alzheimer's dementia patient entorhinal cortex sections with marked phosphorylated-tau labelling. In the AD tissue, phosphorylated-tau containing neurons seemed to be undergoing apoptosis (yellow color: co-localization of phosphorylated-tau and active caspase-3; arrow heads) while the elongated debris were not (green probe: phosphorylated-tau; solid arrows). Panel D shows phosphorylated-tau labelled neurons (presumed α-motor neurons by size and morphology; arrow heads) as well as tau labelled debris-like entities dispersed throughout the neuropil (solid arrows). The "debris" did not co-localize with active caspase-3 (indicated by dashed arrows). Panel E through G shows additional examples of phosphorylated-tau containing neurons both undergoing (yellow color: co-localization of phosphorylated-tau and active caspase-3; arrow heads) and not undergoing (red label only: apoptotic neurons containing phosphorylated-tau; asterisk) apoptosis. Images were captured using a fluorescence microscope under a 40x objective lens. Blue = DAPI (nuclei); red = anti-active caspase-3; green = anti-phosphorylated-tau; and yellow = colocalization of anti-active caspase-3 and anti-phosphorylated-tau. In panels B and C, scale bar = 20 μm. In panels D-G, scale bar = 50 μm.

A

Stigmasterol β-D-glucoside feeding study: Phoshorylated tau aggregates in the lumbar spinal cord at 52 wk

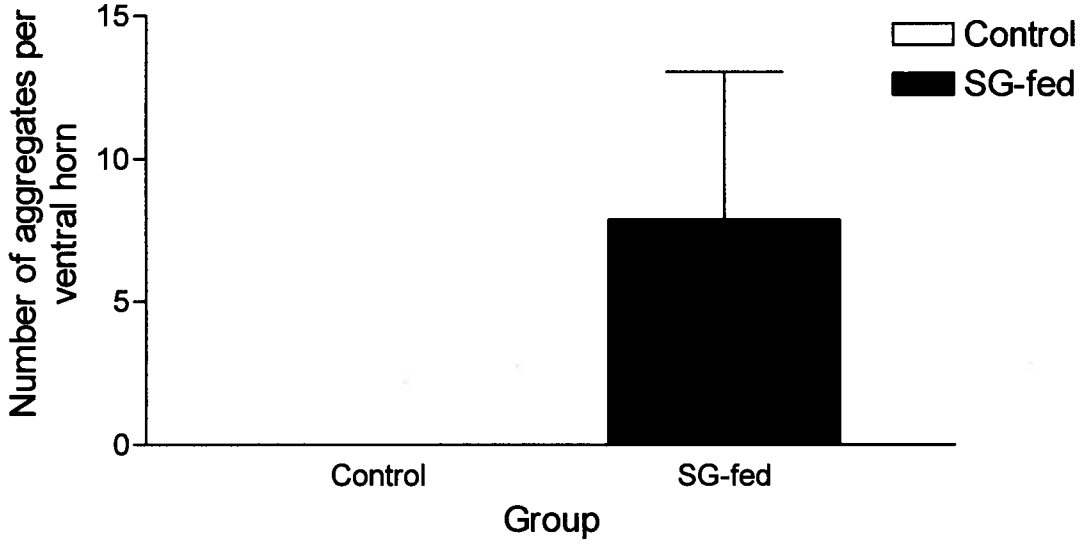

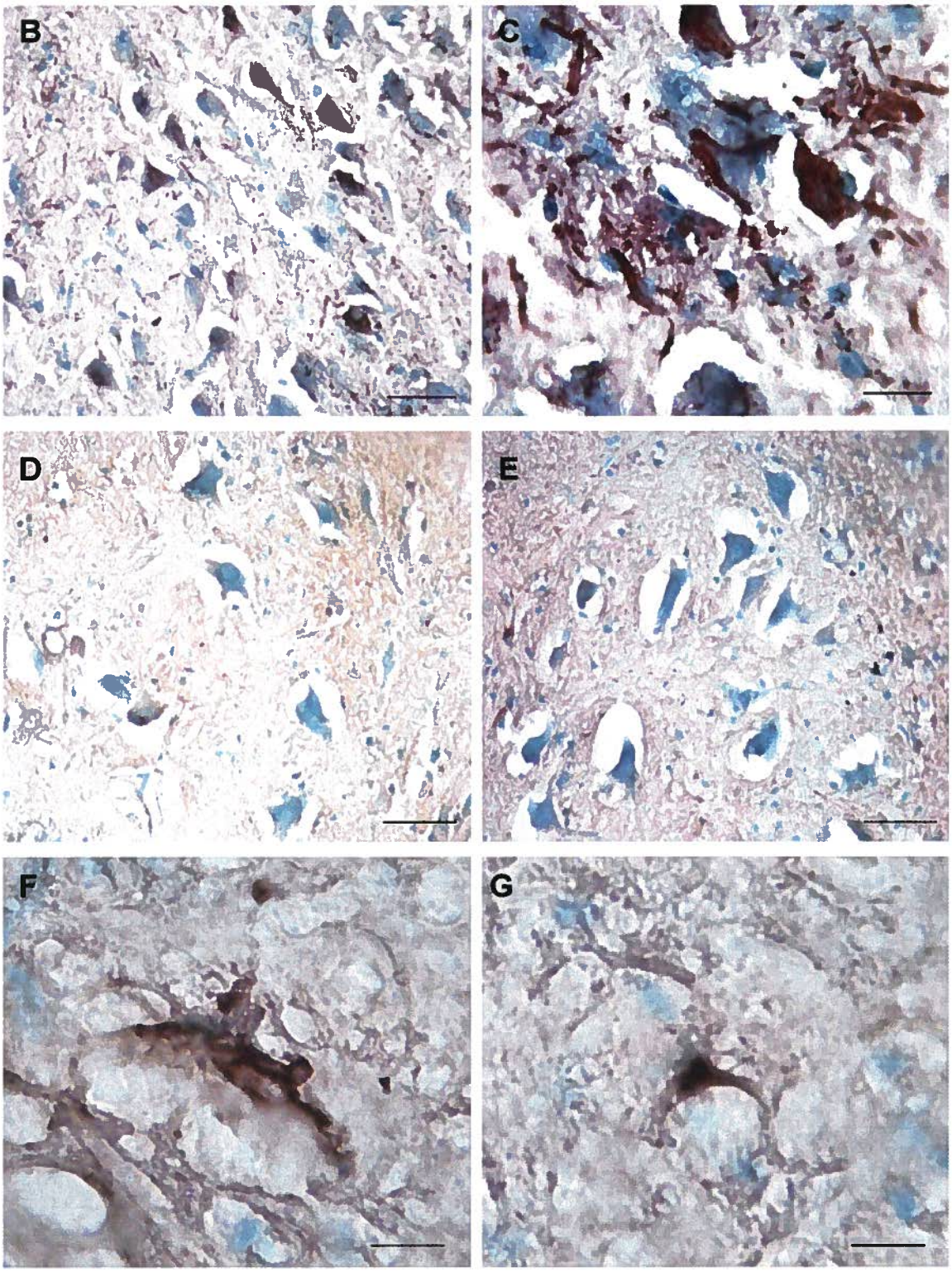
B
C
D
E
F
G

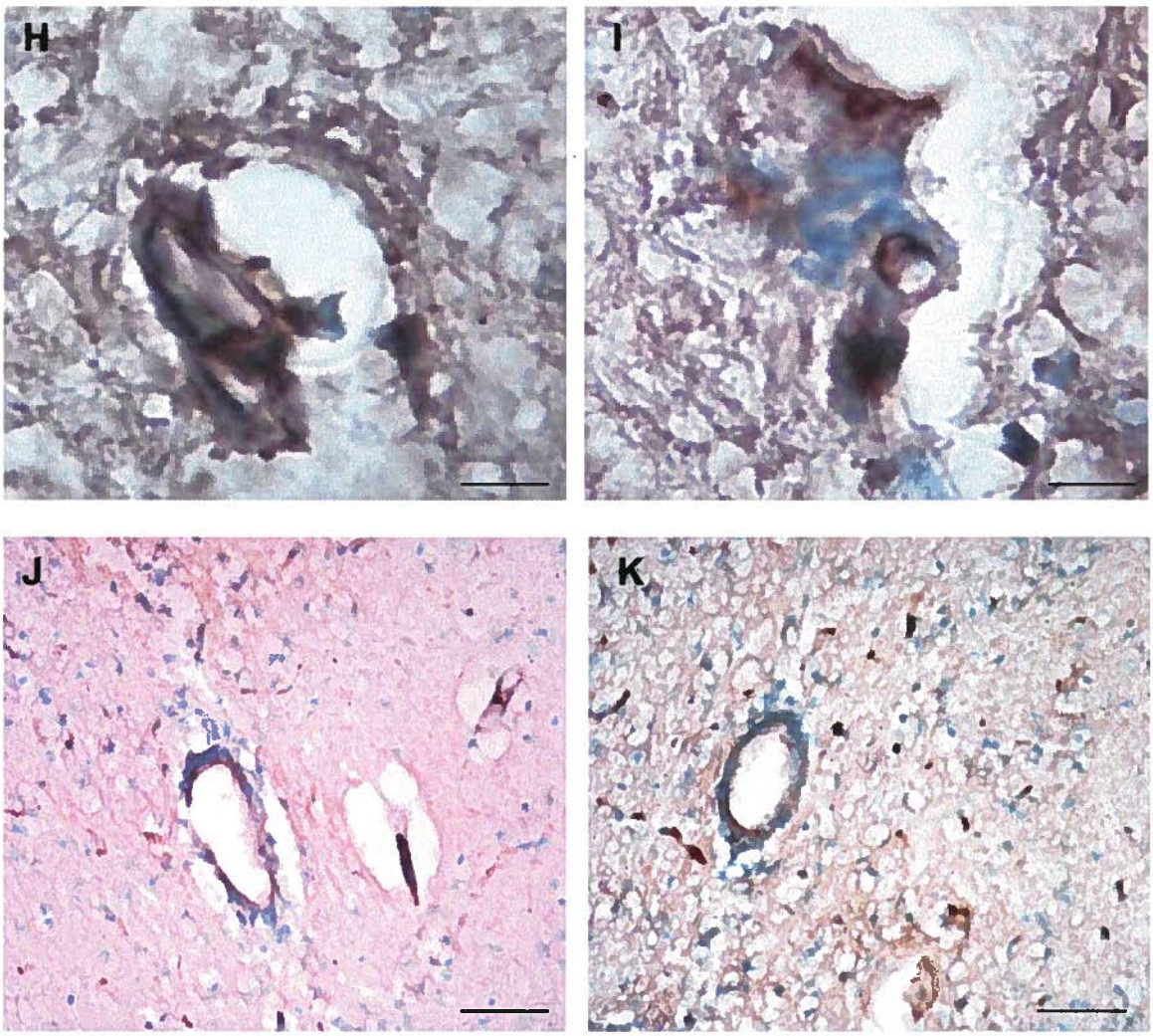
H
I
J
K

Figure 36. **Phoshorylated tau (PHF-tau, AT8 clone) inclusions in the lumbar spinal cord of SG-fed mice.**

Two of eight mice fed to SG and survived to 52 wk exhibited phosphorylated-tau pathology in the lumbar spinal cord. No abnormal accumulation of tau was observed in control animals, SG-fed animals at 35 wk, and in 6 of 8 SG-fed animals at 52 wk. (A) Quantification of phosphorylated-tau inclusions in the lumbar spinal cord of mice at 52 wk. Panels B and C show tau pathology in the entorhinal cortex of an Alzheimer's disease patient (positive control). Panels D and E show the absence of tau aggregation in control animals at 35 and 52 wk, respectively. Panels F-K show pathologic phosphrylated-tau aggregates that occurred in 2 of 8 SG-fed animals survived to 52 wk. Images were captured using a light microscope under a 20x (panels I and H), 40x (panels A, C, D) or 100x (panels B and E-H) objective lens. Scale bar=20 μm (panels B, E-H), 100 μm (panels I and J).

A

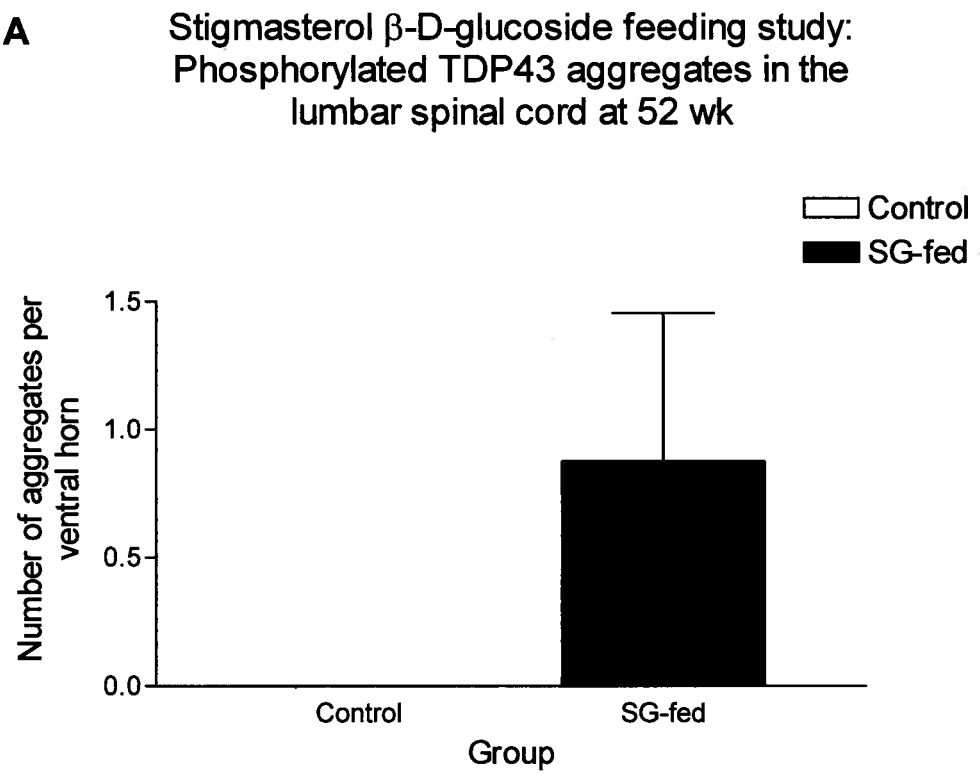
Stigmasterol β-D-glucoside feeding study:
Phosphorylated TDP43 aggregates in the
lumbar spinal cord at 52 wk
Control
SG-fed
Number of aggregates per ventral horn
1.5
1.0
0.5
0.0
Control
SG-fed
Group

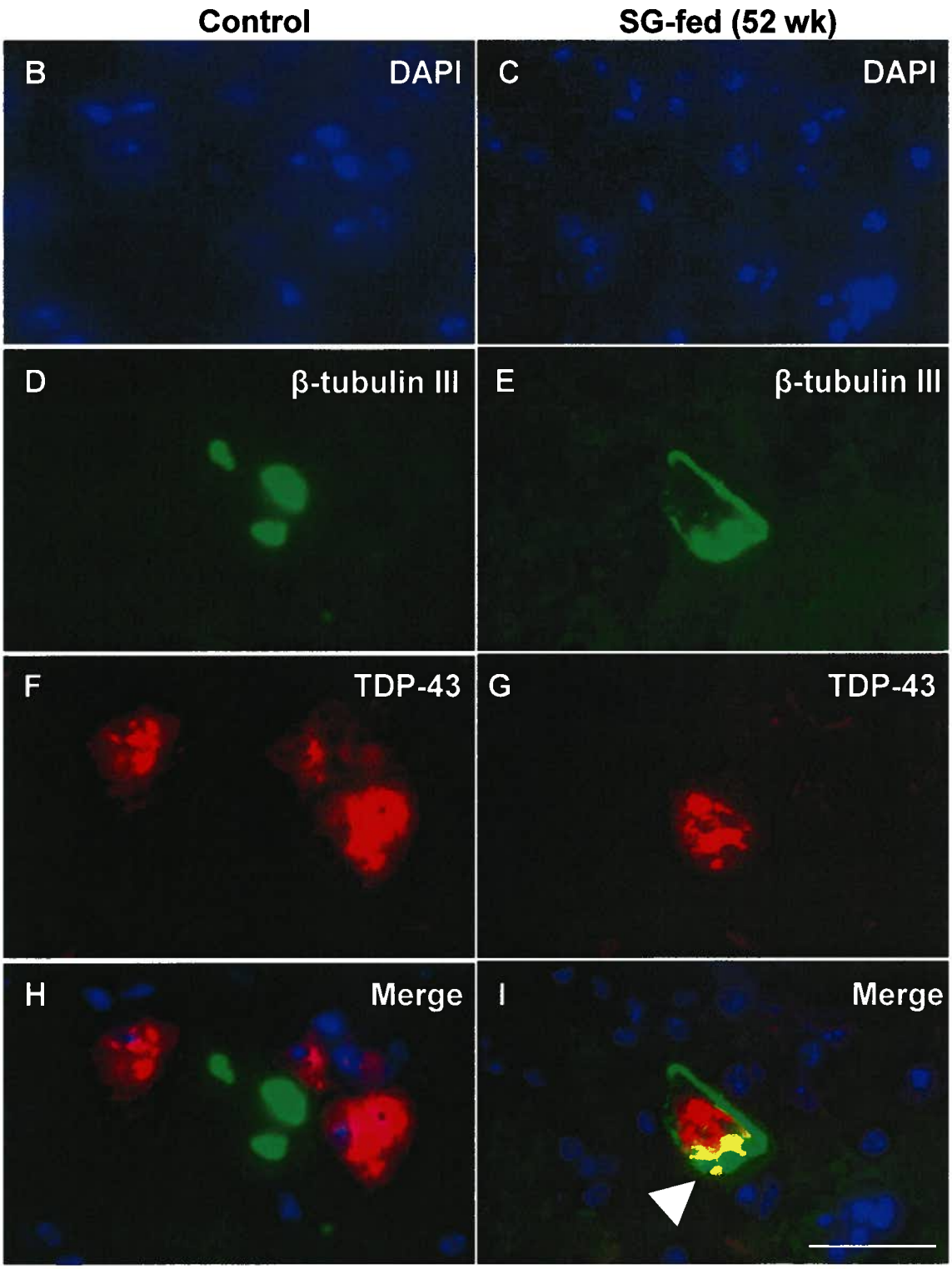
Control
SG-fed (52 wk)
B
DAPI
C
DAPI
D
β-tubulin III
E
β-tubulin III
F
TDP-43
G
TDP-43
H
Merge
I
Merge

Figure 37. **TDP-43 pathology occurs in the lumbar spinal cord of a subset of mice fed SG.**

Two of eight mice fed SG, survived to 52 wk exhibited TAR DNA binding protein (TDP) 43 pathology. In healthy cells, TDP-43 is found in the nucleus, but redistributes and accumulates in the cytosol in neurological conditions, such as in sporadic ALS. No abnormal translocation of TDP-43 was observed in control animals, SG-fed animals at 35 wk, and in the majority of SG-fed animals at 52 wk. The frontal cortex, hippocampus, and motor cortex were also negative in control animals at both time-points. Panel A depicts quantification of pathologic phosphorylated TDP-43-containing aggregates in the lumbar spinal cord. The difference in the total number of phosphorylated TDP-43 inclusions was not statistically significant (Student's t-test: ns, p= 0. 184022; standard deviation control group: 0.00, SG-fed: 1.642081; F-ratio variance: 0.00; p-variance: 1.000000). Panel I depicts a representative pathologic inclusion of a SG-fed animal survived to 52 wk. Pathologic colocalization of β-tubulin III and TDP-43 is indicated by the white arrow head (gold area, panel I). Panel B and C show DAPI nuclear staining; D and E show β-tubulin III (somatic morphology; green); F and G show TDP-43 staining; and H and I show merged images of A-C and E-G respectively. Images were captured using a fluorescence microscope under a 40x objective lens. Scale bar = 50 μm.

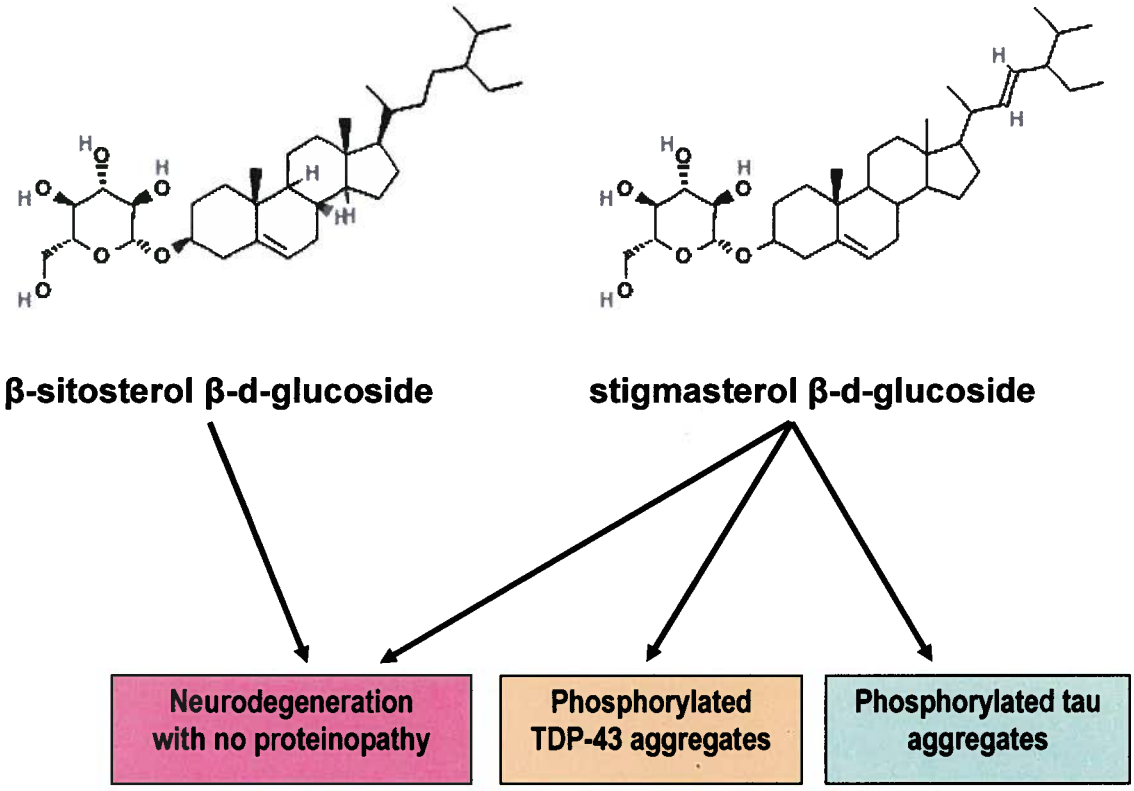

Figure 38. **Summary of the occurrence of proteinopathological inclusions in SG-fed animals.**

The proteino-pathology observed in the SG-fed mice were heterogeneous in that 25% of mice exhibited accumulation of pathological phosphorylated tau, and another 25% of the cohort exhibited accumulation of pathological phosphorylated TDP-43, and the remaining showed no signs of either aggregates. Further, at the same late time point, BSSG-fed animals did not show either form of proteinopathology.

	Time-point 1	Time-point 2
Mouse Strain, sex	CD1 (outbred), male	
Mouse age at study start	20 wk	
Numbers (n)	Control=14; SG-fed=16	Control=7; SG-fed=8
BSSG Feeding Duration	15 wk	15 wk
Post-feeding survival duration	0 wk	17 wk
Mouse age at sacrifice	35 wk	52 wk
Behavioural Tests	Leg extension Rotarod Wirehang Velocity of movement Angular velocity Percent time spent moving Total distance moved (ns) Total distance to zone border (ns) Total turn angle (ns) Forelimb braking (ns) Forelimb propulsion (ns) Forelimb stance width (ns) Forelimb stride length (ns) Hind limb braking (ns) Hind limb propulsion (ns) Hind limb stance width (ns) Hind limb stride length (ns) Hind limb stride frequency (ns)	Leg extension* Rotarod Wirehang* Velocity of movement Angular velocity Percent time spent moving Total distance moved Total distance to zone border* Total turn angle Forelimb braking* Forelimb propulsion* Forelimb stance width Forelimb stride length Hind limb braking* Hind limb propulsion* Hind limb stance width Hind limb stride length Hind limb stride frequency*
Motor Neurons per lumbar cord section	Healthy α-MN (ns) Chromatolytic α-MN (ns) Pyknotic α-MN (ns) Total α-MN: -29%* Total γ-MN (ns)	Healthy α-MN: -55%* Chromatolytic α-MN (ns) Pyknotic α-MN (ns) Total α-MN: -47* Total γ-MN (ns)
	Chromatolytic α-MN (control group & SG-group independently over time) (ns) Pyknotic α-MN (control group and SG-group independently over time) (ns) Total α-MN (control group over time (ns) Total α-MN (SG-fed group over time): -36%* Total γ-MN (control group and SG-group independently over time) (ns)	
Cholinergic cell number Choline acetyl transferase	Cholinergic neurons (-18%)	Cholinergic neurons (-32%)
	Total cholinergic cells (control group over time) (ns) Total cholinergic cells (SG-fed group over time): -32%*	

	Time-point 1	Time-point 2
Mouse Strain, sex	CD1 (outbred), male	
Mouse age at study start	20 wk	
Numbers (n)	Control=14; SG-fed=16	Control=7; SG-fed=8
BSSG Feeding Duration	15 wk	15 wk
Post-feeding survival duration	0 wk	17 wk
Mouse age at sacrifice	35 wk	52 wk
Stress induction Heat shock protein-70 Activating transcription factor-3 Phosphorylated Jun^{ser73}	Anti-Hsp-70: +1036%*** (VHLsc) Anti-Hsp-70: (ns, p=0.9697) (VHTsc)	Anti-Hsp-70: +425%* (VHLsc) Anti-Hsp-70: (ns, p=0.2793) (VHTsc)
	Anti-Hsp-70 Lsc (control group over time) (ns, p=0.7334) Anti-Hsp-70 Lsc (SG-fed group over time) (ns, p=0.1223) Anti-Hsp-70 Tsc (control group over time) (ns, p=0.2967) Anti-Hsp-70 Tsc (SG-fed group over time) (ns, p=0.8319)	
	Anti-ATF-3: +242%***	Anti-ATF-3: +101%**
	Anti-ATF-3 immunoreactive cells (control group over time) (ns) Anti-ATF-3 immunoreactive cells (SG-fed group over time): -48%***	
	Anti-pJun: +199%*	Anti-pJun (ns)
	Anti-pJun immunoreactive cells (control group over time) (ns) Anti-pJun immunoreactive cells (SG-fed group over time) (ns)	
Apoptotic activity Active Caspase-3	Anti-active caspase 3: +78%***	(ns)
	Apoptotic cells (control group over time) (ns) Apoptotic cells (SG-fed group over time) (ns)	
Astrocyte proliferation Glial fibrillary acidic protein	Anti-GFAP: +337%***	Anti-GFAP: +119%*
	Astrocytes (control group over time): +41%* Astrocytes (SG-fed group over time): -30%*	
Microglia proliferation Ionized calcium-binding adaptor molecule-1	Anti-IBA1: +33%**	Anti-IBA1: +59%*
	Anti-IBA-1 immunoreactive cells (control group over time) (ns) Anti-IBA-1 immunoreactive cells (SG-fed group over time) (ns)	
Cytochrome c oxidase activity	(ns)	(ns)
	Optical density (control group over time): -47%*** Optical density (SG-fed group over time): -36%**	
Dopaminergic cells Tyrosine Hydroxylase	-34%***	-39%*
	Optical density (control group over time) (ns) Optical density (SG-group over time): -22%*	
Lipid deposits Oil red O	Lipid deposits Lsc VH: +28%* Lipid deposits dorsal root: Lipid deposits ventral root:	Lipids deposits Lsc VH: +10%* Lipid deposits dorsal root: Lipid deposits ventral root:
	Control Lsc over time: +29%* SG-fed Lsc over time: ns, p=0.4864 Control DR over time: ns, p=0.4864 SG-fed DR over time: ns, p=0.8062 Control VR over time: ns, p=0.1301 SG-fed VR over time: ns, p=0.5478	

	Time-point 1	Time-point 2
Mouse Strain, sex	CD1 (outbred), male	
Mouse age at study start	20 wk	
Numbers (n)	Control=14; SG-fed=16	Control=7; SG-fed=8
BSSG Feeding Duration	15 wk	15 wk
Post-feeding survival duration	0 wk	17 wk
Mouse age at sacrifice	35 wk	52 wk
Phosphorylated tau aggregates	- Lsc VH, motor cortex, hippocampus	+ LscVH (in 2/8 of SG-fed group) - Motor cortex, hippocampus
Phosphorylated TDP-43 aggregates	- Lsc VH, motor cortex, hippocampus	+ LscVH (in 2/8 of SG-fed group) - Motor cortex, hippocampus

*p<0.05; **p<0.01; ***p<0.00
not significant = ns; Lsc = lumbar spinal cord; Tsc = thoracic spinal cord; ventral horn = VH; dorsal root=DR: - = not present; + = present

Table 2. **Summary of neurological outcomes following SG feeding.**

CHAPTER 5 General discussion and future studies

5.1 General discussion

5.1.1 General discussion

Amyotrophic lateral sclerosis-parkinsonism dementia complex (ALS-PDC) is a neurodegenerative cluster of disorders characterized by a combination of varying degrees of amyotrophic lateral sclerosis, Parkinson's dementia, and Alzheimer's dementia features. Epidemiological studies indicate a link between consumption of cycad seeds and disease development. When washed cycad flour was biochemically analyzed, likely neurotoxins turned out to be variant forms of sterol glucosides (Khabazian et al., 2002b). A study that measured the proportion of insoluble sterol glucosides in washed cycad seeds found that β-sitosterol β-D-glucoside (BSSG) is present in the greatest quantity (Khabazian et al., 2002b). In the same study, rat cortical neurons were exposed to various cycad sterol glucosides including BSSG and stigmastersol β-D-glucoside (SG), and the latter was found to be most toxic of the tested sterol glucosides *in vitro* (Khabazian et al., 2002c). The purpose of the present study was to investigate the effects of BSSG and SG on the CNS *in vivo*. Specifically, I set out to determine whether the motor system as a whole and its major physiological players were affected by dietary BSSG and SG exposure. The results were obtained by conducting experiments designed to test the hypotheses that SG and BSSG found in washed cycad flour are contributory to the pathogenesis of ALS-PDC. The sterol glucoside content in the experimental mouse pellets were designed to reflect the body-weight adjusted quantity of each sterol glucoside consumed by Chamorro people. The ability to recreate key aspects of the disease by exposing mice to pure cycad neurotoxic compounds enables us to gain a better understanding of the pathogenesis from initial exposure to behavioural deficits to cellular pathology, which in turn can be used to map the temporal sequence of events in ALS-PDC and other neurological diseases. The results of the present *in vivo* work show that SG is one of the more potent of the cycad sterol glucosides. The present study also shows that BSSG and SG induce behavioural and cellular pathology both distinct and overlapping from

each other. Each study on its own was found to mirror key aspects of ALS-PDC. While each of the studies reflected a relatively small sample, a variety of behavioural and pathological outcomes was observed. The findings are consistent with the variation in behavioural and neurological symptoms seen in humans afflicted with ALS-PDC. Humans with ALS-PDC may have a different combination of varying degrees of ALS, parkinsonism, and dementia features. In both feeding studies, every mouse also exhibited differing degrees of ALS, parkinsonism and dementia phenotypes. Variation was observed with the cellular assessments as well, but nonetheless, each sterol glucoside was found to induce the loss of neurons in specific regions of the CNS. Overall, the present findings add to the cycad-induced murine model of the progressive neurological disease, ALS-PDC.

5.1.2 Potential sources of error

The major source of error is due to the variability among the tested animals. While the mice were age-matched, species-matched, placed in the same living and experimental conditions, variation inevitably exists in every group of animals. An outbred strain of mice was deliberately chosen to reflect the genetic variability in humans. Accordingly, the behavioural and neuropathological outcomes were heterogeneous, but the present studies would have benefited from a larger experimental group. Initially, there was a decent sample size for each of the studies, but in the BSSG study, a request for tissue to be put aside for biochemistry at a time point different from that which was originally planned for the present studies effectively reduced the sample size from 31 to 21. Similarly, in the SG study reductions in the sample size occurred unexpectedly, due to spontaneous illness of several mice reducing the sample size from 35 to 30. Nonetheless, a sufficient number of animals were utilized in each study, providing ample power in statistical analysis. In future, given the opportunity, I would run similar studies with a larger sample size to obtain greater power.

General motor activity for the present studies was conducted under standard light conditions. However, animal behavioural testing would have generated better results had they been conducted on animals housed under a reverse light cycle, where the room is maintained on a circadian lighting cycle with lights on at night and lights off during the day. This method is preferred for mouse behavioural testing since it allows observers to test the mouse during its most active period, rather than when it is normally sleeping (Crawley, 2000). Animal care facilities that strive to meet the needs of multiple users often operate under standard lighting conditions due to practical considerations, which was the case with the animal care facility of the present study. In the future I would propose in my Animal Care Protocol to use circadian light cycle controllers to regulate the daily lighting system (Crawley, 2000). When conducting the behavioural tests in the dark, I would use a red light bulb in the room lamp fixtures or other lighting devices to enable me to see what I am doing since rodents are unable to detect red light (Crawley, 2000).

Stereological practices were not used for the present studies to quantify immunoreactive motor neurons. However, various measures were used to ensure the best quantitative results (described in the Methods, Chapter 2). Where appropriate, motor neurons were sub-grouped and quantified and shown alongside "total" counts. A comparison of motor neuron counts obtained from Nissl body staining and choline acetyl transferase immunofluorescence showed reliability in the quantification protocol. Both methods gave similar data in each of the sterol glucoside feeding studies suggesting that the sampling and histological procedures are reliable.

5.2 Future studies

The involvement of several signalling proteins and cell types has been determined from the current studies. However a detailed analysis has yet to be completed to reveal other proteins, enzymes, and CNS regions involved. Both BSSG and SG feeding were found to induce apoptosis in lumbar spinal cord motor neurons, however, some motor neurons always were spared. It would be

instructive to determine how these motor neurons were able to overcome the stresses that the others succumbed to and by what processes or molecules they were able to accomplish this by. Determination of a specific mechanism or a molecule that permits motor neuron survival will afford information for neurodegenerative disease therapeutic development and targeting.

The timing of animal exposure to the sterol glucosides was standardized to permit comparison amongst the sterol glucoside and cycad flour feeding studies. However, the possibility that the age of exposure to these sterols may have a hand in determining the severity or pattern of changes cannot be ignored. Further work still needs to be done to determine whether the timing of sterol glucoside exposure will change the behavioural and cellular outcomes. For example, exposure to sterol glucosides *in utero*, or in late adulthood, or for intermittent periods of exposure may produce differing outcomes. With respect to this, current work in our laboratory is investigating the effect of *in utero* exposure to sterol glucosides on targeted days when neurons in the substantia nigra and striatum are differentiating. Preliminary results of this study are showing profound differences between the control and sterol glucoside-exposed groups as well as differences as a function of sex (Yemi Banjo, personal communication).

BSSG and SG were singly able to induce neuropathology. However, I believe that ALS-PDC and other neurodegenerative diseases cannot be caused by a single environment or genetic factor. Instead, in the whole animal or person, a gene-toxin interaction likely contributes to the determination of disease acquirement and severity. Challenging animals expressing susceptibility genes such as those for any of the mutant superoxide dismutases or amyloid precursor protein with BSSG or SG alone, together, or in combination with other insoluble cycad sterol glucosides will bring us one step closer to resolving this issue.

In a previous study conducted by Wilson et al (2003, 2004), magnetic resonance microscopy (MRM) scans of cycad-fed mice showed that cycad-treatment induced decreases in the volume of lumbar spinal cord gray matter, striatum, substantia nigra, basal nucleus/internal capsule and olfactory bulb

(granule layer). It would be interesting to assess whether SG or BSSG treatment induces volume decrease in mice and compare with the cycad-fed mice MR scans.

Lastly, while one of the present studies assessed the behavioural and neuropathological outcomes of dietary exposure to SG, it still only looked at two time points. A future study which includes the analysis of mice that survive into late adulthood may provide further insights into the toxic actions of these molecules and its full range of neuropathologic outcomes. The ability to induce a clear temporal sequence of behavioural and pathological changes in the CNS may provide important clues to the overall processes of neurodegeneration. If such data could be correlated to the still unknown stages in human neurological disease, they might provide a wealth of pharmacological targets for early therapeutic intervention.

Reference List

1. Aarsland, D., Andersen, K., Larsen, J. P., Lolk, A., and Kragh-Sorensen, P. (2003) Prevalence and characteristics of dementia in Parkinson disease: an 8- year prospective study. ***Arch Neurol***. **60**, 387-92.

2. Ahlskog, J. E., Waring, S. C., Petersen, R. C., Esteban-Santillan, C., Craig, U. K., O'Brien, P. C., Plevak, M. F., and Kurland, L. T. (1998) Olfactory dysfunction in Guamanian ALS, parkinsonism, and dementia. ***Neurology***. **51**, 1672-7.

3. Alnemri, E. S., Livingston, D. J., Nicholson, D. W., Salvesen, G., Thornberry, N. A., Wong, W. W., and Yuan, J. (1996) Human ICE/CED-3 protease nomenclature. ***Cell***. **87**, 171.

4. Alonso, A. C., Grundke-Iqbal, I., and Iqbal, K. (1996) Alzheimer's disease hyperphosphorylated tau sequesters normal tau into tangles of filaments and disassembles microtubules. ***Nat Med***. **2**, 783-7.

5. Anderson, C. M. and Swanson, R. A. (2000) Astrocyte glutamate transport: review of properties, regulation, and physiological functions. ***Glia***. **32**, 1-14.

6. Arai, T., Hasegawa, M., Akiyama, H., Ikeda, K., Nonaka, T., Mori, H., Mann, D., Tsuchiya, K., Yoshida, M., Hashizume, Y., and Oda, T. (2006) TDP-43 is a component of ubiquitin-positive tau-negative inclusions in frontotemporal lobar degeneration and amyotrophic lateral sclerosis. ***Biochem Biophys Res Commun***. **351**, 602-11.

7. Arasaki, K. and Tamaki, M. (1998) A loss of functional spinal alpha motor neurons in amyotrophic lateral sclerosis. ***Neurology***. **51**, 603-5.

8. Arima, K., Hirai, S., Sunohara, N., Aoto, K., Izumiyama, Y., Ueda, K., Ikeda, K., and Kawai, M. (1999) Cellular co-localization of phosphorylated tau- and NACP/alpha- synuclein-epitopes in lewy bodies in sporadic Parkinson's disease and in dementia with Lewy bodies. ***Brain Res***. **843**, 53-61.

9. Auluck, P. K., Chan, H. Y., Trojanowski, J. Q., Lee, V. M., and Bonini, N. M. (2002) Chaperone suppression of alpha-synuclein toxicity in a Drosophila model for Parkinson's disease. ***Science***. **295**, 865-8.

10. Azoyan, P., Garnier, R., Poitrineau, H., and Taboulet, P. (1991) [Acute poisoning by scilliroside]. ***J Toxicol Clin Exp***. **11**, 189-92.

11. Barbeito, L. H., Pehar, M., Cassina, P., Vargas, M. R., Peluffo, H., Viera, L., Estevez, A. G., and Beckman, J. S. (2004) A role for astrocytes in motor neuron loss in amyotrophic lateral sclerosis. ***Brain Res Brain Res***

Rev. **47**, 263-74.

12. Barlow, C., Hirotsune, S., Paylor, R., Liyanage, M., Eckhaus, M., Collins, F., Shiloh, Y., Crawley, J. N., Ried, T., Tagle, D., and Wynshaw-Boris, A. (1996) Atm-deficient mice: a paradigm of ataxia telangiectasia. ***Cell.*** **86**, 159-71.

13. Barneoud, P. and Curet, O. (1999) Beneficial effects of lysine acetylsalicylate, a soluble salt of aspirin, on motor performance in a transgenic model of amyotrophic lateral sclerosis. ***Exp Neurol.*** **155**, 243-51.

14. Barneoud, P., Lolivier, J., Sanger, D. J., Scatton, B., and Moser, P. (1997) Quantitative motor assessment in FALS mice: a longitudinal study. ***Neuroreport.*** **8**, 2861-5.

15. Becker, J. and Craig, E. A. (1994) Heat-shock proteins as molecular chaperones. ***Eur J Biochem.*** **219**, 11-23.

16. Benn, S. C., Perrelet, D., Kato, A. C., Scholz, J., Decosterd, I., Mannion, R. J., Bakowska, J. C., and Woolf, C. J. (2002) Hsp27 upregulation and phosphorylation is required for injured sensory and motor neuron survival. ***Neuron.*** **36**, 45-56.

17. Bodart, P., Kabengera, C., Noirfalise, A., Hubert, P., and Angenot, L. (2000) Determination of alpha-solanine and alpha-chaconine in potatoes by high-performance thin-layer chromatography/densitometry. ***J AOAC Int.*** **83**, 1468-73.

18. Borenstein, A. R., Mortimer, J. A., Schofield, E., Wu, Y., Salmon, D. P., Gamst, A., Olichney, J., Thal, L. J., Silbert, L., Kaye, J., Craig, U. L., Schellenberg, G. D., and Galasko, D. R. (2007) Cycad exposure and risk of dementia, MCI, and PDC in the Chamorro population of Guam. ***Neurology.*** **68**, 1764-71.

19. Bouic, P. J. (2002) Sterols and sterolins: new drugs for the immune system? ***Drug Discov Today.*** **7**, 775-8.

20. Brich, J., Shie, F. S., Howell, B. W., Li, R., Tus, K., Wakeland, E. K., Jin, L. W., Mumby, M., Churchill, G., Herz, J., and Cooper, J. A. (2003) Genetic modulation of tau phosphorylation in the mouse. ***J Neurosci.*** **23**, 187-92.

21. Bruening, W., Roy, J., Giasson, B., Figlewicz, D. A., Mushynski, W. E., and Durham, H. D. (1999) Up-regulation of protein chaperones preserves viability of cells expressing toxic Cu/Zn-superoxide dismutase mutants associated with amyotrophic lateral sclerosis. ***J Neurochem.*** **72**, 693-9.

22. Buratti, E. and Baralle, F. E. (2001) Characterization and functional

implications of the RNA binding properties of nuclear factor TDP-43, a novel splicing regulator of CFTR exon 9. ***J Biol Chem***. **276**, 36337-43.

23. Calne, D. B. and Eisen, A. (1989) The relationship between Alzheimer's disease, Parkinson's disease and motor neuron disease. ***Can J Neurol Sci***. **16**, 547-50.

24. Campbell, M. E., Mickelsen, O., Yang, M. G., Laqueur, G. L., and Keresztesy, J. C. (1966) Effects of strain, age and diet on the response of rats to the ingestion of Cycas circinalis. ***J Nutr***. **88**, 115-24.

25. Carrell, R. W. and Lomas, D. A. (1997a) Conformational disease. ***Lancet***. **350**, 134-8.

26. Carter, R. J., Lione, L. A., Humby, T., Mangiarini, L., Mahal, A., Bates, G. P., Dunnett, S. B., and Morton, A. J. (1999) Characterization of progressive motor deficits in mice transgenic for the human Huntington's disease mutation. ***J Neurosci***. **19**, 3248-57.

27. Chapillon, P., Lalonde, R., Jones, N., and Caston, J. (1998) Early development of synchronized walking on the rotorod in rats. Effects of training and handling. ***Behav Brain Res***. **93**, 77-81.

28. Chen, B. P., Liang, G., Whelan, J., and Hai, T. (1994) ATF3 and ATF3 delta Zip. Transcriptional repression versus activation by alternatively spliced isoforms. ***J Biol Chem***. **269**, 15819-26.

29. Chen, C., Kano, M., Abeliovich, A., Chen, L., Bao, S., Kim, J. J., Hashimoto, K., Thompson, R. F., and Tonegawa, S. (1995) Impaired motor coordination correlates with persistent multiple climbing fiber innervation in PKC gamma mutant mice. ***Cell***. **83**, 1233-42.

30. Chen, S. and Brown, I. R. (2007) Neuronal expression of constitutive heat shock proteins: implications for neurodegenerative diseases. ***Cell Stress Chaperones***. **12**, 51-8.

31. Chu, H. M., Tan, Y., Kobierski, L. A., Balsam, L. B., and Comb, M. J. (1994) Activating transcription factor-3 stimulates 3',5'-cyclic adenosine monophosphate-dependent gene expression. ***Mol Endocrinol***. **8**, 59-68.

32. Coates, C. and Bakheit, A. M. (1997) The prevalence of verbal communication disability in patients with Parkinson's disease. ***Disabil Rehabil***. **19**, 104-7.

33. Cohen, J. J. (1993) Apoptosis: the physiologic pathway of cell death. ***Hosp Pract (Off Ed)***. **28**, 35-43.

34. Crawley, J. N. (1999) Behavioral phenotyping of transgenic and knockout

mice: experimental design and evaluation of general health, sensory functions, motor abilities, and specific behavioral tests. ***Brain Res.*** **835**, 18-26.

35. Crawley, J. N. (2000) What' s Wrong With My Mouse? : Behavioral Phenotyping of Trangenic and Knockout Mice. 65--69.

36. Crawley, J. N. and Paylor, R. (1997) A proposed test battery and constellations of specific behavioral paradigms to investigate the behavioral phenotypes of transgenic and knockout mice. ***Horm Behav.*** **31**, 197-211.

37. Cruz-Aguado, R., Winkler, D., and Shaw, C. A. (2006) Lack of behavioral and neuropathological effects of dietary b-methylaminoalanine (BMAA) in mice. ***Pharmacol. Biochem. Behav.*** in press.

38. Dauer, W. and Przedborski, S. (2003) Parkinson's disease: mechanisms and models. ***Neuron.*** **39**, 889-909.

39. Dobson, C. M. (1999) Protein misfolding, evolution and disease. ***Trends Biochem Sci.*** **24**, 329-32.

40. Dobson, C. M. (2003) Protein folding and misfolding. ***Nature.*** **426**, 884-90.

41. Dobson, C. M. and Karplus, M. (1999) The fundamentals of protein folding: bringing together theory and experiment. ***Curr Opin Struct Biol.*** **9**, 92-101.

42. Doty, R. L., Perl, D. P., Steele, J. C., Chen, K. M., Pierce, J. D. Jr, Reyes, P., and Kurland, L. T. (1991) Olfactory dysfunction in three neurodegenerative diseases. ***Geriatrics.*** **46 Suppl 1**, 47-51.

43. Dou, F., Netzer, W. J., Tanemura, K., Li, F., Hartl, F. U., Takashima, A., Gouras, G. K., Greengard, P., and Xu, H. (2003) Chaperones increase association of tau protein with microtubules. ***Proc Natl Acad Sci U S A.*** **100**, 721-6.

44. Duncan, M. W., Steele, J. C., Kopin, I. J., and Markey, S. P. (1990) 2-Amino-3-(methylamino)-propanoic acid (BMAA) in cycad flour: an unlikely cause of amyotrophic lateral sclerosis and parkinsonism- dementia of Guam. ***Neurology.*** **40**, 767-72.

45. Durlach, J., Bac, P., Durlach, V., Durlach, A., Bara, M., and Guiet-Bara, A. (1997) Are age-related neurodegenerative diseases linked with various types of magnesium depletion? ***Magnes Res.*** **10**, 339-53.

46. Eilers, A., Whitfield, J., Babij, C., Rubin, L. L., and Ham, J. (1998) Role of the Jun kinase pathway in the regulation of c-Jun expression and

apoptosis in sympathetic neurons. ***J Neurosci***. **18**, 1713-24.

47. Erdmann, A. A., Gao, Z. G., Jung, U., Foley, J., Borenstein, T., Jacobson, K. A., and Fowler, D. H. (2005) Activation of Th1 and Tc1 cell adenosine A2A receptors directly inhibits IL-2 secretion in vitro and IL-2-driven expansion in vivo. ***Blood***. **105**, 4707-14.

48. Fawcett, J. W. and Geller, H. M. (1998) Regeneration in the CNS: optimism mounts. ***Trends Neurosci***. **21**, 179-80.

49. Flint, J., Corley, R., DeFries, J. C., Fulker, D. W., Gray, J. A., Miller, S., and Collins, A. C. (1995) A simple genetic basis for a complex psychological trait in laboratory mice. ***Science***. **269**, 1432-5.

50. Forman, M. S., Schmidt, M. L., Kasturi, S., Perl, D. P., Lee, V. M., and Trojanowski, J. Q. (2002) Tau and alpha-synuclein pathology in amygdala of Parkinsonism-dementia complex patients of Guam. ***Am J Pathol***. **160**, 1725-31.

51. Garruto, R. M., Gajdusek, C., and Chen, K. M. (1980) Amyotrophic lateral sclerosis among Chamorro migrants from Guam. ***Ann Neurol***. **8**, 612-9.

52. Gerlai, R., Millen, K. J., Herrup, K., Fabien, K., Joyner, A. L., and Roder, J. (1996a) Impaired motor learning performance in cerebellar En-2 mutant mice. ***Behav Neurosci***. **110**, 126-33.

53. Gerlai, R. and Roder, J. (1996) Spatial and nonspatial learning in mice: effects of S100 beta overexpression and age. ***Neurobiol Learn Mem***. **66**, 143-54.

54. Hai, T. and Hartman, M. G. (2001) The molecular biology and nomenclature of the activating transcription factor/cAMP responsive element binding family of transcription factors: activating transcription factor proteins and homeostasis. ***Gene***. **273**, 1-11.

55. Hai, T., Wolfgang, C. D., Marsee, D. K., Allen, A. E., and Sivaprasad, U. (1999) ATF3 and stress responses. ***Gene Expr***. **7**, 321-35.

56. Hall, E. D., Oostveen, J. A., and Gurney, M. E. (1998) Relationship of microglial and astrocytic activation to disease onset and progression in a transgenic model of familial ALS. ***Glia***. **23**, 249-56.

57. Hall, W. T. (1987) Cycad (zamia) poisoning in Australia. ***Aust Vet J***. **64**, 149-51.

58. Ham, J., Babij, C., Whitfield, J., Pfarr, C. M., Lallemand, D., Yaniv, M., and Rubin, L. L. (1995) A c-Jun dominant negative mutant protects sympathetic neurons against programmed cell death . ***Neuron***. **14**, 927-

39.

59. Herdegen, T., Skene, P., and Bahr, M. (1997) The c-Jun transcription factor--bipotential mediator of neuronal death, survival and regeneration. ***Trends Neurosci.*** **20**, 227-31.

60. Hirano, A., Arumugasamy, N., and Zimmerman, H. M. (1967) Amyotrophic lateral sclerosis. A comparison of Guam and classical cases. ***Arch Neurol.*** **16**, 357-63.

61. Hirano, A., Kurland, L. T., Krooth, R. S., and Lessell, S. (1961) Parkinsonism-dementia complex, an endemic disease on the island of Guam. I. Clinical features. ***Brain.*** **84**, 642-61.

62. Hirano, A., Malamud, N., Elizan, T. S., and Kurland, L. T. (1966a) Amyotrophic lateral sclerosis and Parkinsonism-dementia complex on Guam. Further pathologic studies. ***Arch Neurol.*** **15**, 35-51.

63. Hirano, A., Malamud, N., and Kurland LT. (1961) Parkinsonism-dementia complex, an endemic disease on the island of Guam. II. Pathological features. ***Brain.*** **84**, 662-79.

64. Hof, P. R., Perl, D. P., Loerzel, A. J., and Morrison, J. H. (1991) Neurofibrillary tangle distribution in the cerebral cortex of parkinsonism-dementia cases from Guam: differences with Alzheimer's disease. ***Brain Res.*** **564**, 306-13.

65. Hof, P. R., Perl, D. P., Loerzel, A. J., Steele, J. C., and Morrison, J. H. (1994) Amyotrophic lateral sclerosis and parkinsonism-dementia from Guam: differences in neurofibrillary tangle distribution and density in the hippocampal formation and neocortex. ***Brain Res.*** **650**, 107-16.

66. Hoffmann, G. R. and Morgan, R. W. (1984) Review: putative mutagens and carcinogens in foods. V. Cycad azoxyglycosides. ***Environ Mutagen.*** **6**, 103-16.

67. Holderith, N. B., Shigemoto, R., and Nusser, Z. (2003) Cell type-dependent expression of HCN1 in the main olfactory bulb. ***Eur J Neurosci.*** **18**, 344-54.

68. Hooper, P. T., Best, S. M., and Campbell, A. (1974) Axonal dystrophy in the spinal cords of cattle consuming the cycad palm, Cycas media. ***Aust Vet J.*** **50**, 146-9.

69. Hsu, J. C., Bravo, R., and Taub, R. (1992) Interactions among LRF-1, JunB, c-Jun, and c-Fos define a regulatory program in the G1 phase of liver regeneration. ***Mol Cell Biol.*** **12**, 4654-65.

70. Ince, P. G. and Codd, G. A. (2005) Return of the cycad hypothesis - does the amyotrophic lateral sclerosis/parkinsonism dementia complex (ALS/PDC) of Guam have new implications for global health? ***Neuropathol Appl Neurobiol***. **31**, 345-53.

71. Iqbal, K. and Grundke-Iqbal, I. (1998) Tau phosphatase activity as a therapeutic target for AD. ***Drug News Perspect***. **11**, 10-4.

72. Jones, B. J. and Roberts, D. J. (1968) A rotarod suitable for quantitative measurements of motor incoordination in naive mice. ***Naunyn Schmiedebergs Arch Exp Pathol Pharmakol***. **259**, 211.

73. Kawamata, T., Akiyama, H., Yamada, T., and McGeer, P. L. (1992) Immunologic reactions in amyotrophic lateral sclerosis brain and spinal cord tissue. ***Am J Pathol***. **140**, 691-707.

74. Kerr, J. F., Wyllie, A. H., and Currie, A. R. (1972) Apoptosis: a basic biological phenomenon with wide-ranging implications in tissue kinetics. ***Br J Cancer***. **26**, 239-57.

75. Khabazian, I., Bains, J. S., Williams, D. E., Cheung, J., Wilson, J. M., Pasqualotto, B. A., Pelech, S. L., Andersen, R. J., Wang, Y. T., Liu, L., Nagai, A., Kim, S. U., Craig, U. K., and Shaw, C. A. (2002a) Isolation of various forms of sterol beta-d-glucoside from the seed of Cycas circinalis: neurotoxicity and implications for ALS-parkinsonism dementia complex. ***J Neurochem***. **82**, 516-28.

76. Kieran, D., Kalmar, B., Dick, J. R., Riddoch-Contreras, J., Burnstock, G., and Greensmith, L. (2004) Treatment with arimoclomol, a coinducer of heat shock proteins, delays disease progression in ALS mice. ***Nat Med***. **10**, 402-5.

77. Kline, M. P. and Morimoto, R. I. (1997) Repression of the heat shock factor 1 transcriptional activation domain is modulated by constitutive phosphorylation. ***Mol Cell Biol***. **17**, 2107-15.

78. Klucken, J., Shin, Y., Masliah, E., Hyman, B. T., and McLean, P. J. (2004) Hsp70 Reduces alpha-Synuclein Aggregation and Toxicity. ***J Biol Chem***. **279**, 25497-502.

79. Kokubo, Y., Kuzuhara, S., and Narita, Y. (2000) Geographical distribution of amyotrophic lateral sclerosis with neurofibrillary tangles in the Kii Peninsula of Japan. ***J Neurol***. **247**, 850-2.

80. Kurland, L. T. (1972) An appraisal of the neurotoxicity of cycad and the etiology of amyotrophic lateral sclerosis on Guam. ***Fed Proc***. **31**, 1540-2.

81. Kurland, L. T. (1988a) Amyotrophic lateral sclerosis and Parkinson's

disease complex on Guam linked to an environmental neurotoxin. ***Trends Neurosci***. **11**, 51-4.

82. Kurland, L. T. and Mulder, D. W. (1954) Epidemiologic investigations of amyotrophic lateral sclerosis. ***Neurology***. **4**, 355-378.

83. Kurland, L. T. and Mulder, D. W. (1987) Age-specific incidence rates for motor neuron disease. ***J Neurol Neurosurg Psychiatry***. **50**, 115-6.

84. Kurland, L. T., Radhakrishnan, K., Williams, D. B., and Waring, S. C. (1994) Amyotrophic lateral sclerosis-parkinsonism-dementia complex on Guam: epidemiologic and etiological perspectives. 109-131.

85. Kwong, L. K., Neumann, M., Sampathu, D. M., Lee, V. M., and Trojanowski, J. Q. (2007) TDP-43 proteinopathy: the neuropathology underlying major forms of sporadic and familial frontotemporal lobar degeneration and motor neuron disease. ***Acta Neuropathol***. **114**, 63-70.

86. Lauckner, J., Frey, P., and Geula, C. (2003) Comparative distribution of tau phosphorylated at Ser262 in pre-tangles and tangles. ***Neurobiol Aging***. **24**, 767-76.

87. Lee, G., Cruz-Aguado, R., Banjo, O. C., and Shaw, C. A. (2007) Characterization of gait analysis, memory, and neuromuscular junction integrity in a mouse model of ALS-PDC.

88. Leenders, K. L., Salmon, E. P., Tyrrell, P., Perani, D., Brooks, D. J., Sager, H., Jones, T., Marsden, C. D., and Frackowiak, R. S. (1990) The nigrostriatal dopaminergic system assessed in vivo by positron emission tomography in healthy volunteer subjects and patients with Parkinson's disease. ***Arch Neurol***. **47**, 1290-8.

89. Lessell, S., Hirano, A., Torres, J., and Kurland, L. T. (1962) Parkinsonism-dementia complex. Epidemiological considerations in the Chamorros of the Mariana Islands and California. ***Arch Neurol***. **7**, 377-85.

90. Levine, S., Saltzman, A., and Kumar, A. R. (2004) A method for peripheral chromatolysis in neurons of trigeminal and dorsal root ganglia, produced in rats by lithium. ***J Neurosci Methods***. **132**, 1-7.

91. Liang, G., Wolfgang, C. D., Chen, B. P., Chen, T. H., and Hai, T. (1996) ATF3 gene. Genomic organization, promoter, and regulation. ***J Biol Chem***. **271**, 1695-701.

92. Lilienfeld, D. E., Perl, D. P., and Olanow, C. W. (1994) Guam Neurodegeneration. 895-908.

93. Lotocki, G., Alonso, O. F., Frydel, B., Dietrich, W. D., and Keane, R. W.

(2003) Monoubiquitination and cellular distribution of XIAP in neurons after traumatic brain injury. ***J Cereb Blood Flow Metab***. **23**, 1129-36.

93. Lu, Z., Rowe, S. P., Brennan, B. B., Davis, S. E., Metzler, R. E., Nau, J. J., Majmudar, C. Y., Mapp, A. K., and Ansari, A. Z. (2005) Unraveling the mechanism of a potent transcriptional activator. ***J Biol Chem***. **280**, 29689-98.

94. Lucking, C. B. and Brice, A. (2000) Alpha-synuclein and Parkinson's disease. ***Cell Mol Life Sci***. **57**, 1894-908.

95. Ly, P. T. and Shaw, C. A. (2007) Steryl glycoside induced cytopathological changes in the motor neuron-derived NSC-34 cells.

96. Mackenzie, I. R., Foti, D., Woulfe, J., and Hurwitz, T. A. (2008) Atypical frontotemporal lobar degeneration with ubiquitin-positive, TDP-43-negative neuronal inclusions. ***Brain***. **131**, 1282-93.

97. Marler, T., Lee, V., and Shaw, C. A. (2005) Cycad Toxins and Neurological Diseases in Guam: Defining Theoretical Experimental Standards for Correlating Human Disease with Environmental Toxins. ***Horticultural Science***. **40**, 1607-1611.

98. Martin, L. J. (1999) Neuronal death in amyotrophic lateral sclerosis is apoptosis: possible contribution of a programmed cell death mechanism. ***J Neuropathol Exp Neurol***. **58**, 459-71.

99. Masliah, E., Rockenstein, E., Veinbergs, I., Mallory, M., Hashimoto, M., Takeda, A., Sagara, Y., Sisk, A., and Mucke, L. (2000) Dopaminergic loss and inclusion body formation in alpha-synuclein mice: implications for neurodegenerative disorders. ***Science***. **287**, 1265-9.

100. McGeer, P. L., Itagaki, S., Akiyama, H., and McGeer, E. G. (1988) Rate of cell death in parkinsonism indicates active neuropathological process. ***Ann Neurol***. **24**, 574-6.

101. Mercado, P. A., Ayala, Y. M., Romano, M., Buratti, E., and Baralle, F. E. (2005) Depletion of TDP 43 overrides the need for exonic and intronic splicing enhancers in the human apoA-II gene . ***Nucleic Acids Res***. **33**, 6000-10.

102. Misiak, M., Kalinowska, M., and Wojciechowski, Z. A. (1991) Characterization of acyllipid: sterol glucoside acyltransferase from oat (Avena sativa L.) seedlings. ***Acta Biochim Pol***. **38**, 43-5.

103. Montine et al., 2008 (in preparation).

104. Morrow, C. E., Bandstra, E. S., Anthony, J. C., Ofir, A. Y., Xue, L., and

Reyes, M. L. (2001) Influence of prenatal cocaine exposure on full-term infant neurobehavioral functioning. ***Neurotoxicol Teratol.*** **23**, 533-44.

105. Muchowski, P. J. and Wacker, J. L. (2005) Modulation of neurodegeneration by molecular chaperones. ***Nat Rev Neurosci.*** **6**, 11-22.

106. Mukai, E. U., Sakakibara, T., Sobue, I., and Chen, K. M. (1982) [The prognosis of amyotrophic lateral sclerosis in Guam and Japan (author's transl)]. ***Rinsho Shinkeigaku.*** **22**, 139-44.

107. Mura, A., Feldon, J., and Mintz, M. (1998) Reevaluation of the striatal role in the expression of turning behavior in the rat model of Parkinson's disease. ***Brain Res.*** **808**, 48-55.

108. Nakagomi, S., Suzuki, Y., Namikawa, K., Kiryu-Seo, S., and Kiyama, H. (2003) Expression of the activating transcription factor 3 prevents c-Jun N-terminal kinase-induced neuronal death by promoting heat shock protein 27 expression and Akt activation. ***J Neurosci.*** **23**, 5187-96.

109. Nestel, P., Cehun, M., Pomeroy, S., Abbey, M., and Weldon, G. (2001) Cholesterol-lowering effects of plant sterol esters and non-esterified stanols in margarine, butter and low-fat foods. ***Eur J Clin Nutr.*** **55**, 1084-90.

110. Neumann, M., Sampathu, D. M., Kwong, L. K., Truax, A. C., Micsenyi, M. C., Chou, T. T., Bruce, J., Schuck, T., Grossman, M., Clark, C. M., McCluskey, L. F., Miller, B. L., Masliah, E., Mackenzie, I. R., Feldman, H., Feiden, W., Kretzschmar, H. A., Trojanowski, J. Q., and Lee, V. M. (2006) Ubiquitinated TDP-43 in frontotemporal lobar degeneration and amyotrophic lateral sclerosis. ***Science.*** **314**, 130-3.

111. Norflus, F., Tifft, C. J., McDonald, M. P., Goldstein, G., Crawley, J. N., Hoffmann, A., Sandhoff, K., Suzuki, K., and Proia, R. L. (1998) Bone marrow transplantation prolongs life span and ameliorates neurologic manifestations in Sandhoff disease mice. ***J Clin Invest.*** **101**, 1881-8.

112. Odle, T. G. (2003) Alzheimer disease and other dementias. ***Radiol Technol.*** **75**, 111-35; quiz 136-9.

113. Ohba, N., Maeda, M., Nakagomi, S., Muraoka, M., and Kiyama, H. (2003) Biphasic expression of activating transcription factor-3 in neurons after cerebral infarction. ***Brain Res Mol Brain Res.*** **115**, 147-56.

114. Patel, Y. J., Payne Smith, M. D., de Belleroche, J., and Latchman, D. S. (2005) Hsp27 and Hsp70 administered in combination have a potent protective effect against FALS-associated SOD1-mutant-induced cell death in mammalian neuronal cells. ***Brain Res Mol Brain Res.*** **134**, 256-

74.

115. Peng, L., Kawagoe, Y., Hogan, P., and Delmer, D. (2002) Sitosterol-beta-glucoside as primer for cellulose synthesis in plants. ***Science***. **295**, 147-50.

116. Perry, T. L., Bergeron, C., Biro, A. J., Hansen S. (1989) Beta-N-methylamino-L-alanine. Chronic oral administration is not neurotoxic to mice. J Neurol Sci. 94:173-80.

117. Plato, C. C., Garruto, R. M., Galasko, D., Craig, U. K., Plato, M., Gamst, A., Torres, J. M., and Wiederholt, W. (2003) Amyotrophic lateral sclerosis and parkinsonism-dementia complex of Guam: changing incidence rates during the past 60 years. ***Am J Epidemiol***. **157**, 149-57.

118. Poorkaj, P., Tsuang, D., Wijsman, E., Steinbart, E., Garruto, R. M., Craig, U. K., Chapman, N. H., Anderson, L., Bird, T. D., Plato, C. C., Perl, D. P., Weiderholt, W., Galasko, D., and Schellenberg, G. D. (2001) TAU as a susceptibility gene for amyotropic lateral sclerosis-parkinsonism dementia complex of Guam. ***Arch Neurol***. **58**, 1871-8.

119. Rao, S. D. and Weiss, J. H. (2004) Excitotoxic and oxidative cross-talk between motor neurons and glia in ALS pathogenesis. ***Trends Neurosci***. **27**, 17-23.

120. Reed, D., Labarthe, D., Chen, K. M., and Stallones, R. (1987) A cohort study of amyotrophic lateral sclerosis and parkinsonism-dementia on Guam and Rota. ***Am J Epidemiol***. **125**, 92-100.

121. Reed, W., Torres, J. M., and Brody, J. A. (1975) ALS and PD on Guam, 1945-1972. II. Familial and genetic studies. ***American Journal of Epidemiology***. **101**, 302-310.

122. Roder, J. K., Roder, J. C., and Gerlai, R. (1996) Memory and the effect of cold shock in the water maze in S100 beta transgenic mice. ***Physiol Behav***. **60**, 611-5.

123. Rodgers-Johnson, P., Garruto, R. M., Yanagihara, R., Chen, K. M., Gajdusek, D. C., and Gibbs, C. J. Jr. (1986) Amyotrophic lateral sclerosis and parkinsonism-dementia on Guam: a 30-year evaluation of clinical and neuropathologic trends. ***Neurology***. **36**, 7-13.

124. Rowland, L. P. and Shneider, N. A. (2001) Amyotrophic lateral sclerosis. ***N Engl J Med***. **344**, 1688-700.

125. Sango, K., McDonald, M. P., Crawley, J. N., Mack, M. L., Tifft, C. J., Skop, E., Starr, C. M., Hoffmann, A., Sandhoff, K., Suzuki, K., and Proia, R. L. (1996) Mice lacking both subunits of lysosomal beta-hexosaminidase

display gangliosidosis and mucopolysaccharidosis. ***Nat Genet.*** **14**, 348-52.

126. Sango, K., Yamanaka, S., Hoffmann, A., Okuda, Y., Grinberg, A., Westphal, H., McDonald, M. P., Crawley, J. N., Sandhoff, K., Suzuki, K., and et, a. l. (1995) Mouse models of Tay-Sachs and Sandhoff diseases differ in neurologic phenotype and ganglioside metabolism. ***Nat Genet.*** **11**, 170-6.

127. Sargsyan, S. A., Monk, P. N., and Shaw, P. J. (2005) Microglia as potential contributors to motor neuron injury in amyotrophic lateral sclerosis. ***Glia.*** **51**, 241-53.

128. Sasaki, S. and Iwata, M. (1999) Immunoreactivity of beta-amyloid precursor protein in amyotrophic lateral sclerosis. ***Acta Neuropathol (Berl).*** **97**, 463-8.

129. Schapira, A. H. and Olanow, C. W. (2003) Rationale for the use of dopamine agonists as neuroprotective agents in Parkinson's disease. ***Ann Neurol.*** **53 Suppl 3**, S149-57; discussion S157-9.

130. Schulz, J. D., Cruz-Aguado, R., Hawkes, E. L., Singh, S., and Shaw, C. A. (2005) Comparative study of the roles of novel cycad toxins versus BMAA in the etiology of ALS-PDC. ***Soc Neurosci. Abstr*** . in press.

131. Schulz, J. D., Khabazian, I., Wilson, J. M., and Shaw, C. A. (2003) A Muring Model of ALS-PDC with Behavioural and Neuropathological Features of Parkinsonism. ***Ann N Y Acad Sci.*** **991**, 326-9.

132. Selkoe, D. J. (2003) Folding proteins in fatal ways. ***Nature.*** **426**, 900-4.

133. Sepkuty, J. P., Cohen, A. S., Eccles, C., Rafiq, A., Behar, K., Ganel, R., Coulter, D. A., and Rothstein, J. D. (2002) A neuronal glutamate transporter contributes to neurotransmitter GABA synthesis and epilepsy. ***J Neurosci.*** **22**, 6372-9.

134. Shaw, C. A. and Wilson, J. M. (2003) Analysis of neurological disease in four dimensions: insight from ALS-PDC epidemiology and animal models. ***Neurosci Biobehav Rev.*** **27**, 493-505.

135. Shaw, C. A., Wilson, J. M., Cruz-Aguado, R., Singh, S., Hawkes, E. L., Lee, V., and Marler, T. (2005) Cycad-Induced Neurodegeneration in a Mouse Model of ALS-PDC: Is the Culprit Really BMAA or is a Novel Toxin to Blame? ***Botanical Review.*** *in press.*

136. Sherman, M. Y. and Goldberg, A. L. (2001) Cellular defenses against unfolded proteins: a cell biologist thinks about neurodegenerative diseases. ***Neuron*** . **29**, 15-32.

137. Shimura, H., Miura-Shimura, Y., and Kosik, K. S. (2004) Binding of tau to heat shock protein 27 leads to decreased concentration of hyperphosphorylated tau and enhanced cell survival. ***J Biol Chem***. **279**, 17957-62.

138. Snow, A. D., Mar, H., Nochlin, D., and Wight, T. N. (1989) Congo red staining on 1 micron de-plasticized sections for detection of lesions in Alzheimer's disease and related disorders. ***Prog Clin Biol Res***. **317**, 383-91.

139. Spencer, P. S., Kisby, G. E., and Ludolph, A. C. (1991) Slow toxins, biologic markers, and long-latency neurodegenerative disease in the western Pacific region. ***Neurology***. **41**, 62-6; discussion 66-8.

140. Spencer, P. S., Palmer, V. S., and Ludolph, A. C. (2005) On the decline and etiology of high-incidence motor system disease in West Papua (southwest New Guinea). ***Mov Disord***. **20 Suppl 12**, S119-26.

141. Spencer, P. S., Ross, S. M., Nunn, P. B., Roy, D. N., and Seelig, M. (1987) Detection and characterization of plant-derived amino acid motorsystem toxins in mouse CNS cultures. ***Prog Clin Biol Res***. **253**, 349-61.

142. Spencer, P. S., Roy, D. N., Ludolph, A., Hugon, J., Dwivedi, M. P., and Schaumburg, H. H. (1986) Lathyrism: evidence for role of the neuroexcitatory aminoacid BOAA. ***Lancet***. **2**, 1066-7.

143. Steele, J. C. and Guzman, T. (1987) Observations about amyotrophic lateral sclerosis and the parkinsonism- dementia complex of Guam with regard to epidemiology and etiology. ***Can J Neurol Sci***. **14**, 358-62.

144. Szumanska, G. and Gadamski, R. (1977) [Histochemical study of rat brain following intoxication with dichlorvos (DDVP)]. ***Neuropatol Pol***. **15**, 523-35.

145. Tabata, R. C., Wilson, J. M., Ly, P., Zwiegers, P., Kwok, D., Van Kampen, J. M., Cashman, N., and Shaw, C. A. (2008) Chronic Exposure to Dietary Sterol Glucosides is Neurotoxic to Motor Neurons and Induces an ALS-PDC Phenotype. ***Neuromolecular Med***. **10**, 24-39.

146. Tsujino, H., Kondo, E., Fukuoka, T., Dai, Y., Tokunaga, A., Miki, K., Yonenobu, K., Ochi, T., and Noguchi, K. (2000) Activating transcription factor 3 (ATF3) induction by axotomy in sensory and motoneurons: A novel neuronal marker of nerve injury. ***Mol Cell Neurosci***. **15**, 170-82.

147. Ungerstedt, U. and Arbuthnott, G. W. (1970) Quantitative recording of rotational behavior in rats after 6-hydroxy-dopamine lesions of the nigrostriatal dopamine system. ***Brain Res***. **24**, 485-93.

148. Valentino, K. M., Dugger, N. V., Peterson, E., Wilson, J. M., Shaw, C. A., and Yarowsky, P. J. (2006) Environmentally induced parkinsonism in cycad-fed rats.

149. Vanni-Mercier, G., Gigout, S., Debilly, G., and Lin, J. S. (2003) Waking selective neurons in the posterior hypothalamus and their response to histamine H3-receptor ligands: an electrophysiological study in freely moving cats. ***Behav Brain Res***. **144**, 227-41.

150. Vaphiades, M. S., Husain, M., Juhasz, K., and Schmidley, J. W. (2002) Motor neuron disease presenting with slow saccades and dementia. ***Amyotroph Lateral Scler Other Motor Neuron Disord***. **3**, 159-62.

151. Verghese, J., Lipton, R. B., Hall, C. B., Kuslansky, G., Katz, M. J., and Buschke, H. (2002) Abnormality of gait as a predictor of non-Alzheimer's dementia. ***N Engl J Med***. **347**, 1761-8.

152. Walker, L. C. and LeVine, H. 3rd. (2002a) Proteopathy: the next therapeutic frontier? ***Curr Opin Investig Drugs***. **3**, 782-7.

153. Walker, L. C. and LeVine, H. 3rd. (2002b) Proteopathy: the next therapeutic frontier? ***Curr Opin Investig Drugs***. **3**, 782-7.

154. Waring, S. C., Esteban-Santillan, C., Reed, D. M., Craig, U. K., Labarthe, D. R., Petersen, R. C., and Kurland, L. T. (2004) Incidence of amyotrophic lateral sclerosis and of the parkinsonism-dementia complex of Guam, 1950-1989. ***Neuroepidemiology***. **23**, 192-200.

155. Wasserstrom, J. A. and Aistrup, G. L. (2005) Digitalis: new actions for an old drug. ***Am J Physiol Heart Circ Physiol***. **289**, H1781-93.

156. Weiss, J. H., Koh, J. Y., and Choi, D. W. (1989) Neurotoxicity of beta-N-methylamino-L-alanine (BMAA) and beta-N- oxalylamino-L-alanine (BOAA) on cultured cortical neurons. ***Brain Res***. **497**, 64-71.

157. Whitehouse, P. J., Price, D. L., Struble, R. G., Clark, A. W., Coyle, J. T., and Delon, M. R. (1982) Alzheimer's disease and senile dementia: loss of neurons in the basal forebrain. ***Science***. **215**, 1237-9.

158. Wikstrom, M., Krab, K., and Saraste, M. (1981) Proton-translocating cytochrome complexes. ***Annu Rev Biochem***. **50**, 623-55.

159. Wilson, J. M., Khabazian, I., Pow, D. V., Craig, U. K., and Shaw, C. A. (2003a) Decrease in glial glutamate transporter variants and excitatory amino acid receptor down-regulation in a murine model of ALS-PDC. ***Neuromolecular Med***. **3**, 105-18.

160. Wilson, J. M., Khabazian, I., Wong, M. C., Seyedalikhani, A., Bains, J. S.,

Pasqualotto, B. A., Williams, D. E., Andersen, R. J., Simpson, R. J., Smith, R., Craig, U. K., Kurland, L. T., and Shaw, C. A. (2002a) Behavioral and neurological correlates of ALS-parkinsonism dementia complex in adult mice fed washed cycad flour. ***Neuromolecular Med***. **1**, 207-21.

161. Wilson, J. M., Petrik, M. S., Blackband, S. J., Grant, S. C., and Shaw, C. A. (2003) Quantitative Measurement of Neurodegeneration in ALS-PDC model using MRI. ***UBC Department of Ophthalmology Research Day Abstracts***. See copy included in application.

162. Wilson, J. M., Petrik, M. S., Grant, S. C., Blackband, S. J., Lai, J., and Shaw, C. A. (2004a) Quantitative measurement of neurodegeneration in an ALS-PDC model using MR microscopy. ***Neuroimage***. **23**, 336-43.

163. Wilson, J. M., Petrik, M. S., Moghadasian, M. H., Grant, S. C., Blackband, S. J., Krieger, C., Craig, U. K., and Shaw, C. A. (2005) The Progression of Motor Deficits and CNS Pathology in ALS-PDC. ***Soc Neurosci. Abstr***. online.

164. Wilson, J. M., Petrik, M. S., Rosebrugh, R. L., Moghadasian, M. H., and Shaw, C. A. (2004a) Dynamic Interaction of Gene and Environment Using APOE Allele Variants in an Animal Model of ALS-PDC. ***Society for Neuroscience Abstracts***. 341.11.

165. Wilson, J. M., Wong, M. C., Seyedalikhani, A., Pasqualotto, B. A., and Shaw, C. A. (2001) Histological Assessment of Cytotoxicity Due to Cycad Feeding in Mice: Implications for ALS-PDC. ***Society for Neuroscience Abstracts***.

166. Winton, M. J., Joyce, S., Zhukareva, V., Practico, D., Perl, D. P., Galasko, D., Craig, U., Trojanowski, J. Q., and Lee, V. M. (2006) Characterization of tau pathologies in gray and white matter of Guam parkinsonism-dementia complex. ***Acta Neuropathol***. **111**, 401-12.

167. Wojciechowski, Z. A. (1983) The biosynthesis of plant steryl glycosides and saponins. ***Biochem Soc Trans***. **11**, 565-8.

168. Wong-Riley, M. (1979) Changes in the visual system of monocularly sutured or enucleated cats demonstrable with cytochrome oxidase histochemistry. ***Brain Res***. **171**, 11-28.

169. Wong-Riley, M. T. (1989) Cytochrome oxidase: an endogenous metabolic marker for neuronal activity. ***Trends Neurosci***. **12**, 94-101.

170. Wong-Riley, M. T., Merzenich, M. M., and Leake, P. A. (1978) Changes in endogenous enzymatic reactivity to DAB induced by neuronal inactivity. ***Brain Res***. **141**, 185-92.

171. Xia, Z., Dickens, M., Raingeaud, J., Davis, R. J., and Greenberg, M. E. (1995) Opposing effects of ERK and JNK-p38 MAP kinases on apoptosis. ***Science***. **270**, 1326-31.

172. Yanagihara, R., Garruto, R. M., Gajdusek, D. C., Tomita, A., Uchikawa, T., Konagaya, Y., Chen, K. M., Sobue, I., Plato, C. C., and Gibbs, C. J. Jr. (1984) Calcium and vitamin D metabolism in Guamanian Chamorros with amyotrophic lateral sclerosis and parkinsonism-dementia. ***Ann Neurol***. **15**, 42-8.

173. Yokoyama, K., Ikebe, S., Komatsuzaki, Y., Takanashi, M., Mori, H., Mochizuki, H., and Mizuno, Y. (2002) [A 68-year-old woman with dementia and parkinsonism]. ***No To Shinkei***. **54**, 175-84.

174. Yoshida, T., Limmroth, V., Irikura, K., and Moskowitz, M. A. (1994) The NOS inhibitor, 7-nitroindazole, decreases focal infarct volume but not the response to topical acetylcholine in pial vessels. ***J Cereb Blood Flow Metab***. **14**, 924-9.

175. Zhang, Z. X., Anderson, D. W., Lavine, L., and Mantel, N. (1990) Patterns of acquiring parkinsonism-dementia complex on Guam. 1944 through 1985. ***Arch Neurol***. **47**, 1019-24.

176. Zoccolella, S., Palagano, G., Fraddosio, A., Russo, I., Ferrannini, E., Serlenga, L., Maggio, F., Lamberti, S., and Iliceto, G. (2002) ALS-plus: 5 cases of concomitant amyotrophic lateral sclerosis and parkinsonism. ***Neurol Sci***. **23 Suppl 2**, S123-4.

177. Zourlidou, A., Payne Smith, M. D., and Latchman, D. S. (2004) HSP27 but not HSP70 has a potent protective effect against alpha-synuclein-induced cell death in mammalian neuronal cells. ***J Neurochem***. **88**, 1439-48.

Appendix A

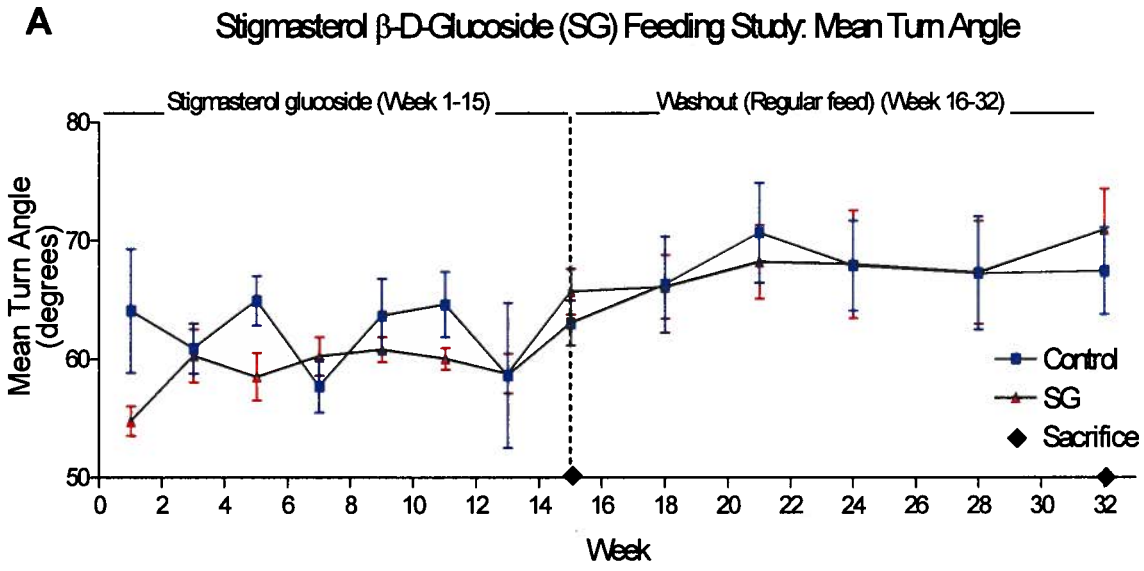
A
Stigmasterol β-D-Glucoside (SG) Feeding Study: Mean Turn Angle
Stigmasterol glucoside (Week 1-15)
Washout (Regular feed) (Week 16-32)
Mean Turn Angle (degrees)
80
70
60
50
0 2 4 6 8 10 12 14 16 18 20 22 24 26 28 30 32
Week
Control
SG
Sacrifice

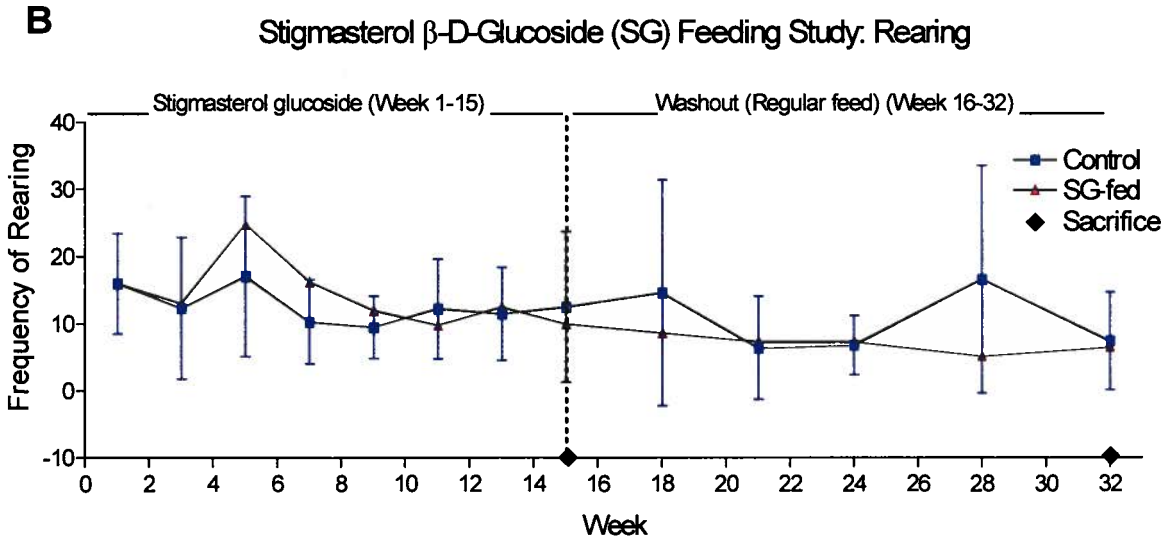
B
Stigmasterol β-D-Glucoside (SG) Feeding Study: Rearing
Stigmasterol glucoside (Week 1-15)
Washout (Regular feed) (Week 16-32)
Frequency of Rearing
40
30
20
10
0
-10
0 2 4 6 8 10 12 14 16 18 20 22 24 26 28 30 32
Week
Control
SG-fed
Sacrifice

C

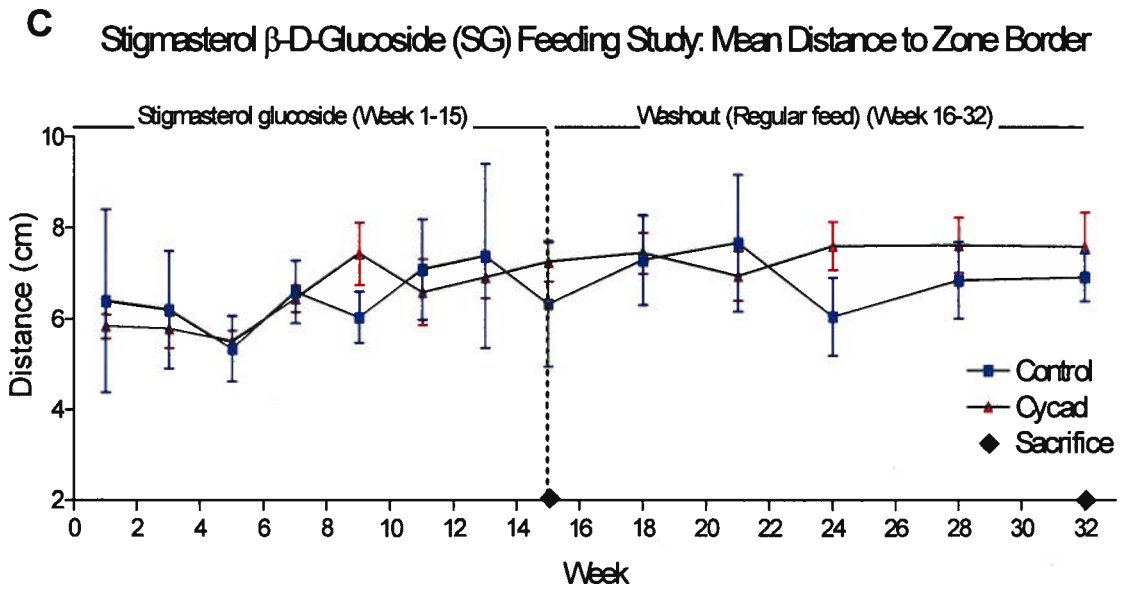
Stigmasterol β-D-Glucoside (SG) Feeding Study: Mean Distance to Zone Border
Stigmasterol glucoside (Week 1-15)
Washout (Regular feed) (Week 16-32)
Distance (cm)
Week
Control
Cycad
Sacrifice

D

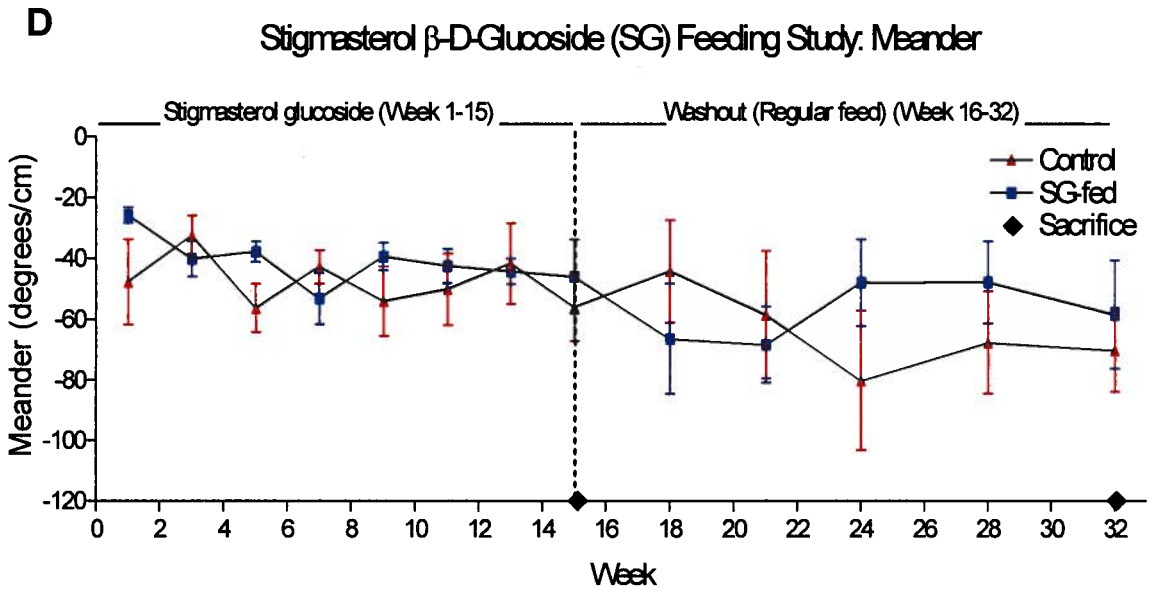
Stigmasterol β-D-Glucoside (SG) Feeding Study: Meander
Stigmasterol glucoside (Week 1-15)
Washout (Regular feed) (Week 16-32)
Meander (degrees/cm)
Week
Control
SG-fed
Sacrifice

E

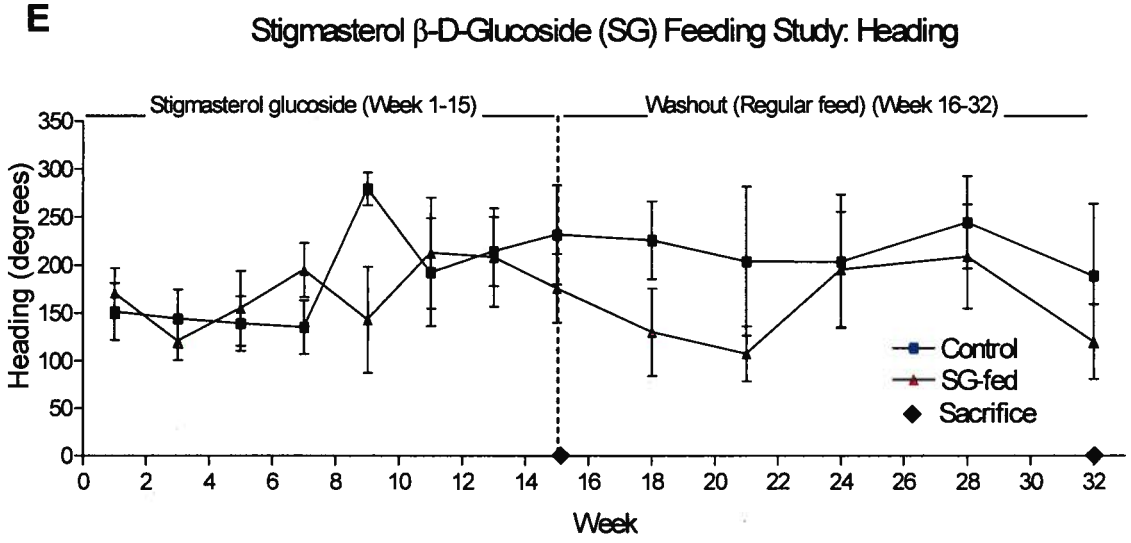
Stigmasterol β-D-Glucoside (SG) Feeding Study: Heading
Stigmasterol glucoside (Week 1-15)
Washout (Regular feed) (Week 16-32)
Heading (degrees)
Week
Control
SG-fed
Sacrifice

F

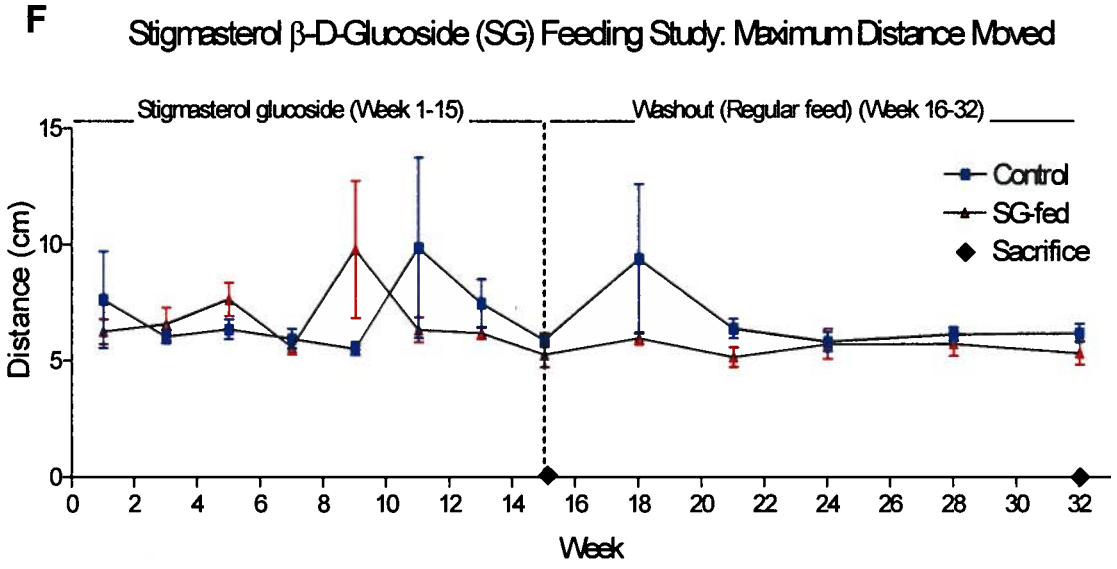
Stigmasterol β-D-Glucoside (SG) Feeding Study: Maximum Distance Moved
Stigmasterol glucoside (Week 1-15)
Washout (Regular feed) (Week 16-32)
Distance (cm)
Week
Control
SG-fed
Sacrifice

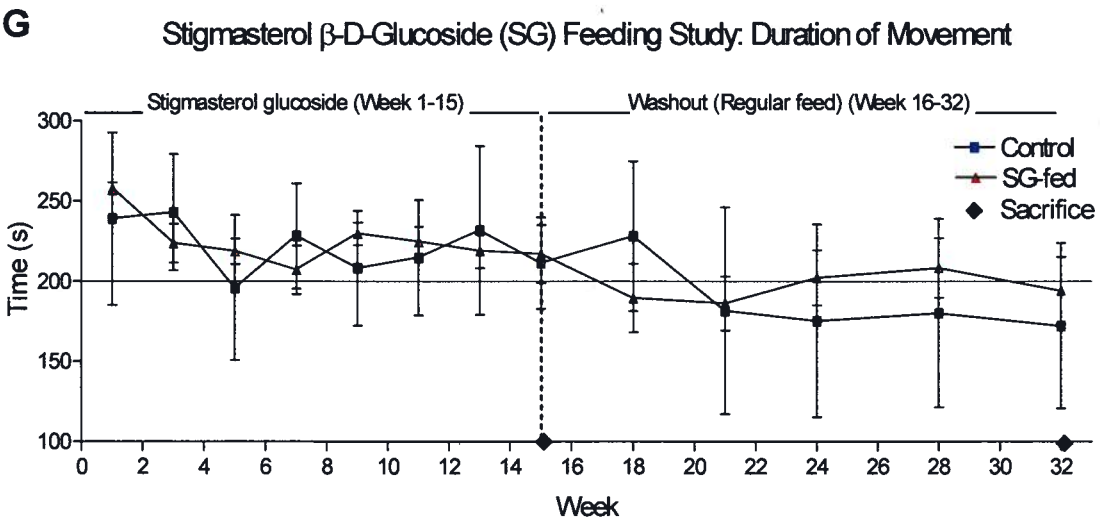

Figure 39. **Open field test performances of SG-fed animals show that dietary exposure induces hyperactivity, anxiety, and tighter, more frequent rotations.**

SG-fed mice showed a trend in greater general movement velocity (A), angular velocity (B), percent of time spent moving (C), and total distance travelled (D) compared to age-matched controls, as measured by an automated open field camera and analysis program. SG-fed animals also showed a propensity to stay away from the periphery of the arena, which is indicative of anxiety (E) and spinning behaviour at tight angles (F). The Student's t-test revealed a significant difference between groups at a single time point in the total distance to the zone border (*$p<0.05$), however, the behavioural findings obtained through the automated open field testing system did not detect significant differences otherwise.

A

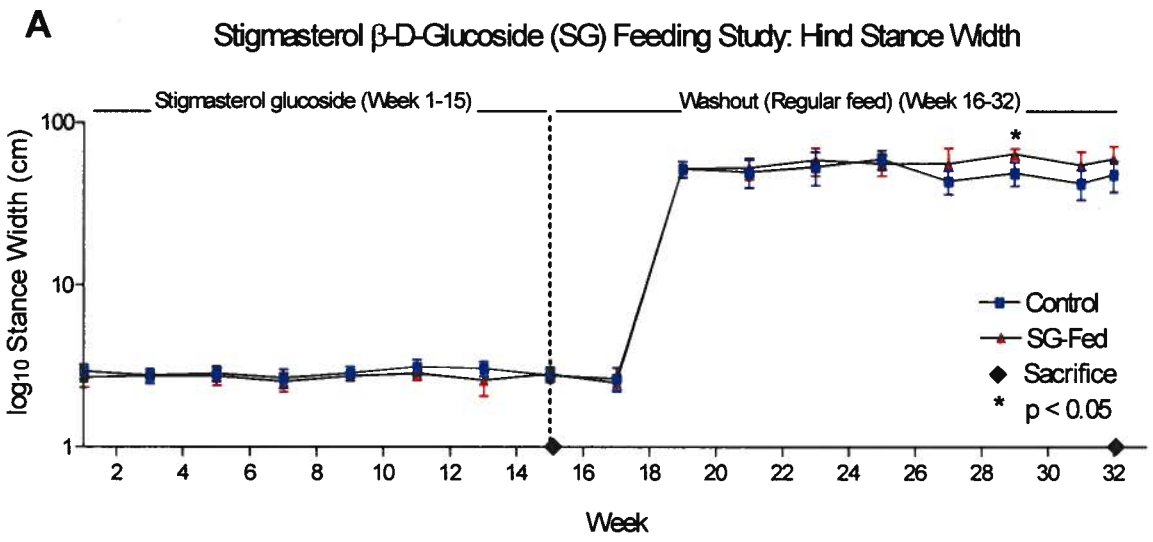
Stigmasterol β-D-Glucoside (SG) Feeding Study: Hind Stance Width
Stigmasterol glucoside (Week 1-15)
Washout (Regular feed) (Week 16-32)
log10 Stance Width (cm)
100
10
1
2 4 6 8 10 12 14 16 18 20 22 24 26 28 30 32
Week
Control
SG-Fed
Sacrifice
* p < 0.05

B

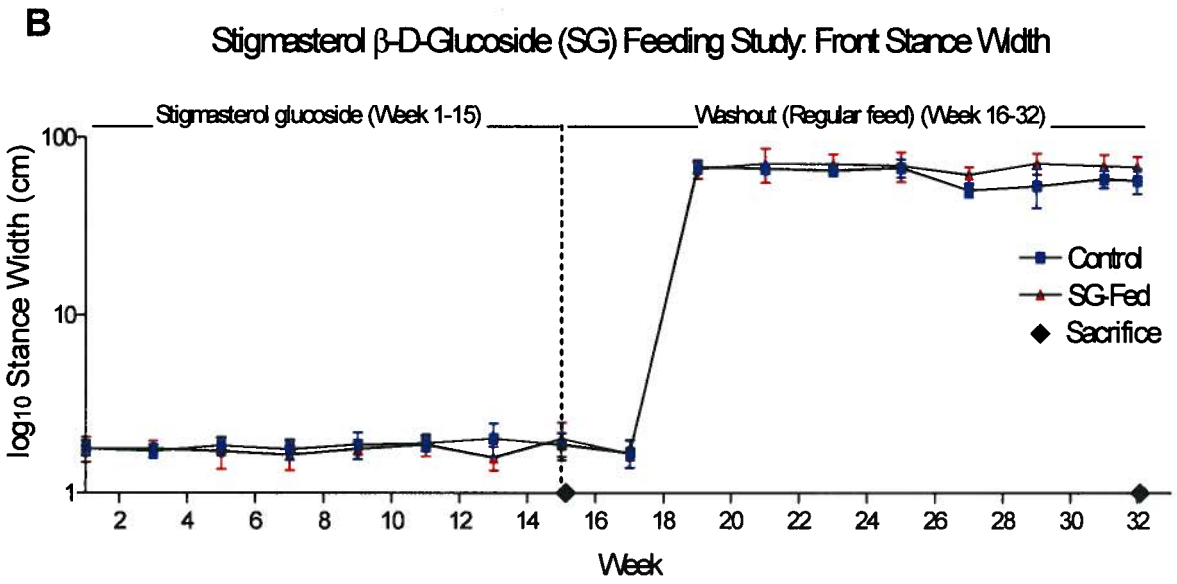
Stigmasterol β-D-Glucoside (SG) Feeding Study: Front Stance Width
Stigmasterol glucoside (Week 1-15)
Washout (Regular feed) (Week 16-32)
log10 Stance Width (cm)
100
10
1
2 4 6 8 10 12 14 16 18 20 22 24 26 28 30 32
Week
Control
SG-Fed
Sacrifice

C

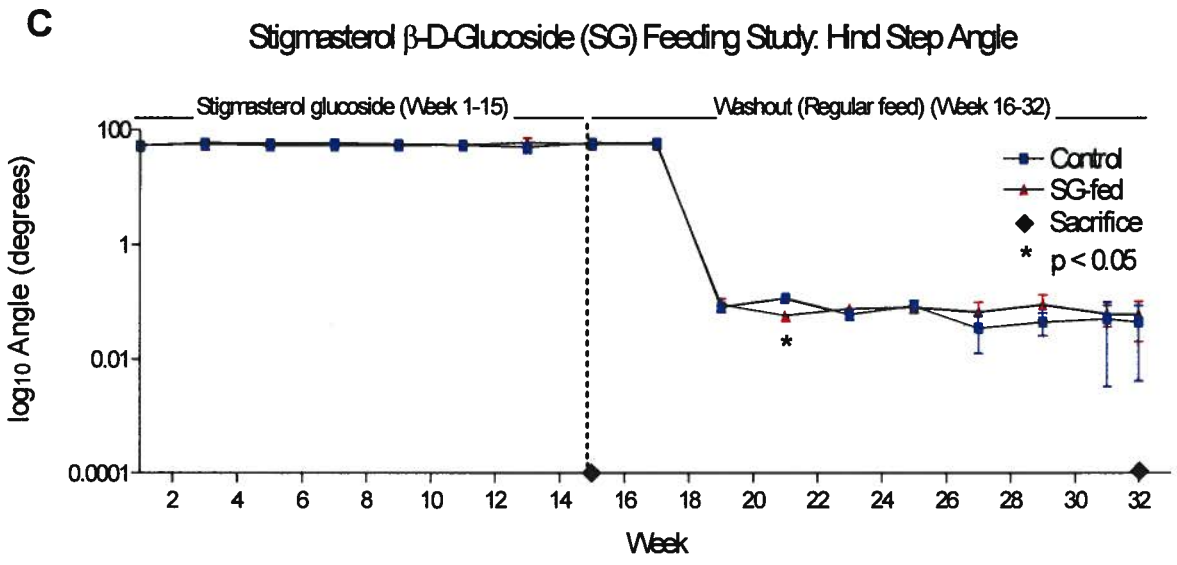
Stigmasterol β-D-Glucoside (SG) Feeding Study: Hind Step Angle
Stigmasterol glucoside (Week 1-15)
Washout (Regular feed) (Week 16-32)
log10 Angle (degrees)
100
1
0.01
0.0001
2 4 6 8 10 12 14 16 18 20 22 24 26 28 30 32
Week
Control
SG-fed
Sacrifice
* p < 0.05
*

D

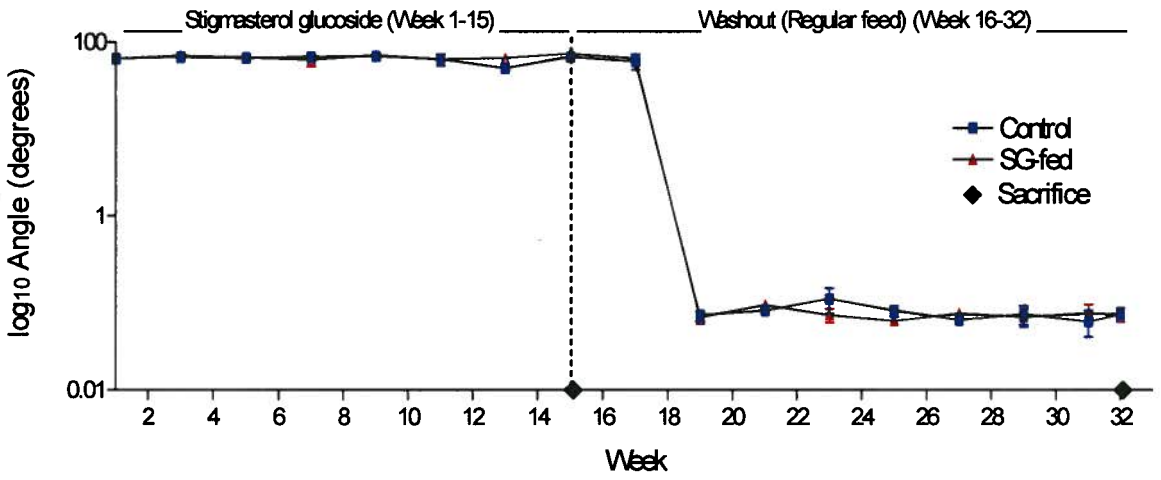
Stigmasterol β-D-Glucoside (SG) Feeding Study: Front Step Angle
Stigmasterol glucoside (Week 1-15)
Washout (Regular feed) (Week 16-32)
log10 Angle (degrees)
100
1
0.01
2 4 6 8 10 12 14 16 18 20 22 24 26 28 30 32
Week
Control
SG-fed
Sacrifice

E

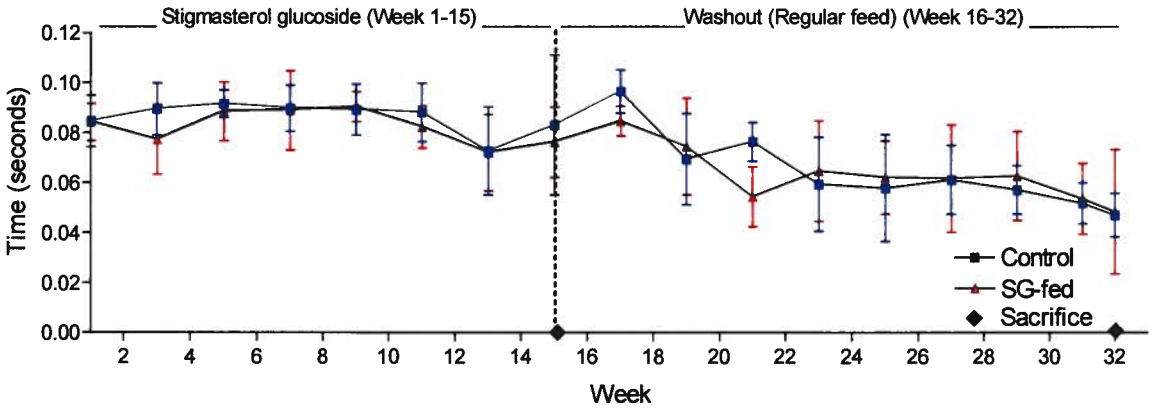
Stigmasterol β-D-Glucoside (SG) Feeding Study: Left Front Swing
Stigmasterol glucoside (Week 1-15)
Washout (Regular feed) (Week 16-32)
Time (seconds)
0.12
0.10
0.08
0.06
0.04
0.02
0.00
2 4 6 8 10 12 14 16 18 20 22 24 26 28 30 32
Week
Control
SG-fed
Sacrifice

F

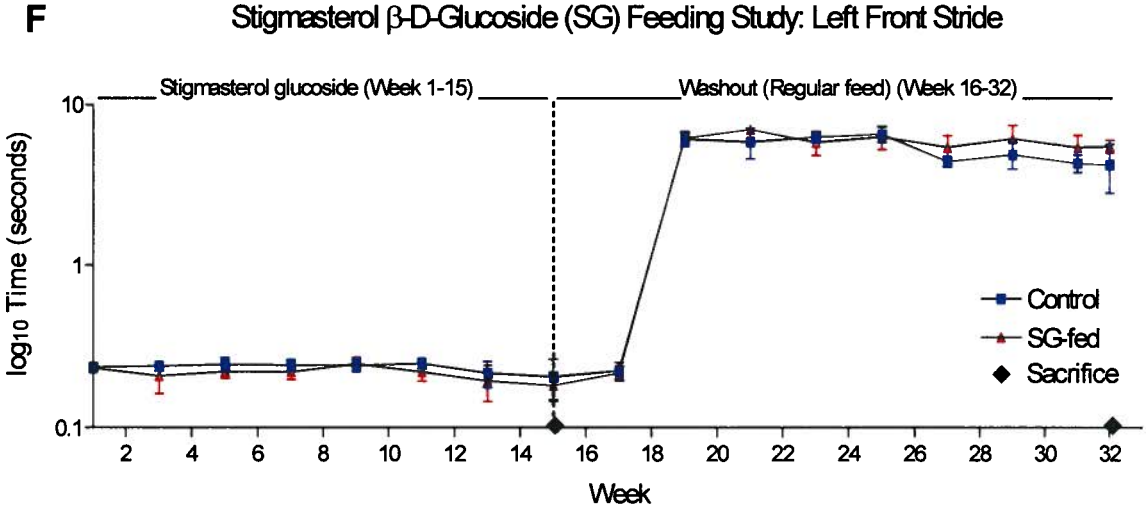
Stigmasterol β-D-Glucoside (SG) Feeding Study: Left Front Stride
Stigmasterol glucoside (Week 1-15)
Washout (Regular feed) (Week 16-32)
log10 Time (seconds)
10
1
0.1
2 4 6 8 10 12 14 16 18 20 22 24 26 28 30 32
Week
Control
SG-fed
Sacrifice

G

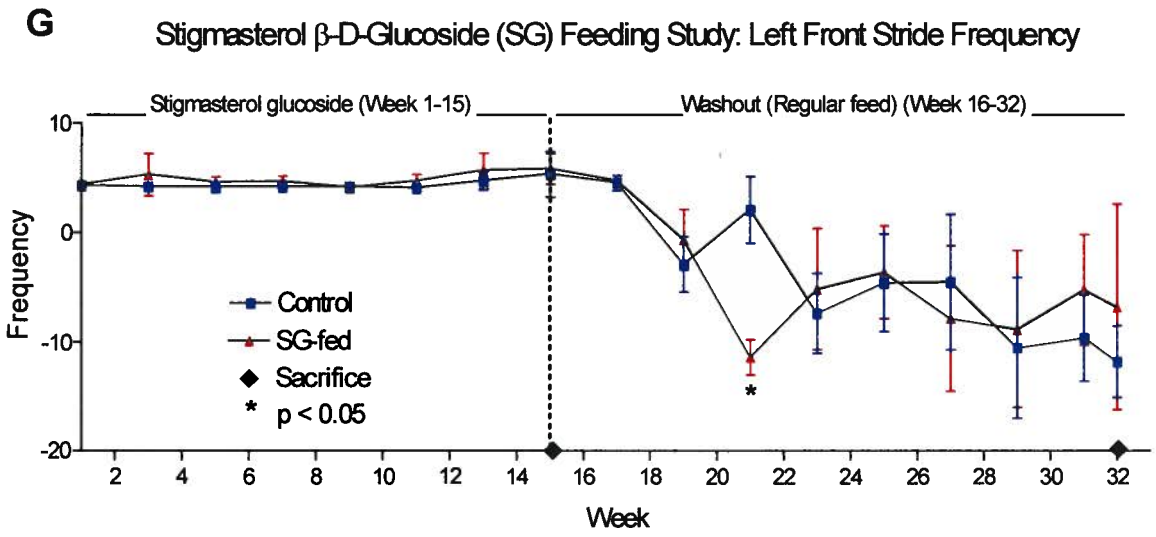
Stigmasterol β-D-Glucoside (SG) Feeding Study: Left Front Stride Frequency
Stigmasterol glucoside (Week 1-15)
Washout (Regular feed) (Week 16-32)
Frequency
Control
SG-fed
Sacrifice
* p < 0.05
Week

H

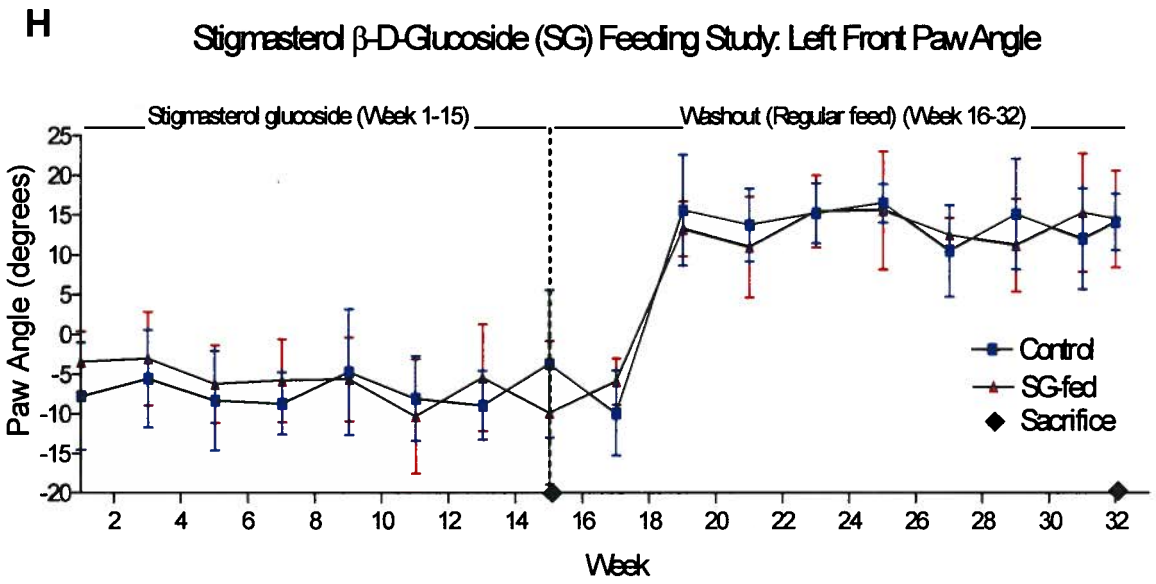
Stigmasterol β-D-Glucoside (SG) Feeding Study: Left Front Paw Angle
Stigmasterol glucoside (Week 1-15)
Washout (Regular feed) (Week 16-32)
Paw Angle (degrees)
Control
SG-fed
Sacrifice
Week

I

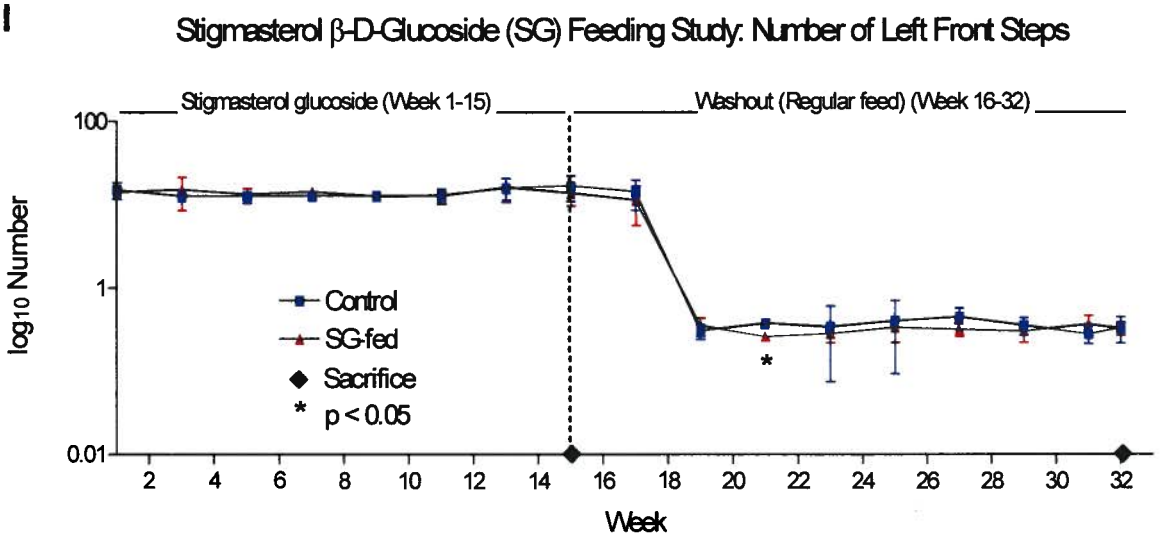
Stigmasterol β-D-Glucoside (SG) Feeding Study: Number of Left Front Steps
Stigmasterol glucoside (Week 1-15)
Washout (Regular feed) (Week 16-32)
log10 Number
100
1
0.01
Control
SG-fed
Sacrifice
* p < 0.05
2 4 6 8 10 12 14 16 18 20 22 24 26 28 30 32
Week

J

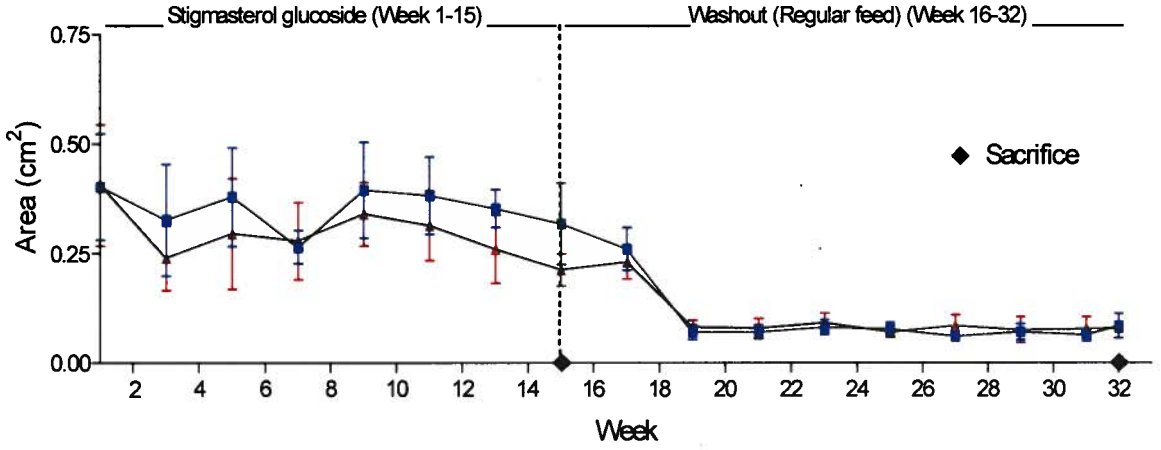
Stigmasterol β-D-Glucoside (SG) Feeding Study: Left Front Paw Area at Peak Stance
Stigmasterol glucoside (Week 1-15)
Washout (Regular feed) (Week 16-32)
Area (cm2)
0.75
0.50
0.25
0.00
Sacrifice
2 4 6 8 10 12 14 16 18 20 22 24 26 28 30 32
Week

K

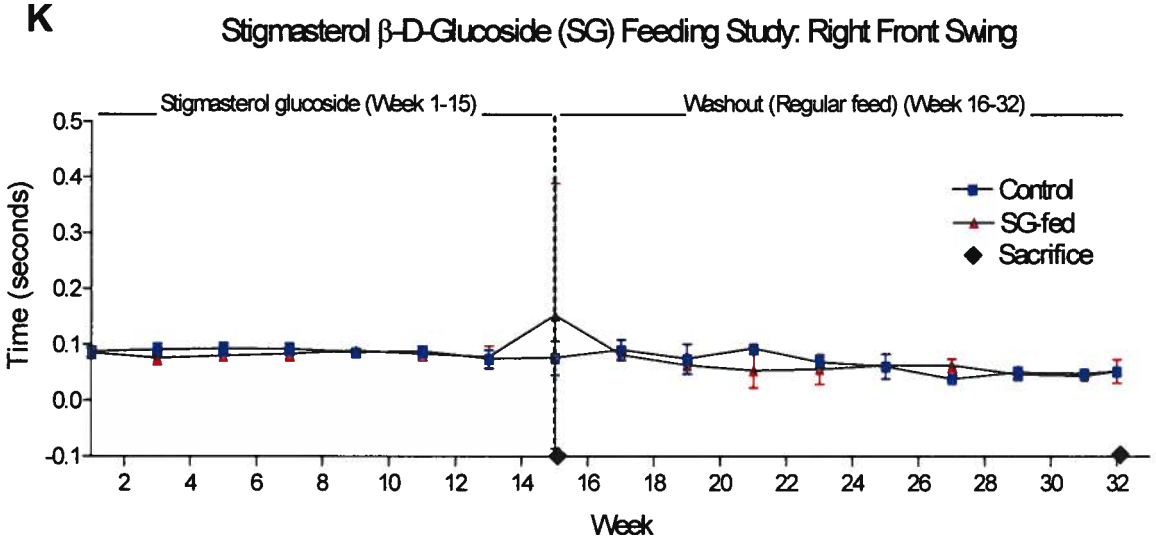
Stigmasterol β-D-Glucoside (SG) Feeding Study: Right Front Swing
Stigmasterol glucoside (Week 1-15)
Washout (Regular feed) (Week 16-32)
Time (seconds)
0.5
0.4
0.3
0.2
0.1
0.0
-0.1
2 4 6 8 10 12 14 16 18 20 22 24 26 28 30 32
Week
Control
SG-fed
Sacrifice

L

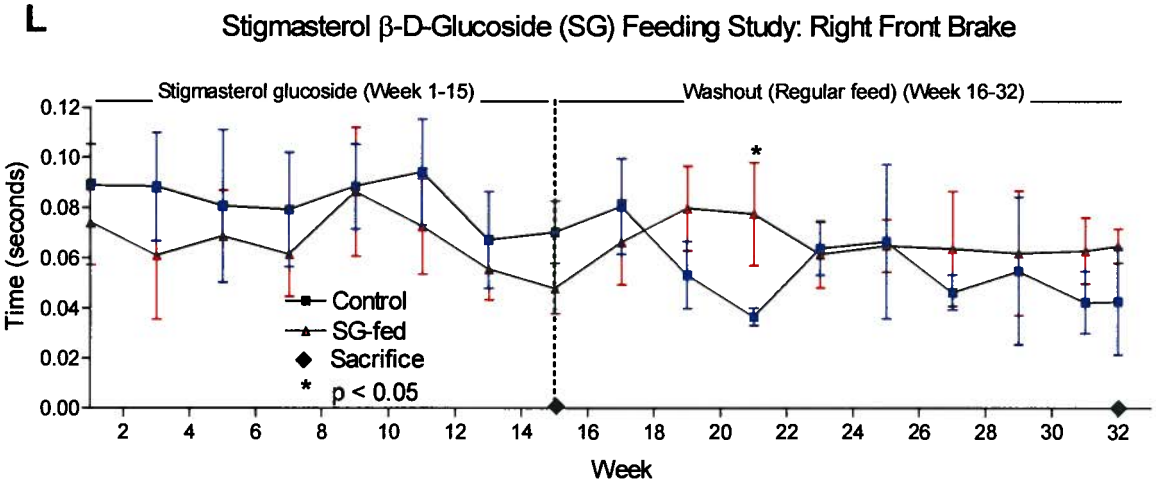
Stigmasterol β-D-Glucoside (SG) Feeding Study: Right Front Brake
Stigmasterol glucoside (Week 1-15)
Washout (Regular feed) (Week 16-32)
Time (seconds)
0.12
0.10
0.08
0.06
0.04
0.02
0.00
2 4 6 8 10 12 14 16 18 20 22 24 26 28 30 32
Week
Control
SG-fed
Sacrifice
* p < 0.05
*

M

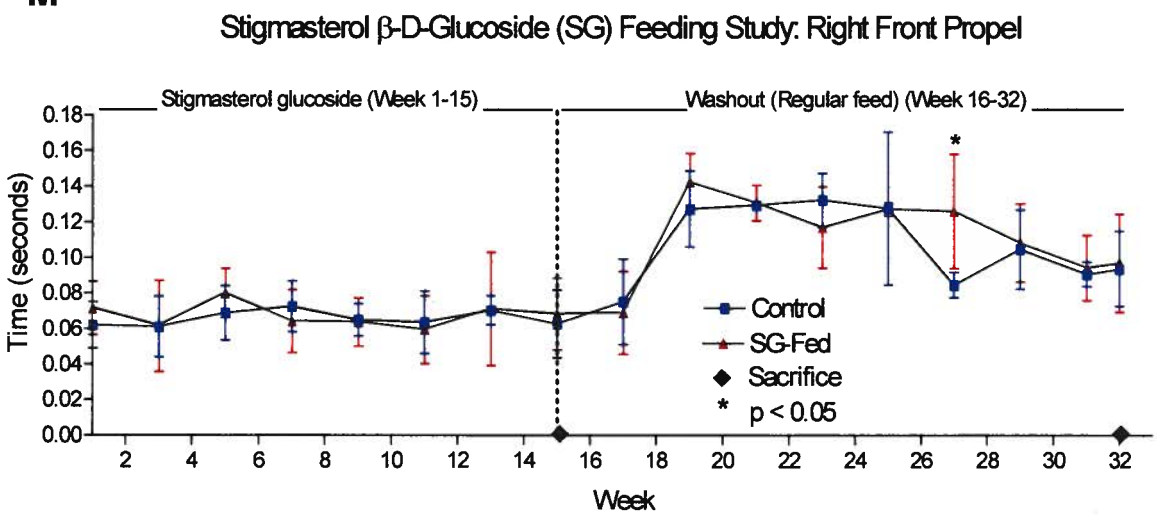
Stigmasterol β-D-Glucoside (SG) Feeding Study: Right Front Propel
Stigmasterol glucoside (Week 1-15)
Washout (Regular feed) (Week 16-32)
Time (seconds)
0.18
0.16
0.14
0.12
0.10
0.08
0.06
0.04
0.02
0.00
2 4 6 8 10 12 14 16 18 20 22 24 26 28 30 32
Week
Control
SG-Fed
Sacrifice
* p < 0.05

N

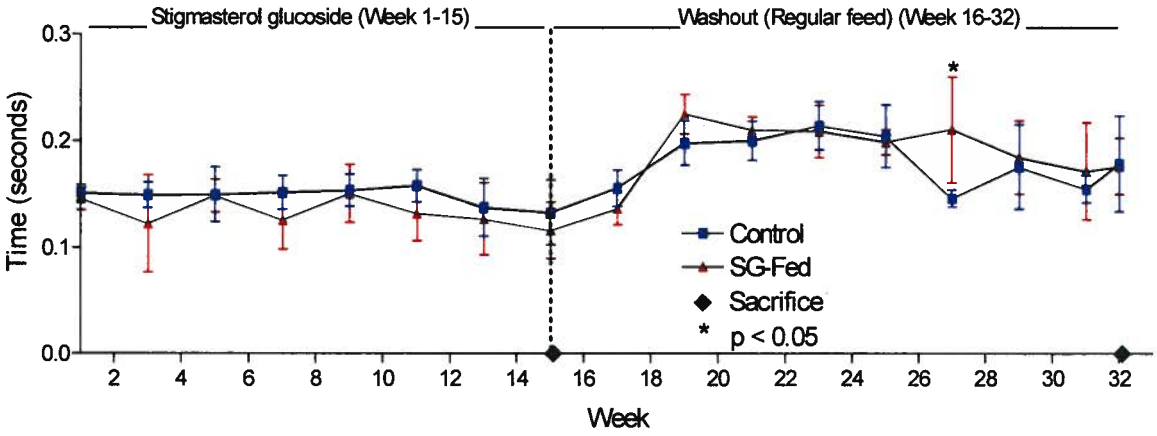
Stigmasterol β-D-Glucoside (SG) Feeding Study: Right Front Stance
Stigmasterol glucoside (Week 1-15)
Washout (Regular feed) (Week 16-32)
Time (seconds)
0.3
0.2
0.1
0.0
2 4 6 8 10 12 14 16 18 20 22 24 26 28 30 32
Week
Control
SG-Fed
Sacrifice
* p < 0.05

O

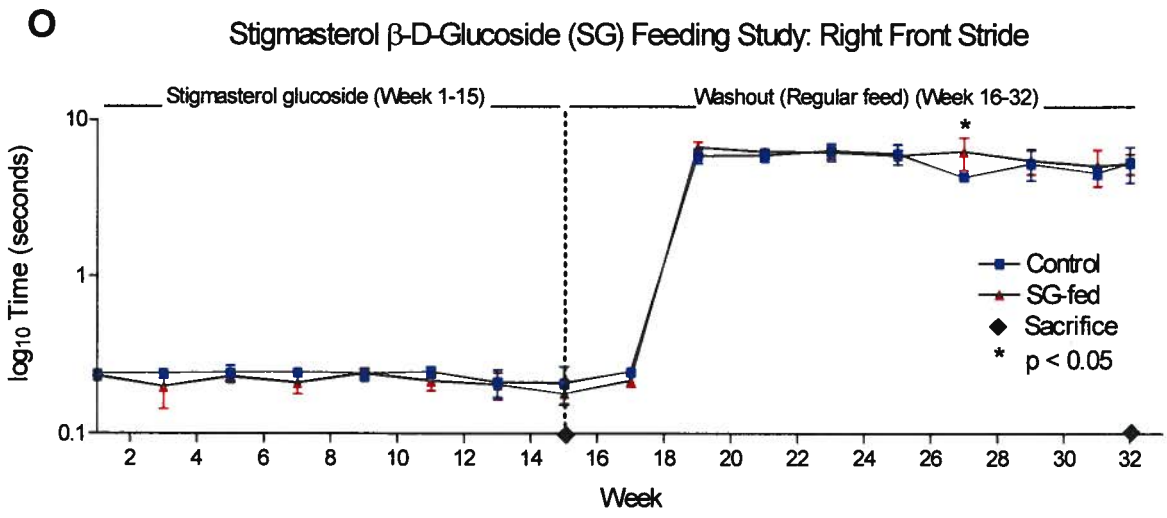
Stigmasterol β-D-Glucoside (SG) Feeding Study: Right Front Stride
Stigmasterol glucoside (Week 1-15)
Washout (Regular feed) (Week 16-32)
log10 Time (seconds)
10
1
0.1
2 4 6 8 10 12 14 16 18 20 22 24 26 28 30 32
Week
Control
SG-fed
Sacrifice
* p < 0.05

P

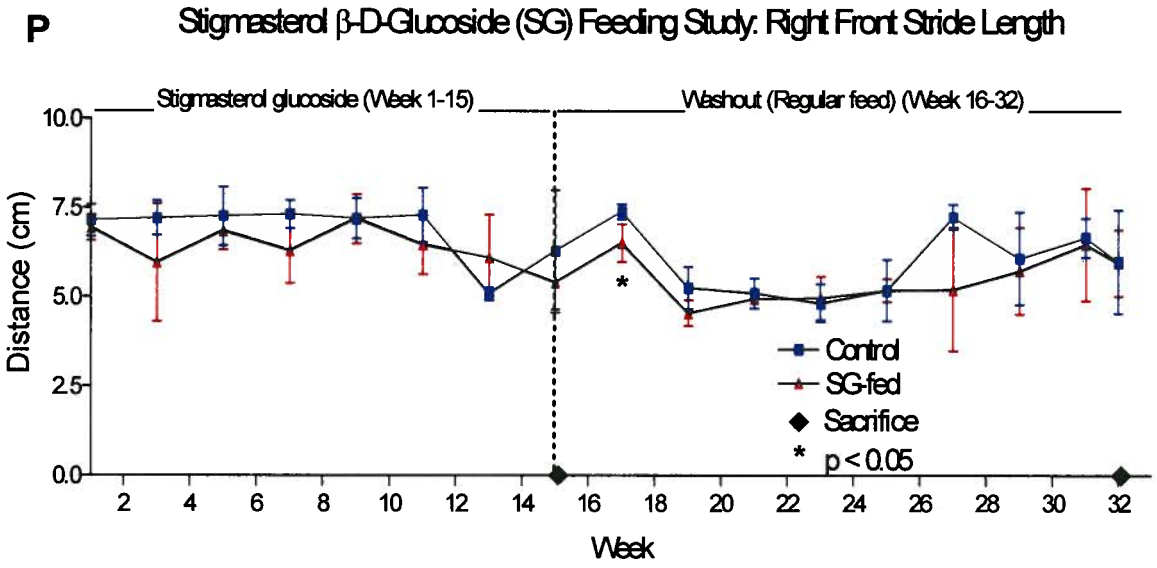
Stigmasterol β-D-Glucoside (SG) Feeding Study: Right Front Stride Length
Stigmasterol glucoside (Week 1-15)
Washout (Regular feed) (Week 16-32)
Distance (cm)
10.0
7.5
5.0
2.5
0.0
2 4 6 8 10 12 14 16 18 20 22 24 26 28 30 32
Week
Control
SG-fed
Sacrifice
* p < 0.05

Q

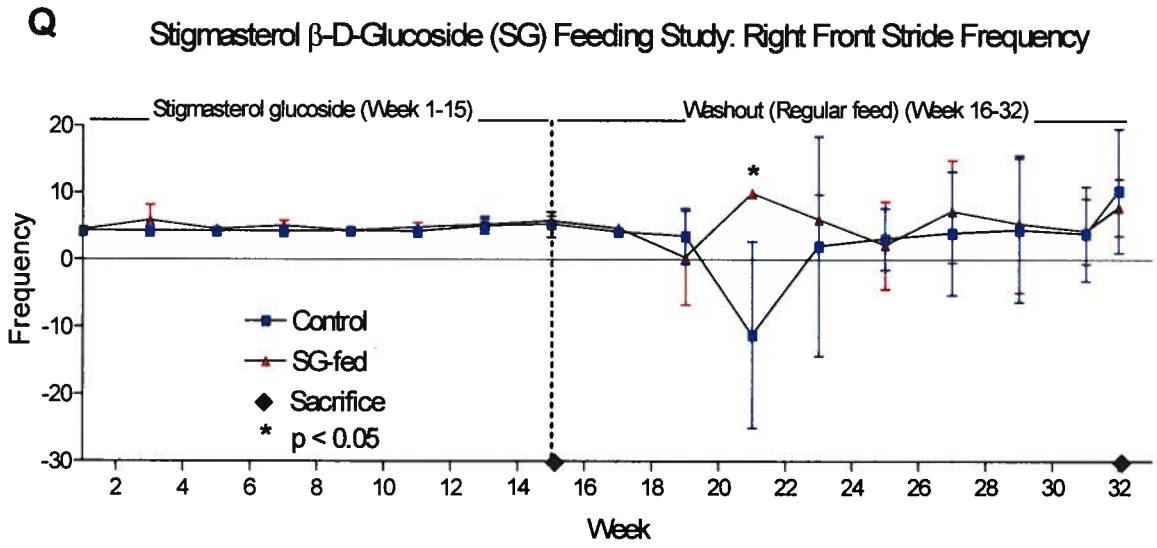
Stigmasterol β-D-Glucoside (SG) Feeding Study: Right Front Stride Frequency
Stigmasterol glucoside (Week 1-15)
Washout (Regular feed) (Week 16-32)
Frequency
Week
Control
SG-fed
Sacrifice
* p < 0.05
*

R

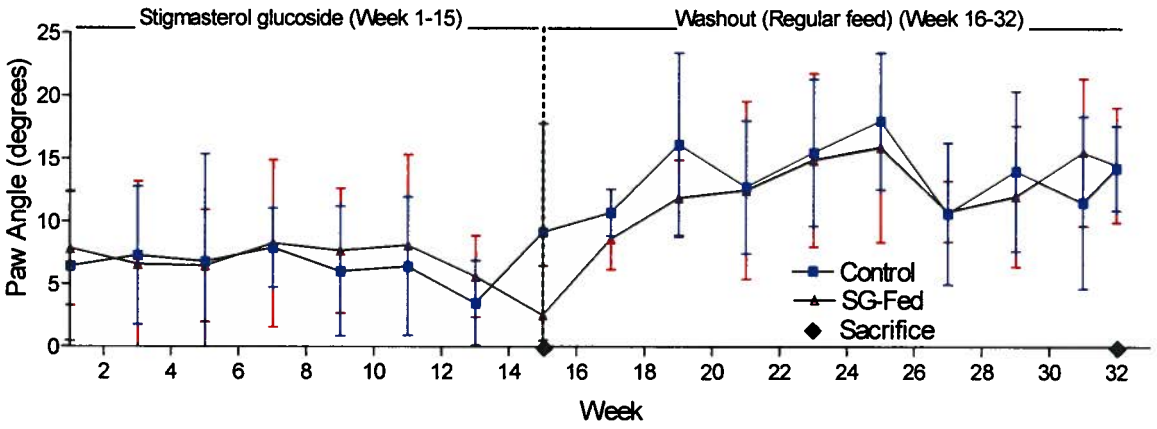
Stigmasterol β-D-Glucoside (SG) Feeding Study: Right Front Paw Angle
Stigmasterol glucoside (Week 1-15)
Washout (Regular feed) (Week 16-32)
Paw Angle (degrees)
Week
Control
SG-Fed
Sacrifice

S

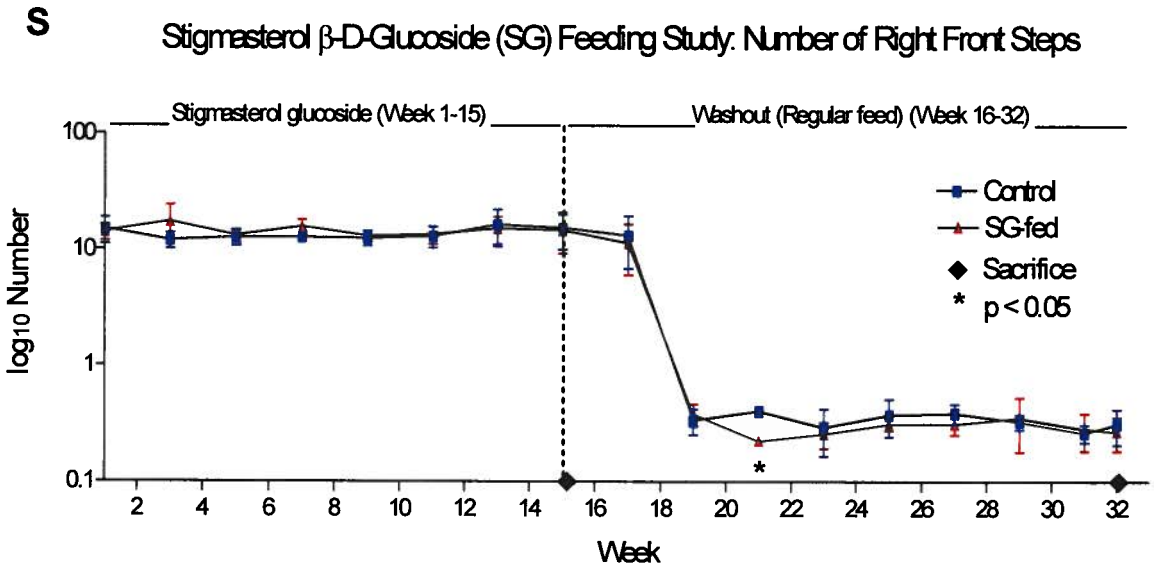
Stigmasterol β-D-Glucoside (SG) Feeding Study: Number of Right Front Steps
Stigmasterol glucoside (Week 1-15)
Washout (Regular feed) (Week 16-32)
log10 Number
100
10
1
0.1
Control
SG-fed
Sacrifice
* p < 0.05
*
2 4 6 8 10 12 14 16 18 20 22 24 26 28 30 32
Week

T

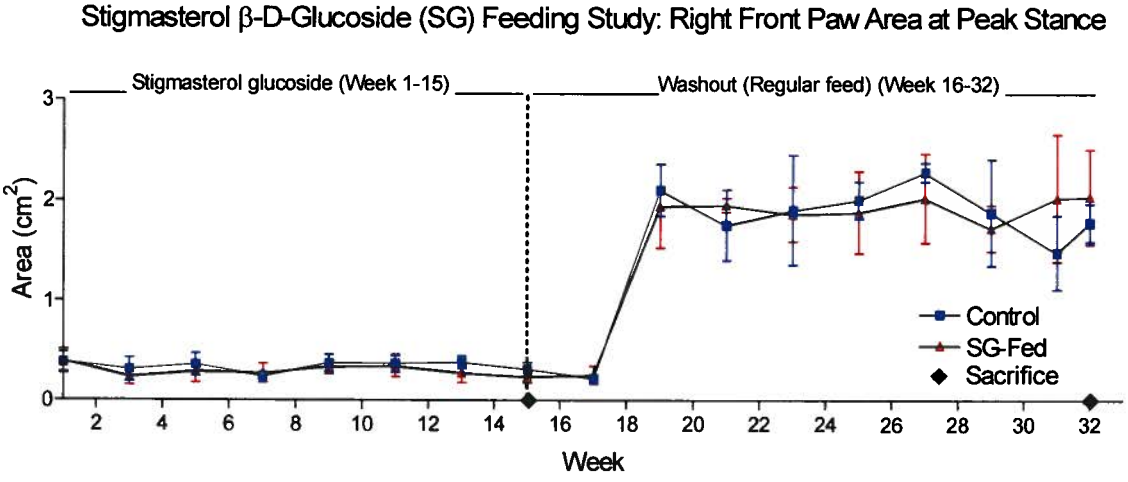
Stigmasterol β-D-Glucoside (SG) Feeding Study: Right Front Paw Area at Peak Stance
Stigmasterol glucoside (Week 1-15)
Washout (Regular feed) (Week 16-32)
Area (cm2)
3
2
1
0
Control
SG-Fed
Sacrifice
2 4 6 8 10 12 14 16 18 20 22 24 26 28 30 32
Week

U

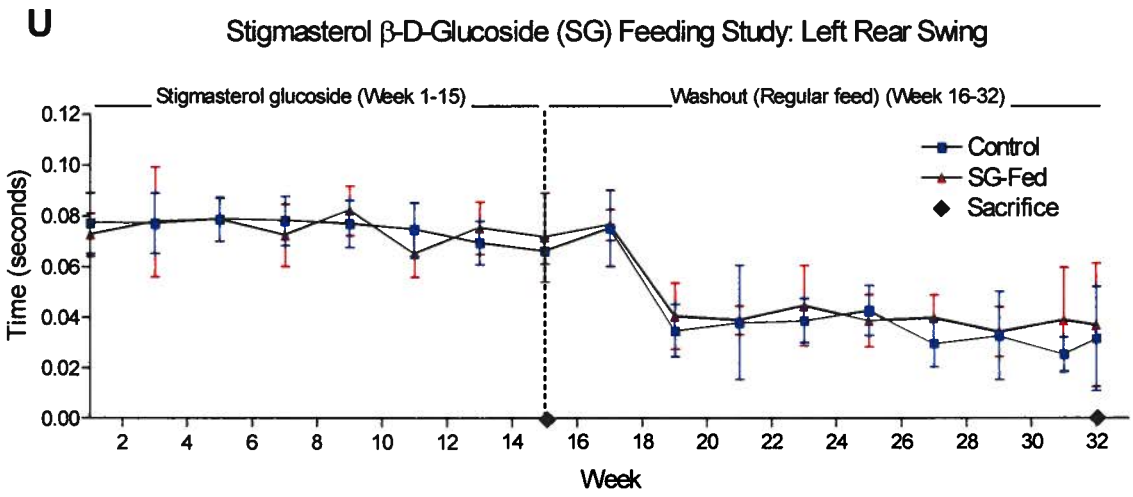
Stigmasterol β-D-Glucoside (SG) Feeding Study: Left Rear Swing
Stigmasterol glucoside (Week 1-15)
Washout (Regular feed) (Week 16-32)
Control
SG-Fed
Sacrifice
Time (seconds)
0.12
0.10
0.08
0.06
0.04
0.02
0.00
2 4 6 8 10 12 14 16 18 20 22 24 26 28 30 32
Week

V

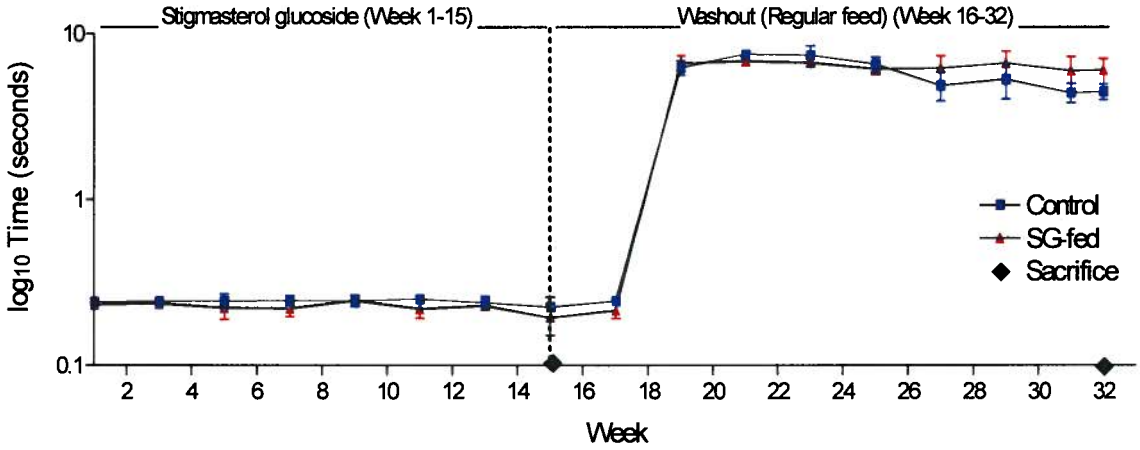
Stigmasterol β-D-Glucoside (SG) Feeding Study: Left Rear Stride
Stigmasterol glucoside (Week 1-15)
Washout (Regular feed) (Week 16-32)
Control
SG-fed
Sacrifice
log10 Time (seconds)
10
1
0.1
2 4 6 8 10 12 14 16 18 20 22 24 26 28 30 32
Week

W

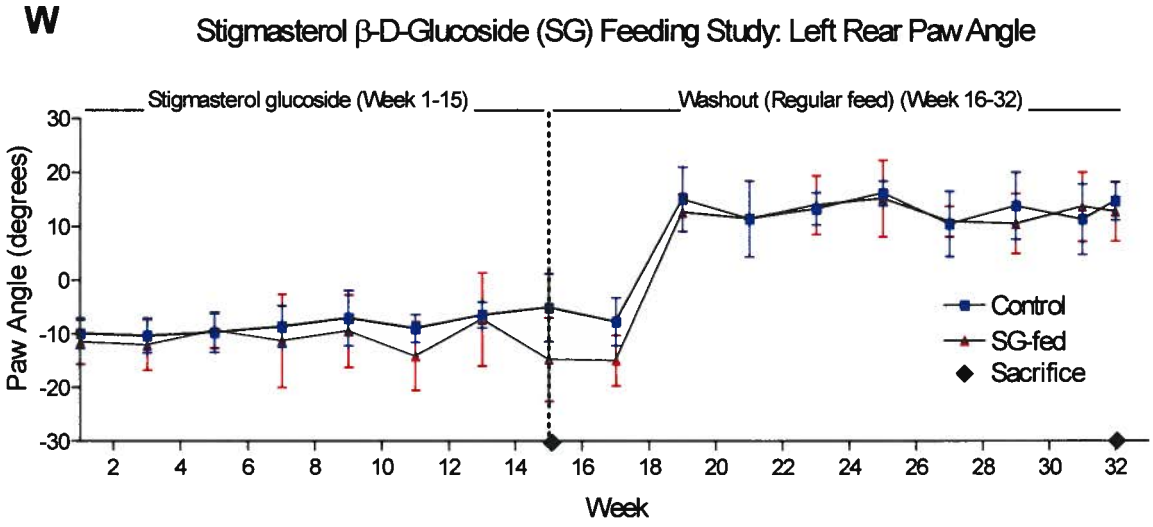
Stigmasterol β-D-Glucoside (SG) Feeding Study: Left Rear Paw Angle
Stigmasterol glucoside (Week 1-15)
Washout (Regular feed) (Week 16-32)
Paw Angle (degrees)
30
20
10
0
-10
-20
-30
2
4
6
8
10
12
14
16
18
20
22
24
26
28
30
32
Week
Control
SG-fed
Sacrifice

X

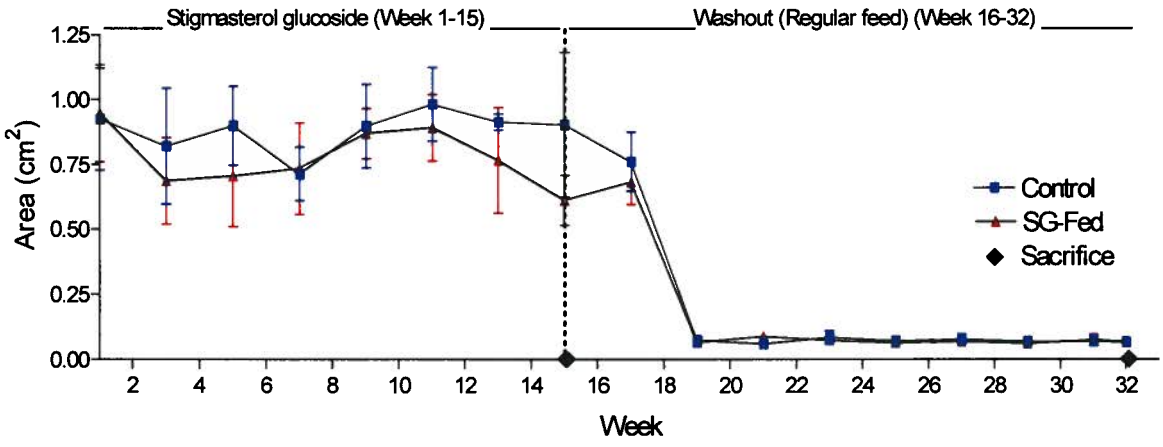
Stigmasterol β-D-Glucoside (SG) Feeding Study: Left Rear Paw Area at Peak Stance
Stigmasterol glucoside (Week 1-15)
Washout (Regular feed) (Week 16-32)
Area (cm2)
1.25
1.00
0.75
0.50
0.25
0.00
2
4
6
8
10
12
14
16
18
20
22
24
26
28
30
32
Week
Control
SG-Fed
Sacrifice

Y

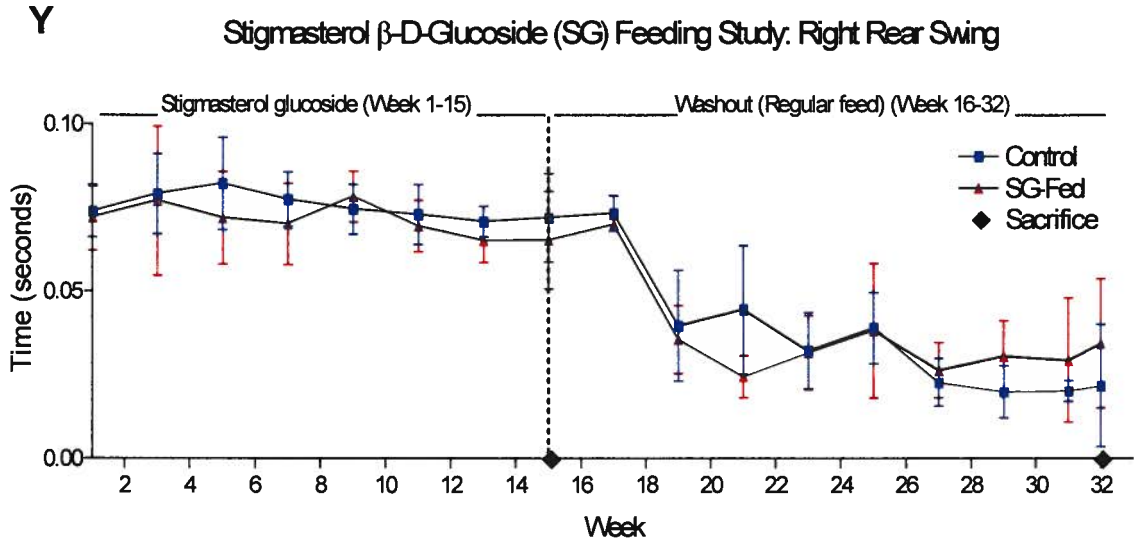
Stigmasterol β-D-Glucoside (SG) Feeding Study: Right Rear Swing
Stigmasterol glucoside (Week 1-15)
Washout (Regular feed) (Week 16-32)
Control
SG-Fed
Sacrifice
Time (seconds)
0.10
0.05
0.00
2 4 6 8 10 12 14 16 18 20 22 24 26 28 30 32
Week

Z

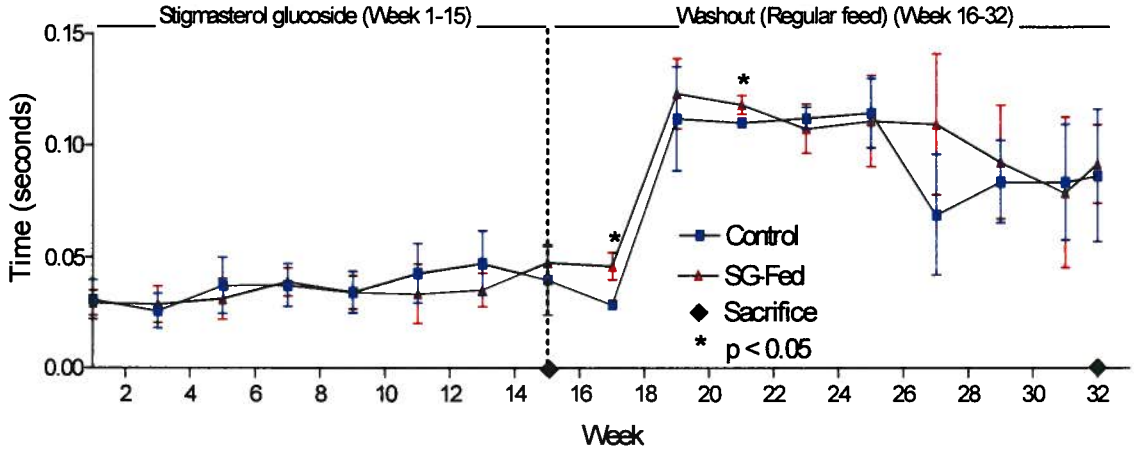
Stigmasterol β-D-Glucoside (SG) Feeding Study: Right Rear Brake
Stigmasterol glucoside (Week 1-15)
Washout (Regular feed) (Week 16-32)
Control
SG-Fed
Sacrifice
* p < 0.05
Time (seconds)
0.15
0.10
0.05
0.00
2 4 6 8 10 12 14 16 18 20 22 24 26 28 30 32
Week

AA

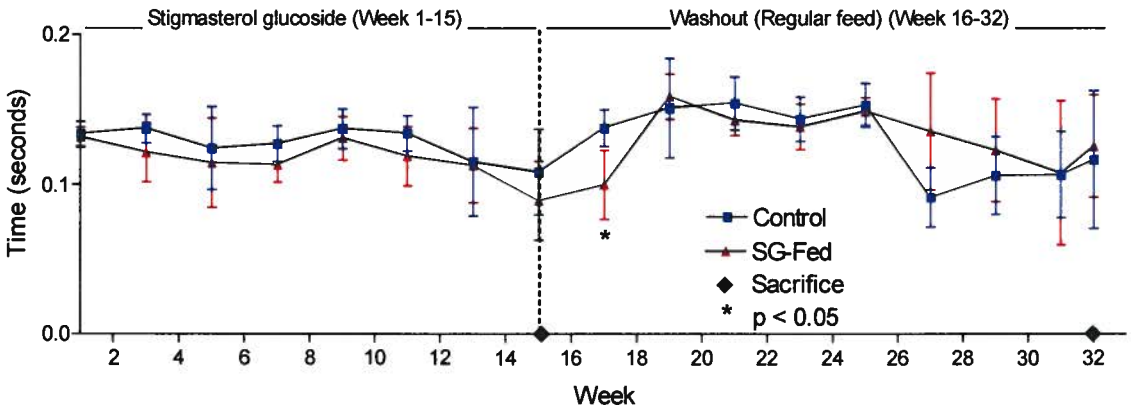
Stigmasterol β-D-Glucoside (SG) Feeding Study: Right Rear Propel
Stigmasterol glucoside (Week 1-15)
Washout (Regular feed) (Week 16-32)
Time (seconds)
0.2
0.1
0.0
2 4 6 8 10 12 14 16 18 20 22 24 26 28 30 32
Week
Control
SG-Fed
Sacrifice
* p < 0.05

BB

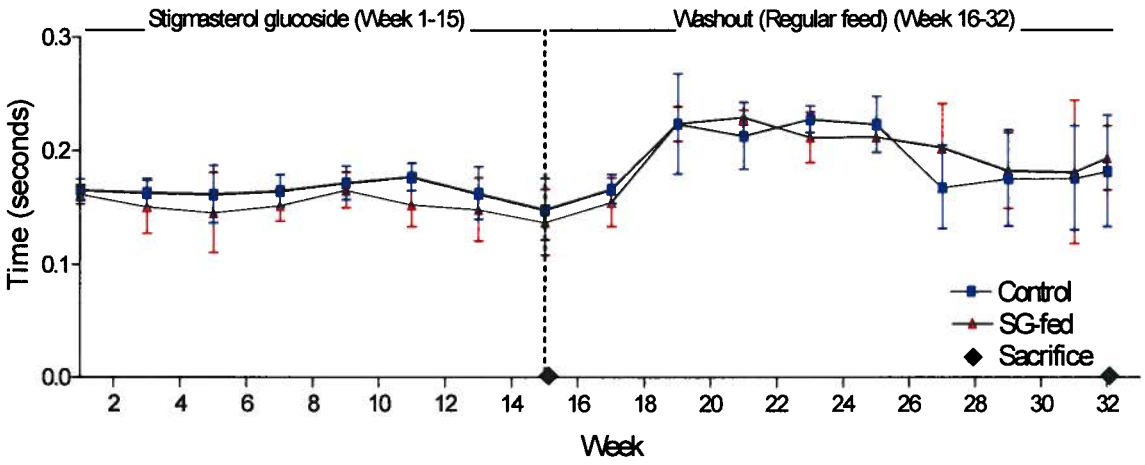
Stigmasterol β-D-Glucoside (SG) Feeding Study: Right Rear Stance
Stigmasterol glucoside (Week 1-15)
Washout (Regular feed) (Week 16-32)
Time (seconds)
0.3
0.2
0.1
0.0
2 4 6 8 10 12 14 16 18 20 22 24 26 28 30 32
Week
Control
SG-fed
Sacrifice

CC

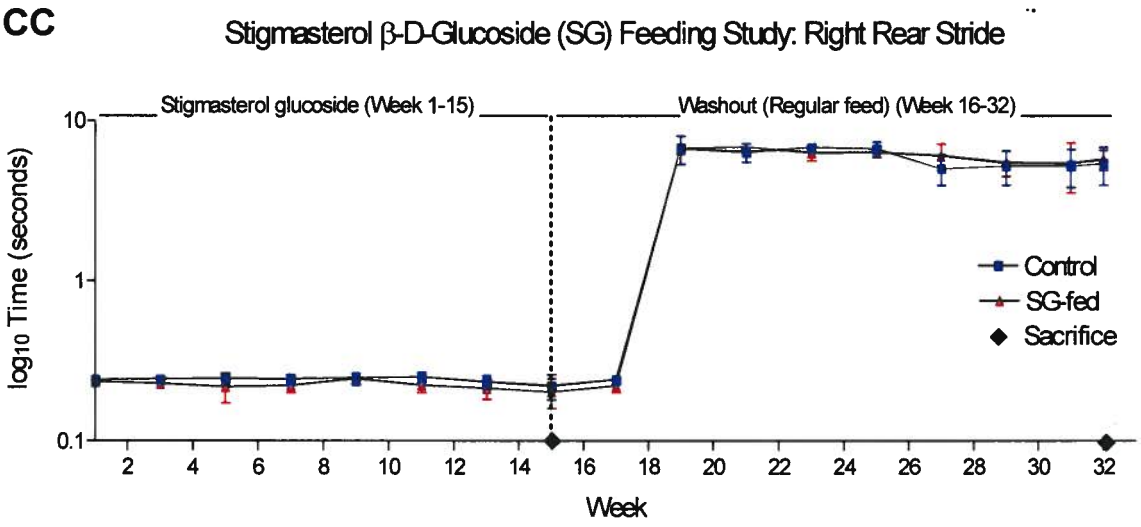
Stigmasterol β-D-Glucoside (SG) Feeding Study: Right Rear Stride
Stigmasterol glucoside (Week 1-15)
Washout (Regular feed) (Week 16-32)
log10 Time (seconds)
10
1
0.1
Control
SG-fed
Sacrifice
2 4 6 8 10 12 14 16 18 20 22 24 26 28 30 32
Week

DD

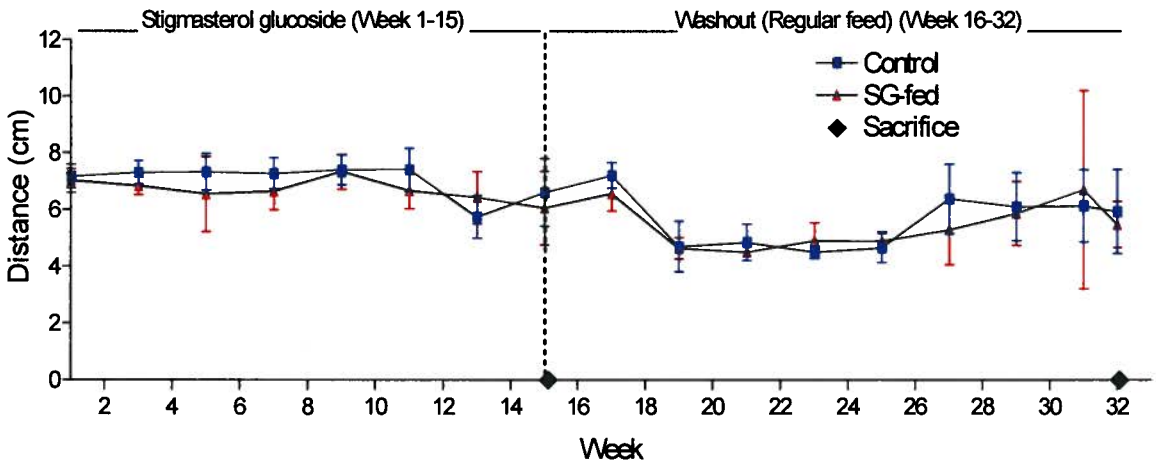
Stigmasterol β-D-Glucoside (SG) Feeding Study: Right Rear Stride Length
Stigmasterol glucoside (Week 1-15)
Washout (Regular feed) (Week 16-32)
Distance (cm)
12
10
8
6
4
2
0
Control
SG-fed
Sacrifice
2 4 6 8 10 12 14 16 18 20 22 24 26 28 30 32
Week

EE Stigmasterol β-D-Glucoside (SG) Feeding Study: Right Rear Paw Angle

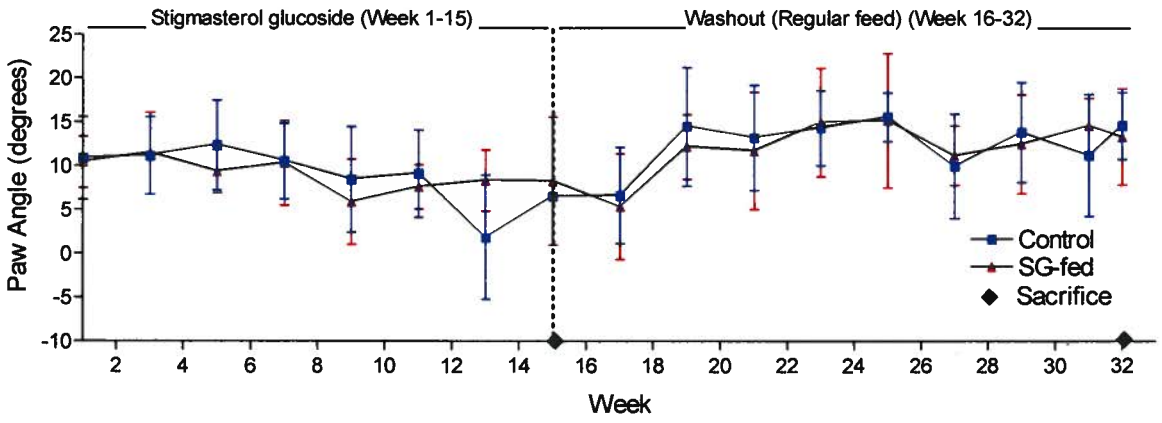

FF Stigmasterol β-D-Glucoside (SG) Feeding Study: Number of Right Rear Steps

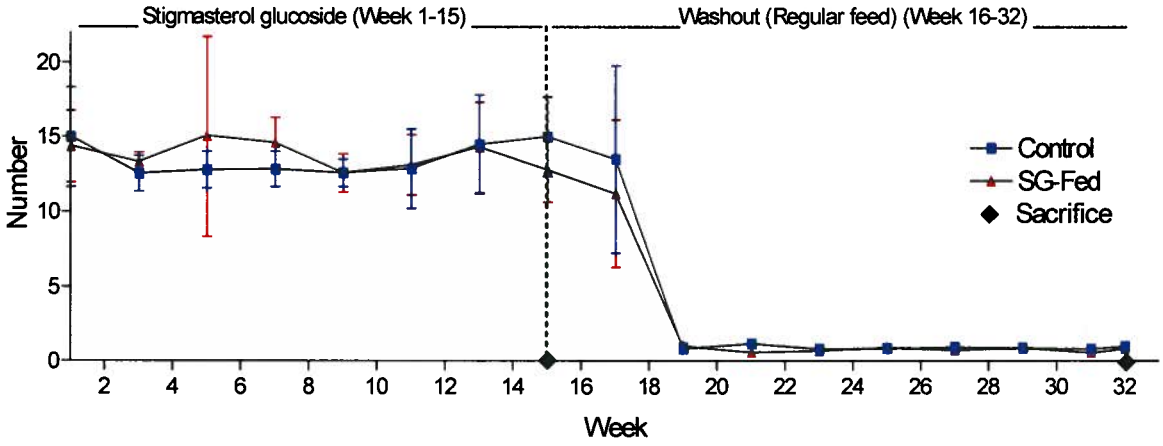

GG Stigmasterol β-D-Glucoside (SG) Feeding Study: Right Rear Paw Area at Peak Stance

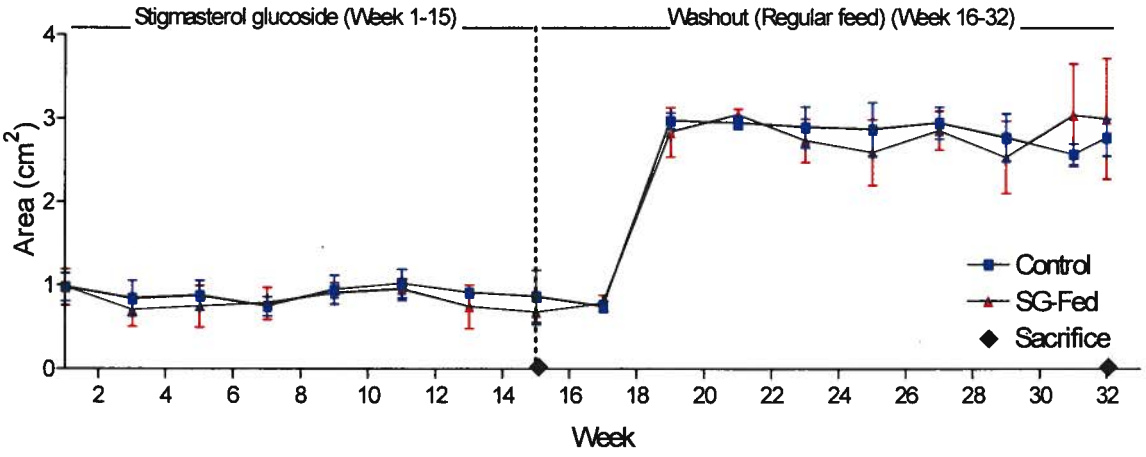

HH Stigmasterol β-D-Glucoside (SG) Feeding Study: Right Rear Stride Frequency

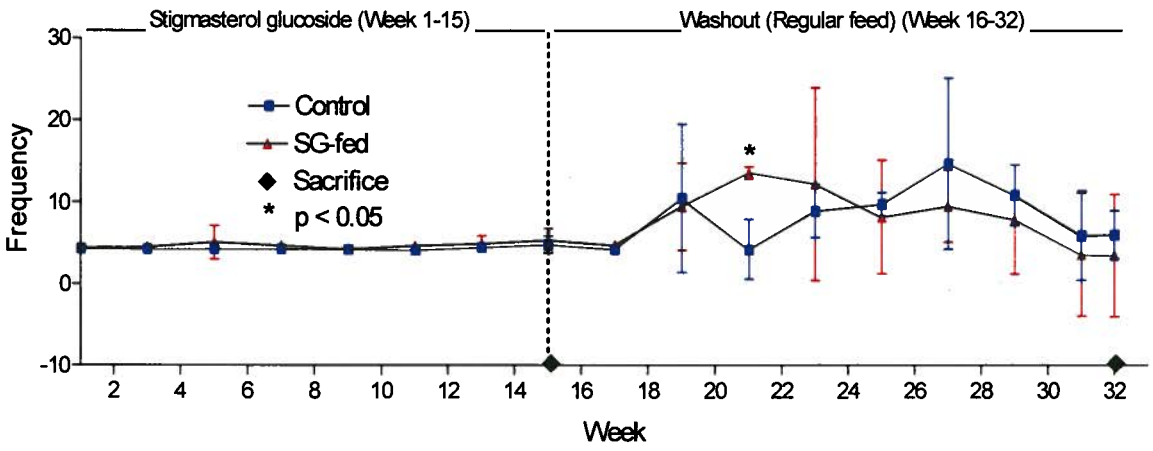

Figure 40. **Gait indices of SG-exposed mice and their age-matched controls.**

Additional gait indices also obtained with computer-assisted vertical plane videography system and analysis software.

Appendix B

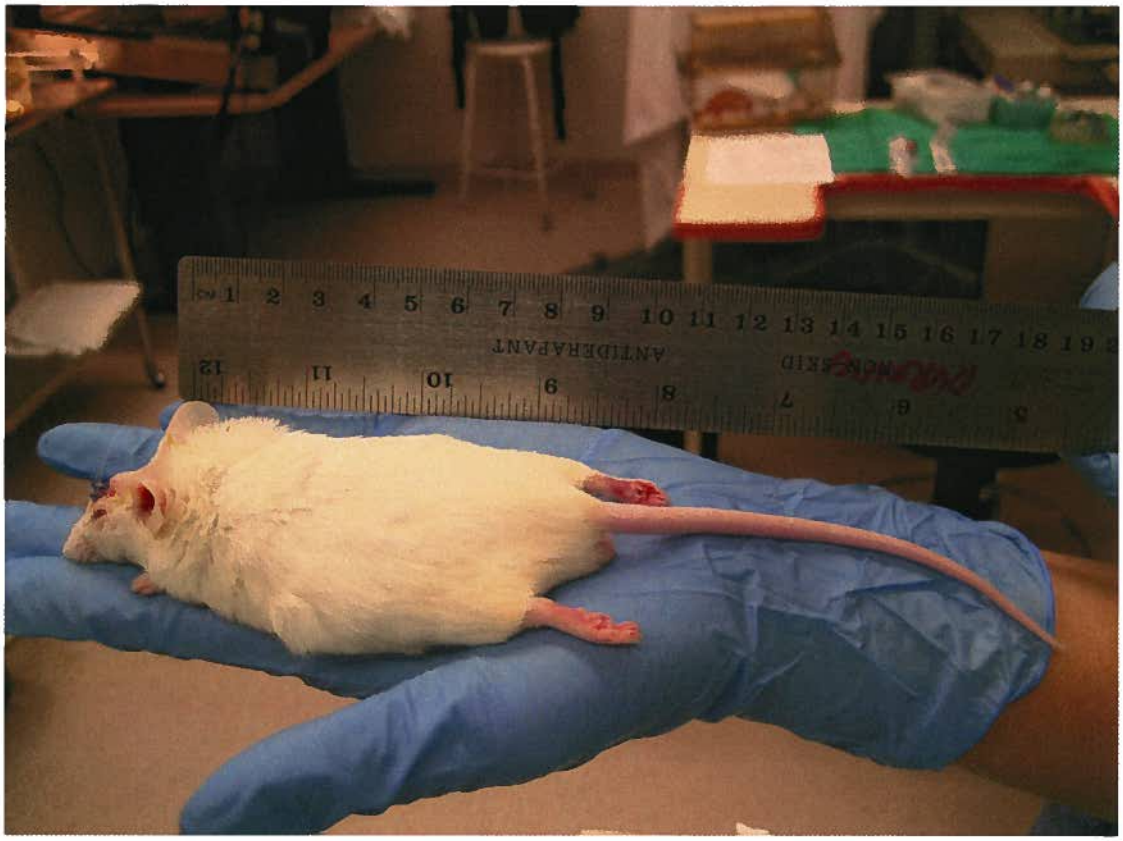

Figure 41. **Photograph showing the length of a mouse at the beginning of the sterol glucoside feeding studies.**

Appendix C

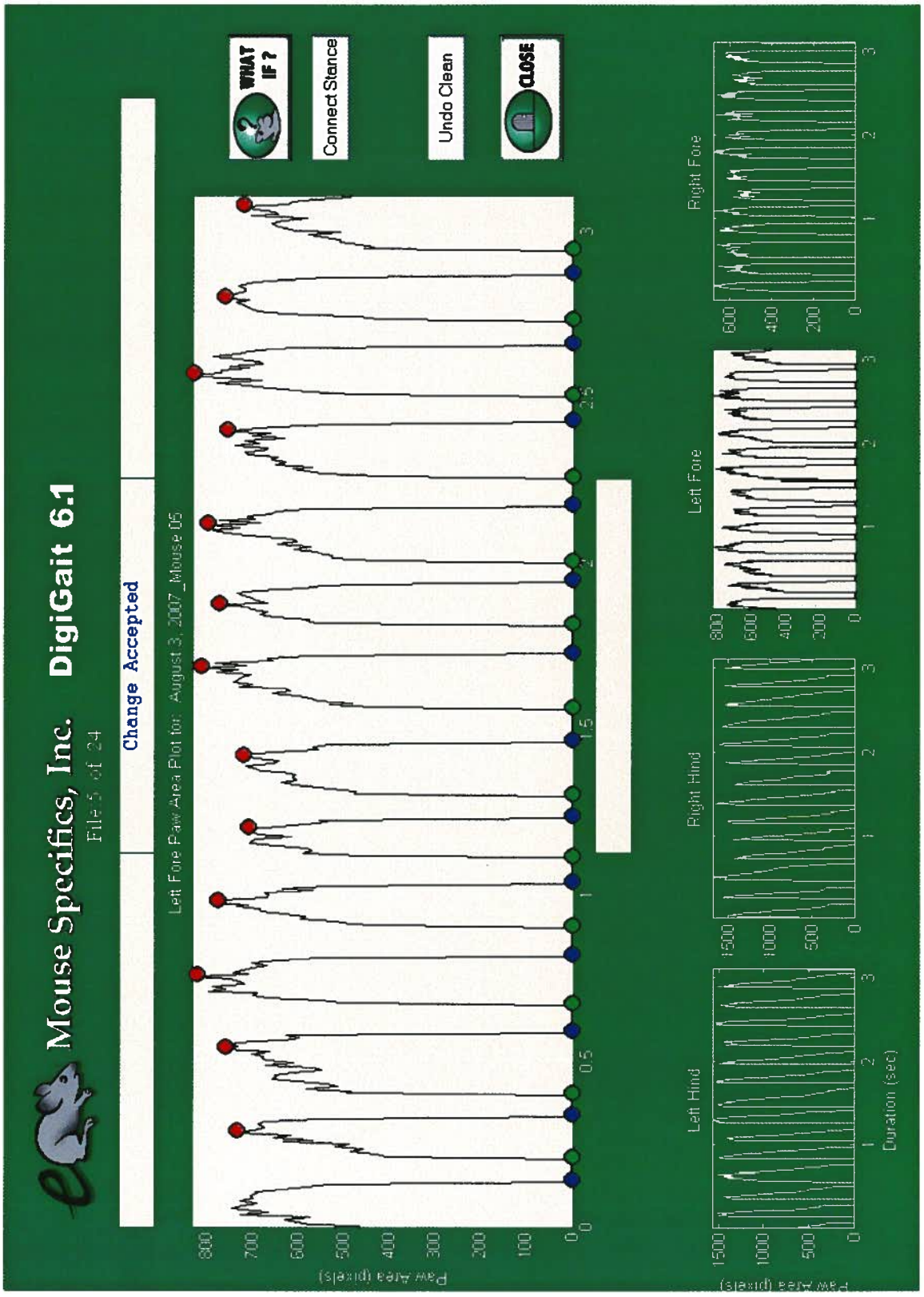
Mouse Specifics, Inc.
DigiGait 6.1
File 5 of 24
Change Accepted
Left Fore Paw Area Plot for: August 3, 2007_Mouse 05
WHAT IF ?
Connect Stance
Undo Clean
CLOSE
Paw Area (pixels)
Duration (sec)
Left Hind
Right Hind
Left Fore
Right Fore

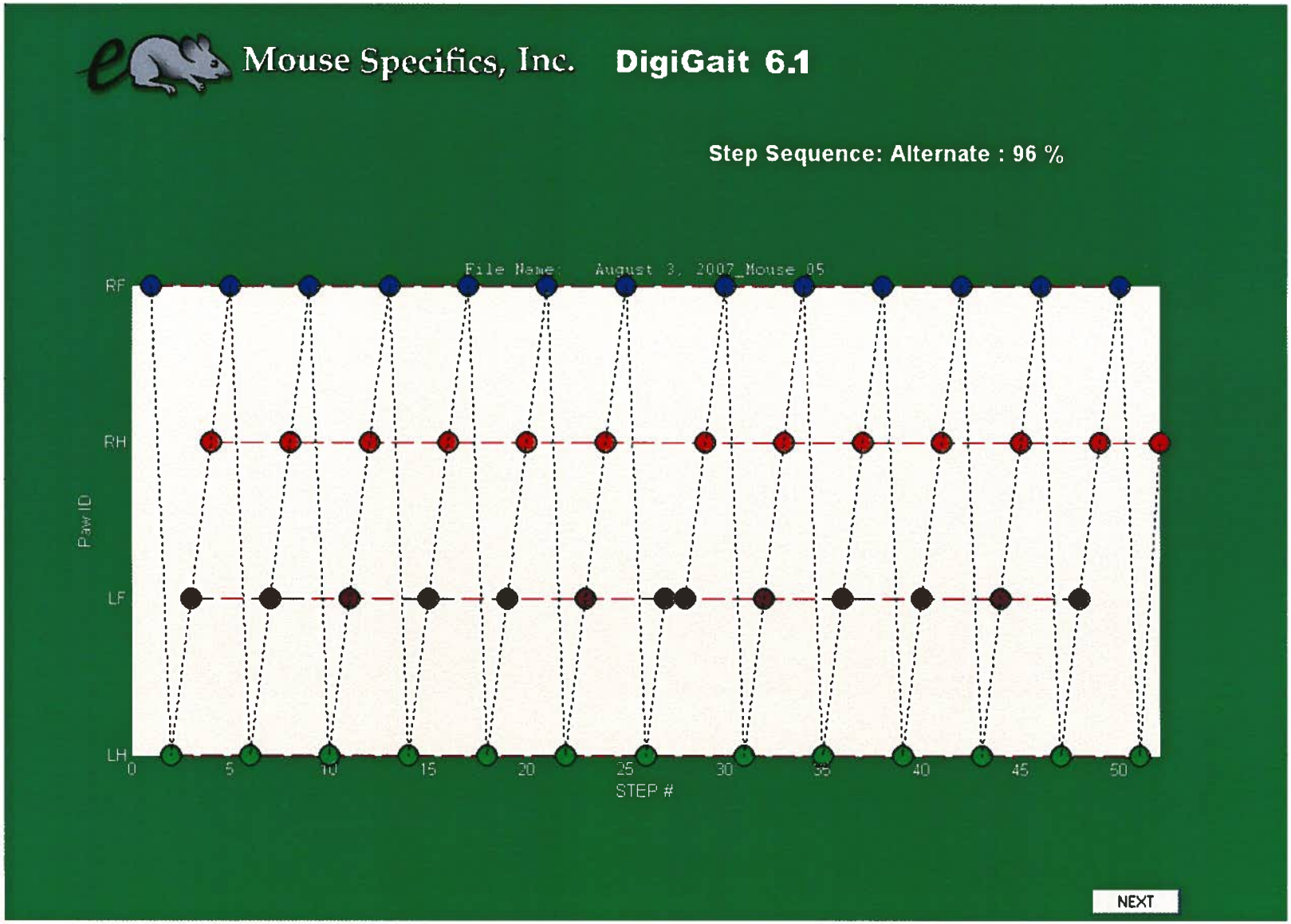
Mouse Specifics, Inc.
DigiGait 6.1
Step Sequence: Alternate : 96 %
File Name: August 3, 2007_Mouse 05
RF
RH
LF
LH
Paw ID
0
5
10
15
20
25
30
35
40
45
50
STEP #
NEXT

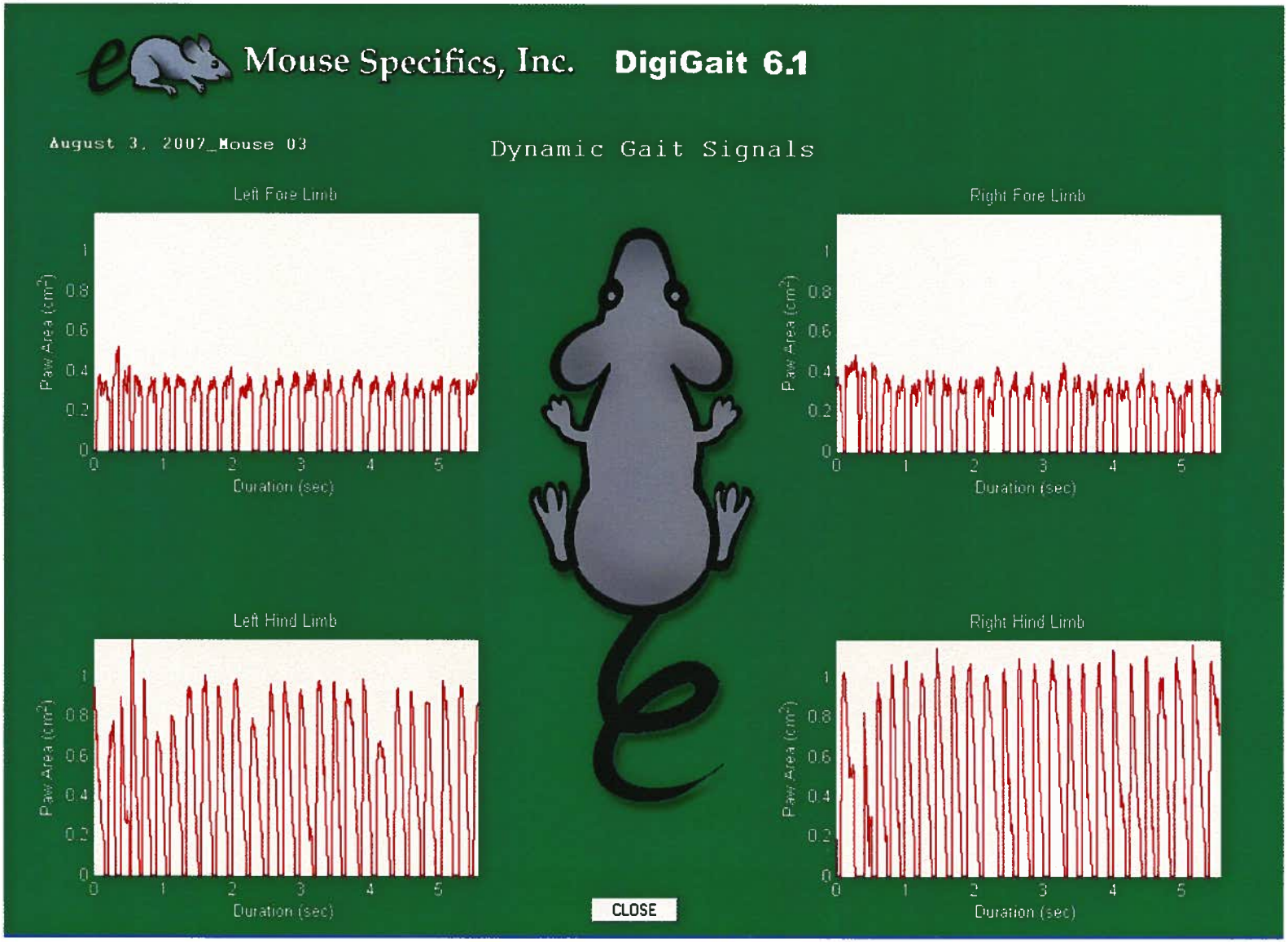
Mouse Specifics, Inc. DigiGait 6.1
August 3, 2007_Mouse 03
Dynamic Gait Signals
Left Fore Limb
Right Fore Limb
Left Hind Limb
Right Hind Limb
Paw Area (cm²)
Duration (sec)
CLOSE

Figure 42. **Screen shots of the ventral plane videography analysis in progress.**